A COMPUTATIONAL APPROACH TO THE FREE RADICAL POLYMERIZATION OF ACRYLATES AND METHACRYLATES

by

İsa Değirmenci

M. S., Chemistry, Boğaziçi University, 2005 (Turkey)

B. S., Marmara University, 2002 (Turkey)

Submitted to the Institute for Graduate Studies in
Science and Engineering of Boğaziçi University (Turkey)
and
the Faculty of Engineering of Ghent University (Belgium)
in fulfillment of the requirements for the degree of
the bi-nationally supervised
Joint Doctor of Philosophy

Supervisors :

Prof. Dr. Ir. V. Van Speybroeck (UGent, Faculty of Engineering)

Prof. Dr. Viktorya Aviyente (Boğaziçi University, Department of Chemistry)

Boğaziçi University

2010

MEMBERS OF THE EXAMINATION BOARD

Chair

Prof. Dr. Ir. Luc Taerwe, Dean Faculty of Engineering (IR14)

Reading Committee

Prof. Dr. Filip Du Prez (WE07)

Prof. Dr. Michel Waroquier (WE05)

Prof. Dr. Nurcan Tüzün, Istanbul Technical University, Department of Chemistry

Prof. Dr. Ir. Veronique Van Speybroeck (IR17), Supervisor

Other Members

Prof. Dr. Duygu Avcı, Department of Chemistry, Boğaziçi University, Istanbul

Prof. Dr. Viktorya Aviyente , Supervisor, Department of Chemistry, Boğaziçi University, Istanbul

Prof. Dr. Dimitri Van Neck (WE05)

Prof. Dr. Marie-Françoise Reyniers (IR12)

Dr. Saron Catak (IR17)

NEDERLANDSTALIGE SAMENVATTING

EEN COMPUTATIONALE STUDIE VAN VRIJE RADICALAIRE POLYMERIZATIE VAN ACRYLATEN EN METACRYALTEN.

In dit doctoraatswerk worden computationele moleculaire modelleringsmethoden aangewend om verschillende aspecten te bestuderen die van belang zijn bij de vrije radicalaire polymerizatieprocessen van acrylaten en methacrylaten. Vrije radicalaire polymerizatie vormt één van de belangrijkste chemische processen die gebruikt wordt in de industrie om een brede waaier van polymeren te produceren. Met dit proces kunnen een grote variëteit van vinyl monomeren omgezet worden naar hoog moleculair moleculair gewicht polymeer materialen, zonder dat een uitgebreide zuivering van commercieel beschikbare monomeren en oplosmiddelen nodig is. Anderzijds kent het proces ook een aantal tekortkomingen zoals de moeilijke beheersing van een aantal eigenschappen die de macromoleculaire structuren kenmerken zoals het moleculair gewicht, de polydispersiteit, eindfunctionaliteit, ketting architectuur, en de samenstelling. Om de eigenschappen van de geproduceerde materialen te optimaliseren is het van primordiaal belang dat een goed inzicht wordt verkregen in de relatie tussen de structuur van het monomeer, het reactiemechanisme en de uiteindelijk verkregen macroscopische eigenschappen. In deze thesis werd een dergelijke studie uitgevoerd voor acrylaten en methacrylaten, waarbij verschillende aspecten worden bekeken.

De reacties die voorkomen gedurende het vrije radicalaire polymerizatie proces kunnen ruwweg onderverdeeld worden in vier klassen van radicalaire reacties : (i) initiatie waarbij radicalen worden gegenereerd (2) propagatie waarbij radicalaire additiereacties zorgen voor een verdere ketengroei (3) transferreacties van reactieve radicalaire species op monomeer of solvent (4) terminatiereacties waarbij radicalen verdwijen door disproportionering of radicalaire recombinatiereacties. Het overgrote deel van de reacties bestudeerd in deze thesis behoren tot de klasse van de propagatiereacties. Aangezien sommige experimentele waarden waarvan gebruik gemaakt werd informatie geven over de

globale polymerizatiesnelheid, waarbij ook terminatiereacties en transferreacties bepalend zijn, werden ook sommige van deze reacties gemodelleerd. Tijdens de gemodelleerde transferreacties wordt het radicalair centrum overgedragen op een monomeer dat op zich een reactief intermediair wordt dat een nieuwe propagatie kan initiëren. Transferreacties zijn voornamelijk belangrijk voor het bepalen van het globale moleculair gewicht van het bekomen polymeer.

In een eerste deel van deze thesis werden gasfase reacties gemodelleerd van een serie van acrylaten en methacrylaten waarvan experimentele gegevens voorhanden waren betreffende de globale polymerizatiesnelheid. Hierbij werd als doel gesteld een duidelijke relatie vast te stellen tussen de structuur van het monomeer en de polymerizatiesnelheid. Deze laatste grootheid wordt bepaald door $k_p/k_t^{1/2}$, waarbij k_p de reactiesnelheid is van de de propagatie en k_t de reactiesnelheidsconstante van de terminatie. In deze studie werd de variatie van de propagatiesnelheid bestudeerd voor monomeren met verschillende eindgroepen met variatie van lineair naar cyclische groepen en verschillen in de polarizatie van de groep. De geometriën en frequenties werden bepaald met behulp van de B3LYP/6-31+G(d) methodologie en de energiën werden verder verfijnd met behulp van de BMK/6-311+G(3df,2p)//B3LYP/6-31+G(d) elektronische methode. Verder werden de partitiefuncties verfijnd door ook de rotatie rond de vormende binding in een model te beschrijven dat rekening houdt met de verschillende optredende minima. De rotationele potentialen werden tevens bepaald met het B3LYP/6-31+G(d) niveau. Algemeen kan gesteld worden dat de snelheidsconstanten van de propagatie de experimentele trend inzake polymerizatiesnelheid goed weergeven. Voor 2-dimethylaminoethyl acrylaat werd evenwel gevonden dat transferreacties een grote rol spleen. De reactiesnelheidsconstanten van de disproportioneringsreacties waren te klein om een belangrijke bijdrage te leveren tot de terminatie.

In een tweede deel van de thesis werd het polymerizatiegedrag bestudeerd van een serie gesubstitueerde alfa acrylaten. Het is wel gekend dat door invoering van een hetero-atoom in de alfa een belangrijke invloed kan hebben op de reactiekinetiek. Dit effect werd onderzocht voor de volgende monomeren : methyl acrylaat (MA), methyl methacrylaat (MMA), ethyl α-fluoroacrylaat (EFA), ethyl α-chloroacrylaat (ECA), ethyl α-cyanoacrylaat (ECNA), methyl α-hydroxymethacrylaat (MHMA). Verschillende elektronische structuur

methoden werden onderzocht om na te gaan welke methode beste geschikt is om de experimenteel gevonden trends te verklaren. Volgende DFT functionalen werden in beschouwing genomen : BMK, BB1K, MPW1B95, MPW1K en MPWB1K. Van de verschillende geteste methoden werd gevonden dat de MPWB1K/6-311+G(3df,2p)// B3LYP/6-31+G(d) het meest geschikt is om de experimenteel gevonden trends te verklaren. Bovendien werd het effect van de ketenlengte op de radicalaire reactiekinetiek onderzocht. Daartoe werden radicalaire species van verschillende lengtes bekeken gaande van dimeren, trimeren en tetrameren. Verder werd rekening gehouden met verschillende reacties die aanleiding kunnen geven tot verscheidene tacticiteiten van het finaal polymeer. De modelleringsresultaten slagen erin om de experimenteel waargenomen verhouding van 66/33 voor syndiotactisch versus isotactisch te reproduceren.

In een derde deel van de thesis werd aandacht besteed aan het correct in rekening brengen van solventeffecten op radicalaire additiereacties van belang bij de polymerizatie van methylmetacrylaat (MMA). De controle van de stereochemie bij de vrije radicalaire polymerizatie van MMA is een belangrijk aandachtspunt om de finale fysische eigenschappen te controleren. In dit werk werd de invloed van verschillende solventen op de tacticiteit onderzocht. Volgende solventen werden in beschouwing genomen : methanol (CH3OH) and in 1,1,1,3,3,3-hexafluoro-2-(trifluoromethyl)propan-2-ol ((CF3)3COH). De geometrie-optimalisaties werden uitgevoerd met behulp van de B3LYP/6-31+G(d) methodologie terwijl voor de verdere kinetiek evaluatie opnieuw verschillende methoden werden geëvalueerd (B3LYP/6-31+G(d), B3LYP/6-311+G(3df,2p), MPWB1K/6-311+G(3df,2p) and B2PLYP/6-31+G(d)). De solventomgeving werd in rekening gebracht zowel door het in beschouwing nemen van expliciete solventinteracties door introduceren van additionele solvenmoleculen in het model als door continue solventmodellen. In deze laatste modellen wordt het gesimuleerd moleculaire model ingebed in een omgeving die gekarakteriseerd wordt door een vaste diëlectrische constante die karakteristiek is voor het specifiek solvent. Uit de modelleringsresultaten is gebleken dat solventen die in staat zijn om waterstofbruggen te vormen met de carbonyl zuurstoffen van de backbone in staat zijn de vorming van isotactische structuren te onderdrukken. Methanol is in dit opzicht minder effect door de relatief kleine grootte van de molecule en de zwakkere sterkte van de waterstofbruggen. De studie heeft aangetoond dat het mogelijk is om experimenteel gevonden trends in tacticiteit te verklaren in functie van verschillende solventen.

Deze gevolgde aanpak werd ook gevolgd voor acrylzuren en methacrylzuren waarbij experimenteel gevonden werd dat acrylzuren sneller polymerizeren dan methacrylzuren.

Naast de studie van acrylaten en methacrylaten werd gedurende het verloop van dit thesiswerk ook meegewerkt aan een aantal andere projecten die van belang zijn voor de vrije radicalaire polymerizatie van andere monomeren. De resultaten van deze studies zijn opgenomen in het hoofdstuk 8 de huidige thesis.

Finaal kan gesteld worden dat het huidig werk een moderne stand van zaken geeft omtrent de mogelijkheid om vrije radicalaire processen te modelleren met huidige computationele technieken. Hierbij werd verschillende malen nagegaan in hoeverre verschillende elektronische structuurmethoden in staat zijn om de experimenteel bevonden trends te verklaren. Over het algemeen kan besloten worden dat de MPWB1K/6-311+G(3df,2p)//B3LYP/6-31+G(d) methodologie het meest geschikt is om de vrije radicalaire processen adequaat te beschrijven. Het bijzonder uitdagend probleem over de invloed van solventen werd ook bekeken. Het is hierbij vooral belangrijk expliciete solventmoleculen toe te voegen aan het moleculaire model aangezien dergelijke methoden in staat zijn om expliciete interacties die werkzaam zijn in de transitietoestand te beschrijven. Het huidig werk toont aan dat modelleringstechnieken in staat zijn om belangrijke experimenteel bevonden trends te verklaren. Uiteraard zal nog uitgebreid toekomstig onderzoek nodig zijn om de modellering ook predictief toe te passen op een breed scala van industrieel belangrijke monomeren.

ENGLISH SUMMARY

A COMPUTATIONAL APPROACH TO THE FREE RADICAL POLYMERIZATION OF ACRYLATES AND METHACRYLATES

Free radical polymerization (FRP) is one of the most favorable chemical reactions employed in both industry- and laboratory-scale chemical productions, because it can convert a wide variety of vinyl monomers into high molecular weight polymeric materials without extensive purification of commercially available monomers and solvents. On the other hand, the poor control of some of the key elements of macromolecular structures such as molecular weight (MW), polydispersity, end functionality, chain architecture, and composition are some important limitations for FRP. If the behavior of monomers during the FRP is well identified and understood, these limitations can be adjusted to moderate levels. In this work, the free radical polymerization of some highly useful acrylates and methacrylates have been explored and the origins of the structure-reactivity relationship have been investigated.

The mechanism of the free radical polymerization process basically consists of four different types of reaction families involving free radicals: (1) radical generation from non radical species (initiation), (2) radical addition to a substituted alkene (propagation), (3) chain transfer reactions, (4) termination reactions (termination by combination and termination by disproportionation). A variety of topics have been included in this thesis to study structure reactivity relations for acrylates and methacrylates.

Most of the reactions studied in this thesis are propagation reactions. However in some cases, also the termination reactions and chain transfer reactions have been modeled as they also influence the overall rate of polymerization. During chain transfer reaction to monomer, the radical center is transferred to the monomer, thereby generating a small radical species originating from the former monomer. This new radical can reinitiate the

propagation by attacking a second monomer. Chain transfer reactions mainly control the overall molecular weight of the formed polymer.

In a first part of this work gas phase calculations have been performed on a series of acrylates and methacrylates for which experimental rates of polymerization are available in order to directly correlate the polymerization rate to the monomer structure. The experimental polymerizability behavior is expressed as $k_p/k_t^{1/2}$, where k_p is the rate coefficient of propagation and k_t is the rate coefficient of termination. In this study, the reactivity of a series of acrylates and methacrylates is modeled in order to understand the effect of the pendant group size, the polarity of a pendant group, and the nature of the pendant group (linear vs cyclic) on their polymerizability. The geometries and frequencies are calculated with the B3LYP/6-31+G(d) methodology whereas the energetics and kinetics of these monomers have been studied using the two-component BMK/6-311+G(3df,2p)//B3LYP/6-31+G(d) level of theory. For rotations about forming/ breaking bonds in the transition state, an uncoupled scheme for internal rotations has been applied with potentials determined at the B3LYP/6-31+G(d) level. Generally the rate constants for propagation *k*p mimic the qualitative polymerization trend of the monomers modeled and can be used with confidence in predicting the polymerizability behavior of acrylates. However in the case of 2-dimethylaminoethyl acrylate, chain transfer is found to play a major role in inhibiting the polymerization. On the other hand, the disproportionation reaction turns out to be too slow to be taken into consideration as a termination reaction.

In a second part of this thesis, attention was focused on the polymerization behavior of alpha substituted acrylates. It is well known that the introduction of a heteroatom in the α-position of acrylates can influence the reaction kinetics. This effect was explored and it we indeed could rationalize the experimentally observed trend for the propagation of the following monomers: methyl acrylate (MA), methyl methacrylate (MMA), ethyl α-fluoroacrylate (EFA), ethyl α-chloroacrylate (ECA), ethyl α-cyanoacrylate (ECNA), methyl α-hydroxymethacrylate (MHMA). Various DFT functionals such as BMK, BB1K, MPW1B95, MPW1K, and MPWB1K were used to model the relative propagation kinetics of the monomers. Among the methodologies used MPWB1K/6-311+G(3df,2p)// B3LYP/6-31+G(d) was found to yield the best qualitative agreement with experiment. Chain length effects were explored by examining addition reactions of monomeric, dimeric, trimeric and

tetrameric radicals to the monomers. The tacticity of the widely used monomers methyl acrylate, methyl methacrylate has also been modeled by considering all the alternatives of attack of the radical in the 3D-space around the monomer. This study has confirmed qualitatively the experimental syndiotactic/isotactic ratio of 66/3 for methyl methacrylate. Finally the kinetics of the initiation to polymerization for methyl acrylate and methyl methacrylate is also successfully reproduced.

In a third part of this thesis, we focused on the influence of solvent on the tacticity of free radical polymerization of methyl methacrylate. The control of stereochemistry in the free radical polymerization of methylmethacrylate (MMA) is important because the physical properties of PMMA are often significantly affected by the main-chain tacticity. In this study, the role of the solvent on the tacticity of MMA polymerization has been investigated by considering the propagation rate constants for the syndiotactic and isotactic free radical polymerization of MMA in vacuum, in methanol (CH_3OH) and in 1,1,1,3,3,3-hexafluoro-2-(trifluoromethyl)propan-2-ol ($(CF_3)_3COH$). All geometry optimizations have been carried out with the B3LYP/6-31+G(d) methodology. The kinetics of the propagating dimer have been evaluated with the B3LYP/6-31+G(d), B3LYP/6-311+G(3df,2p), MPWB1K/6-311+G(3df,2p) and B2PLYP/6-31+G(d) methodologies. The role of the solvent has been investigated by using explicit solvent molecules and also by introducing a polarizable continuum model (IEF-PCM) with a dielectric constant specific to the solvent. Experimentally, the free radical polymerization of MMA in $(CF_3)_3COH$ is found to be highly syndiotactic (*rr* = 93 per cent): the stereoeffects of fluoroalcohols are claimed to be due to the hydrogen-bonding interaction of the alcohols with the monomers and growing species. This modeling study has revealed the fact that the solvents CH_3OH and $(CF_3)_3COH$, which are H-bonded with the carbonyl oxygens located on the same side of the backbone hinder the formation of the isotactic PMMA to some extent. Methanol is less effective in reducing the isotacticity because of its small size and also because of the relatively loose hydrogen bonds (~ 1.9 Å) with the carbonyl oxygens. The methodologies used in this study reproduce the solvent effect on the free radical polymerization kinetics of MMA in a satisfactory way.

The previous methodology was also applied acrylic acid(AA) methacrylic acid (MAA) For AA and MAA early studies indicated that the polymerization rates vary

strongly with pH and degree of ionization, which was ascribed to alteration of the propagation rate rather than termination rate. Both for MAA and AA it was found that the propagation rate constant of non-ionized monomers increases by more than one order of magnitude in going from the bulk to a highly dilute system. These effects were ascribed by specific interactions in the transition state. The effect of adding water to the propagation rate of MAA and AA has been investigated. The experimentally observed trends were reproduced for both monomers. Moreover it was shown that both the AA and MAA polymerizing system prefers to be solvated by water molecules instead of solvating with the monomer itself.

In addition to the main part of the thesis concerning acrylates and methacrylates, some research was performed in collaboration with other researchers from the Bogazici University on chain transfer reactions. These results are taken up in chapter 8 of the thesis.

This work brings a new perspective to the modeling of free radical polymerization reactions and provides a deeper insight into the factors that affect polymerizability of a various monomers. However, the scope of exploring the FRP reactions is very large and highly useful examples are not limited to the ones discussed in this study. Lots of DFT methodologies have been tested against the experimental results in order to assess the level of theory for modeling the FRP. In all cases, the MPWB1K/6-311+G(3df,2p)//B3LYP/6-31+G(d) methodology is found to reproduce the experimental trend the best as cost effective method. We were able to show that specific solvent interactions in the transition state could explain some experimentally seen trends. Future work will undoubtedly uncover many other important aspects of the FRP reactions.

TABLE OF CONTENTS

MEMBERS OF THE EXAMINATION BOARD ii

NEDERLANDSTALIGE SAMENVATTING iii

ENGLISH SUMMARY vii

TABLE OF CONTENTS xi

LIST OF SYMBOLS/ ABBREVIATIONS xiv

1. INTRODUCTION 1

1.1. Free Radical Polymerization 1

1.2. Free Radical Polymerization Kinetics 5

1.3. The Stereocontrol in the FRP of Acrylates and Methacrylates 7

1.4. Computational Approach to Free Radical Polymerization 10

1.5. References 11

2. RESEARCH OBJECTİVES. 18

3. COMPUTATIONAL DETAILS 20

3.1. Quantum Mechanics 20

3.2. Ab initio Methods 22

3.3. Semi-empirical Methods 28

3.4. Density Functional Theory 30

3.5. LCAO Approximation and Basis Sets. 33

3.6. Solvation Models 35

3.7. Continuum Solvation Models 35

3.8. References 37

4. DFT STUDY OF FREE-RADICAL POLYMERIZATION OF ACRYLATES AND METHACRYLATES 42

4.1. Introduction 42

4.2. Computational Methodology 46

4.2.1. Reaction mechanism of free radical polymerization 46

4.2.2. Reaction kinetics 48

4.2.3. Computatinal Details 49

4.3. Results and Discussion 50

4.4. Conclusions 73

4.5. References 73

5. DFT STUDY ON THE PROPAGATION KINETICS OF FREE-RADICAL POLYMERIZATION OF α–SUBSTITITED ACRYLATES 80

5.1. Introduction 80

5.2. Methodology 83

5.2.1. Reaction mechanism 83

5.2.2. Computational Procedure 83

5.2.3. Reaction kinetics 84

5.3. Results and Discussion 84

5.4. Conclusions 102

5.5. References 103

6. MODELING THE SOLVENT EFFECT ON THE TACTICITY IN THE FREE RADICAL POLYMERIZATION OF METHYL METHACRYLATE 107

6.1. Introduction 107

6.2. Computational Procedure 109

6.3. Results 112

6.2.1. A. Free Radical Polymerization of MMA in CH_3OH as solvent 113

6.2.2. B. Free Radical Polymerization of MMA in perfluoro-tert-butyl alcohol$(CF_3)_3COH$ 122

6.2.3. C. Comparison of Free Radical Polymerization of MMA in CH_3OH and in $(CF_3)_3COH$ 126

6.4. Conclusions 128

6.5. References 129

7. ROLE OF SOLVENT ON THE PROPAGATION KINETICS OF ACRYLIC ACID AND METHACRYLIC ACID 134

7.1. Introduction 134

7.2. Computational Procedure 136

7.3. Results 137

7.4. Conclusions 148

7.5. References 149

8. ROLE OF CHAIN TRANSFER AGENTS IN FREE RADICAL POLYMERIZATION KINETICS 154

8.1. Introduction 154

8.2. Methodology and Computational Procedure 156

8.3. Results 161

8.2.1. Propagation of Ethelene 161

8.2.2. Chain transfer in the propagation of ethelene 162

8.2.3. Level of theory study 170

8.4. Conclusions 172

8.5. References 173

9. GENERAL CONCLUSIONS 178

LIST OF SYMBOLS/ABBREVIATIONS

E	Electronic energy
$E[\rho(\mathbf{r})]$	Electronic energy from electron density
$E_{\mathrm{C}}[\rho(\mathbf{r})]$	Correlation energy
$E_{\mathrm{C}}^{\mathrm{DFT}}$	DFT Correlation energy
$E_{\mathrm{X}}[\rho(\mathbf{r})]$	Exchange energy
$E_{\mathrm{X}}^{\mathrm{DFT}}$	DFT exchange energy
$E_{\mathrm{X}}^{\mathrm{exact}}$	Exact exchange energy
$E_{\mathrm{X}}^{\mathrm{HF}}$	Hartree-Fock exchange energy
$E_{\mathrm{XC}}[\rho(\mathbf{r})]$	Exchange correlation energy functional
$\hat{f}_i\,(1)$	Fock operator
f	Initiator efficiency
$F(\mathbf{r}_s)$	Electric field perpendicular to the surface
$\widehat{H}$	Hamiltonian operator
$\widehat{H}^{\mathrm{core}}(1)$	Core-Hamiltonian operator
h	Planck's constant
$\hat{J}_j(1)$	Coulomb operator
$J[\rho(\mathbf{r})]$	Coulomb energy
J_{ij}	Coulomb integral
$\widehat{K}_j(1)$	Exchange operator
K_{ij}	Exchange integral
k_B	Boltzmann's constant
k_p	The rate constant of the propagation reaction
k_d	The decomposition rate constant of the initiation reaction
k_{ct}	The rate constant of the chain transfer reaction
k_{td}	The rate constant of the termination by disproportionation reaction
k_{tc}	The rate constant of the termination by coupling reaction
k_t	The rate constant of the termination reaction
R_p	Rate of polymerization
$T[\rho(\mathbf{r})]$	Kinetic energy of interacting electrons

$T_s[\rho(\mathbf{r})]$	Kinetic energy of the non-interacting electrons
$U_{\mathrm{XC}}^{\lambda}$	Potential energy of exchange-correlation at intermediate coupling strength
U_x^{σ}	Exchange energy density
$V_{\mathrm{ee}}[\rho(\mathbf{r})]$	Interelectronic interactions
$V_{\mathrm{ext}}(\mathbf{r})$	External potential
V_{KS}	Kohn-Sham potential
$V_{\sigma}(\mathbf{r})$	Potential from the surface charge
$V_{\mathrm{XC}}[\mathbf{r}_1]$	Exchange-correlation potential
Å	Angstrom
$\Delta E_{\mathrm{C}}^{\mathrm{GC}}$	Gradient correction to the correlation energy
$\Delta E_{\mathrm{X}}^{\mathrm{GC}}$	Gradient correction to the exchange energy
$\Delta E_0^{\ddagger}$	Energy of activation
$\Delta E_{dis}^{\ddagger}$	Distortion energy
$\Delta E_{int}^{\ddagger}$	Interaction energy
$\Delta G^{\ddagger}$	Activation Gibbs free energy
$\Delta H^{\ddagger}$	Enthalpy of activation
$\Delta S^{\ddagger}$	Entropy of activation
ΔH_{theor}	Heat relased per mole of double bonds reacted
ε_{C}	Correlation contribution to energy density
ε_{X}	Exchange contribution to energy density
$\varepsilon_{\mathrm{XC}}(\rho(\mathbf{r}))$	Energy density
ε	Dielectric constant
λ	Interelectronic coupling strength
$\rho(\mathbf{r})$	Electron density
$\sigma(\mathbf{r}_s)$	Charge density on the surface of the cavity
δ	Partial charge
μ	Dipole moment
χ_i	Spin orbital
ψ_i	Kohn-Sham orbitals
Q_{PRC}	Prereactive complex's partition function

Q_R	Reactants partition functions
Q_{TS}	Transition state's partition function
Q/s	Heat flow per second

AA	Acrylic Acid
AM1	Austin method 1
B3LYP	Becke-3-Lee-Yang-Parr
B88	Becke 88
BMK	Boese-Martin for kinetics
B-LYP	Becke-Lee-Yang-Parr
CC	Coupled cluster
CNDO	Complete neglect of differential overlap
CI	Configuration interaction
DFT	Density functional theory
ECA	Ethyl chloro acrylate
ECNA	Ethyl cyano acrylate
EFA	Ethyl fluoro acrylate
EHMA	Ethyl alpha-hydroxymethacrylate
FRP	Free radical polymerization
GC	Gradient corrected
GGA	Generalized gradient approximation
HEA	Hydroxyethyl acrylate
HF	Hartree-Fock
HMA	Alpha-hydroxymethacrylate
HO	Harmonic oscillator approximation
HR	Hindered rotor approximation
HOMO	Highest occupied molecular orbital
IEFPCM	Integral equation formalism polarized continuum model
INDO	Intermediate neglect of differential overlap
IRC	Intrinsic reaction coordinate
LCAO	Linear combination of atomic orbitals
LDA	Local density approximation
LUMO	Lowest unoccupied molecular orbital

LYP	Lee-Yang-Parr
MA	Methyl acrylate
MAA	Methacrylic acid
MCSF	Multiconfiguration self consistent field
MHMA	Methyl alpha-hydroxymethacrylate
MINDO/3	Modified intermediate neglect of differential overlap/3
MMA	Methyl methacrylate
MNDO	Modified neglect of diatomic overlap
MO	Molecular orbital
MP	Moller-Plesset
MP2	Second order perturbation
MP3	Third order perturbation
MP4	Fourth order perturbation
MRCI	Multi-reference configuration interaction
NBO	Natural bond orbital
NDDO	Neglect of diatomic differential overlap
NIPAM	N-isopropylacrylamide
PCM	Polarizable continuum model
PES	Potential energy surface
PFTB	Perfluoro-tert-butyl alcohol
PM3	Parameterization method 3
PMMA	Poly methy methacrylate
PAA	Poly (allyl alcohol)
PVA	Poly (vinyl alcohol)
RE	Reactant complex
RHMA	Alkyl alpha-hydroxymethacrylate
SCF	Self-consistent field
SCRF	Self-consistent reaction field theory
SOI	Secondary orbital interaction
STO	Slater type orbital
TBHMA	Tert-butyl alpha-hydroxymethacrylate
TS	Transition state
TST	Transition state theory

UEG	Uniform electron gas
VDW	Van der Waals
VWN	Vosko-Wilk-Nusair
ZPVE	Zero-point vibration energy

1. INTRODUCTION

1.1. Free Radical Polymerization

Conventional free-radical polymerization (FRP) is a very important commercial process for preparing high molecular weight polymers because it can be employed for polymerization of many vinyl monomers under mild reaction conditions, requiring the absence of oxygen, but tolerant to water, and can be conducted over a large temperature range (-80 to 250°C) [1,2]. The main limitation of FRP is the poor control of some of the key elements of macromolecular structures such as molecular weight (MW), polydispersity, end functionality, chain architecture, and composition. Well-defined polymers with precisely controlled structural parameters are accessible by ionic living polymerization; however, ionic living polymerization requires stringent conditions and are limited to a relatively small number of monomers [3-5].

The free radical polymerization process via chain mechanism, basically consists of four different types of reactions involving free radicals: (1) radical generation from non radical species (initiation), (2) radical addition to a substituted alkene (propagation), (3) chain transfer reaction, (4) termination reaction (termination by combination and termination by disproportionation) [1]. The initiation step is considered to proceed via two reactions. The first is the production of free radicals by heat or light. The usual case is the homolytic dissociation of an initiator or a catalyst *I* to yield a pair of radicals $R\bullet$

$$I \xrightarrow{k_d} 2R\bullet \qquad (1.1)$$

where k_d is the rate constant for the catalyst dissociation. The second part of the initiation involves the addition of this radical to the first monomer molecule to produce the chain initiating species $M_1\bullet$

$$R_1\bullet + M \xrightarrow{k_i} M_1\bullet \qquad (1.2)$$

where M represents a monomer molecule and k_i is the rate constant for the initiation step (Eq. 1.2). For the polymerization of $CH_2=CXY$, Eq. 1.2 takes the form

$$R\bullet + CH_2 = CXY \longrightarrow R - CH_2 - CXY\bullet \tag{1.3}$$

(The radical $R\bullet$ is often referred to as an initiator radical or a primary radical.)

The propagation consists of the growth of $M_1\bullet$ by the successive additions of large numbers of monomer molecules. Each addition creates a new radical which has the same identity as the previous one, except that it is larger by one monomer unit. The successive additions may be represented by

$$M_1\bullet + M \xrightarrow{k_p} M_2\bullet \tag{1.3}$$

$$M_2\bullet + M \xrightarrow{k_p} M_3\bullet \tag{1.4}$$

$$M_3\bullet + M \xrightarrow{k_p} M_4\bullet \tag{1.5}$$

etc., etc.

or in general terms

$$M_n\bullet + M \xrightarrow{k_p} M_{n+1}\bullet \tag{1.6}$$

where k_p is the rate constant for propagation. Propagation with growth of the chain to high polymer proportions takes place very rapidly. The value of k_p for most monomers is in the range 10^2-10^4 liter/mole-sec.

The propagating radical may attack to another monomer by chain transfer and the radical center may be transferred to another chain, so that the molecular weight of the propagating polymer can be controlled.

$$M_n \bullet + R - H \xrightarrow{k_{ct}} M_n - H + R \bullet \tag{1.7}$$

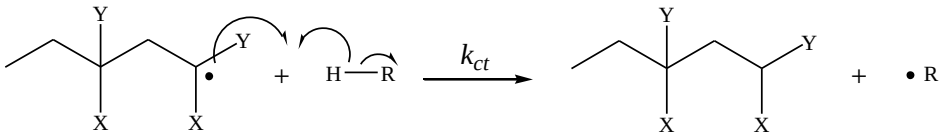

(1.8)

k_{ct} in these reactions is the rate constant for the chain transfer reaction. According to the reactivity of the new radical center a new growing species is generated or propagating and the radical is terminated.

At some point, the propagating polymer chain stops growing and terminates. The termination with the annihilation of the radical centers occurs by bimolecular reaction between radicals. Two radicals react with each other by *combination* (*coupling* (k_{tc})),

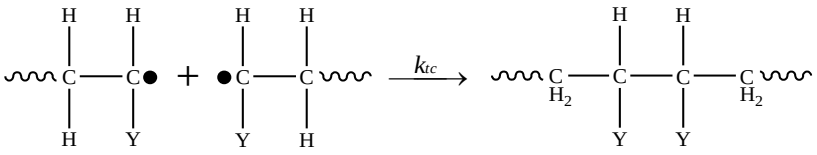

(1.9)

or, more rarely, by *disproportionation* in which a hydrogen radical that is *beta* to a radical center is transferred to another radical center (k_{td}). This results in the formation of two polymer molecules-one saturated and one unsaturated.

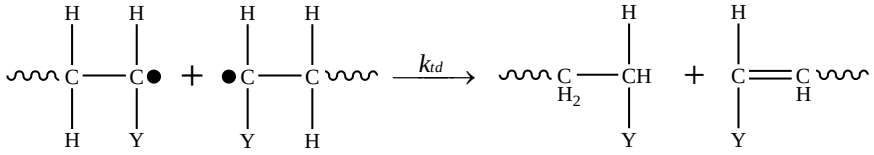

(1.10)

Termination can also occur by a combination of coupling and disproportionation. The two different modes of termination can be represented in general terms by

$$M_n\bullet + M_m\bullet \xrightarrow{k_{tc}} M_{n+m} \tag{1.11}$$

$$M_n\bullet + M_m\bullet \xrightarrow{k_{td}} M_n + M_m \tag{1.12}$$

where k_{tc} and k_{td} are the rate constants for termination by coupling and disproportionation, respectively. One can also express the termination step by

$$M_n\bullet + M_m\bullet \xrightarrow{k_t} \text{dead polymer} \tag{1.13}$$

where the particular mode of termination is not specified

$$k_t = k_{tc} + k_{td} \tag{1.14}$$

The term *dead polymer* signifies the cessation of growth for the propagating radical. The propagation reaction would proceed indefinitely until all the monomers in a reaction system are exhausted. Typical termination rate constants are in the range of 10^6-10^8 liter/mole-sec or orders of magnitude greater than the propagation rate constants. The much greater value of k_t (whether k_{tc} or k_{td}) compared to k_p does not prevent propagation

because the radical species are present in very low concentrations and because the polymerization rate is dependent on only the one-half power of k_t.

1.2. Free Radical Polymerization Kinetics

When the reaction kinetics is considered, the rate of initiation (υ_i) according to the initiation reaction may be given as

$$\upsilon_i = 2fk_d[I] \tag{1.15}$$

where f is the initiator efficiency, k_d is the rate constant for the decomposition of the initiator and I is the concentration of the initiator. The initiator efficiency factor is used since all the generated free radicals are not able to initiate polymer growth. Sometimes recombination between radicals may take place. Initiator efficiency may take values between zero and one.

The rate of termination (υ_t) is a bimolecular process so that

$$\upsilon_t = 2k_t[M^\bullet]^2 \tag{1.16}$$

where k_t and M stand for the termination rate constant and the concentration of the monomer respectively. The rate constant $2k_t$ is actually ($k_{tc} + k_{td}$).

The overall rate of polymerization is calculated by the aid of the steady-state approximation. The steady-state approximation assumes that, after an initial induction period, an interval during which the consentrations of intermediates, rise from zero, and during the major part of the reaction, the rates of change of concentrations of all reaction

intermediates are negligibly small [6]. According to the steady state approximation for the FRP, the initiation is relatively small but continuous. The termination speeds up as the active radical concentration builds and the termination removes (kills) active radicals. Therefore it is an excellent approximation to assume that rate of initiation of radicals is equal to the rate of termination of radicals.

$$\upsilon_i = \upsilon_t \tag{1.17}$$

$$2fk_d[I] = 2k_t[M^\bullet]^2 \tag{1.18}$$

$$[M^\bullet] = \left(\frac{fk_d[I]}{k_t} \right)^{1/2} \tag{1.19}$$

Thus, rate of propagation (υ_p) may be given as

$$\upsilon_p = k_p[M][M^\bullet] = k_p[M]\left(\frac{fk_d[I]}{k_t} \right)^{1/2} \tag{1.20}$$

where k_p stands for the propagation rate constant. In the derivation of polymerization rate, the propagation (k_p) and termination (k_t) rate coefficients are assumed to be chain length and conversion independent [7].

The overall homopolymerization rate constant, *k*, is based on the kinetic expression for homopolymerization [8]

$$R_p = k[I]^{1/2}[M] \tag{1.21}$$

Then, the expression for *k* is

$$k = \frac{k_p}{k_t^{1/2}}(fk_d)^{1/2} \tag{1.22}$$

1.3. The Stereocontrol in the FRP of Acrylates and Methacrylates

Stereoregularity is taken into account because it affects many important properties of the polymers, such as solubility, crystallinity, melting point, glass transition temperature, and mechanical strength. The overall tacticity of the polymer chain is determined by the regularity in the configuration of the pseudochiral centers. If the R groups of pseudochiral centers are randomly distributed on the two sides of the polymer chain plane the polymer is *atactic*. In an *isotactic* structure, the two adjacent monomer units consist of meso (*m*) diads, all the R groups are located on one side of the plane of the polymer chain. In a *syndiotactic* structure, the two adjacent monomer units consist of racemo (*r*) diads, all the R groups are located alternately on the opposite side of the plane of the polymer chain (Scheme 1.1).

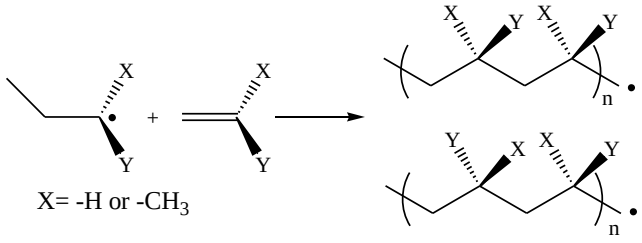

Scheme 1.1. Representation of isotactic and syndiotactic radical polymerization of various acrylates and methacrylates.

The fractions of *isotactic* and *syndiotactic diads* are referred to as (*m*) and (*r*), respectively. *Triad* tacticity describes *isotactic*, *syndiotactic*, and *heterotactic triads*, whose fractions are described as (*mm*), (*rr*), and (*mr*), respectively.

When free radical polymerizations yield *tactic* structures (either isotactic or syndiotactic) they are termed as *stereospecific polymerizations* and the polymer structures are termed as *stereoregular polymers*.

The stereoregular polymers are significantly different from the corresponding non-stereoregular polymers in terms of their physical properties. Crystallinity can be given as a property which is significantly affected by stereoregularity of the polymer chain. While *atactic* polymers are amorphous (noncrystalline), the corresponding *isotactic* and *syndiotactic* polymers are usually obtained as highly crystalline materials. Crystallinity leads to high physical strength and increased solvent and chemical resistance as well as difference in other properties which depend on crystallinity [10].

The stereospecificity for radical polymerization in solution can be affected significantly by the bulkiness in the monomer structure. Free radical polymerization of aliphatic methacrylates give polymer products which have an excess of syndiotactic over isotactic diads (such as MMA and tBut-MA), probably due to the steric repulsion among the R-methyl and pendent ester groups of the incoming monomer, growing radical, penultimate, and penpenultimate units in the antistaggered gauche conformations of the planar polymer chain [11].

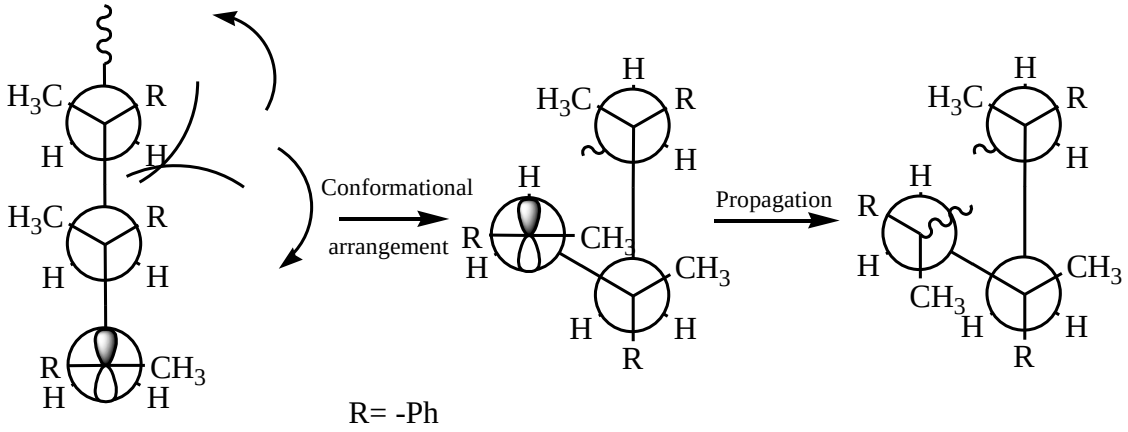

Schema 2. Schematic models for the steric effect of bulky pendant groups of a methacrylate during polymerization.

Methacrylates which have highly bulky pendant group can be arranged in a variety of ways depending on the reaction medium.

Methacrylate versus Acrylate

Radical polymerization of the acrylate derivatives has a greater tendency to afford almost atactic polymers regardless of the monomer structure and polymerization temperature [12-17]. When the bulkiness of the pendant group of acrylates is increased, the syndiotacticity of the obtained polymers slightly increases which is different from the polymerization of the methacrylates. The steric repulsion in the antistaggered gauche conformations of the planar polymer chain can leads to this effect.

Stereoregularity of some special monomers can be affected by the solvent such as, methacrylates bearing aromatic groups show a change in the tacticity of the polymer products. This is probably due to the π-stacking interaction or specific interactions between the aromatic ring and growing radicals [18-21]. For example, 2-naphthyl methacrylate gave an isotactic-rich polymer in *n*-hexane (*mm*/*mr*/*rr* = 58/24/18), whereas that obtained in benzene was rather syndiotactic (*mm*/*mr*/*rr* = 14/39/47) [22-25]. In addition to this usage of some fluoroalcohol solvents can alter the stereochemistry of MMA (*mm*/*mr*/*rr* = 3/22/75) [26,27]. Syndiospecifity increased due to the hydrogen-bonding interaction between the alcohol and monomers or growing species. A recent study on this subject has

illustrated the effect of solvent on stereoregularity of MMA by the aid of quantum chemical tools [28].

1.4. Computational Approach to Free Radical Polymerization

The accurate measurement of the rate and equilibrium constants of the free-radical polymerization processes is crucial for the development of suitable kinetic models. On the other hand computational quantum chemistry offers an attractive strategy for modeling free radical polymerization processes including the calculation of the rate and equilibrium constants of any individual chemical reaction.

In the last fifteen years, quantum chemical methods have been proven to yield accurate and useful kinetic tools in the field of free radical polymerization. These methods can provide reliable qualitative or semi-quantitative information on the nature of the transition state and/or on the effects of the substituents on the kinetic and thermodynamics of key reactions. Computational studies have also played a major role in establishing the importance of the penultimate unit effect in free radical copolymerization [29-34], in clarifying the origin of defect structures in vinyl chloride polymerization [35-37]. These methods have contributed greatly to our understanding of the mechanism and structure-reactivity trends in both conventional and controlled free radical polymerization [29-53]. Computational chemistry has been used with success in understanding the controlled radical polymerization processes such as atom transfer radical polymerization (ATRP) [54-59], nitroxide mediated polymerization (NMP) [60-64], reversible addition fragmentation chain transfer (RAFT) polymerization [65-74], thioketone mediated polymerization (TKMP) [75,76] and cobalt-mediated polymerization (CMP) [77]. These experiences in field of the modeling of FRP reactions kinetics individually provide an implementation of improved kinetic models for use in optimization and process control, and the rational design of improved reagents. For example, fluorodithioformates [78,79] which are multipurpose RAFT agents that control radical polymerization were designed by usage of quantum chemical tools. They have subsequently been synthesized and shown to control radical polymerization [80,81]. Recently it has also been shown that ‘chemical accurate’ values of the propagation rate constant can be obtained for vinyl chloride and acrylonitrile polymerization [48-53] by the aid of high-level ab initio molecular calculations.

Overall highly accurate methods are computationally very intensive, with their computational cost scaling rapidly with the size of the system. For example, modeling more than the oligomeric size of species of acrylates or methacrylates would only be feasible with lower-cost computational procedures. On the other hand, low-level quantum-chemical methods should be used with care since oversimplified chemical models may lead to large errors in the resulting kinetic data.

1.5. References

1. Moad, G. and D. H. Solomon, *The Chemistry of Free Radical Polymerization*, Pergamon, Oxford, 1995.
2. Matyjaszewski, K. and S. G. Gaynor, in *Applied Polymer Science*, C. D. Craver and C. E. Carraher, Jr., Pergamon Press, Oxford, 2000, p. 929.
3. Szwarc, M., *Carbonions, Living Polymers and Electron Transfer Process*, Interscience: New York, 1968.
4. Hsieh, H. L. and R. P. Quirk, *Anionic Polymerization, Principles and Practical Applications*. Marcel Dekker, New York, 1996.
5. Matyjaszewski, K. ed., *Cationic Polymerizations: Mechanisms, Synthesis and Applications*. Marcel Dekker, New York, 1996.
6. Moad, G. Moad and D. H. Solomon, *The Chemistry of Free Radical Polymerization*, Pergamon, Oxford, 1995.
7. Atkins, P. and J. De Paula, *Atkins' Physical Chemistry*, 8th ed.; Oxford University Press, New York, 2006.
8. Beuermann, S. and M. Buback, "Rate Coefficients of Free Radical Polymerization Deduced from Pulsed Laser Experiments", *Prog. Polym. Sci.*, 27, 191-254, 2002.

9. Fernández-Garcia, M., M. Fernández-Sanz and E. L. Madruga, "A Kinetic Study of Butyl Acrylate Free Radical Polymerization in Benzene Solution", *Macromol. Chem. Phys.*, 201, 1840-1845, 2000.

10. Odian, G. *Principles of Polymerization*; Wiley-Interscience, New York,1991.

11. Moad, G.; Solomon, D. H.; Spurling, T. H.; Johns, S. R.; Willing, R. I. "Tacticity of Poly(Methyl Methacrylate) - Evidence for A Penultimate Group Effect in Free-Radical Polymerization" *Aust. J. Chem.* **1986**, *39*, 43.

12. Pino, P.; Suter, U. W. "Some Aspects of Stereoregulation in the Stereospecific Polymerization of Vinyl Monomers" *Polymer* **1976**, *17*, 977.

13. Bovey, F. A.; Hood, F. P.; Anderson, E. W.; Kornegay, R. L. *J. Phys. Chem.* **1967**, *71*, 312.

14. Minagawa, M.; Miyano, K.; Takahashi, M.; Yoshii, F. "Infrared Characteristic Absorption Bands of Highly Isotactic Poly(Acrylonitrile)" *Macromolecules* **1988**, *21*, 2387.

15. Mijangos, C.; Martinez, G.; Millen, J. L. "Dependence of Glass-Transition Temperature T_g on Tacticity of Poly(Viny1 Chloride). A Preliminary Study by Differential Scanning Calorimetry" *Makromol Chem.* **1988**, *189*, 567.

16. Matsuzaki, K.; Uryu, T.; Ishida, A.; Ohki, T.; Takeuchi, M. "Stereoregularity of Poly(methyl Acrylate)" *J. Polym. Sci.: Part A-1* **1967**, *5*, 2167.

17. Matsuzaki, K.; Uryu, T.; Ishida, A.; Takeuchi, M. *J. Polym. Sci.: Part C* **1967**, *16*, 2099.

18. Nishino, J.; Nakata, H.; Sakaguchi, Y. "Stereoregularities of Ring-Containing Polymethacrylates Obtained by Radical Polymerization" *Polym. J.* **1971**, *5*, 555.

19. Boudevska, H.; Popminchev, V. "Polymerization of Methacrylates Containing Aromatic Nuclei With Different Electron Donating Capacity" *Makromol. Chem.* **1971**, *143*, 19.

20. Kamachi, M.; Satoh, J.; Liaw, D. J.; Nazakura, S.-I. "Solvent Effects on Radical Polymerization of Vinyl Benzoate and Phenyl Methacrylate" *Macromolecules* **1977**, *10*, 501.

21. Boudevska, H.; Brutchkov, C. "The Influence of Intermolecular Interactions on the Polymerization, 3 Radical Polymerization of 1-Naphthyl Methacrylate and 2-Naphthyl Methacrylate in Acetone and Acetonitrile" *Makromol. Chem.* **1979**, *180*, 1661.

22. Nishino, J.; Nakata, H.; Sakaguchi, Y. *Polym. J.* **1971**, *5*, 555.

23. Boudevska, H.; Popminchev, V. "Polymerization of Methacrylates Containing Aromatic Nuclei With Different Electron Donating Capacity" *Makromol. Chem.* **1971**, *143*, 19.

24. Kamachi, M.; Satoh, J.; Liaw, D. J.; Nazakura, S.-I. *Macromolecules* **1977**, *10*, 501.

25. Boudevska, H.; Brutchkov, C. *Makromol. Chem.* **1979**, *180*, 1661.

26. Isobe, Y.; Yamada, K.; Nakano, T.; Okamoto, Y. *Macromolecules* **1999**, *32*, 5979–5981.

27. Isobe, Y.; Yamada, K.; Nakano, T.; Okamoto, Y. *J. Polym. Sci., Part A: Polym. Chem.* **2000**, *38*, 4693–4703.

28. Değirmenci, İ.; Eren, Ş.; Aviyente, V.; De Sterck, B.; Hemelsoet, K.; Van Speybroeck, V.; Waroquier, M.; *Macromolecules*, **2010**, *43*, 5602–5610.

29. J. P. A. Heuts, Sudarko, R. G. Gilbert, Macromol. Symp. 1996, 111, 147.

30. J. P. A. Heuts, R. G. Gilbert, I. A. Maxwell, Macromolecules 1997, 30, 726.

31. M. L. Coote, T. P. Davis, L. Radom, THEOCHEM 1999, 461–462, 91.

32. M. L. Coote, T. P. Davis, L. Radom, Macromolecules 1999, 32, 5270.

33. M. L. Coote, T. P. Davis, L. Radom, Macromolecules 1999, 32, 2935.

34. P. Cieplak, A. Kaim, J. Polym. Sci., A 2004, 42, 1557.

35. J. Purmova, K. F. D. Pauwels, W. van Zoelen, E. J. Vorenkamp, A. J. Schouten, M. L. Coote, Macromolecules 2005, 38, 6352.

36. K. Van Cauter, B. J. Van Den Bossche, V. Van Speybroeck, M. Waroquier, Macromolecules 2007, 40, 1321.

37. J. Purmova´, K. F. D. Pauwels, M. Agostini, M. Bruinsma, E. J. Vorenkamp, A. J. Schouten, M. L. Coote, Macromolecules 2008, 41, 5527.

38. G. Leroy, J.-P. Dewispelaere, H. Benkadour, C. Wilante, Macromol. Theory Simul. 1996, 5, 269.

39. J. P. A. Heuts, R. G. Gilbert, L. Radom, J. Phys. Chem. 1996, 100, 18997.

40. D. M. Huang, M. J. Monteiro, R. G. Gilbert, Macromolecules 1998, 31, 5175.

41. J. S.-S. Toh, D. M. Huang, P. A. Lovell, R. G. Gilbert, Polymer 2001, 42, 1915.

42. J. Filley, J. T. Mc Kinnon, D. T. Wu, G. H. Ko, Macromolecules 2002, 35, 3731.

43. C.-G. Zhan, D. A. Dixon, J. Phys. Chem. A 2002, 106, 10311.

44. S. C. Thickett, R. G. Gilbert, Polymer 2004, 45, 6993.

45. K. Van Cauter, K. Hemelsoet, V. Van Speybroeck, M. F. Reyniers, M. Waroquier, Int. J. Quantum Chem. 2004, 102, 454.

46. S. Salman, A. Z. Albayrak, D. Avci, V. Aviyente, J. Polym. Sci., A 2005, 43, 2574.

47. H. Günaydin, S. Salman, N. S. Tüzün, D. Avci, V. Aviyente, Int. J. Quantum Chem. 2005, 103, 176.

48. E. I. Izgorodina, M. L. Coote, Chem. Phys. 2006, 324, 96.

49. K. Van Cauter, V. Van Speybroeck, P. Vansteenkiste, M.-F. Reyniers, M. Waroquier, ChemPhysChem 2006, 7, 131.

50. I. Degirmenci, D. Avci, V. Aviyente, K. Van Cauter, V. Van Speybroeck, M. Waroquier, Macromolecules 2007, 40, 9590.

51. I. Degirmenci, V. Aviyente, V. Van Speybroeck, M. Waroquier, Macromolecules 2009, 42, 3033.

52. Değirmenci, İ.; Eren, Ş.; Aviyente, V.; De Sterck, B.; Hemelsoet, K.; Van Speybroeck, V.; Waroquier, M.; *Macromolecules,* **2010**, *43*, 5602–5610.

53. Furuncuoğlu, T.; Uğur, İ.; Değirmenci, İ.; Aviyente, V. *Macromolecules* **2010**, 43, 1823-1835.

54. M. B. Gillies, K. Matyjaszewski, P.-O. Norrby, T. Pintauer, R. Poli, P. Richard, Macromolecules 2003, 36, 8551.

55. D. A. Singleton, D. T. Nowlan, III, N. Jahed, K. Matyjaszewski, Macromolecules 2003, 36, 8609.

56. K. Matyjaszewski, R. Poli, Macromolecules 2005, 38, 8093.

57. C. Y. Lin, M. L. Coote, A. Petit, P. Richard, R. Poli, K. Matyjaszewski, Macromolecules 2007, 40, 5985.

58. W. Tang, Y. Kwak, W. Braunecker, N. V. Tsarevsky, M. L. Coote, K. Matyjaszewski, J. Am. Chem. Soc. 2008, 130, 10702.

59. C. Y. Lin, M. L. Coote, A. Gennaro, K. Matyjaszewski, J. Am. Chem. Soc. 2008, 130, 12762.

60. P. Marsal, M. Roche, P. Tordo, P. de Sainte Claire, J. Phys. Chem. A 1999, 103, 2899.

61. D. Gigmes, A. Gaudel-Siri, S. R. A. Marque, D. Bertin, P. Tordo, P. Astolfi, L. Greci, C. Rizzoli, Helv. Chim. Acta 2006, 89, 2312.

62. A. Kaim, E. Megiel, J. Polym. Sci., A 2005, 44, 914.

63. A. Kaim, J. Polym. Sci., A 2006, 45, 232.

64. E. Megiel, A. Kaim, J. Polym. Sci., A 2008, 46, 1165.

65. S. C. Farmer, T. E. Patten, J. Polym. Sci., A Polym. Chem. 2002, A40, 555.

66. M. L. Coote, L. Radom, J.Am. Chem. Soc. 2003, 125, 1490.

67. M. L. Coote, L. Radom, Macromolecules 2004, 37, 590.

68. M. L. Coote, Macromolecules 2004, 37, 5023.

69. A. Feldermann, M. L. Coote, M. H. Stenzel, T. P. Davis, C. Barner- Kowollik, J. Am. Chem. Soc. 2004, 126, 15915.

70. M. L. Coote, D. J. Henry, Macromolecules 2005, 38, 1415.

71. M. L. Coote, E. H. Krenske, E. I. Izgorodina, Macromol. Rapid Commun. 2006, 27, 473.

72. E. I. Izgorodina, M. L. Coote, Macromol. Theory Simul. 2006, 15, 394.

73. H. Chaffey-Millar, M. H. Stenzel, T. P. Davis, M. L. Coote, C. Barner-Kowollik, Macromolecules 2006, 39, 6406.

74. L. Nebhani, S. Sinnwell, C. Y. Lin, M. L. Coote, M. H. Stenzel, C. Barner-Kowollik, J. Polym. Sci.,A Chem. 2009, in press (JPOL-A-09-0575).

75. A. Ah Toy, H. Chaffey-Millar, T. P. Davis, M. H. Stenzel, E. I. Izgorodina, M. L. Coote, C. Barner-Kowollik, Chem. Commun. 2006, 835.

76. H. Chaffey-Millar, E. I. Izgorodina, C. Barner- Kowollik, M. L. Coote, J. Chem. Theory Comput. 2006, 2, 1632.

77. A. Debuigne, Y. Champouret, R. Jerome, R. Poli, C. Detrembleur, Chem. Eur. J. 2008, 14, 4046.

78. M. L. Coote, D. J. Henry, Macromolecules 2005, 38, 5774.

79. M. L. Coote, E. I. Izgorodina, G. E. Cavigliasso, M. Roth, M. Busch, C. Barner-Kowollik, Macromolecules 2006, 39, 4585.

80. A. Theis, M. H. Stenzel, T. P. Davis, M. L. Coote, C. Barner- Kowollik, Aust. J. Chem. 2005, 58, 437.

81. C. W. Barner- Kowollik, M. L. Coote, T. P. Davis, M. H. Stenzel, A. Theis, Polymerization agent. 2006 International Patent Number WO2006122344 A1.

82. Nakano, T.; Okamoto, Y. *Chem. Rev.* **2001**, *101*, 4013. Matsumoto, A. In *Handbook of Radical Polymerization*; Matyjaszewski, K., Davis, T. P., Eds.; Wiley: New York, 2002; pp 691-773.

83. Valdebenito, A.; Encinas, M. V. *Polymer* **2005**, *46*, 10658–10662.

2. RESEARCH OBJECTIVES

Because of its advantages such as compatibility, convenience, and applicability, free radical polymerization (FRP) is widely used in industrial fields. Due to the general interest in the field, the kinetics of FRP have been thoroughly investigated experimentally and computationally. In this work, the general aim is to elucidate computationally the structure-reactivity relationship of acrylates and methacrylates in order to rationalize the chain transfer process, the solvent effect on the kinetics of free radical polymerization and the tacticity of the products.

In the Chapter 3, the basic principles of computational approaches used throughout this study are presented. The various methodologies used in this study such as semi-empirical, ab initio, density functional methods and continuum solvation models have been discussed.

In the Chapter 4, the effect of the pendant group size, its polarity, its cyclic character have been presented. Alkyl α-hydroxymethacrylates are used in industry because they can provide hydrophilicity, crosslinking sites and/or functionality for subsequent reactions. The electronic effect of the hydroxymethyl ester group is important in facilitating the polymerization. This effect can even overcome the steric effect of an acrylic t-butyl ester group. In this chapter the effect of an electron withdrawing and an electron donor group have been modeled in order to understand the effect of polar groups on the polymerizability. It is also known that cyclic pendant groups on acrylate monomers accelerate the FRP, thus the effect of a cyclic pendant group on FRP has also been monitored.

In the Chapter 5, the polymerization behavior of the alpha substituted acrylates has been scrutinized. Introduction of a heteroatom into the α-position of acrylates is known to influence the reaction kinetics of a monomer; a heteroatom would withdraw a singlet electron from the propagating radical inductively and stabilize the propagating radicals.

Thus it is important to understand the polymerization behavior of a monomer with a heteroatom at the alpha position. The chain length dependency of the propagation rate constant has been considered during this study. For this purpose the chain length dependency of acylates and methacrylates has been discussed by modeling monomeric, dimeric, trimeric, and tetrameric radical addition to a monomer.

In the Chapter 6, the role of solvent on controlling stereoregularity of a PMMA has been investigated. Stereoregularity affects many important properties of the polymers, such as solubility, crystallinity, melting point, glass transition temperature, and mechanical strength [82]. The development of stereoregulation methods for radical polymerization can contribute to the industrial production of polymers with improved properties. This topic aims to elucidate the effect of the solvent in stereoregulating the radical polymerization by the aid of quantum chemical tools. In this respect, methanol and 1,1,1,3,3,3-hexafluoro-2-(trifluoromethyl)propan-2-ol have been considered by examining their effect on the propagation rate constants for the syndiotactic and isotactic free radical polymerization of MMA.

In the Chapter 7, the role of water as solvent on the propagation kinetics of acrylic acid and methacrylic acid has been covered. Water-soluble polymers have been used widely in industrial applications because of their high technical importance. Kinetic properties of of nonionized MAA and AA are strongly affected inclusion of water as solvent. As an example the propagation rate constant increases by more than 10 order of magnitude in passing from the bulk system to a highly dilute system.

In the Chapter 8, the role of chain transfer agents in free radical polymerization kinetics has been investigated. The molecular weight control of polymers is a subject of increasing interest since many of their properties such as physical and mechanical properties depend on the chain length [83]. In this chapter, quantum mechanical calculations have been used to model and understand the role of chain transfer agents in the free radical polymerization of ethylene.

The general conclusions of the computational work conducted in this thesis on free radical polymerization is taken up in 9.

3. COMPUTATIONAL DETAILS

3.1. Quantum Mechanics

The solution of Schrödinger equation and its evaluations are the starting point for discussion of quantum mechanics. Unfortunately, the Schrödinger equation can be solved exactly for only a few problems, such as the particle in a box, the harmonic oscillator, the particle on a ring, the particle on a sphere and the hydrogen atom. Therefore, no exact solutions can be found for systems that involve three (or more) interacting particles. An approximate solution to the Schrödinger equation can be done by all electronic structure methods for many electron atoms and molecules.

The linear combination of atomic orbitals (the LCAO approach) is well known quantum mechanical calculations which is performed on molecules each molecular spin orbital [1]. The molecular orbital calculation simply involves finding the combination of the atomic orbitals that have the proper symmetries and that give the lowest electronic energy.

All ab initio quantum chemistry methods are based on Hartree-Fock (HF) method for modeling molecules. The Hartree-Fock method uses an iterative, fixed–point type algorithm in order to solve equations. Therefore, this method is also called the self-consistent field (SCF) method. That is, the orbitals are improved from cycle to cycle until the electronic energy reaches a constant minimum value and the orbitals no longer change.

Within the HF method, the antisymmetric *N*-body wavefunction is approximated by a single Slater determinant of *N*-spin orbitals. However, this approximation does not take into account Coulomb correlation, leading to a total electronic energy higher than the exact solution of the non-relativistic Schrödinger equation within the Born-Oppenheimer approximation. That is, the molecular orbitals of the HF method are optimized by

evaluating the energy of an electron in each molecular orbital moving in the mean field of all other electrons, rather than including the instantaneous repulsion between electrons.

However, the probability of finding an electron at a certain position in space depends on the position of the other electron. The motions of the electrons are correlated giving rise to a lower energy than HF formalism would suggest. Post-Hartree-Fock (post-HF) methods are developed to improve the electron correlation on the HF method where electron repulsions are only averaged. There are a number of ways in which the electron correlation effects can be incorporated into ab initio molecular orbital calculations. Moller-Plesset perturbation theory, configuration interaction and coupled cluster methods are among the most popular ones. Unfortunately, the added accuracy of the post-HF methods comes with the price of added computational cost.

An alternative approach to the electronic structure of atoms and molecules is density functional theory (DFT). DFT has enjoyed a growing interest due to its reduced computational cost for increased accuracy. DFT is based on the fact that there is a relationship between the total electronic energy and the overall electronic density. Therefore, DFT calculates the overall electronic density distribution, which is a function of only three variables, instead of the complicated many-body wavefunction that depends on three spacial variables for each of the N electrons. A key feature of the density functional theory is the way in which correlation effects are incorporated from the beginning by the term which is known as exchange-correlation potential. The major problem is that the exact functional for exchange and correlation are not known but approximations permit quite accurate calculations. Alterations to the functional or the inclusion of additive terms aim to improve the accuracy of the method and constitute a current research topic.

Semi-empirical methods are based on HF formalism but involve many approximations and some parameters from experimental data. The electron correlation effects are partially taken into account by the use of empirical parameters. They are especially valuable for treating large molecules where higher level of theories bring unaffordable computational cost.

In brief, all ab initio, DFT and semi-empirical calculations treat the linear combination of atomic orbitals (expressed by Gaussian functions) using iterative computations, which establish a self-consistent electric field and minimize the energy of the system. In ab initio and DFT calculations, electron-electron repulsion is specifically taken into account, while the semi-empirical method appears to be an intermediate cost effective approach.

3.2 Ab initio Methods

Ab initio methods are based on quantum mechanics calculations that solve the molecular Schrödinger equation associated with the molecular Hamiltonian. It is very difficult to find an analytical solution to the Schrödinger equation because of the electron-electron interaction terms. Therefore, a particular approximation is rigorously defined on first principles − the quantum theory − and the equation is then solved by numerical iterative methods within an error margin that is defined beforehand. Available computational techniques provide very detailed and reliable numerical solutions for the wavefunctions and energies [2,3].

The time-independent Schrödinger equation has the form:

$$\hat{H}\psi = E\psi \tag{3.1}$$

where E is the electronic energy, ψ is the wavefunction describing the system and $\hat{H}$ is the Hamiltonian operator, which involves kinetic and potential energy terms.

Because of the correlated motions of particles, to express accurate wave functions for many-particle systems are extremely difficult. The mass of the nuclei is much higher than the mass of the electron. For practicle purposes, electronic relaxation with respect to the nuclear motion is instantaneous. The nuclei of molecular systems are moving much more slowly than electrons. In order to simplify the problem somewhat, Born-Oppenheimer approximation is used. According to this approximation, motions of the nuclei and the electron are decoupled. As a result the total wavefunction for the molecule can be formed:

$$\Psi_{\text{tot}}(\text{nuclei}, \text{electrons}) = \Psi(\text{electrons})\Psi(\text{nuclei}) \tag{3.2}$$

The total energy then equals the sum of the nuclear energy and the electronic energy. As the nuclei are considered as fixed, the nuclear energy includes only the electrostatic repulsion between the positively charged nuclei:

$$\sum_{A=1}^{M} \sum_{B=A+1}^{M} \frac{Z_A Z_B}{R_{AB}} \tag{3.3}$$

On the other hand, the electronic energy comprises the kinetic and potential energy of the electrons moving in the electrostatic field of the nuclei together with the electron-electron repulsion and it can be approximated by solving the Schrödinger equation associated with the electronic Hamiltonian operator.

The electronic Hamiltonian operator in atomic units is:

$$\widehat{H} = -\frac{1}{2}\sum_{i=1}^{N} \nabla_i^2 - \sum_{i=1}^{N}\sum_{A=1}^{M} \frac{Z_A}{r_{iA}} + \sum_{i=1}^{N}\sum_{j=i+1}^{N} \frac{1}{r_{ij}} \tag{3.4}$$

where the first term is the kinetic energy operator, the second term is the operator for the attraction between the electrons and the nuclei, and finally the third term is the interelectonic repulsion operator for an *N* electron *M* nuclei system.

Ψ can be approximated as an antisymmetrized product of *N* orthonormal spin orbitals χ_1, χ_1,…, χ_N with a Slater determinant, where each spin orbital is the product of a spatial function and a spin function. The expectation value of the energy can be determined by calculating the following integral:

$$E = \frac{\int \Psi^* \widehat{H} \Psi d\tau}{\int \Psi^* \Psi d\tau} \tag{3.5}$$

It is possible to write the energy expression in a concise form that distinguishes the three types of interaction that contribute to the total electronic energy of the system. The first contribution is from the kinetic and potential energy of each electron moving in the field of nuclei. The energy associated with this contribution for the molecular orbital χ_i:

$$H_{ii}^{core} = \int \chi_i(1)\left(-\frac{1}{2}\nabla_i^2 - \sum_{A=1}^{M}\frac{Z_A}{r_{iA}}\right)\chi_i(1)\,d\tau_1 \tag{3.5}$$

For *N* electrons in *N* molecular orbitals this contribution to the total energy is:

$$E_{\text{total}}^{\text{core}} = \sum_{i=1}^{N}\int \chi_i(1)\left(-\frac{1}{2}\nabla_i^2 - \sum_{A=1}^{M}\frac{Z_A}{r_{iA}}\right)\chi_i(1)\,d\tau_1 = \sum_{i=1}^{N} H_{ii}^{\text{core}} \tag{3.6}$$

The second contribution to the energy is due to the electrostatic repulsion between electron pairs and is calculated from the integrals:

$$J_{ij} = \iint \chi_i(1)\chi_j(2)\left(\frac{1}{r_{12}}\right)\chi_i(1)\chi_j(2)\,d\tau_1 d\tau_2 \tag{3.7}$$

The total electrostatic interaction between the electron in orbital χ_i and the other *N*-1 electrons is a sum of all such integrals, where the summation index *j* runs from 1 to *N*, excluding *i*:

$$\begin{aligned} E_i^{\text{Coulomb}} &= \sum_{j\neq i}^{N}\iint \chi_i(1)\chi_j(2)\left(\frac{1}{r_{12}}\right)\chi_i(1)\chi_j(2)\,d\tau_1 d\tau_2 \\ &\equiv \sum_{j\neq i}^{N}\iint \chi_i(1)\chi_i(1)\left(\frac{1}{r_{12}}\right)\chi_j(2)\chi_j(2)\,d\tau_1 d\tau_2 \end{aligned} \tag{3.8}$$

The total contribution to the electronic energy of the system is obtained as a double summation over all electrons, taking care to count each interaction only once:

$$E_{\text{total}}^{\text{Coulomb}} = \sum_{i=1}^{N}\sum_{j=i+1}^{N}\iint \chi_i(1)\chi_j(2)\left(\frac{1}{r_{12}}\right)\chi_i(1)\chi_j(2)\,d\tau_1 d\tau_2$$

$$= \sum_{i=1}^{N}\sum_{j=i+1}^{N} J_{ij} \qquad (3.9)$$

The third contribution to the energy is known as exchange 'interaction', although this has no classical counterpart. It arises as a result of the correlation of the motions of electrons with parallel spins. Electrons of the same spin tend to 'avoid' each other, so they experience a lower Coulombic repulsion leading to a more favorable energy. The exchange interaction involves integrals of the form:

$$K_{ij} = \iint \chi_i(1)\chi_j(2)\left(\frac{1}{r_{12}}\right)\chi_j(1)\chi_i(2)\,d\tau_1 d\tau_2 \qquad (3.10)$$

The exchange energy between the electron in spin orbital χ_i and the other N-1 electrons is:

$$E_i^{\text{exchange}} = \sum_{j\neq i}^{N}\iint \chi_i(1)\chi_j(2)\left(\frac{1}{r_{12}}\right)\chi_j(1)\chi_i(2)\,d\tau_1 d\tau_2 \qquad (3.11)$$

The total exchange energy is given by:

$$E_{\text{total}}^{\text{exchange}} = \sum_{i=1}^{N}\sum_{j=i+1}^{N}\iint \chi_i(1)\chi_j(2)\left(\frac{1}{r_{12}}\right)\chi_j(1)\chi_i(2)\,d\tau_1 d\tau_2$$

$$= \sum_{i=1}^{N}\sum_{j=i+1}^{N} K_{ij} \qquad (3.12)$$

The ground state energy (called HF energy at this level of approximation) in a closed-shell system containing N electrons and N/2 orbitals can be expressed by:

(3.13)

$$E = 2\sum_{i=1}^{N/2} H_{ii}^{\text{core}} + \sum_{i=1}^{N/2}\sum_{j=1}^{N/2}\left(2J_{ij} - K_{ij}\right)$$

Finally, the variational theorem provides us with a mechanism to the find the best solution to the problem, since there is no 'correct' solution for many-body systems. The theorem states that energy calculated from an approximation to the exact wavefunction will always be higher than the true energy. This means the better the wavefunction, the lower the energy. The 'best' wavefunction is thus obtained when the energy is minimum. This is where the first derivative of energy, δE, will be zero.

The fock operator, $\hat{f}_i\,(1)$, is an effective one electron Hamiltonian for the electron in a polyelectronic system and has the following form:

$$\hat{f}_i\,(1) = \widehat{H}^{\text{core}}(1) + \left\{\sum_{j=1}^{N} \hat{J}_j(1) - \widehat{K}_j(1)\right\} \tag{3.14}$$

where three operators that represent the contributions to the energy of the spin orbital χ_i are introduced. These are the core Hamiltonian operator, $\widehat{H}^{\text{core}}(1)$:

$$\widehat{H}^{\text{core}}(1) = -\frac{1}{2}\nabla_1^2 - \sum_{A=1}^{M}\frac{Z_A}{r_{1A}} \tag{3.15}$$

the Coulomb operator, $\hat{J}_j(1)$:

$$\hat{J}_j(1) = \int \chi_j(2)\left(\frac{1}{r_{12}}\right)\chi_j(2)\,d\tau_2 \tag{3.16}$$

and the exchange operator, $\widehat{K}_j(1)$:

$$\widehat{K}_j(1) = \int \chi_j(2)\left(\frac{1}{r_{12}}\right)\chi_i(2)\,d\tau_2 \tag{3.17}$$

The Hartree-Fock equations then take the standard eigenvalue form:

$$\hat{f}_i \chi_i = \varepsilon_i \chi_i \tag{3.18}$$

The Hartree-Fock equation, however, is based on an assumption that each electron moves in a 'fixed' field of the nuclei and the other electrons. Therefore, any solution for one electron will have an effect on the solutions for the other electrons. Moreover, spin functions which have to be the solutions of the equation already appear in the coulomb and exchange operators. The general strategy to solve these equations is self-consistent field approach. An initial set of trial solutions χ_i are used to calculate the Coulomb and exchange operators. Solving the HF equations give a second set of solutions, χ_i, which are used in the next iteration. The SCF method thus gradually refines the individual electronic solutions that correspond to lower and lower total energies. The solutions are said to be self-consistent at the point where the results for all electrons remain unchanged.

Hartree-Fock theory is very helpful for providing initial, first-level predictions for many systems. It performs reasonably well for computing the structures and vibrational frequencies of stable molecules and some transition states. However, the Hartree-Fock method does not take into account the electron correlation resulting from the instantaneous repulsions between electrons. So it is not suitable for the accurate modeling of the energetics of reactions and bond dissociation.

Since electrons are correlated, the probability of finding an electron at a certain position depends on the position of other electrons. This requires that the instantaneous electron correlation should be included into the wavefunction. Methods that include electron correlation such as configuration interaction (CI), coupled cluster (CC) and perturbation theory are called post-Hartree-Fock methods [4].

Confuguration interaction method uses a variational wavefunction that is a linear combination of configuration state functions built from spin orbitals [5]. Coupled cluster theory is one of the elegant techniques for estimating the electron correlation [6]. Coupled cluster calculations start from the HF molecular orbital method, then a linear combination

of excited Slater determinants are produced by acting an excitation operator on the Slater determinant constructed from HF molecular orbitals.

The Møller-Plesset perturbation theory (MP) treats the effect of electronic interactions as a perturbation to a system consisting of non-interacting electrons [7]. The first order perturbation introduces the interaction between the electrons in the ground state and is equal to the Hartree-Fock theory. The second order perturbation (MP2) takes into account the interaction of the doubly excited configurations with the ground state configuration. The third order perturbation (MP3) adds the contribution of doubly excited configurations interacting with each other. The fourth order perturbation (MP4) brings in interactions involving single, double and quadruple excitations.

There are other correlated methods [5], such as multiconfiguration SCF (MCSCF) and multi-reference configuration interaction (MRCI). Although they use a single determinant as reference, they employ similar perturbation or configuration interaction methods to improve the description of electron correlation.

Despite the high accuracy of post-HF methods, they are very expensive methods to treat the correlation energy.

3.3. Semi-empirical Methods

Semi-empirical methods are characterized by their use of parameters derived from experimental data in order to simplify the approximation to the Schrödinger equation. As such, they are relatively inexpensive and can be practically applied to very, very large molecules. The semi-empirical quantum-mechanical methods developed by Dewar and coworkers [8-17] have been successful at reproducing molecular energies, replicating molecular structures and interpreting chemical reactions [18,19].

To overcome some of the computational difficulties, approximations are made in which several of the integrals involving core orbitals are replaced by parameters. The number of two-electron integrals calculated is reduced, by simply ignoring them or

calculating them in an approximate fashion. Three levels of approximation have been defined by Pople and Beveridge, in which certain two-electron integrals are neglected [20].

The first is known as the complete neglect of differential overlap (CNDO) [21,22]. It assumes the atomic orbitals to be spherically symmetrical when evaluating electron repulsion integrals. The directionality of p-orbitals was included only via the one-electron resonance integrals, the size of which depends on the orientations and distances of the orbitals and on a constant assigned to each type of bond.

The second, known as intermediate neglect of differential overlap (INDO), contains all terms that CNDO contains and includes all one-center two-electron integrals [23]. The third is known as neglect of diatomic differential overlap (NDDO) in which all two-electron two-center integrals involving charge clouds arising from pairs of orbitals on an atom were retained.

In 1975, Dewar and coworkers published the MINDO/3 method, which is a modified version of the INDO method [8-11]. MINDO/3 uses a set of parameters in approximation. These parameters, along with the constants used to evaluate the resonance integrals, allow the results to be fitted as closely as possible to experimental data.

The first practical NDDO method was introduced by Dewar and Thiel in 1977 [12-14] called modified neglect of diatomic overlap (MNDO), the model was parameterized on experimental molecular geometries, heats of formation, dipole moments and ionization potentials. The orbital exponents and the core integral were again treated as empirical parameters to be determined in the fitting procedure.

The inability of MNDO has lead to a reexamination of the model, leading to the Austin Model 1 (AM1) [15]. In this model a term was added to MNDO to correct for the excessive repulsions at van der Waals distances. For this purpose, each atom was assigned a number of spherical gaussians, which were intended to mimic long-range correlation effects.

The third parameterization of MNDO is the Parametric Method Number 3 (PM3) [16,17], AMl being the second. In PM3, the parameters were optimized using a large set of reference molecular data. This allowed 12 elements to be optimized simultaneously [24]. The PM3 method has been used in this study for conformational search.

Semi-empirical and ab initio methods differ in the trade-off made between computational cost and accuracy of the result. Semi-empirical calculations are relatively inexpensive. They provide reasonable qualitative descriptions of molecular systems and fairly accurate quantitative prediction of energies and structures for systems where good parameter sets exist. Semi-empirical methods may only be used for systems where parameters have been developed for all of their component atoms. In addition to this, semiempirical models have a number of well-known limitations. Types of problems on which they do not perform well include hydrogen bonding, transition structures, and molecules containing atoms for which they are poorly parameterized.

3.4. Density Functional Theory

Density functional theory (DFT) is based on the Hohenberg-Kohn proposed in 1964 [25,26] and is an alternative many-body technique to solve the electronic many-body problem. The basic quantity is not yet the wavefunction but the one-electron density $\rho(\mathbf{r})$. The first theorem states that the electron density $\rho(\mathbf{r})$ determines the external potential $V_{\text{ext}}(\mathbf{r})$, i.e. the potential due to the nuclei. The second theorem introduces the variational principle. Hence, the electron density can be computed variationally and from this quantity all other properties of the molecular system can be deduced such as the position of the nuclei, the energy, the wave function and other related parameters.

The electron density is defined as:

$$\rho(x) = N \int \cdots \int |\Psi(x_1, x_2, \cdots, x_n)|^2 dx_1 dx_2 \cdots dx_n \tag{3.19}$$

where *x* represents both spin and spatial coordinates of electrons.

The electronic energy can be expressed as a functional of the electron density:

$$E[\rho(\mathbf{r})] = \int V_{\text{ext}}(\mathbf{r})\rho(\mathbf{r})d\mathbf{r} + T[\rho(\mathbf{r})] + V_{\text{ee}}[\rho(\mathbf{r})] \tag{3.20}$$

The first term arises from the interaction of the electrons with an external potential $V_{\text{ext}}(\mathbf{r})$, typically due to the Coulomb interaction with the nuclei. $T[\rho(\mathbf{r})]$ is the kinetic energy of the interacting electrons and $V_{\text{ee}}[\rho(\mathbf{r})]$ is the interelectronic interaction energy.

For practical purposes DFT always uses the Kohn-Sham scheme to effectively find the solutions of the electron density. In this scheme the connection is made with a non-interacting many-body problem which is fully characterized by one-particle orbitals. The latter are referred as Kohn-Sham orbitals. The main advantage of introducing such orbitals is that within an interacting many-body problem exact forms are know for some energy terms such as the kinetic energy. Of course these energy terms do not correspond to their counterparts in the interacting system. Making use of this non-interacting system, the electronic energy may be rewritten as:

$$E[\rho(\mathbf{r})] = \int V_{\text{ext}}(\mathbf{r})\rho(\mathbf{r})d\mathbf{r} + T_s[\rho(\mathbf{r})] + J[\rho(\mathbf{r})] + E_{\text{XC}}[\rho(\mathbf{r})] \tag{3.21}$$

where $J[\rho(\mathbf{r})]$ is the electron-electron Coulomb energy, which is also known as the Hartree electrostatic energy:

$$J[\rho(\mathbf{r})] = \frac{1}{2}\iint \frac{\rho(\mathbf{r}_1)\rho(\mathbf{r}_2)}{|r_1 - r_2|} d\mathbf{r}_1 d\mathbf{r}_2 \tag{3.22}$$

$T_s[\rho(\mathbf{r})]$ is the kinetic energy of the non-interacting electrons:

$$T_s[\rho(\mathbf{r})] = \sum_{i=1}^{N} \int \psi_i(\mathbf{r}) \left(-\frac{\nabla^2}{2}\right) \psi_i(\mathbf{r}) d\mathbf{r} \tag{3.23}$$

and $E_{\text{XC}}[\rho(\mathbf{r})]$ contains contributions from exchange and correlation.

The full expression for the energy of an *N*-electron system within the Kohn-Sham scheme is:

$$E[\rho(\mathbf{r})] = -\sum_{A=1}^{M}\int \frac{Z_A}{|\mathbf{r}-\mathbf{R}_A|}\rho(\mathbf{r})d\mathbf{r} + \sum_{i=1}^{N}\int \psi_i(\mathbf{r})\left(-\frac{\nabla^2}{2}\right)\psi_i(\mathbf{r})d\mathbf{r} + \frac{1}{2}\iint \frac{\rho(\mathbf{r}_1)\rho(\mathbf{r}_2)}{|r_1-r_2|}d\mathbf{r}_1 d\mathbf{r}_2 + E_{\mathrm{XC}}[\rho(\mathbf{r})] \tag{3.24}$$

Equation (3.25) acts to define the exchange-correlation energy functional, $E_{\mathrm{XC}}[\rho(\mathbf{r})]$, which can be expressed as the sum of an exchange functional $E_{\mathrm{X}}[\rho(\mathbf{r})]$ and a correlation functional $E_{\mathrm{C}}[\rho(\mathbf{r})]$, although it contains also a contribution due to the difference between the true kinetic energy of the system and $T_s[\rho(\mathbf{r})]$.

In the Kohn-Sham density functional theory, a reference system of independent non-interacting electrons in a common, one-body potential V_{KS} yielding the same density as the real fully-interacting system is considered. More specifically, a set of independent reference orbitals ψ_i satisfying the following independent particle Schrödinger equation are imagined:

$$\left[-\frac{1}{2}\nabla^2 + V_{\mathrm{KS}}\right]\psi_i = \varepsilon_i\psi_i \tag{3.25}$$

with the one-body potential V_{KS} defined as:

$$V_{\mathrm{KS}} = V_{\mathrm{ext}}(\mathbf{r}) + \frac{\delta J[\rho(\mathbf{r})]}{\delta\rho(\mathbf{r})} + \frac{\delta E_{\mathrm{XC}}[\rho(\mathbf{r})]}{\delta\rho(\mathbf{r})} \tag{3.26}$$

$$V_{\mathrm{KS}} = -\sum_{A=1}^{M}\frac{Z_A}{r_{1A}} + \frac{1}{2}\iint \frac{\rho(\mathbf{r}_2)}{r_{12}}d\mathbf{r}_2 + V_{\mathrm{XC}}[\mathbf{r}_1] \tag{3.27}$$

where $V_{\mathrm{XC}}[\mathbf{r}]$ is the exchange-correlation potential and is related to exchange-correlation energy by:

$$V_{\mathrm{XC}}[\mathbf{r}] = \frac{\delta E_{\mathrm{XC}}[\rho(\mathbf{r})]}{\delta \rho(\mathbf{r})} \tag{3.28}$$

The independent orbitals ψ_i are known as Kohn-Sham orbitals and give the exact density by:

$$\rho(\mathbf{r}) = \sum_{i}^{N} |\psi_i|^2 \tag{3.29}$$

If the exact form of the exchange-correlation functional is known, DFT would be an exact many-body technique. Unfortunately the exact form of this functional is not known and approximate forms need to be proposed. Today there are a wealth of functionals available which have varying accuracy depending on the properties one is interested in and depending on the specific nature of the molecular system that is treated. Excellent reviews are available in a variety of textbooks [72]. In general functional can be categorized into following classes : (i) Local Density Based Functionals (ii) Gradient Corrected functional (GGA) (iii) Hybrid Functionals and (iv) Meta-hybrid functionals. In each of the chapter including the applications, the specific functionals that were used are properly introduced.

3.5. LCAO approximation and Basis Sets

In all of the above methods i.e. Hartree-Fock based methods, post-Hartree-Fock based methods, semi-empirical methods and Density Functional Theory methods, the wavefunction is at first instance approximated as a Slaterdeterminat which is made up of one-electron orbitals. In practice these one-electron orbitals or **molecular orbitals** are constructed as linear combinations of atomic orbitals. This approach is referred as the **LCAO** approach. These molecular orbitals are constructed in order to fulfill to correct molecular symmetry and to give also the lowest electronic energy [1]. In addition the atomic orbitals are expressed in terms of basis functions, which are mathematical description of the orbitals. In practice the molecular orbitals are thus expressed in terms of a set of basis functions. Larger basis sets more accurately approximate the orbitals by imposing fewer restrictions on the locations of the electrons in space.

In 1951, Roothaan proposed the Hartree-Fock orbitals as linear combinations of a complete set of known functions, called basis functions. There are two types of set of basis functions for atomic Hartree-Fock calculations, Slater-type functions and Gaussian-type functions.

In the simplest Hartree-Fock model, the number of basis functions on each atom is as small as possible that is only large enough to accommodate all the electrons and still maintain spherical symmetry. As a consequence, the molecular orbitals have only limited flexibility. If larger basis sets are used, the number of adjustable coefficients in the variational procedure increases, and an improved description of the molecular orbitals is obtained. Very large basis sets will result in nearly complete flexibility. The limit of such an approach termed the Hartree-Fock limit represents the best that can be done with a single electron configuration.

There are numerous different Gaussian basis sets with which SCF calculations can be carried out. The most widely used are those developed by Pople and co-workers. The simplest and lowest basis set is called STO-3G. This means that the Slater-type orbitals are represented by three gaussian functions. It is a minimal basis set which means that it has only as many orbitals as are necessary to accommodate the electrons of the neutral atom.

The next level of basis sets developed by Pople is referred to as the split-valence basis sets. The problem of any minimal basis set is its inability to expand or contract its orbitals to fit the molecular environment. One solution to the problem is to use split valence or double zeta basis sets in which the basis are split into two parts, an inner, compact orbital and an outer, more diffuse one. Thus the size of the atomic orbital that contributes to the molecular orbital can be varied within the limits set by the inner and outer basis functions. Split-valence basis set splits only the valence orbitals in this way, whereas double zeta basis also have split core orbitals.

For greater flexibility the split-valence basis set can be augmented with polarization functions. In polarization basis sets, which are the next level of improvement in basis set, d

orbitals are added to all heavy atoms is designated with a * or (d). Polarization can be added to hydrogen atoms as well, this would be done by **.

Diffuse functions are large-size versions of s- and p-type functions (as opposed to the standard valence-size functions). They allow orbitals to occupy a larger region of space. Basis sets with diffuse functions are important for systems where electrons are relatively far from the nucleus: molecules with lone pairs, anions and other systems with significant negative charge, systems in their excited states, and so on. The 6-31+G (d) basis set is the 6-31G (d) basis set with diffuse functions added to heavy atoms. The double plus version, 6-31++G (d), adds diffuse functions to the hydrogen atoms as well. The 6-31+G* and the 6-31+G** split valence basis sets have been used for gas phase calculations in this study, with the addition of polarization and diffused functions on heavy atoms as well as polarization functions on hydrogens for the 6-31+G**.

3.6. Solvation Models

In recent years, there have been a large number of theoretical studies on solvated systems, for reactivity, structure or properties. As an (over)simplification, we can identify two distinct classes: the so-called explicit solvent models and the continuum models. The main difference is that in the first approach the molecular nature of the solvent molecules is maintained as a discrete number of solvent molecules are explicitely added into the model, whereas in the second a macroscopic (continuous) description is used. The latter models are generally referred to as Polarizable Continuum Models (PCM). An alternative is to choose for a combined model in which a limited number of solvent molecules are treated explicitly while the remainder of the solvent is included by a continuum. These are the so-called implicit/explicit solvent models.

3.7. Continuum Solvation Models

In continuum solvation models [67,68], the solvent is represented as a uniform polarizable medium characterized by its static dielectric constant ϵ. In basic continuum solvation models, the solute is described at a homogenous quantum mechanical (QM) level and the solute-solvent interactions are limited to those of electrostatic terms.

The total solvation free energy may be written as

$$\Delta G_{solvation} = \Delta G_{cavity} + \Delta G_{disportion} + \Delta G_{electrostatic} \tag{3.30}$$

In this representation, ΔG_{cavity} is the energetic cost of creating a cavity in the medium producing a destabilization effect. Dispersion interactions between solvent and solute add stabilization to solvation free energy term expressed as $\Delta G_{dispersion}$. The latter electrostatic term, $\Delta G_{electrostatic}$, has a stabilization effect and furthermore it appears to be responsible for the main structural changes of the solute.

The solute charge distribution within the cavity induces a polarization of the surrounding medium, which in turn induces an electric field within the cavity called the *reaction field*. This field then interacts with solute charges, providing additional stabilization. The effect of the reaction field may be modeled by an appropriately distributed set of induced polarization charges on the surface S of the dielectric. The charge density on the surface of the cavity, $\sigma(\mathbf{r}_s)$, is given by the standard electrostatics in terms of the dielectric constant, ϵ, and the electric field perpendicular to the surface, $F(\mathbf{r}_s)$, generated by the charge distribution within the cavity

$$4\pi\epsilon\sigma(\mathbf{r}_s) = (\epsilon - 1)F(\mathbf{r}_s) \tag{3.31}$$

Once $\sigma(\mathbf{r}_s)$ is determined, the associated potential is added as an extra term to the Hamiltonian operator

$$H = H_0 + V_\sigma \tag{3.32}$$

$$V_\sigma(\mathbf{r}) = \int \frac{\sigma(\mathbf{r}_s)}{|\mathbf{r} - \mathbf{r}_s|} d\mathbf{r}_s \tag{3.33}$$

The potential of the surface charge V_σ is given by the molecular charge distribution but also enters the Hamiltonian and thus influences the molecular wave function, the procedure is therefore iterative.

In the Polarized Continuum solvation Models (PCM), the solute is embedded in a cavity defined by a set of spheres centered on atoms (sometimes only on heavy atoms), having radii defined by the van der Waals radius of the atoms multiplied by a predefined factor (usually 1.2). The cavity surface is then subdivided into small domains (called tesserae), where the polarization charges are placed. Among the many solutions to the electrostatic problem is the Integrated Equation Formalism (IEF) originally formulated by Cancés and Menucci [69-71]. The IEF-PCM method is a recent development in the polarized continuum models and has been utilized for solvent calculations in this study. It is based on the use of operators largely exploited in the theory of integral equations. The concept of cavity and of its tessellation is conserved. The IEF formalism is in fact able to treat a larger class of electrostatic problems.

Apart from the apparent surface charge (ASC) methods, other solutions for calculating the electrostatic solute-solvent interactions in continuum models have been proposed such as, multipole expansion (MPE) methods, generalized Born approximation (GBA), image charge (IMC) methods, finite element methods (FEM) and finite difference methods (FDM).

3.8. References

1. Clark, T., *A Handbook of Computational Chemistry*, John Willey&Sons, Canada, 1985.

2. Hehre, W. J., L. Radom, P. R. Schleyer and J. A. Pople, *Ab Initio Molecular Orbital Theory*, John Willey and Sons, New York, 1986.

3. Lowe, J. P., *Quantum Chemistry*, 2nd Ed., Academic Press, 1993.

4. Wang, L. C. and R. J. Boyd, "The effect of electron correlation on the electron density distributions of molecules: Comparison of perturbation and configuration interaction methods", *J. Chem. Phys.*, Vol. 90, pp. 1083-1091, 1989.

5. Cramer, C. J., *Essentials of Computational Chemistry: Theories and Models*, John Wiley & Sons Ltd., USA, 2004.

6. Cizek, J., "On Correlation Problem in Atomic and Molecular Systems. Calculation of Wavefunction Components in Ursell-Type Expansion Using Quantum-Field Theoretical Methods", *J. Chem. Phys.*, Vol. 45, pp. 4256-4266, 1966.

7. Pople, J. A. and R. Seeger, "Electron Density in Møller-Plesset Theory", *J. Chem. Phys.*, 62, 4566, 1975.

8. Bingham, R. C., M. J. S. Dewar and D. H. Lo, "Ground States of Molecules. XXV. MINDO/3. An Improved Version of MINDO Semi-Empirical SCFMO Method", *J. Am. Chem. Soc.*, Vol. 97, pp. 1285-1293, 1975.

9. Bingham, R. C., M. J. S. Dewar and D. H. Lo, "Ground States of Molecules. XXVI. MINDO/3. Calculations for Hydrocarbons", *J. Am. Chem. Soc.*, Vol. 97, pp. 1294-1301, 1975.

10. Bingham, R. C., M. J. S. Dewar and D. H. Lo, "Ground States of Molecules. XXVII. MINDO/3. Calculations for CHON Species", *J. Am. Chem. Soc.*, Vol. 97, pp. 1302-1306, 1975.

11. Bingham, R. C., M. J. S. Dewar and D. H. Lo, "Ground States of Molecules. XXVIII. MINDO/3. Calculations for Compunds Containing Carbon, Hydrogen, Fluorine and Chlorine", *J. Am. Chem. Soc.*, Vol. 97, pp. 1307-1310, 1975.

12. Dewar, M. J. S. and W. Thiel, "Semiempirical Model for 2-Center Repulsion Integrals in NDDO Approximation", *Theor. Chim. Acta.*, Vol. 46, pp. 89-104, 1977.

13. Dewar, M. J. S. and W. Thiel, "Ground-States of Molecules. 38. MNDO Method – Approximations and Parameters", *J. Am. Chem. Soc.*, Vol. 99, pp. 4899-4907, 1977.

14. Dewar, M. J. S. and W. Thiel, “Ground-States of Molecules. 39. MNDO Results for Molecules Containing Hydrogen, Carbon, Nitrogen, and Oxygen”, *J. Am. Chem. Soc.*, Vol. 99, pp. 4907-4917, 1977.

15. Dewar, M. J. S., Zoebisch, E. G. Healy, E. F. and J. J. P. Stewart, “AM1: A New General Purpose Quantum Mechanical Molecular Model”, *J. Am. Chem. Soc.*, Vol. 107, pp. 3902-3909, 1985.

16. Stewart, J. J. P., “Optimization of parameters for semi-empirical methods. I. Method.”, *J. Comp. Chem.*, Vol. 10, pp. 209-220, 1989.

17. Stewart, J. J. P., “Optimization of Parameters for Semiempirical Methods Applications”, *J. Comp. Chem.*, Vol. 10, pp. 221-264, 1990.

18. Pilar, F. L., *Elementary Quantum Chemistry*, Mc-Graw-Hill, New York, 1990.

19. Hirst, D. M. A., *Computational Approach to Chemistry*, Blackwell Scientific Publications, Oxford, 1990.

20. Pople, J. A. and D. L. Beveridge, *Approximate Molecular Orbital Theory*, Mc-Graw-Hill, New York, 1970.

21. Pople, J. A. and G. A. Segal, “Approximate Self-Consistent Molecular Orbital Theory. II. Calculations with Complete Neglect of Differential Overlap”, *J. Chem. Phys.*, Vol. 43, pp. S136-S149, 1965.

22. Pople, J. A., D. P. Santry and G. A. Segal, “Approximate Self-Consistent Molecular Orbital Theory. I. Invariant Procedures”, *J. Chem. Phys.*, Vol. 43, pp. S129-S135, 1965.

23. Pople, J. A., D. L. Beveridge and P. A. Dobosh, "Approximate Self-Consistent Molecular Orbital Theory. V. Intermediate Neglect of Differential Overlap", *J. Chem. Phys.*, Vol. 47, pp. 2026-2033, 1967.

24. Levine, I. N., *Quantum Chemistry,* Prentice-Hall, New Jersey, 1991.

25. Parr, R. G. and W. Yang, *Density-Functional Theory of Atoms and Molecules*, Oxford University Press, New York, 1989.

26. Handy, N. C., "Density Functional Theory", in: B. O. Roos (ed.), *Lecture Notes in Quantum Chemistry*, Vol. 2, pp. 91-123, Springer-Verlag, Berlin, 1994.

67. Tomasi, J., B. Mennucci and E. Cancès, "The IEF version of the PCM solvation method: an overview of a new method addressed to study molecular solutes at the QM ab initio level", *Mol. Struct. (THEOCHEM)*, Vol. 464, pp. 211-226, 1999.

68. Tomasi, J., M. Benedetta and R. Cammi, "Quantum Mechanical Continuum Solvation Models", *Chem. Rev.*, Vol. 105, pp. 2999-3093, 2005.

69. Cancès, E., B. Mennucci and J. Tomasi, "Evaluation of Solvent Effects in Isotropic and Anisotropic Dielectrics and in Ionic Solutions with a Unified Integral Equation Method: Theoretical Bases, Computational Implementation, and Numerical Applications", *J. Chem. Phys.*, Vol. 107, pp. 3032-3041, 1997.

70. Mennucci, B., E. Cancès and J. Tomasi, "evaluation of solvent effects in isotropic and anisotropic dielectrics andin ionic solutions with a unified integral equation method: theoretical bases, computational implementation, and numerical applications", *J. Phys. Chem. B*, Vol. 101, pp. 10506-10517, 1997.

71. Mennucci, B. and J. Tomasi, "Continuum Solvation Models: A New Approach To The Problem Of Solute's Charge Distribution And Cavity Boundaries", *J. Chem. Phys.*, Vol. 106, pp. 5151-5158, 1997.

72. Wolfram, K.; Holthausen, M. C., “Chemist's Guide to Density Functional Theory” 2th Ed. 2001.

4. DFT STUDY OF FREE-RADICAL POLYMERIZATION OF ACRYLATES AND METHACRYLATES: STRUCTURE-REACTIVITY RELATIONSHIP

4.1. Introduction

Radical polymerization processes are complex since they involve many different reactions [1]. In a simple homopolymerization reaction, initiation, propagation and termination steps occur, and the propagating species may undergo a variety of chain transfer processes. The absolute and relative rates of these individual steps govern the overall rate of polymerization, the molecular weight and the chain architecture. The ability to measure the rates of these individual reactions, and the study of reaction mechanisms are extremely important and instructive as they lead to the development of accurate kinetic models and better methods for controlling the free-radical polymerization. Computational quantum chemistry has become a powerful tool to study directly the individual reactions within a complex process and to extract accurate mechanistic information such as geometries and relative rates of the elementary reactions [2].

Photoinitiated polymerization of acrylates and methacrylates is used for the rapid production of polymeric cross-linked materials with defined properties. It is widely employed in the performance applications where emphasis is put on the mechanical as well as optical properties. These applications are typically dental restorative fillers, fiber-optic coatings, optical adhesives, aspherical lenses for CD applications and contact lenses [3]. In a typical formulation, acrylated multifunctional oligomers and small molecule monofunctional and multifunctional acrylates are used to adjust viscosity, rate of curing and final film properties.

The polymerization rate is directly related to the monomer structure. The relationship between monomer structure and reactivity was investigated extensively in the late 1980s and 1990s by Decker et al. using several model monofunctional acrylates with various pendant groups ranging from cyclic carbonates and oxazolidones to dioxolanes and

oxetanes [4]. Comprehension of the influence of molecular structure on acrylate reactivity has been sought ever since the first publications with acrylates and methacrylates. Decker's report on acrylates with a very high intrinsic reactivity assigned importance to hydrogen bonding as a potential reason for high rates of polymerization R_p.[5] Andrzejewska reported a heteroatom effect in the side chain which led to higher reactivity [6]. Hoyle et al. have investigated the relationship between the photopolymerization rate of hydroxyalkyl acrylates and their structure [7]. The photopolymerization rates of hydroxyalkyl acrylates are higher than those observed for typical monofunctional acrylate monomers and rival those of multifunctional monomers. However, even though the photopolymerization practice is well established, there are still limitations to this process. These limitations include residual unsaturation, oxygen inhibition, polymerization speed, and polymer properties. A typical method to increase the polymerization rate is to utilize monomers with more than one vinyl group. By increasing the monomer functionality, diffusion limitations are encountered earlier in the polymerization, and termination is also hindered earlier. This early reduction in termination leads to stronger autoacceleration and greater polymerization rates. These highly cross-linked materials have increased moduli, they are hard and brittle. However, increasing the cross-linking density leads to the residual unsaturation. The tradeoff between polymerization rate and residual unsaturation is important for the development and selection of monomers for use in polymerization applications. There is a desire to counteract these limitations and develop monomers that polymerize to a higher extent of reaction with greater polymerization rates [8].

The reactivity of a series of acrylates was determined experimentally by Jansen et al. and a relation was found with the degree of hydrogen bonding as well as with the polarity of the monomer [3]. It was suggested that the propagation step of polymerization is influenced by hydrogen bonding while the dipole moment influences the termination rate constant. Lee et al. studied the influence of hydrogen bonding for hydroxyalkyl acrylates specifically because these systems show a behavior that differs from conventional acrylates, a decrease of polymerization rate with increasing temperature has been observed [7]. They presumed that the termination rates are greatly reduced by hydrogen bonding when polymerizing at lower temperatures, leading to an enhanced polymerization rate. In the mid 80's, the radical homopolymerization and copolymerization behavior of methacrylic esters containing heteroatoms at the α-position of alkyl groups have been

investigated to elucidate the effects of structures on reactivity [9].These investigations have revealed that the introduction of a heteroatom into the methyl group increases the reactivity of these monomers due to polar effects. The first such monomer investigated is that containing the hydroxymethyl group at the α-position, ethyl α -hydroxymethacrylate (EHMA) [9c].

Recently, some of the current authors published an ab initio study on the free radical polymerization of acrylates and phosphoacrylates in order to understand the mechanistic behavior of their free radical polymerization reactions [10]. Furthermore the different factors controlling the reactivity of a large series of carbon-centered radicals toward the methyl acrylate monomer were examined computationally by Lalevee et al [11].

In this study, the structure-reactivity relationship of three different classes of acrylates has been investigated on an ab initio basis using Density Functional Theory (DFT) with the aim of elucidating the effect of alkyl, polar and cyclic pendant groups on their polymerizabilities. Elementary steps corresponding to propagation, disproportionation and chain transfer have been studied.

The first class of acrylates aims to investigate the effect of pendant group size on the polymerizability. Mathias et al. have been pursuing the chemistry of α-hydroxymethacrylate (HMA) derivatives for several years [12]. Alkyl α-hydroxymethacrylates (RHMA) derivatives give faster photopolymerization rates than typical methacrylates [13]. In this study, the free radical polymerizability of a series of alkyl α-hydroxymethacrylates (MHMA, EHMA, and TBHMA) is investigated in an attempt to analyze in details the effects exerted by the bulky groups on their polymerizability. Experimentally, it is known that α-substituted methacrylate MHMA polymerizes faster than EHMA, and TBHMA [13,14].

A second class of monomers investigates the effect of polar groups on the polymerizability of acrylates. More specifically the effect of an electron withdrawing (-CN) and an electron donor group (-$N(CH_3)_2$) on the polymerizability of acrylates is studied. It is known experimentally that 2-cyanoethyl acrylate (M-CN) polymerizes 13

times faster than 2-dimethylaminoethyl acrylate (M-N$(CH_3)_2$) and modeling is expected to shed light on this issue [3a].

Finally in the third class, the effect of cyclic pendant groups in acrylates is modeled by comparison of a cyclic ether (2,3-epoxypropyl acrylate) with a straight-chain ether (2-methoxyethyl acrylate) since the former is known to polymerize twice as fast as the latter.

The three classes of acrylates are shown in Figure 4.1.

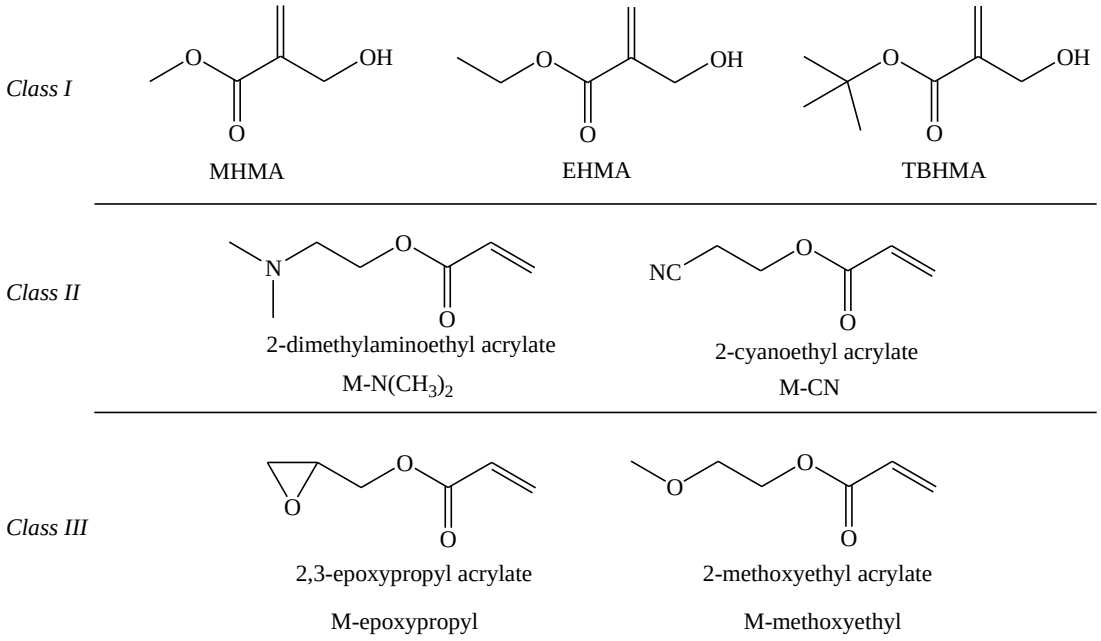

Figure 4.1. Monomers considered in this study

The experimentally determined rates of polymerization (R_p) of the various monomers are summarized in Table 4.1.

Table 4.1. Experimental rates of polymerization (R_p) of the substituted acrylates modeled in this study.

No	**Name**	**R_p (mol $L^{-1}s^{-1}$)**	**T(K)**
M1	Methyl α-hydroxymethacrylate (**MHMA)**	3.70E-02 [12]	303.15
M2	Ethyl α-hydroxymethacrylate (**EHMA)**	3.00E-02 [12]	303.15
M3	t-Butyl α-hydroxymethacrylate (**TBHMA)**	1.60E-02 [12,14]	303.15
M4	2-dimethylaminoethyl acrylate **(M-N(CH_3)$_2$)**	1.04E+00 [3a]	298.15
M5	2-cyanoethyl acrylate (**M-CN)**	13.90E+00 [3a]	298.15
M6	2,3-epoxypropyl acrylate **(M-epoxypropyl)**	4.11E+00 [3a]	298.15
M7	2-methoxyethyl acrylate (**M-methoxyethyl)**	2.67E+00 [3a]	298.15

4.2. Computational Methodology

4.2.1. Reaction mechanism of free radical polymerization

The free-radical polymerization proceeds via a chain mechanism, which basically consists of four elementary reactions i.e. initiation, propagation, chain transfer and

termination [15].

(1) radical generation from non-radical species (initiation)

$I \xrightarrow{k_d} 2R.$

Accordingly, initiators with similar decomposition rates and initiating efficiencies should bring about similar initiation rates irrespective of the monomer.

(2) radical addition to a substituted alkene (propagation)

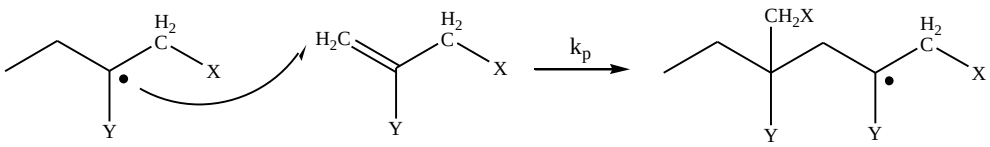

(3) atom transfer (chain transfer) reactions

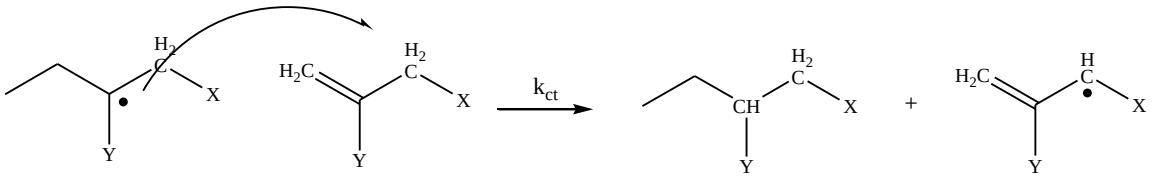

(4) atom abstraction reactions (termination by disproportionation)

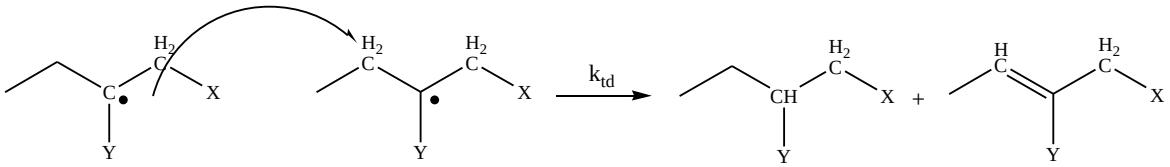

and radical-radical recombination reactions (termination by coupling)

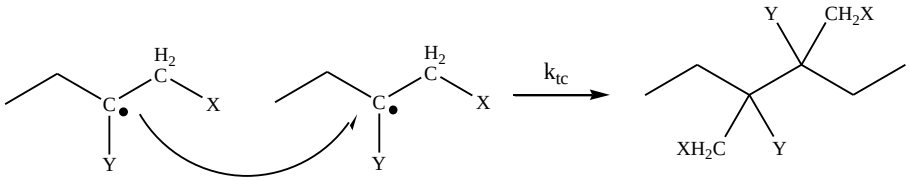

In this study, the radical chain is modeled by a monomer to which a methyl radical is attached as is illustrated in the reaction schemes above.

4.2.2. Reaction kinetics

The reaction rate constants (k_p, k_{ct}, and k_{td}) are calculated by using the conventional Transition State Theory (TST) [16]. Within the Transition State Theory (TST) the rate constant of a bimolecular reaction A+B →C is related to the molecular properties of the reacting specie(s) [17].

$$k(T) = \frac{k_B T}{h} K_C^{\neq}$$

$$K_C^{\neq} = \frac{q_{TS}}{q_A q_B} e^{-\Delta E_0 / k_B T}$$

where k_B represents Boltzmann's constant, T is the temperature, h is the Planck's constant, ΔE_0 represents the molecular energy difference between the activated complex and the reactants (with inclusion of zero point vibrational energies), and q_{TS}, q_A and q_B are the molecular partition functions of the transition state and reactants, respectively. The rate constant is expressed per unit volume, per mol and per unit time. The molecular properties, such as geometries, ground state energies and frequencies that are required for the evaluation of the partition functions, and the reaction barrier are obtained by ab initio molecular calculations. The kinetic parameters are deduced from fitting the results of the TST expression to the Arrhenius rate law in a specific temperature range. In our case the temperature range of experimental relevance is 250-350K. A conformer search analysis has been carried out for all the structures in order to locate the energetically most stable points on the potential energy surface. IRC calculations have been performed to justify the nature of the transition state structures.

The rate of polymerization, R_p, is given by

$$R_p = -\frac{d[M]}{dt} = k_p \left(f \frac{k_d}{k_t} \right)^{0.5} [M][I]^{0.5}$$

where k_p, k_d and k_t are the rate coefficients corresponding to the propagation, initiator decomposition and termination steps. f is the initiator efficiency, [M] and [I] are the concentrations of the monomer and initiator respectively. In this study, the polymerization behavior of monomers whose experimental conditions are more or less similar have been considered. Thus, the parameters related to the initiator- the initiator efficiency f and the rate of the initiator decomposition k_d are taken to be similar under similar experimental conditions.

4.2.3. Computational details

All calculations were carried out with the Gaussian 03 software package [19]. The geometry optimizations are performed at the B3LYP/6-31+G(d) level of theory [20] whereas single point calculations were performed with the new hybrid density functional BMK , which is especially suitable for kinetics and reaction mechanisms [21]. There is a general consensus that B3LYP methods provide excellent low-cost performance for structure optimizations [22]. For energy predictions, however, B3LYP is less accurate and the use of other more advanced functionals with a more reliable performance for reaction energies is desirable. Recent studies have shown that the new hybrid meta-GGA-functional such as BMK (Boese-Martin for kinetics) performs much better with an overall accuracy of maximum 8 kJ/mol for the barrier heights [23]. The combination of a high percentage of Hartree-Fock exchange with terms dependent on the kinetic energy density in the functional is the origin of the surprisingly good performance of BMK. BMK can actually be considered as a reliable general-purpose functional whose domain of applicability has been expanded to cover transition states without losing its accuracy for geometry optimizations. A lot of recent studies confirm these findings [24]. The results are thus obtained with the two-component method BMK/6-311+G(3df,2p)//B3LYP/6-31+G(d). The transition states were verified to have only one imaginary frequency corresponding to the reaction coordinate. It was confirmed by CASSCF(3,6)/6-31+G(d) calculations that the transition states for disproportionation have a single determinant character.

For the construction of the partition functions corresponding to the internal motions of the molecule a mixed HO/HR approach was adopted. The rotations about the forming or

breaking bonds in the transition states were treated using the 1D-HR approach [25]. Several studies have indicated that the account of this specific mode gives the largest corrections to the original HO partition functions, as it allows finding a variety of possible transition states in terms of the rotational angle [26]. All the other internal motions were treated in the standard HO model. The rotational potentials were determined at the B3LYP/6-31+G(d) level of theory and the modified partition function was determined following the procedure outlined in reference 25.

4.3. Results and Discussion

As outlined in the introduction, the monomers chosen can be classified in three different classes. The monomers in *Class I* have been chosen in order to assess the effect of the size of pendant groups on the polymerizability of acrylates, those in *Class II* are expected to enlighten the effect of polarity on the polymerizabilty of acrylates whereas those in *Class III* will shed light on the effect of cyclic pendant group on the rate of polymerization of acrylates.

A. Class I: **The Effect of Pendant Groups Size on the Polymerizability of Acrylates**

Structures of the monomers

Among the various conformers of MHMA the structures corresponding to the lowest stationary points on the Potential Energy Surface (PES) are MHMA-1 (0.00 kcal/mol), MHMA-2 (1.20 kcal/mol), MHMA-3 (1.11 kcal/mol). The relative energies of the structures displayed in Figure 4.2 include the zero point energies. The internal hydrogen bond between the alcoholic hydrogen and the carbonyl oxygen stabilizes MHMA-1. In MHMA-3 the H-bond is with the carboxyl oxygen rather than the carbonyl oxygen. MHMA-2 is an extended conformation and does not show intramolecular hydrogen bonds.

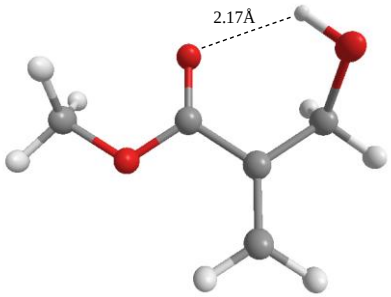

MHMA-1 (H-bond, 0.00 kcal/mol)

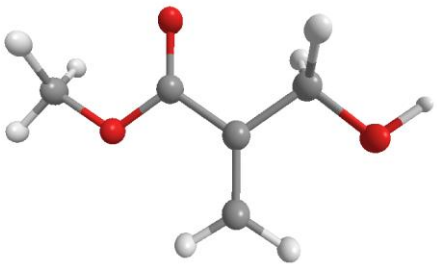

MHMA-2 (+1.20 kcal/mol)

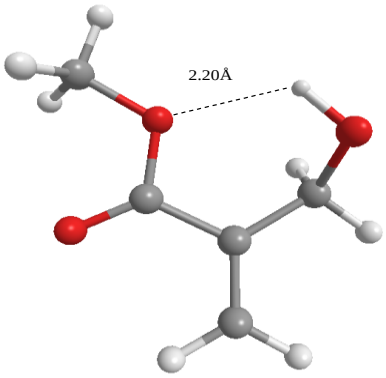

MHMA-3 (+1.11 kcal/mol)

Figure 4.2. Structures of the various conformers of methyl α-hydroxymethacrylate were determined at the B3LYP/6-31+G(d) level of theory. Energies are determined at the BMK/6-311+G(3df,2p)//B3LYP/6-31+G(d) level of theory.

The structures of the energetically most stable conformers of MHMA, EHMA and TBHMA are very similar to each other, the H-bond between the alcoholic hydrogen and the carbonyl oxygen is 2.168 Å, to 2.155 Å, and 2.142 Å in MHMA, EHMA and TBHMA respectively and stabilizes these species. Notice that in every case the *anti* conformer is more stable than the *syn* due to intramolecular hydrogen bonds. The radicals MHMAR, EHMAR, TBHMAR have a methyl group attached to the olefinic double bond of the monomers (CH_3-CH_2-C.-(CH_2OH)(CO)-O-R where R=CH_3,C_2H_5,C_4H_9). The global minima for these radicals have similar structures as the monomers themselves, they are all stabilized by intramolecular hydrogen bonds between the OH group and the carbonyl oxygen (1.977 Å in MHMAR, 1.965 Å in EHMAR, and 1.967 Å and in TBHMAR). The radicalic nature of MHMAR causes an electron delocalization and charge separation (δ_O = -0.562, δ_H = 0.506) as compared to the neutral MHMA (δ_O = -0.542, δ_H = 0.492) and this causes a shortening in the hydrogen bonds.

Influence of hydrogen bonding in the preorganisation of the reactants

We investigated the influence of hydrogen bonding on the reaction kinetics for the propagation reaction of the first monomer, MHMA. Four different transition states (TS1, TS2, TS3 and TS4) have been located, depending on the nature of the hydrogen bonds. The first transition state TS1 has two intramolecular hydrogen bonds (1.96 Å and 2.15 Å) whereas the distance of the forming C-C bond (hereafter referred as the critical distance) is 2.25 Å. A second transition state TS2 has one intermolecular (1.92 Å) and one intramolecular (2.16 Å) H-bond with a critical distance of 2.20 Å. TS3 has two intermolecular bonds (1.93 Å and 2.00 Å) with a critical distance of 2.30 Å. TS4 has two intramolecular H-bonds (2.18 Å and 2.00 Å) with a critical distance of 2.25 Å. TS4 (0.00) is more stable than TS1 (+2.02 kcal/mol), TS2 (+7.51 kcal/mol) and TS3 (+8.05 kcal/mol). IRC calculations starting from the transition state structures have been carried out in order to generate the corresponding reactant complexes. The relative energies of the various reactant complexes and transition states are given in Scheme 4.1. The complexes corresponding to each transition structure bear the same nomenclature i.e. RE1 is the reactant complex corresponding to TS1. The reactant complex RE1 with 2 intermolecular H-bonds (1.89 Å each) is stabilized by 4.33 kcal/mol with respect to the separated reactants. RE2 has 1 inter (2.26 Å) and 1 intramolecular H bond (2.12 Å) and is 2.64 kcal/mol less stable than RE1. RE3 with 2 intermolecular H-bonds (2.05 Å, 2.04 Å) and RE4 with 2 intramolecular H-bonds (2.00 Å, 2.00 Å) are less stable than RE1 by 7.46 and 2.14 kcal/mol respectively. The stability of RE4 can be attributed to the strength of the hydrogen bonds: 2.00 Å in RE4 as compared to 1.89 Å in RE1. The reactant species in the most stable complex RE1 are not properly organized for the propagation reaction to start. Presumably the intermolecular H-bonds in the most stable complex RE1 loosen and a reorganisation of the reactant molecules takes place allowing the propagation reaction to proceed through the most favorable transition state structure TS4. In Scheme 4.1, the propagation barrier, $E_{0,}$ for MHMA starting from the separate reactants is 4.67 kcal/mol.

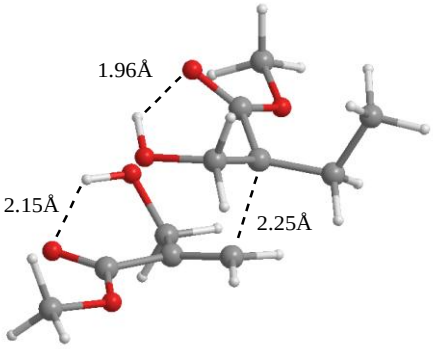

TS1

(E_0 = -881.385607 Hartree)

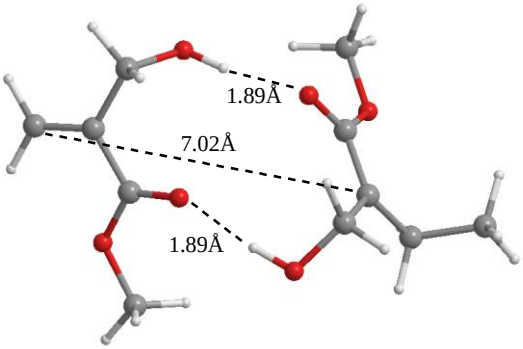

RE1

(E_0 = -881.403160 Hartree)

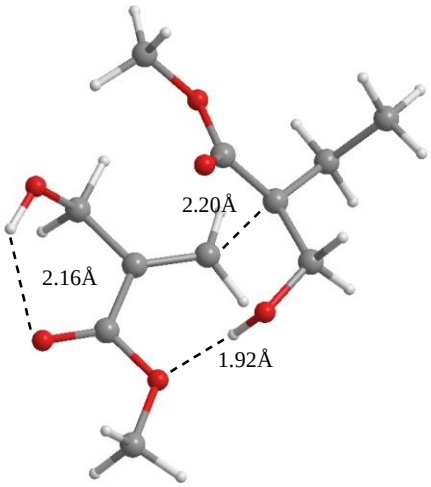

TS2

(E_0 = -881.376854 Hartree)

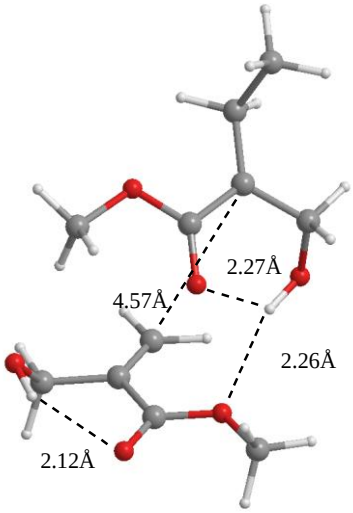

RE2

(E_0= -881.398948 Hartree)

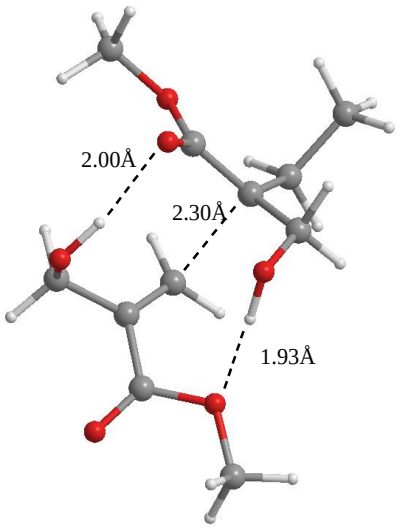

TS3

(E_0 = -881.375993 Hartree)

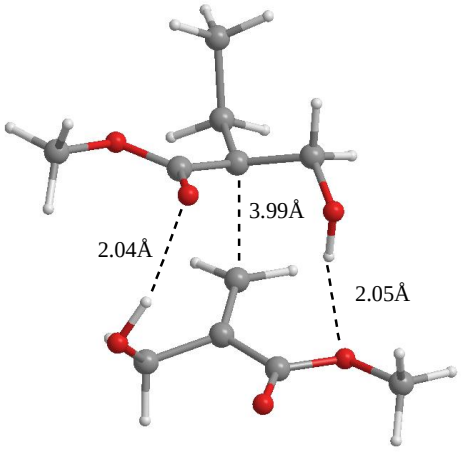

RE3

(E_0 = -881.391277 Hartree)

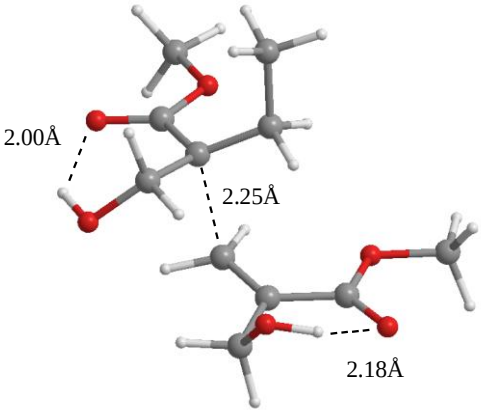

TS4

(E_0 = -881.388819 Hartree)

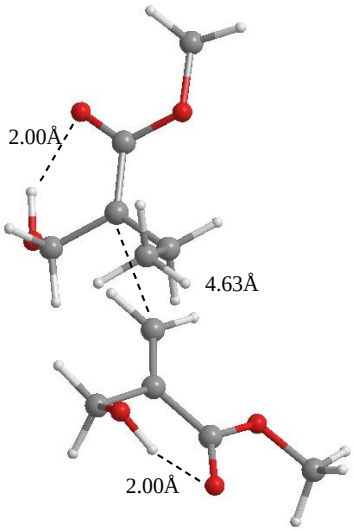

RE4

(E_0 = -881.399746 Hartree)

Figure 4. 3. Various transition structures and their corresponding reactant complexes for MHMA (BMK/6-311+G(3df,2p)//B3-LYP/6-31+G(d). E_0 is defined as the ground state energy with inclusion of zero point vibrational energy.

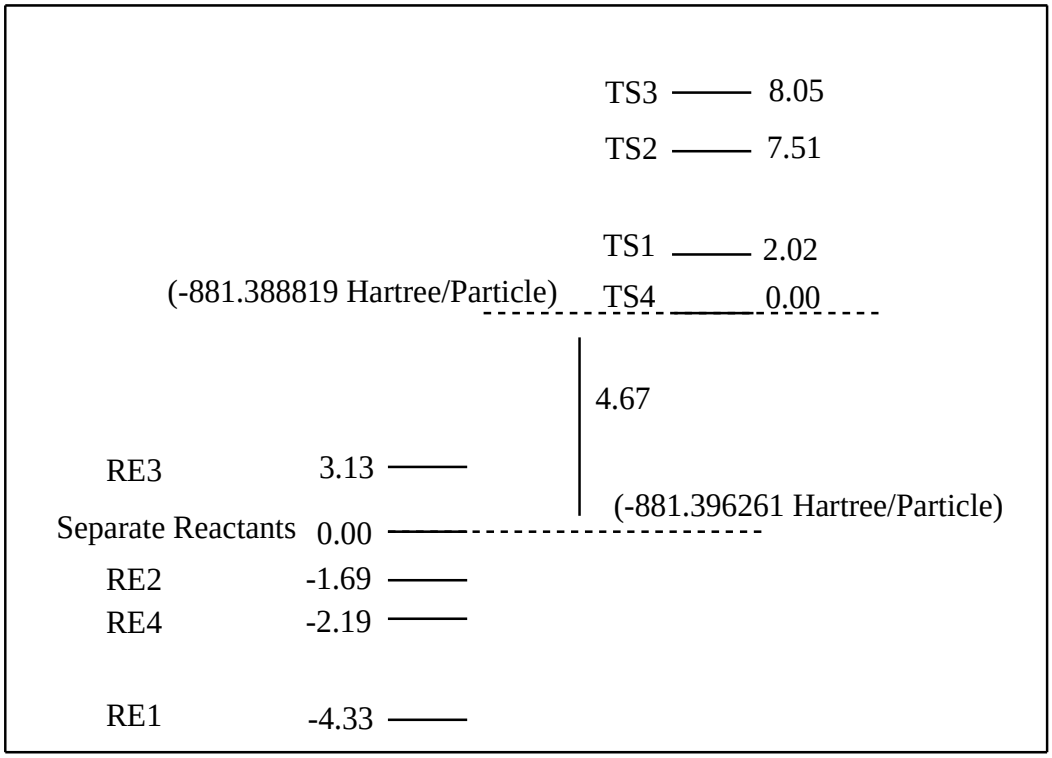

Scheme 4. 1. Relative energies (E_0), in kcal/mol, for the various transition structures and their corresponding reactant complexes for MHMA (BMK/6-311+G(3df,2p)//B3-LYP/6-31+G(d), kcal/mol).

Avcı et al. have investigated the experimental rates of polymerization of TBHMA as a function of temperature (Table 4.2) [14]. Instantaneous rates of polymerization were calculated according to following equation:

$$Rate = \frac{(Q/s)M}{n\Delta H_{theor} m}$$

where ΔH_{theor} is the heat released per mole of double bonds reacted (ΔH_{theor}=13.1 kcal/mol for methacrylate double bonds), *Q/s* is the heat flow per second, *M* is the molar mass of the monomer, *n* the number of double bonds per monomer molecule, and m is the mass of the monomer in the sample. Generally, the rate is expected to increase with temperature however in this case due to the presence of intermolecular hydrogen bonding the rate reaches a limiting value. The fact that the rate of polymerization reaches an almost constant value (0.0160) as the temperature increases, suggests that the heat absorbed is used to destroy the intermolecular H-bonds which might form prior to the polymerization

process. Lee et al. report the correlation between the effect of temperature on hydrogen bonding and the effect of temperature on the polymerization rate for the photopolymerization rate of hydroxalkyl acrylates [7]. They also observe a decrease in the rate of polymerization as a function of time for hydroxyethyl acrylate (HEA) which is found to display intermolecular hydrogen bonds. Our computational results confirm the presence of intermolecular H-bonds in the most stable prereactive complex RE1. In order to proceed the polymerization, the intermolecular H-bonds in the prereactive complex breaks down; the radical attacks the monomer through TS4 which is the lowest stable transition state. All plausible transition structures, except for TS3, have intramolecular H-bonds. Thus, even though the monomers preorganize through intermolecular H-bonds, the most favorable intermediate along the propagation reaction is stabilized by intramolecular H-bonds. As claimed by Davis in the study on the propagation reaction in the free radical polymerization of EHMA, complex formation between hydroxy-containing compounds is very probable [27]. De La Rosa et al. have carried out detailed atomistic modeling of the dense glassy isotactic and syndiotactic poly(allyl alcohol)(PAA) and poly(vinyl alcohol))(PVA). PVA, where 6-membered rings between the lateral groups are formed, is stabilized by intramolecular hydrogen bonds [28]. In PAA, the intramolecular hydrogen bonds represent about 60 per cent of the total hydrogen bonds. In the case of PVA where 8 membered rings would form between neighboring groups, intramolecular bonds are of lower occurrence. This study confirms the occurrence of intramolecular hydrogen bonds whenever 6-membered rings can form as shown above for MHMA.

Table 4.2. Experimental rates of polymerization (s^{-1}) and per cent conversion for TBHMA.

T(ºC)	Rate	Per cent conversion
35	0.0137	61.9
40	0.0160	69.3
50	0.0161	63.8
65	0.0162	56.1
70	0.0144	46.1

Reaction kinetics

The reaction kinetics have been calculated by considering the most stable transition state, TS4 and the separated reactants. The transition states for the propagation reactions corresponding to the other monomers EHMA and TBHMA show a large similarity with each other in the sense that each monomer moiety in the transition state is stabilized by an intramolecular H-bond and a critical distance of about 2.25Å (Figure 4.4). However due to steric hindrance, the propagation reaction for TBHMA is expected to be less facile than the one for MHMA. TBHMA characterized by a bulky isobutyl pendant group has indeed the largest activation energy for propagation, i.e. 6.16 kcal/mol compared to 5.60 for MHMA. The effect of the ester side chain on the propagation kinetics of alkyl methacrylates has been monitored by the pulsed-laser polymerization technique [30]. This study has shown an increase in k_p with ester chain length. In *Class I* monomers, where the α-substituent is α-hydroxymethyl instead of methyl, the experimentally observed and calculated rates of polymerization decrease with chain length. This behavior can be rationalized by the presence of intramolecular hydrogen bonding which leads to the formation of 6-membered rings and prevents the approach of bulky groups.

Experimentally it is known that small, aliphatic radicals terminate predominantely by coupling and methylmethacrylate undergoes termination both by coupling and disproportionation. The extent of disproportionation in MMA increases from 67 per cent at 25ºC to 80 per cent at 80ºC [18]. It is also known that termination by disproportionation increases when the propagating radical is sterically hindered or has more α-hydrogens available for transfer. For monomers of *Class I*, there is no experimental evidence for the mode of termination. In this study, we have checked whether disproportionation as shown in Scheme 4.2 might be the major termination process. The rate constant, k_{td} depicts the kinetics of the transfer of hydrogen between two radicals (Figure 4.5). The termination by coupling has not been modeled as these reactions where two radicals couple need advanced and very expensive molecular modeling techniques which are beyond the scope of this study. The accurate a priori prediction of the high-pressure rate coefficient for radical-radical combination reactions has been a difficult challenge since the location of the reaction bottleneck shifts dramatically as a function of the energy and the angular momentum of the collision [31]. Recently an ab initio transition state theory based

procedure at the CASPT2/cc-pvdz level within variable reaction coordinate transition state theory (VRC-TST) for accurately predicting the combination kinetics of two alkyl radicals has been reported by Klippenstein et al [32]. However, these methodologies need to be tested for radicals involving unsaturated and resonantly stabilized radicals like the ones in this study.

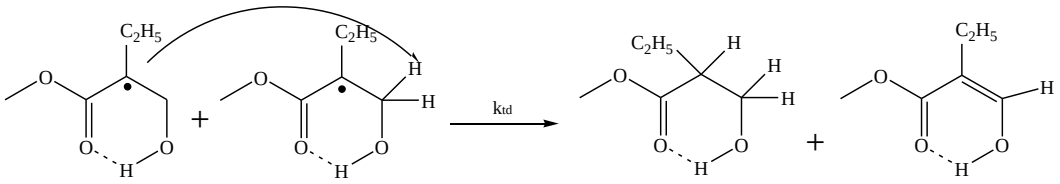

Scheme 4. 2. Mechanism for the disproportionation reaction in *Class I* monomers

The activation barriers for the disproportionation reactions are higher than the ones for the propagation reactions as expected (Table 4.3). The values of k_p reproduce the desired trend in that steric hinderance inhibits the rate of propagation:i.e. k_p(MHMA)> k_p(EHMA)> k_p(TBHMA). As is evidenced by the magnitude of k_{td} , the disproportionation reaction is quite slow and is probably not the rate determining step for the termination process of monomers of *Class I.* Considering the ratio $k_p/k_{td}^{1/2}$ as indicator of the polymerizability trend overestimates the importance of disproportionation within the termination process. Overall, the relative experimental trend in polymerizability for monomers of *Class I* is relatively well reproduced with the relative propagation rate constants k_p. As indicated in the last two columns of Table 4.3, from the reaction rates of disproportionation it might be that coupling would be important for termination.

Table

4.3. Energetics (BMK/6-311+G(3df,2p)//B3LYP/6-31+G(d), kcal/mol), rate coefficients (L.mol-1.s)[a] for monomers in *Class I*. (250K<T<350K). k_p(rel) is the relative polymerization rate coefficient and R_{exp}(rel) is the relative polymerization rate with respect to MHMA monomer.

	Propagation Reaction				Disproportionation Reaction			
Monomers	A	E_a	ΔH	k_p	E_a	k_{td}	$k_{p(rel)}$	R_{exp}(rel)
MHMA	1.46E+02	5.60	-18.2	1.62E-02	16.15	1.59E-09	1.00	1.00
EHMA	7.49E+01	5.96	-17.7	4.75E-03	16.55	3.52E-10	0.29	0.81
TBHMA	1.27E+02	6.16	-17.3	4.52E-03	17.73	4.85E-11	0.28	0.43

[a]Rate coefficients calculated at 300K, were corrected by using the HR correction factors of 1.33 for MHMA, 1.39 for EHMA and 1.10 for TBHMA in the propagation and by 1.74 for MHMA, 1.61 for EHMA and 1.92 for TBHMA in the disproportionation reactions respectively. These factors are included in the calculations.

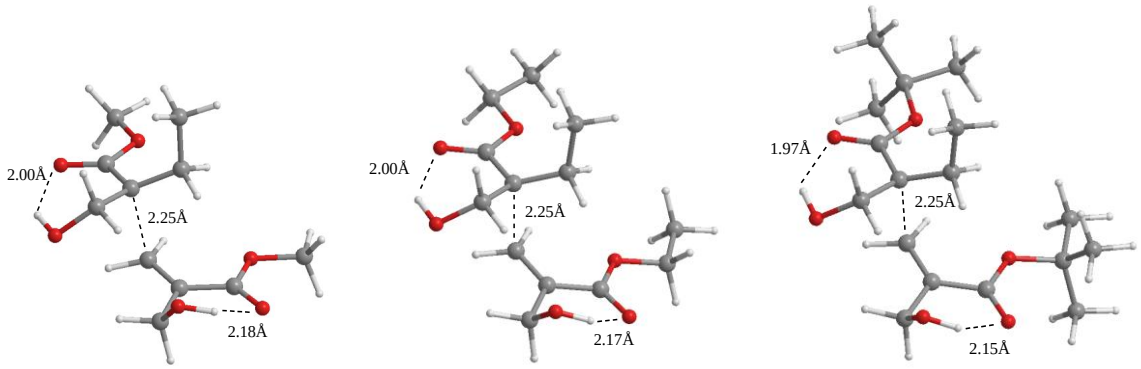

Figure 4.4. Transition states of the propagation for MHMA, EHMA and TBHMA (B3LYP/6-31+ G(d)).

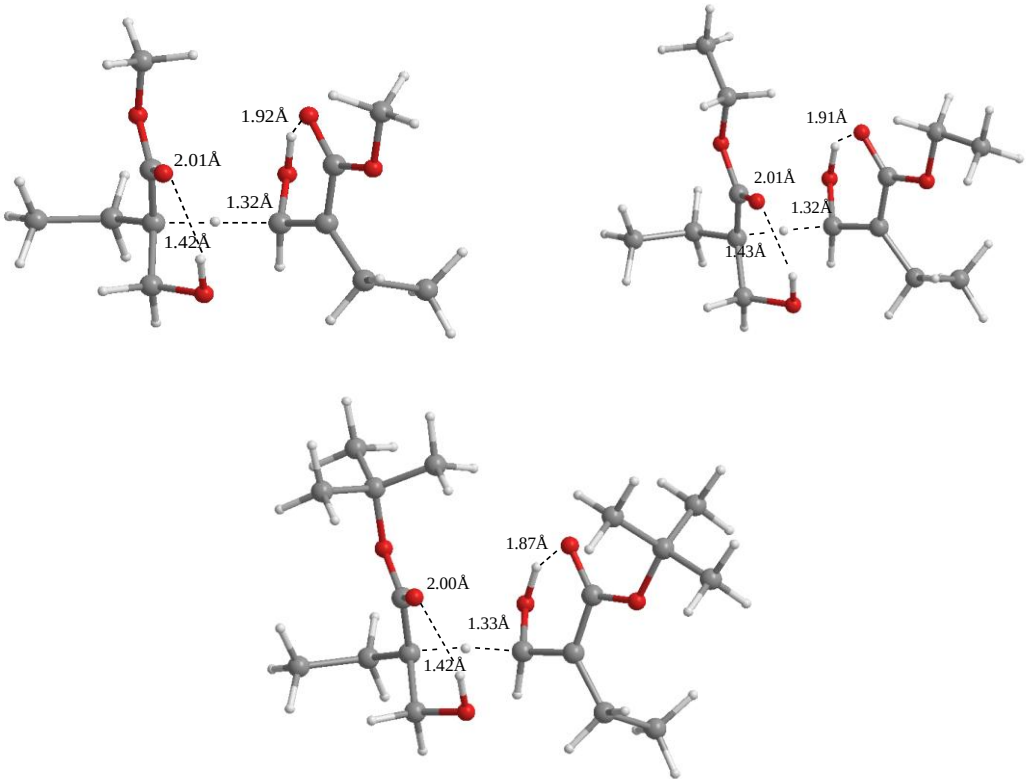

Figure 4.5. Transition states of the disproportionation for MHMA, EHMA and TBHMA (B3LYP/6-31+ G(d)).

Influence of internal rotation about the forming bond on the reaction kinetics.

The rotation about the forming bond in the transition state has been modeled using the 1D-HR approach as introduced in reference 25. MHMA and EHMA show very similar rotational profiles: two additional minima come into play but they all lie higher in energy than the reference conformer. Moreover a substantial energy barrier is needed to reach the other transition states, due to large steric hindrance between the bulky subsituents of the radical and the monomer. For TBHMA the potential is characterized by higher rotational barriers due to the presence of additional bulky groups which prevent rotation in the transition state. Rotational potentials for the propagation reaction of monomers are displayed in Figure 4.6. The correction factors are 1.33 (1.74), 1.39 (1.61) and 1.10 (1.92) for the propagation (disproportionation) reactions of MHMA, EHMA and TBHMA

respectively. The correction factors by applying the 1D-HR approach all lie close to one, as all additional transition states that come into play lie substantially higher in energy than the reference conformer.

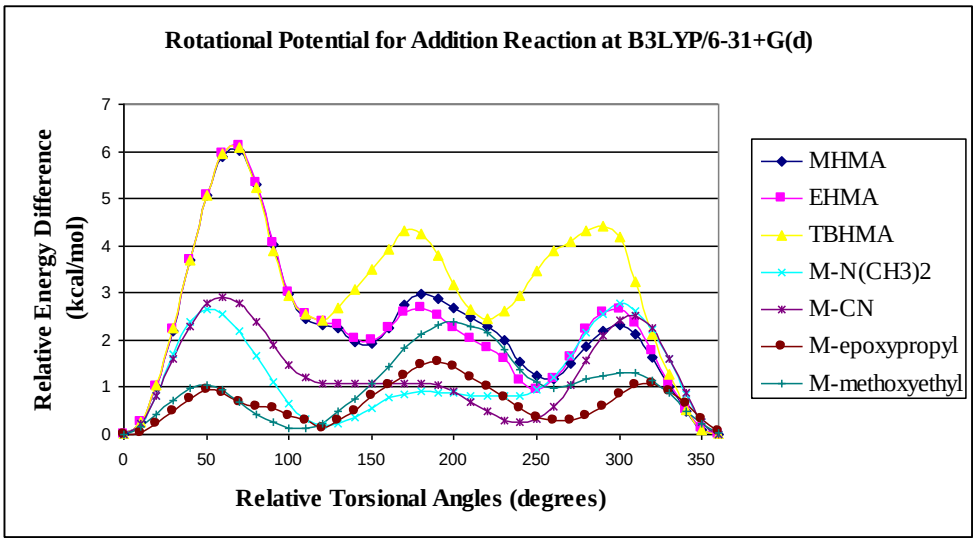

Figure 4.6. Rotational potentials (B3LYP/6-31+G(d)) for the propagation reactions.

How important is the chain transfer to the monomer for Class I monomers?

An important class of reactions that can influence the normal propagation is the chain transfer to monomer in which the radical is transferred to the monomer by hydrogen abstraction or hydrogen transfer. The rate constant for chain transfer to monomer is referred to as $k_{ct.}$ Thereby a small radical species is generated originating from the former monomer which can re-initiate by attacking a second monomer. The rate constant for re-initiation is called k_a.

During a free radical polymerization reaction, the radical R·can either propagate by attacking the monomer with the rate constant k_p (propagation reaction)

$$M + R\cdot \xrightarrow{k_p} M\text{-}R\cdot$$

or abstracting a hydrogen from the monomer with the rate constant k_{ct}(chain-transfer reaction).

$$M + R\cdot \xrightarrow{k_{ct}} R\text{-}H + (M\text{-}H)\cdot$$

Chain transfer yields a saturated compound (R-H) and a new radical whose hydrogen has been abstracted (M-H)·(Figure 4.7). The results in Table 4.4 show that chain transfer in unimportant for this class of monomers.

$$(M\text{-}H)\cdot + M \xrightarrow{k_a} \text{polymer}$$

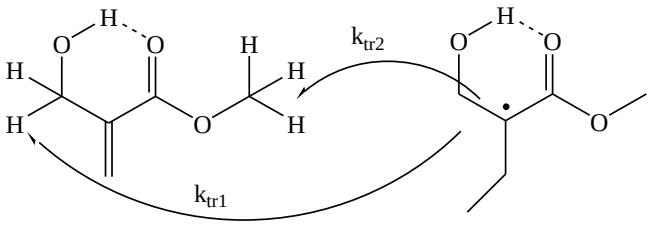

Figure 4.7. Mechanism for the chain transfer reaction for MHMA in *Class I* monomers.

Table 4.4. Energetics (BMK/6-311+G(3df,2p)//B3LYP/6-31+G(d), kcal/mol), rate coefficients (L.mol-1.s) for chain transfer for monomers in *Class I*. (250K<T<350K). k_{ct1} and k_{ct2} are the chain transfer rate coefficients of α-hydrogens and R (alkyloxy)-hydrogens respectively, k_p is the propagation rate constant.

Monomers		A	E_a	k_{ct1}	k_{ct2}	k_p
MHMA	R-hydrogen	3.62E+03	21.88	---	1.26E-12	1.62E-02
	α-hydrogen	2.76E+03	13.76	5.19E-07	---	
EHMA	R-hydrogen	2.63E+07	26.24	---	1.00E-11	4.75E-03
	α-hydrogen	1.63E+03	13.95	2.25E-07	---	
TBHMA	R-hydrogen	2.65E+03	25.35	---	8.15E-15	4.52E-03
	α-hydrogen	7.57E+02	14.05	8.97E-08	---	

Benchmark calculations on solvent and level of theory (LOT) study on the propagation reaction of EHMA.

Benchmark calculations have been carried out for EHMA since experimental results [27] were already present in the literature. All the functionals reproduce the experimental trend qualitatively in that the propagation rate constant decreases in polar medium. The

effect of a polar environment was taken into account by use of the self-consistent reaction field (SCRF) theory, utilizing the integral equation formalism-polarizable continuum [33] (IEF-PCM) model in solution. Bondi radii [34] scaled by a factor of 1.2 were used for all solvent calculations. Notice that even though special interactions with the solvent (H-bonding) are not taken into account, the experiemenal trend is quite well reproduced with geometries taken from B3LYP/6-31+G(d) with all functionals and even slightly better with BMK (Table 4.5).

Table 4.5. Propagation rate constant (k_p) for EHMA. The geometries of the reactants and transition structure were optimized at B3LYP/6-31+G(d) level of theory, the rate constant k_p(L.mol-1.s) was calculated at various levels of theory. The solvent effect was included with the IEF_PCM methodology. The experimental values are taken from reference 27 (250K<T<350K).

Solvent	E	B3PW91/ 6-31+G*	MPW1K/ 6-31+G*	MPW1PW91 /6-31+G*	B3LYP /6-31+G*	BMK/ 6-31+G*	Exp.[27] k_p
Gas*	-	1.01E-04	1.34E-03	1.97E-03	-	4.75E-03	
Toluene	2.3	5.13E-06	6.42E-05	9.60E-05	1.46E-06	3.95E-04	1600
Chloroform	4.8	4.25E-07	4.38E-06	7.62E-06	1.26E-07	2.82E-05	909
Ethanol	24.3	5.63E-08	4.92E-07	9.73E-07	1.73E-08	3.29E-06	589

* Energetics in the gas phase are at the 6-311+G(3df,2p) level.

B. Class II: **Effect of Polar Groups on the Polymerizability of Acrylates**

Structures of the monomers

The *syn* and *anti* conformations for M-N$(CH_3)_2$ and M-CN have been modeled and the ones lowest in energy (E_0) are displayed in Figure 4.8. For both monomers the *syn* conformations have been found to be more stable at the B3LYP/6-31+ G(d) level. The structures corresponding to the global minima for the monomers and the radicals are quite extended, minimizing the unfavorable steric interactions and maximizing the favorable bifurcated C=O ...H interactions.

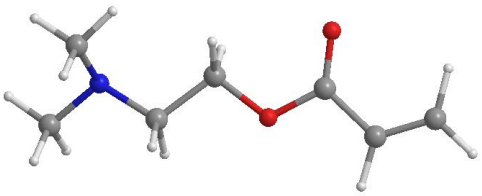

M-N(CH_3)$_2$ *syn* (0.00 kcal/mol)

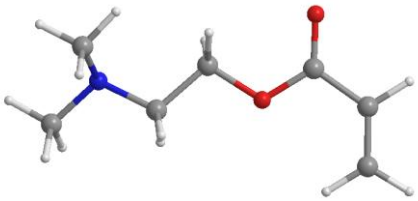

M-N(CH_3)$_2$ *anti* (0.63 kcal/mol)

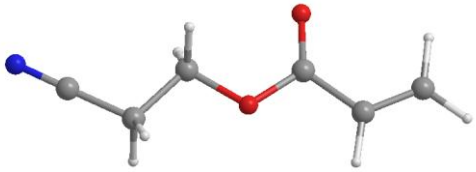

M-CN *syn* (0.00 kcal/mol)

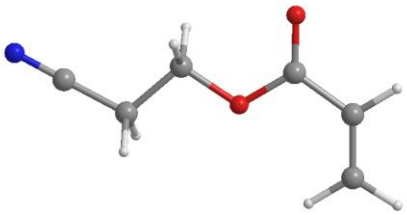

M-CN *anti* (0.77 kcal/mol)

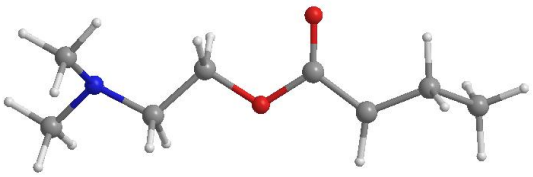

M-N(CH_3)$_2$-R

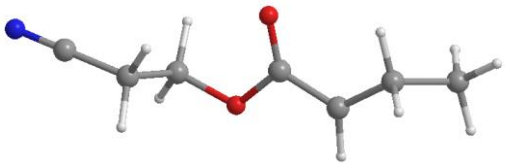

M-CN-R

Figure 4.8. Most stable *syn* and *anti* conformers of M-N(CH_3)$_2$, M-CN, M-N(CH_3)$_2$-R, M-CN-R calculated at the B3LYP/6-31+G(d) level of theory.

Reaction kinetics

The transition states for propagation of monomers M-N(CH_3)$_2$ and M-CN are shown in Figure 4.9. The distance of the forming bond for the transition states of *Class II* is slightly larger than for monomers of *Class I* (2.29 Å versus 2.25Å). It can be anticipated that the activation energy for *Class II* monomers will be higher, as for addition reactions to double bonds a correlation exist between the critical distance and the activation energy. For more information we refer to the review paper by Fisher and Radom [29]. We have checked whether termination is dominated by disproportionation. In this case the barriers for rotation are significantly lower than for *Class I* monomers, due to considerably less steric hindrance between subsitutents of the monomer and the radical. The double bond of the olefin is now unsubstituted at one end, explaining the easier rotation about the forming

bond. Additional minima along the rotational potential have nearly the same energy as the reference conformer. Consequently the correction factors for propagation are larger than for *Class I* monomers, i.e. 3.33 and 2.91 for M-N(CH_3)$_2$ and M-CN respectively. These factors obtained by applying the 1D-HR approach are non negligible and might be important for a correct reproduction of the polymerization trend.

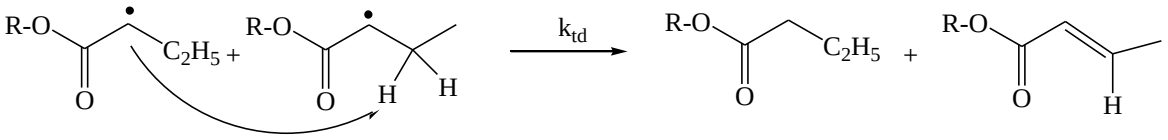

Scheme 4.3. Mechanism for the disproportionation reaction in *Class II* and *Class III*

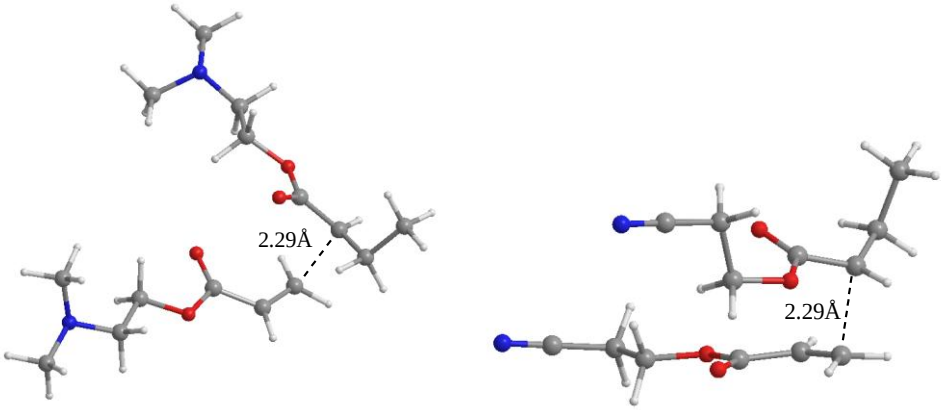

Figure 4.9. Transition states of propagation for M-N(CH_3)$_2$) and M-CN (B3-LYP/6-31+G(d).

Table 4.6. Energetics (BMK/6-311+G(3df,2p)//B3LYP/6-31+G(d), kcal/mol), rate coefficients (L.mol-1.s)[a] for monomers in *Class II*. (250K<T<350K). k_p(rel) is the relative polymerization rate coefficient and R_{exp}(rel) is the relative polymerization rate with respect to M-N$(CH_3)_2$.

	Propagation Reaction			Kinetics			
Monomers	A	E_a	ΔH	k_p	k_{td}	$k_{p(rel)}$	R_{exp}(rel)
M-N$(CH_3)_2$	1.86E+02	6.74	-19.97	7.05E-03	2.98E-12	1.00	1.00
M-CN	3.06E+02	6.78	-19.70	9.57E-03	2.12E-12	1.36	12.60

[a]Rate coefficients for propagation were corrected by using the HIR correction factors of 3.33 for M-N$(CH_3)_2$ and 2.91 for M-CN.

The activation barrier for propagation of *Class II* monomers is slightly higher than the one for *Class I* monomers, whereas the preexponential factors show more subtle variations with respect to *Class I*. M-CN is smaller and more compact than M-N$(CH_3)_2$ and its preexponential factor is larger than the one for M-N$(CH_3)_2$, thus $\Delta S^{\#}$ is larger for the former. The entropy of activation, $\Delta S^{\#}$ renders k_p larger in the case of M-CN even though the activation barriers for the propagation reaction are more or less similar. As in *Class I*, for monomers of *Class II* the disproportionation pathway is not rate determining in terms of termination. The trend in k_p (1.4:1) mimics qualitatively the experimental trend (14:1) however consideration of the propagation rate constant only, underestimates the polymerization trend on a quantitative basis. To understand the discrepancy further, the role of side reactions for these monomers has been investigated by modeling the chain transfer reactions.

How important is the chain transfer to the monomer for Class II monomers?

As displayed in Table 4.7, the chain transfer rate constant k_{ct1} is the one for the abstraction of the most labile H's - those on the carbon atom bearing the -N$(CH_3)_2$ and CN groups, k_{ct2} is the chain transfer rate constant for abstraction of H's from the N$(CH_3)_2$ group in M-N$(CH_3)_2$ and from –CH_2-(O)- group in M-CN, k_{ct3} is the chain transfer rate constant for abstraction of H's from the –CH_2-(O)- group in M-N$(CH_3)_2$. The overall chain transfer constant $k_{ct\ (total)}$ for M- N$(CH_3)_2$ (1.14E-05) is much larger than the transfer rate

constant for M-CN (1.00E-08) indicating that the polymerization in the case of M-$N(CH_3)_2$ is inhibited by chain transfer. Schematic representation of the chain transfer reactions for *Class II* monomers are given in Figure 4.10.

Furthermore, depending on the magnitude of the chain transfer rate constant k_{ct}, reinitiation can compete with propagation. Comparison of k_p and k_a requires normalization of k_a by the normalization factor k_{ct}/k_p. Therefore a modified rate constant k_a' (k_a'= k_a x k_{ct}/k_p) has been introduced.

If $k_{ct} << k_p$, then the effect of chain transfer on the reaction is determined by comparing k_a' with k_p.[1] The results in Table 4.7 demonstrate that re-initiation is unimportant for M-CN for which $k_a' << k_p$. However for M-$N(CH_3)_2$ re-initiation can compete with the propagation reaction and this is expected to decrease the polymerizability of the latter.

Tunneling corrections have been introduced with Eckart [35] and Wigner [36] methodologies in order to test the effect of tunneling on chain transfer via hydrogen abstraction. Part B and C on Table 4.7 mimic the same qualitative trend as the results in Part A. The value of k_a' with both methods emphasizes further the importance of reinitiation for M-$N(CH_3)_2$.

Overall, for monomers in *Class II* where the nature of the substituents is completely different, i.e. $N(CH_3)_2$ vs CN , modeling side reactions such as chain transfer and reinitiation is quite important. Even though the propagation rate constants reproduce the experimental behavior of these monomers qualitatively, the role of chain transfer must be emphasized in understanding the experimental behavior of these monomers.

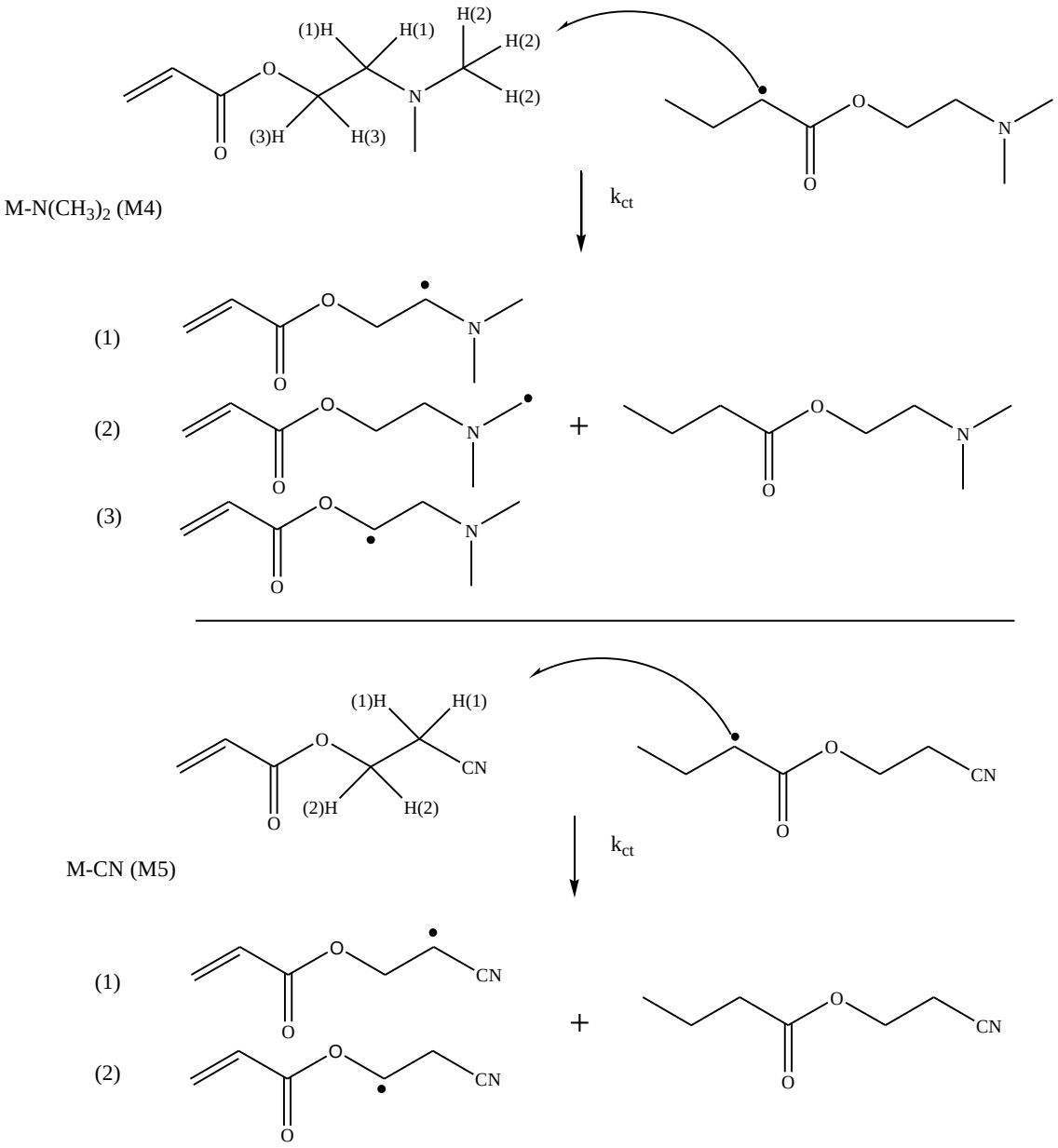

Figure 4.10. Schematic representation of the chain transfer reactions for monomers M-$N(CH_3)_2$ and M-CN.

Table 4.7. Reinitiation rate constants for M-$N(CH_3)_2$, M-CN, (BMK/6-311+G(3df,2p)// B3LYP/6-31+G(d)).

PART A * Reinitiation rate constants

Monomer	k_{ct1}	k_{ct2}	k_{ct3}	$k_{ct\,(total)}{}^{*}$	k_a	k_p	k_a'
M-$N(CH_3)_2$	2.24E-06	1.15E-06	4.45E-10	1.14E-05	8.88E-01	7.05E-03	1.43E-03
M-CN	4.93E-09	5.44E-10	---	1.09E-08	2.50E-03	9.57E-03	2.86E-09

PART B. Reinitiation rate constants with Eckart tunneling and free rotor corrections

Monomer	k_{ct1}	k_{ct2}	k_{ct3}	$k_{ct\ (total)}$*	k_a	k_p	k_a'
M-$N(CH_3)_2$	4.67E-05	2.08E-05	4.45E-10	2.18E-04	8.88E-01	7.05E-03	2.75E-02
M-CN	3.01E-07	5.44E-10	---	6.03E-07	2.50E-03	9.57E-03	1.58E-07

PART C** Reinitiation rate constants with Wigner tunneling and free rotor corrections

Monomer	k_{ct1}	k_{ct2}	k_{ct3}	$k_{ct\ (total)}$*	k_a	k_p	k_a'
M-$N(CH_3)_2$	7.08E-06	3.53E-06	4.45E-10	3.53E-05	8.88E-01	7.05E-03	4.45E-03
M-CN	1.81E-08	5.44E-10	---	3.74E-08	2.50E-03	9.57E-03	9.77 E-09

*For M-$N(CH_3)_2$ $k_{ct\ (total)} = 2x\ k_{ct1} + 6x\ k_{ct2} + 2x\ k_{ct3}$; for M-CN, $k_{ct\ (total)} = 2x\ k_{ct1} + 2x\ k_{ct2}$. Rate coefficients were corrected by using the Free Rotor correction factors for M-$N(CH_3)_2$ (5.0, 4.6, and 8.5 for k_{ct1}, k_{ct2}, and k_{ct3}) and for M-CN (7.1, 7.3 for k_{ct1}, k_{ct2}).
**For M-$N(CH_3)_2$, $k_{ct\ (total)} = 3.16(2k_{ct1}) + 3.07(6k_{ct2}) + 2k_{ct3}$.
For M-CN $k_{ct\ (total)} = 3.68(2\ k_{ct1}) + (2\ k_{ct2})$

Charge distributions and dipole moments

Based on AM1 calculations, Jansen has attributed the outstanding polymerizability of M-CN to its higher dipole moment (3.7 D) in comparison to the one of M-$N(CH_3)_2$ (2.01D) [3]. We have calculated (B3LYP/6-31+G(d)) the dipole moment of both M-$N(CH_3)_2$ and M-CN as described by Jansen by averaging it over five conformers. Our findings are such that M-CN has a higher average dipole moment $\langle\mu\rangle$, (4.65D) as compared to the one of M-$N(CH_3)_2$ (2.38D). Due to their high dipole moments M-CN molecules are expected to be well organized and facilitate the polymerization.

$$\langle\mu\rangle = \sum_j D_j \frac{e^{\frac{-\Delta H_j}{RT}}}{\sum_j e^{\frac{-\Delta H_j}{RT}}}$$

The Mulliken charge distributions in M-N$(CH_3)_2$, M-N$(CH_3)_2$R , M-CN and M-CNR have been used to predict the electrostatic interactions between the radical center and the unsaturated C (Table 4.8). The electrostatic force of attraction is 0.019 ((-0.528)(0.193)/$(2.29)^2$) in the case of M-CN and its radical; it is 0.015 ((-0.534)(0.152)/$(2.29)^2$) in the case of M-N$(CH_3)_2$, and its radical. This finding supports further the fact that the polymerization is more facile in the case of M-CN.Overall, the dipole moments and Mulliken charge distributions complement the data generated for the kinetics of these two monomers.

Table 4.8. Mulliken charges on the monomer and radical atoms of Class *II* (B3LYP/6-31+G(d)).

Compounds	Mulliken charges
M-N$(CH_3)_2$	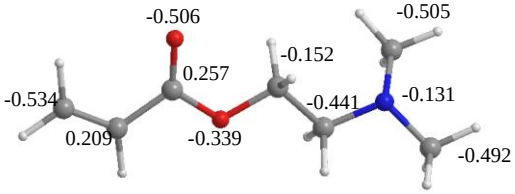
M-N$(CH_3)_2$-R	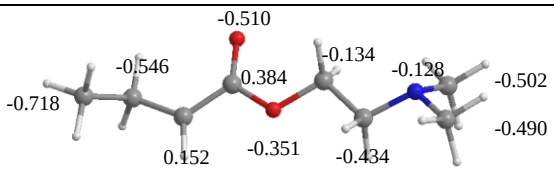
M-CN	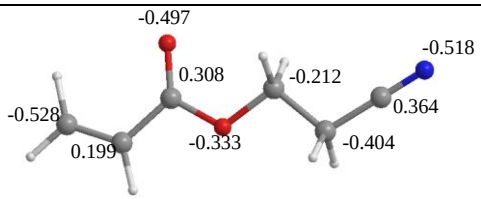
M-CN-R	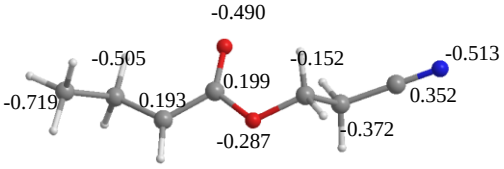

C. Class III: **Effect of cyclic pendant groups in acrylates**

Structures of the monomers

The structures corresponding to global minima for the monomers and the radicals are in the *syn* conformation, quite extended and similar to each other. Most stable geometries and their energy (E_0) for monomers are displayed in Figure 4.11.

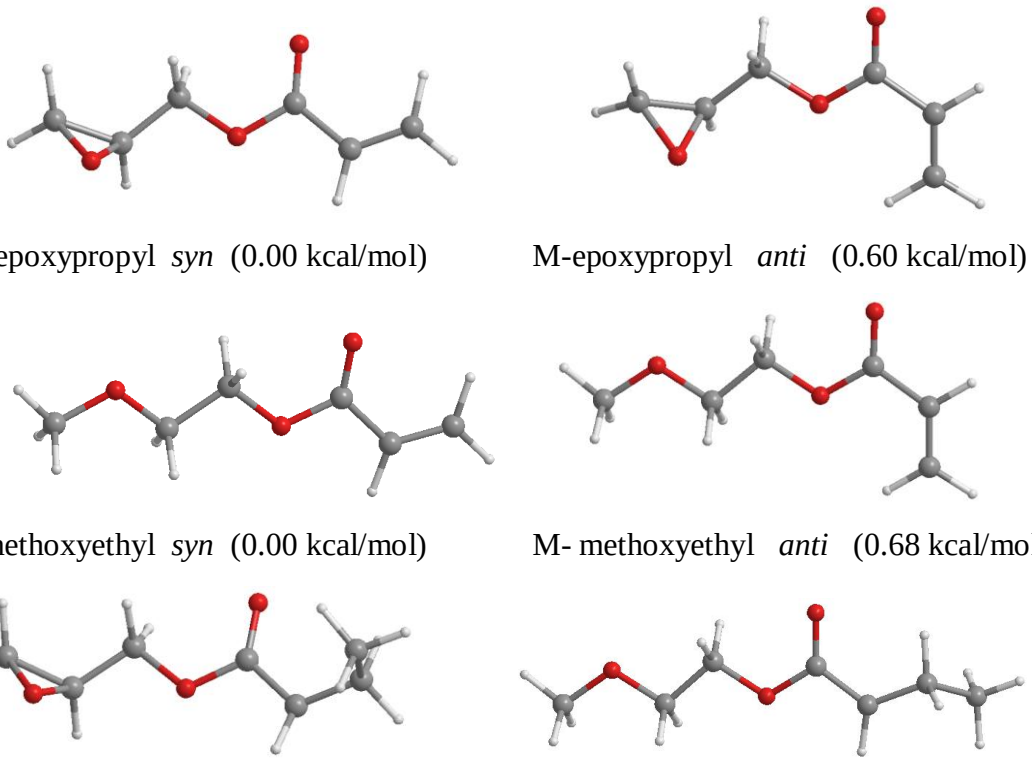

Figure 4.11. 3D structures for M-epoxypropyl, M-epoxypropyl-R, M-methoxypropyl and M-methoxyethyl-R (B3LYP/6-31+G(d)).

The transition states for propagation are shown in Figure 4.12. The structures of the transition states of the propagation reactions for M-epoxypropyl and M-methoxyethyl are different than for *Class II* monomers (dihedrals about forming bonds ~ -60º,90º) as the pendant groups are situated on the opposite side of the forming bond (dihedrals about forming bonds ~180º,90º) . The rotational potentials about the forming bond are shown in Figure 4.6.

Reaction Kinetics

The propagation reaction is favored for M-epoxypropyl. The activation energy for propagation and disproportionation for monomers of *Class III* are slightly higher than the values found for monomers of *Class I* and *II*. The trend in k_p values (1.2:1) mimics almost quantitatively the experimental trend (1.5:1). Notice that the rate constant for the disproportionation reaction k_{td} is very small as in the other cases and can not be considered as the rate determining step for termination.

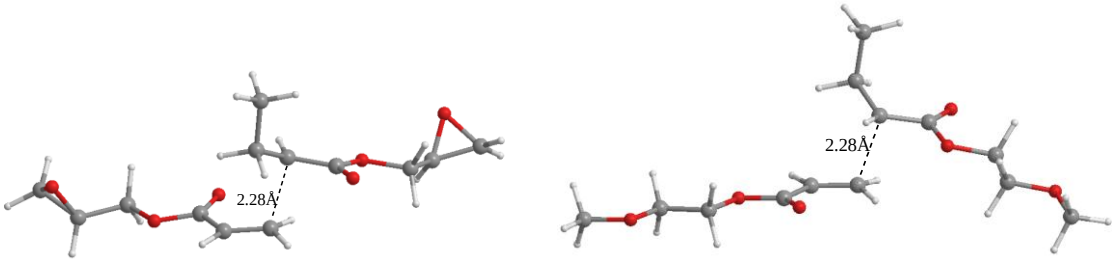

Figure 4.12. Transition states of the propagation reactions for M-epoxypropyl and M-methoxyethyl (B3-LYP/6-31+G(d)).

Table 4.9. Energetics (BMK/6-311+G(3df,2p)//B3LYP/6-31+G(d), kcal/mol), rate coefficients (L.mol-1.s)[a] for monomers in *Class III*. (250K<T<350K). k_p(rel) is the relative polymerization rate coefficient and R_{exp}(rel) is the relative polymerization rate with respect to M-methoxyethyl.

	Propagation Reaction			Kinetics			
Monomers	A	E_a	ΔH	k_p	k_{td}	$k_{p(rel)}$	R_{exp}(rel)
M-epoxypropyl	1.45E+03	6.95	-20.36	3.72E-02	2.71E-11	1.20	1.54
M-methoxyethyl	2.27E+03	7.10	-20.26	3.11E-02	1.05E-11	1.00	1.00

[a]Rate coefficients were corrected by using the HIR correction factors of 3.22 for M-epoxypropyl and 2.21 for M-methoxyethyl

4.4. Conclusion

In this study, polymerization trends within three class of acrylates/methacrylates was modeled by density functional based methods. Experimentally it was found that the effect of pendant group size, the polarity of the pendant group and the nature of a cyclic pendant group, can influence the polymerization rate substantially. The rates for propagation were calculated using the transition state theory in the relevant temperature range using the two component BMK/6-311+G(3df,2p) //B3LYP/6-31+G(d) level of theory. Moroever the hindered rotor approach was applied for rotation of the monomer and radical about the forming bond. For *Class I*, the effect of additional transition states by rotating about the forming bond is very small, as they are substantially higher in energy and the rotational barriers are relatively large. For *Class II* and *Class III* monomers the effect is non-negligible with correction factors of about three.

Overall within the present approach the polymerization trends are qualitatively well reproduced with k_p within each class. However, within *Class II* when the polar groups exibit large structural differences the chain transfer to monomer can contribute largely in inhibiting the polymerization. For all monomers it was investigated whether disproportionation would be the major route for termination. This seems not to be the case, most probably coupling will be important.

4.5. References

1. G.Odian, Principles of Polymerization, Wiley Interscience, New York, 1991.

2. (a) Accurate ab initio prediction of propagation rate coefficients in free-radical polymerization: Acrylonitrile and vinyl chloride Izgorodina, E. I.; Coote, M. L. *Chemical Physics*, **2006**, *324*, 96-110. (b) A Theoretical Study of Propagation Rate Coefficients for Methacrylonitrile and Acrylonitrile. Huang, D. M.; Monteiro, M. J.; Gilbert, R. G. *Macromolecules* **1998**, *31*, 5175-5187. c) Ab Initio Study of Free-Radical Polymerizations: Cost-Effective Methods to Determine the Reaction Rates.

Van Speybroeck, V.; Van Cauter, K.; Coussens, B.; Waroquier, M. *ChemPhysChem* **2005**, *6*, 180-189.

3. (a) Fast Monomers: Factors Affecting the Inherent Reactivity of Acrylate Monomers in Photoinitiated Acrylate Polymerization. Jansen, J. F. G. A.; Dias, A. A.; Dorschu, M.; Coussens, B. *Macromolecules* **2003,** *36*, 3861-3873. b) Effect of Dipole Moment on the Maximum Rate of Photoinitiated Acrylate Polymerizations. Jansen, J. F. G. A.; Dias, A. A.; Dorschu, M.; Coussens, B. *Macromolecules* **2002,** *35*, 7529-7531.

4. (a) Real-Time Kinetic Study of Laser-Induced Polymerization. Decker, C.; Moussa, K. *Macromolecules* **1989,** *22*, 4455-4462; (b) A new class of highly reactive acrylic monomers, 2[a)] Light-induced copolymerization with difunctional oligomers. Decker, C.; Moussa, K., *Makromol.Chem*. **1991**, *192*, 507-522; (c) Light-Induced Polymerization of New Highly Reactive Acrylic Monomers. Moussa, K.; Decker, C. *J. Polym. Sci., Polym. Chem.* **1993**, *31*, 2197-2203; (d) A New Class of Highly Reactive Acrylic Monomers, 1 Light-Induced Polymerization. Decker, C.; Moussa, K. *Makromol. Chem. Rapid Commun.* **1990**, *11*, 159. (e) Photopolymerization De Monomeres Multifunctionnels –V. Resines Polyurethennes- Acrylates. Decker, C.; Moussa, K. *Eur. Polym. J.* **1991**, *27*, 881-889.

5. Decker, C.; Moussa, K. *Polym. Mater Sci. Eng.* **1989,** *60*, 547

6. Polymerization Kinetics of Photocurable Acrylic Resins, Andrzejewska, E.; Andrzejewski, M. *Polym.Sci.Part A: Polym.Chem*. **1998**, *36*, 665-678.

7. Influence of Hydrogen Bonding on Photopolymerization Rate of Hydroxyalkyl Acrylates. Lee, T. Y.; Roper, T. M.; Jönsson, E. S.; Guymon, C. A.; Hoyle, C. E. *Macromolecules* **2004**, *37*, 3659-3665.

8. Effect of Aryl Substituents on the Reactivity of Phenyl Carbamate Acrylate Monomers. Beckel, E. R.; Nie, J.; Stansbury, J. W.; Bowman, C. N. *Macromolecules* **2004,** *37*, 4062-4069.

9. (a) Radical-Initiated Homo- and Copolymerization of Methoxymethyl Methacrylate. Ueda, M.; Ishibashi, S.; Suzuki, T.; Masuko, T.; Pittman, C.U. *J Polym Sci: Part A: Polym. Chem. Ed*. **1984**, *22*, 2305-2316; (b) Radical-Initiated Homopolymerization

and Copolymerization of Methylthiomethyl Methacry late. Ueda, M.; Yazawa, M.; Suzuki, T.; Pittman, C.U. *J Polym Sci: Part A: Polym. Chem. Ed.* **1986**, *24*, 3177-3189; (c) Radical-Initiated Homopolymerization and Copolymerization of Ethyl α-Hydroxymethylacrylate. Ueda, M.; Koyama, T.; Mano, M.; Yazawa, M. *J. Polym. Sci.: Part A: Polym. Chem. Ed*, **1989**, *27*, 751-762.

10. (a) Modeling the Free Radical Polymerization of Acrylates. Gunaydin, H.; Salman, S.; Tuzun, N. S.; Avci, D.; Aviyente, V. *Int. J. Quant. Chem.* **2005**, 103, 176-189. (b) Synthesis and Modeling of New Phosphorus-Containing Acrylates. Salman, S.; Ziylan Albayrak A.; Avcı, D.; Aviyente, V. *Journal of Polymer Science: Part A: Polymer Chemistry*, **2005**, *43*, 2574-2583.

11. Lalevee, J.; Allonas, X.; Fouassier, J. P. "Reactivity of Carbon-Centered Radicals Toward Acrylate Double Bonds: Relative Contribution of Polar vs Enthalpy Effects" *J. Phys. Chem. A.*, **2004**, *108*, 4326-4334.

12. Avci, D.; Mathias, L. J.; Thigpen, K. "Photopolymerization Studies of Alkyl and Aryl Ester Derivatives of Ethyl α-Hydroxymethylacrylate" *J. Polym. Sci., Part A: Polym. Chem.*, **1996**, *34*(15), 3191-3201.

13. Smith, T. J.; Shemper, B. S.; Nobles, J. S.; Casanova, A. M.; Ott, C.; Mathias, L. J. "Crosslinking kinetics of methyl and ethyl (α-hydroxymethyl)acrylates: effect of crosslinker type and functionality" *Polymer*, **2003,** *44*, 6211-6216.

14. Avci, D. *Private Communications,* **2006.**

15. "*Handbook of Radical Polymerization*" edited by K.Matyjaszewski and T. P. Davis, Wiley-Interscience, A John Wiley and Sons, Inc.Publication, **2002**.

16. (a) Laidler, K. J.; Hase, W. L.; Hynes, J. T. "Current Status of Transition-State Theory" *J. Phys. Chem.*, **1983**, *87*, 2664-2682. (b) Laidler, K. J.; King, M. C. "The Development of Transition-State Theory" *J. Phys. Chem.*, **1983**, *87*, 2657-2664. (c) Pechukas, P. "Transition State Theory" *Ann. Rev. Phys. Chem.*, **1981**, *32*, 159-177, (d) Pechukas, P. *Ber. Bunsen-Ges. Phys. Chem.*, **1982**, *86*, 372. (e) Truhlar, D.; Garrett, B. C.; Klippenstein, S. J. "Current Status of Transition-State Theory" *J. Phys. Chem.*, **1996**, *100*, 12771-12800.

17. “Physical Chemistry: A Molecular Approach” by Donald A. McQuarrie, John D. Simon, University Science Books, 1997.

18. (a) Bonta, G.; Gallo, B. M.; Russo, S.; Uliana, C. “Radiochemical Study of The Radical Copolymerization of Styrene and Methyl Methacrylate” *Polymer*, **1976**, *17*, 217-220. (b) Ayrey, G.; Humphrey, M. J.; Poller, R. C. “Radiochemical Studies of Free-Radical Vinyl Polymerizations: 7. Polymerization of Methyl Acrylate” *Polymer*, **1977**, *18*, 840-844. (c) Bamford, C. H.; Eastmond, G. C.; Whittle, D. “Network Formation III-Influence of Organometallic Initiator on NetworkStructure” *Polymer*, **1969**, *10*, 771-783.

19. Gaussian 03, Revision C.02, Frisch, M. J.; Trucks, G. W.; Schlegel, H. B.; Scuseria, G. E.; Robb, M. A.; Cheeseman, J. R.; Montgomery, Jr., J. A.; Vreven, T.; Kudin, K. N.; Burant, J. C.; Millam, J. M.; Iyengar, S. S.; Tomasi, J.; Barone, V.; Mennucci, B.; Cossi, M.; Scalmani, G.; Rega, N.; Petersson, G. A.; Nakatsuji, H.; Hada, M.; Ehara, M.; Toyota, K.; Fukuda, R.; Hasegawa, J.; Ishida, M.; Nakajima, T.; Honda, Y.; Kitao, O.; Nakai, H.; Klene, M.; Li, X.; Knox, J. E.; Hratchian, H. P.; Cross, J. B.; Bakken, V.; Adamo, C.; Jaramillo, J.; Gomperts, R.; Stratmann, R. E.; Yazyev, O.; Austin, A. J.; Cammi, R.; Pomelli, C.; Ochterski, J. W.; Ayala, P. Y.; Morokuma, K.; Voth, G. A.; Salvador, P.; Dannenberg, J. J.; Zakrzewski, V. G.; Dapprich, S.; Daniels, A. D.; Strain, M. C.; Farkas, O.; Malick, D. K.; Rabuck, A. D.; Raghavachari, K.; Foresman, J. B.; Ortiz, J. V.; Cui, Q.; Baboul, A. G.; Clifford, S.; Cioslowski, J.; Stefanov, B. B.; Liu, G.; Liashenko, A.; Piskorz, P.; Komaromi, I.; Martin, R. L.; Fox, D. J.; Keith, T.; Al-Laham, M. A.; Peng, C. Y.; Nanayakkara, A.; Challacombe, M.; Gill, P. M. W.; Johnson, B.; Chen, W.; Wong, M. W.; Gonzalez, C.; and Pople, J. A.; Gaussian, Inc., Wallingford CT, **2004**.

20. Becke, A. D. “Density-Functional Exchange-Energy Approximation With Correct Asymptotic Behavior” *Phys. Rev. A.*, **1988**, *38*, 3098-3100. (b) Lee, C.; Yang, W; Parr, R. G. “Development of The Colle-Salvetti Correlation-Energy Formula Into A Functional of The Electron Density” *Physical Review B.*, **1988**, *37*, 785-789. (c) Becke, A. D., “Density-Functional Thermochemistry. III. The Role of Exact Exchange” *J. Chem. Phys.*, **1993**, *98*, 5648-5652.

21. Hemelsoet, K.; Moran, D.; Van Speybroeck, V.; Waroquier, M.; Radom, L. "An Assessment of Theoretical Procedures for Predicting the Thermochemistry and Kinetics of Hydrogen Abstraction by Methyl Radical from Benzene" *J. Phys. Chem. A*, **2006**, *110*, 8942-8951.

22. (a) Gomez-Balderas, R.; Coote, M. L.; Henry, D. J.; Radom, L. "Reliable Theoretical Procedures for Calculating the Rate of Methyl Radical Addition to Carbon-Carbon Double and Triple Bonds" *J. Phys. Chem. A* , **2004**, *108*, 2874-2883. (b) Coote, M. L. "Reliable Theoretical Procedures for the Calculation of Electronic-Structure Information in Hydrogen Abstraction Reactions" *J. Phys. Chem. A*, **2004**, *108*, 3865-3872.

23. Boese, A. D.; Martin, J. M. L. "Development of Density Functionals For Thermochemical Kinetics" *J. Chem. Phys*. **2004**, *121*, 3405-3416.

24. Wood, G.P.F.; Rauk, A.; Radom, L. "Modeling β-Scission Reactions of Peptide Backbone Alkoxy Radicals: Backbone C-C Bond Fission" *J. Chem. Theory Comput*. **2005**, *1*, 889-899; Miller, D. J. Smith, D. M.; Chan. B.; Radom ,L. "Transfer Hydrogenation Between Ethane and Ethene: A Critical Assessment of Theoretical Procedures" *Molecular Physics* **2006**, *104*, 777-794. Wood, G. P. F.; Moran, D.; Jacob, R.; Radom, L. "Bond Dissociation Energies and Radical Stabilization Energies Associated With Model Peptide-Backbone Radicals" *J. Phys. Chem. A* **2005**, *109*, 6318-6325. Hemelsoet, K.; *J. Phys. Chem. A* **2006**, *110*, 8942-8951.

25. Van Speybroeck, V.; Van Neck, D.; Waroquier, M.; Wauters, S.; Saeys, M.; Marin, G. B. "Ab Initio Study of Radical Addition Reactions: Addition of a Primary Ethylbenzene Radical to Ethene (I)" *J. Phys. Chem. A* **2000,** *104* (46): 10939-10950, Vansteenkiste, P.; Van Speybroeck, V.; Marin, G. B.; Waroquier, M., *J. Phys. Chem. A* **2003**, *107* (17): 3139-3145. Van Speybroeck, V.; Vansteenkiste, P.; Van Neck, D.; Waroquier, M. "Ab Initio Calculation of Entropy and Heat Capacity of Gas-Phase *n*-Alkanes Using Internal Rotations" *Chem. Phys. Lett*., **2005**, 402, 479-484.

26. Van Cauter, K.; Van Speybroeck, V.; Vansteenkiste, P.; Reyniers, M. F.; Waroquier, M. "Ab Initio Study of Free-Radical Polymerization: Polyethylene Propagation Kinetics" *ChemPhysChem*, **2006**, *7* (1): 131-140 .

27. Morrison, D.A.; Davis, T. P. “Studies On The Propagation Reaction In The Free Radical Polymerization of Ethyl α-Hydroxymethacrylate” *Macromol.Chem.Phys.*, **2000**, *201*, 2128-2137.

28. De La Rosa, A.; Heux, L.; Cavaille, J. Y.; Mazeau, K. “Molecular modeling of the mobility of poly(allyl alcohol), PAA, and poly(vinyl alcohol), PVA” *Polymer*, **2002**, *43*, 5665-5677.

29. Fischer, H.; Radom, L. “Factors Controlling the Addition of Carbon-Centered Radicals to Alkenes-An Experimental and Theoretical Perspective” *Angew. Chem. Int. Ed*. **2001**, *40*, 1340-1371.

30. Zammit, M.D.; Coote, M. L.; Davis, T. P.; Willett, G.D. *Macromolecules*, **1998**, *31*, 955-963.

31. (a) Troe, J., Chem. Rev. **2003**, *103*, 4565. (b) Wardlaw, D. W.; Marcus, R. A. *Adv. Chem. Phys*., **1988**, *70*(Part 1), 231. (c) Klippenstein, S. J., in the Chemical Dynamics and Kinetics of Small Radicals, ed. K. Liu and A. F. Wagner, World Scientific, Singapore, **1995**, Part 1, p. 120. (d) Truhlar, D. G.; Garrett, B. C.; Klippenstein, S. J. *J. Phys. Chem*., **1996**, *100*, 12771-12800. (e) Hase, W. L., *Acc. Chem. Res*., **1983**, *16*, 258.

32. Klippenstein, S. J.; Georgievskii, Y.; Harding, L. B. “Predictive Theory For The Combination Kinetics of Two Alkyl Radicals” *Phys. Chem. Chem. Phys*., **2006**, *8*, 1133-1147.

33. a) Tomasi, J.; Mennucci, B.; Cancès, E. *J. Mol. Struct. (THEOCHEM)* **1999**, *464*, 211. b) Cancès, M. T.; Mennucci, B.; Tomasi, J. *J. Chem. Phys*. **1997**, *107*, 3032. c) Mennucci, B. Tomasi, J. *J. Chem. Phys.* **1997**, 106, 5151. d) Mennucci, B. ; Cancès, E.; Tomasi, J. *J. Phys. Chem. B* **1997**, *101*, 10506.

34. Bondi, A. *J. Phys. Chem.* **1964**, *68*, 441.

35. Eckart, C. “Penetration Of A Potential Barrier” *Phys. Rev.* **1930**, *35*, 1303-1309.

36. Wigner, E. Z. *Phys. Chem. B* **1932**, *19*, 203.

5. DFT STUDY ON THE PROPAGATION KINETICS OF FREE-RADICAL POLYMERIZATION OF α–SUBSTITITED ACRYLATES

5.1. Introduction

Radical polymerization processes are complex processes involving many different reactions. Even in simple homopolymerization, initiation, propagation and termination steps occur, and also the propagating species may undergo chain transfer processes. The rates of these individual steps govern the overall rate of polymerization. In the literature, widely deviating values have been reported for rate coefficients. Pulsed laser polymerization size-exclusion chromatography (PLP-SEC) techniques have been used for propagation rate constants, k_p, measurements [1,2]. The ability to measure the rates of the individual reactions, and to study the reaction mechanisms and their structure-reactivity relationships will lead to the development of better kinetic models and better methods for controlling free radical polymerization [3]. From an experimental point of view the relation between the polymer chain length and the observed propagation rates for the bulk free-radical polymerization of styrene and methyl methacrylate has been studied by several groups. Olaj et al. observed a slight decrease of k_p in terms of chain length [4]. Willemse showed that k_p is only dependent on chain length in the oligomeric range [5], but this point of view has been rejected again by Olaj et al [6]. The latter claim that a long-range chain length dependence of k_p extends over several hundreds of propagation steps. This fact is interpreted in terms of a decrease of the monomer concentration at the site of propagation caused by the segments already added to the growing chain [4-6]. The use of quantum chemistry to calculate rate coefficients for free radical polymerization is expected to complement the experimental findings. Heuts et al. have used the transition state theory to predict accurate absolute rate coefficients in free-radical polymerization [7,8]. They have suggested the low frequency torsional mode of the forming bond to be treated as one-dimensional hindered internal rotor [9]. This model has been adopted by Van Speybroeck et al. who compared the calculated rate coefficients for radical addition reactions with a

two-dimensional method [10,11]. The latter have shown that the chain length dependence of the calculated propagation rate coefficient in polyethylene converges by the hexyl radical. Huang et al. have calculated the propagation rate coefficients of acrylonitrile and methacrylonitrile using a “heavy” unimer [12]. In this study, the frequency factor of methacrylonitrile has shown excellent agreement with experiment, but the barrier was highly dependent on the level of theory. Coote et al. have developed a systematic methodology for calculating accurate propagation rate coefficients in the free radical polymerization of acrylonitrile and vinyl chloride [13]. For small to medium-sized polymer systems the G3(MP2)-RAD methodology gave accurate results. For larger systems, G3(MP2)-RAD barriers have been approximated via an ONIOM-based approach in which the core is studied at G3(MP2)-RAD level and the substituent effects are modeled with the ROMP2/6-311+G(3df,2p) methodology [3]. Yu et al. have applied a similar systematic methodology to methyl acrylate (MA) and methyl methacrylate (MMA) monomers. B3LYP with five different basis sets (6-31G(d), 6-31G(d,p), 6-311G(d,p), 6-311+G(d,p), and 6-311G(3df,2p)), MPWB1K/6-31G(d,p) and B1B95/6-31G(d,p) were used in order to investigate the influence of the method and the basis set on the propagation kinetics of this class of monomers [14]. Recently, Değirmenci et al. have studied the reactivity of a series of acrylates and methacrylates in order to understand the effect of the pendant group size, the polarity of a pendant group and the nature of the pendant group (linear vs cyclic) on their polymerizability [15]. As we mentioned in our previous study on the free-radical polymerization of acrylates and methacrylates direct comparison between experiment and theory is not trivial and we tend to focus on relative trends rather than on the reproduction of absolute experimental values [15].

In this study, we model the propagation kinetics of six monomers displayed in Figure 5.1. The experimental propagation rate constants are known and are tabulated in Table 5.1. While the relative propagation rates of the monomers are discussed, various DFT functionals have been tested and the chain length dependence of the polymerization kinetics has been investigated. The tacticity of the widely used monomers MA and MMA has also been modeled. Comparison of the computational findings with experimental results is expected to shed light on the free radical polymerization (FRP) mechanism of this class of monomers.

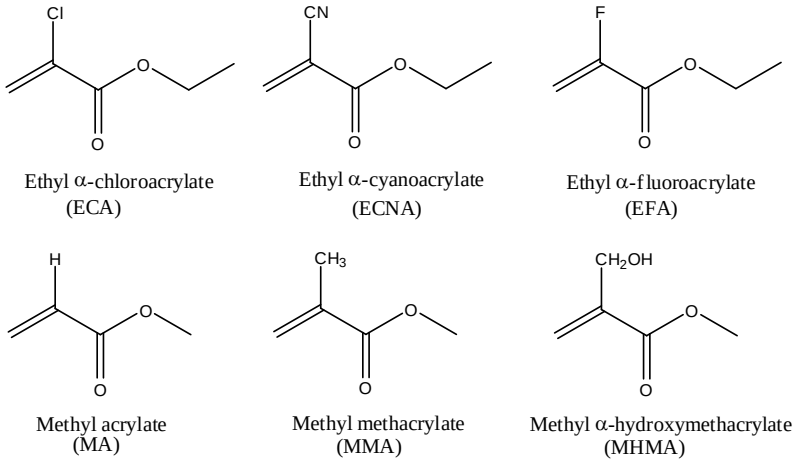

Figure 5.1. α -substituted acrylates considered in this study.

Table 5.1. Experimental propagation rate constants (k_p) of the α-substituted acrylates considered in this study at 30 ºC.

	Name	**k_p (m^3/mol.s)**	**Relative (k_p)**
M1	Ethyl α-chloroacrylate (ECA)	1.66E-00[c]	4.56
M2	Ethyl α-cyanoacrylate (ECNA)	1.62E-00[c]	4.46
M3	Ethyl α-fluoroacrylate (EFA)	1.12E-00[c]	3.08
M4	Methyl acrylate (MA)	1.48E+01[a,b]	40.67
M5	Methyl methacrylate (MMA)	3.64E-01 ± 0.020[a,b]	1.00
M6	Methyl α-hydroxymethacrylate (MHMA)	0.037[d]	-

References: [a] [16], [b] [17], [c] [18], [d] [19], [d] This is the rate of polymerization in $mol.L^{-1}.s^{-1}$.

5.2. Methodology

5.2.1. *Reaction Mechanism*

The free radical polymerization is known to start by the generation of free radicals from the non-radicalic species (initiator).

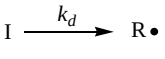

(initiation)

The radical R$^{\cdot}$, taken as the methyl ($CH_3^{\cdot}$) radical, adds to the acrylate monomer and forms a backbone with 3 C atoms. This species then adds to the monomer to generate the propagating polymer chain (propagation reaction).

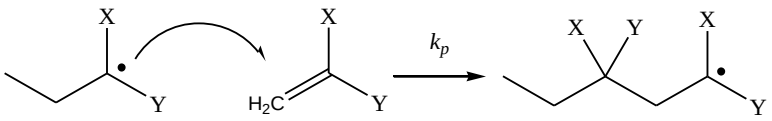

(propagation)

The propagation kinetics of the above mentioned reaction is modeled in this study. This scheme assumes head to tail propagation which was recently shown to be most favorable [20].

5.2.2. *Computational Procedure*

All geometry optimizations were performed by using the Gaussian 03 program package [21]. The B3LYP method is known to yield good ground state geometries but also to underestimate predictions for reaction barriers and to badly reproduce weak interaction energies [22]. We used the B3LYP/6-31+G(d) methodology for locating the stationary points along the potential energy surface since it is a cost effective method and was already used to model the free radical propagation reaction steps [14,15]. Various density functional methods BMK [23], BB1K [24,25], MPW1B95 [25], MPW1K [26], and MPWB1K [25], have been employed for the computation of the energetics starting from

the B3LYP/6-31+G(d) optimized structures. It is known that the more exact exchange is taken into account in DFT methods, the larger become reaction barriers resulting from the calculations [26]. The functionals fulfilling these requirements are BMK, MPW1K and MPWB1K and are expected to yield good results for kinetics and more particular higher (and presumably more realistic) barrier heights [23,25,26]. The best agreement with experiment has been in fact reproduced with the MPWB1K/6-311+G(3df,2p)// B3LYP/6-31+G(d) methodology.

5.2.3. *Reaction Kinetics*

The conventional transition state theory (TST) is used to calculate the rate constants. The rate equation of a bimolecular reaction $A+B\rightarrow C$ is given by [27]

$$k(T)=\frac{k_B T}{h}K_C^{\neq}$$

$$K_C^{\neq}=\frac{q_{TS}}{q_A q_B}e^{-\Delta E_0/k_B T}$$

where k_B represents Boltzmann's constant, T is the temperature, h is Planck's constant, ΔE_0 represents the molecular energy difference between the activated complex and the reactants (with inclusion of zero point vibrational energies), and q_{TS}, q_A and q_B are the molecular partition functions of the transition state and reactants, respectively.

5.3. Results and Discussion

Geometrical Features of the monomers and the radicals

A conformational search for the monomers and the radicals was carried out in order to find out the most stable structure of these species (Scheme 5.1). For all the species, the s-*cis* ($C_1C_2C_4O_7 = 0^o$) and s-*trans* ($C_1C_2C_4O_7 = 180^o$) conformers have the lowest energies (Figure 5.2.). All the monomers except MMA and MHMA are more stable in their s-*cis* conformations. Note that the s-*trans* conformer of MMA is 0.26 kcal/mol more stable than

its s-*cis* conformer and the barrier between the two conformers is around 5 kcal/mol (Figure 5.2). The s-*cis* preference of the monomers has been attributed to the stabilizing long range – $(C_1)H\ldots O_7$ interactions. The relative energies of the s-*cis*/s-*trans* monomers and syn/anti radicals ranges from 0.3 to 1.8 kcal/mol (Table 5.2).

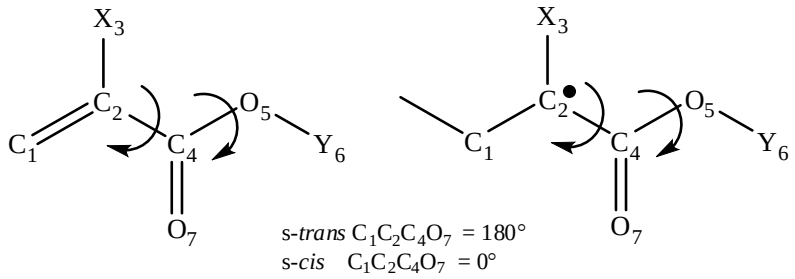

Scheme 5.1. Schematic representation of the monomers and their radicals.

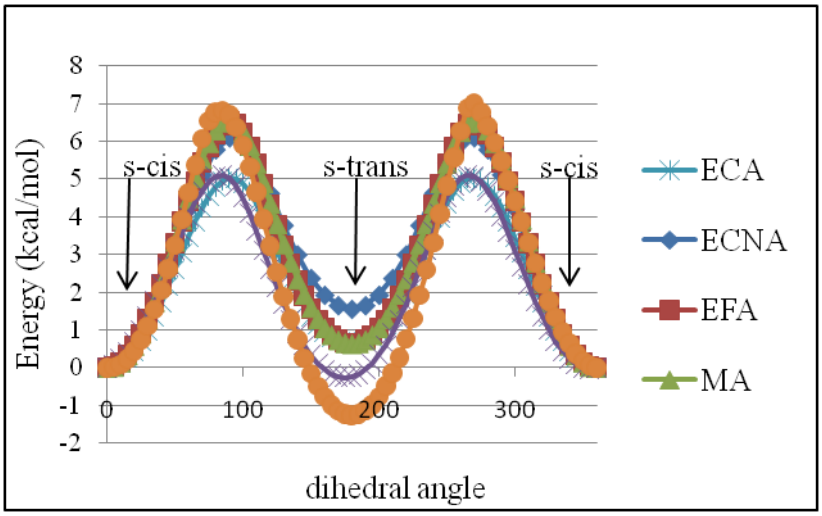

Figure 5.2. Rotational potential (kcal/mol) as a function of the dihedral angle ($C_1C_2C_4O_7$) for monomers M1-M6.

Table 5.2. Relative energies (kcal/mol) of the s-*cis* and s-*trans* conformers of the monomers and their radicals (B3LYP/6-31+G(d)).

	Monomer		Radical	
ECA(s-*cis)*	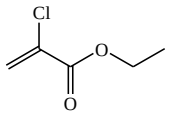	-0.60	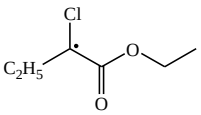	-1.14
ECA(s-*trans)*	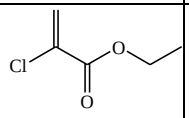	0.00	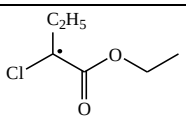	0.00
ECNA (s-*cis)*	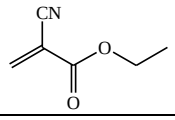	-1.47	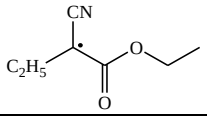	-1.74
ECNA(s-*trans)*	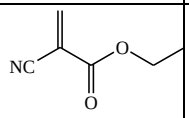	0.00	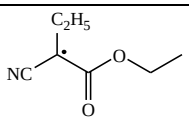	0.00
EFA (s-*cis)*	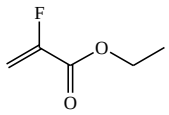	-0.61	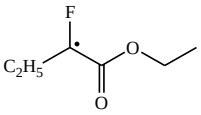	-1.14
EFA(s-*trans)*	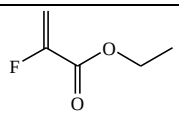	0.00	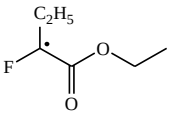	0.00
MA (s-*cis)*	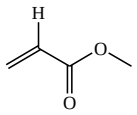	-0.64	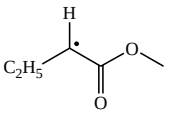	-0.54
MA(s-*trans)*	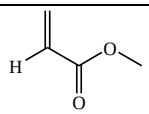	0.00	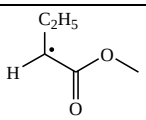	0.00
MMA (s-*cis)*	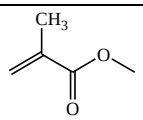	0.00	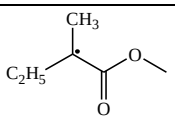	-0.06
MMA(s-*trans)*	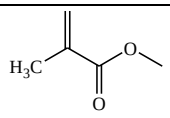	-0.26	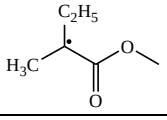	0.00
MHMA(s-*cis)*	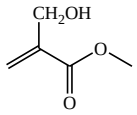	0.00	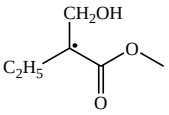	0.00
MHMA(s-*trans)*	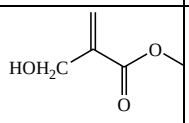	-1.11	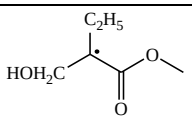	-0.99

In order to dissect the different stabilizing factors in s-*cis* and s-*trans* conformations, NBO analysis at the B3LYP/6-311+G(3df,2p)//B3LYP/6-31+G(d) level has been carried out for MA and MMA [28]. The hyperconjugative energy of 'donor-acceptor' (bond-antibond) interactions in the NBO analysis has been considered to quantify the bond delocalization energy. For MA, the hyperconjugative interaction energy for the *s-cis* conformer is 7.56 kcal/mol higher than the one for its *s-trans* conformer. Similarly, for MMA the *s-cis* conformer is more stabilized (8.82 kcal/mol) than the *s-trans* conformer due to hyperconjugative interactions. The main contribution to the stabilization of the monomer structure comes from anti-bonding interactions between BD*(2) $C_4 = O_7 \rightarrow$ BD*(2) $C_1 = C_2$**.** On the other hand, both in the s-*cis* and s-*trans* conformers of MA and MMA, the charge separations lead to electrostatic interactions that play a crucial role (Figure 5.3).Close inspection of the electrostatic attraction forces reveal the fact that in both cases the s-*trans* conformer is favored over the s-*cis.* However notice also that in the case of s-*trans* MMA the carbonyl oxygen,O_7, is in close proximity with 4 H atoms whereas in the case of s-*trans* MA the carbonyl oxygen interacts only with 3 H's. Thus, the extra stabilization of the s-*trans* MMA with respect to the s-*cis* MMA can be attributed to the long range attractive interactions between the carbonyl oxygen and the methyl group. This stabilizing interaction is missing in MA. Overall, even though delocalization stabilizes the s-*cis* conformations of MA and MMA, the electrostatic interactions between the methyl group and the carbonyl oxygen can be considered as the major source stabilizing the s-*trans* conformation of MMA.

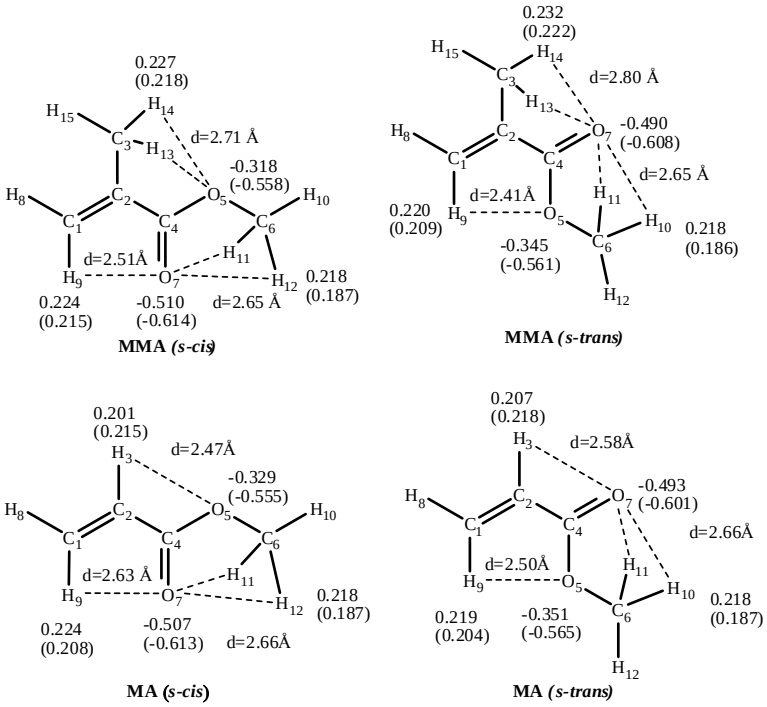

Figure 5.3. Mulliken and NBO charges (in parenthesis) of the most stable s-*cis* and s-*trans* conformers of MMA and MA.

Tacticity of MA and MMA

Although various effective methods of stereoregulation have been devised for anionic and coordination polymerizations, only limited successful examples are known for free-radical polymerization even though many classes of polymers are industrially produced by radical catalysis [2,29]. Therefore, the stereoregulation of radical polymerization is an especially challenging goal. The tacticity of vinyl polymers often significantly affects the properties of the polymers. However, many industrially important vinyl polymers including poly(methyl methacrylate) (PMMA) and polystyrene (PS) are produced by radical polymerization, which is more versatile and economical compared with other types of polymerizations, but is generally poor in stereocontrol. Hence, the development of stereoregulation methods for radical polymerization can contribute to the industrial production of polymers with improved properties [2]. The control of the stereochemistry in acrylate polymerizations is important because physical properties of acrylate polymers are often significantly influenced by the main-chain tacticity. In a recent experimental study the syndiotactic/isotactic ratio of MMA has been found to be 66/3 [29]. Thus, in this study, the tacticity of the polymerizing chain has been analyzed prior to the

kinetics of propagation. We demonstrate that the growing polymer radical, which is generated from the s-*trans* and s-*cis* conformers of the monomer, produces two different stereoisomers. The transition structures for all the monomers under investigation have been located by considering the attack of the radical in the form of $CH_3CH_2C.(X)$-$C(O)$-OCH_3 to the monomer ($H_2C=C(X)$-$C(O)$-OCH_3). As depicted in Scheme 5.2, there are two approaches of the radical to the monomer leading to distinct transition states, labeled (+) and (-). Attack from the (+) direction yields syndiotactic products while attack from the (-) direction yields isotactic products, emphasizing that the direction of attack ((+) or (-)) specifies the tacticity of the final product. Overall we have located eight different transition states generated by the attack of the syn and anti conformers of each radical to the s-*cis* and s-*trans* conformers of the monomer. The tacticity of the products, as well the reaction barriers relative to the most favorable transition state are given in Table 5.3.

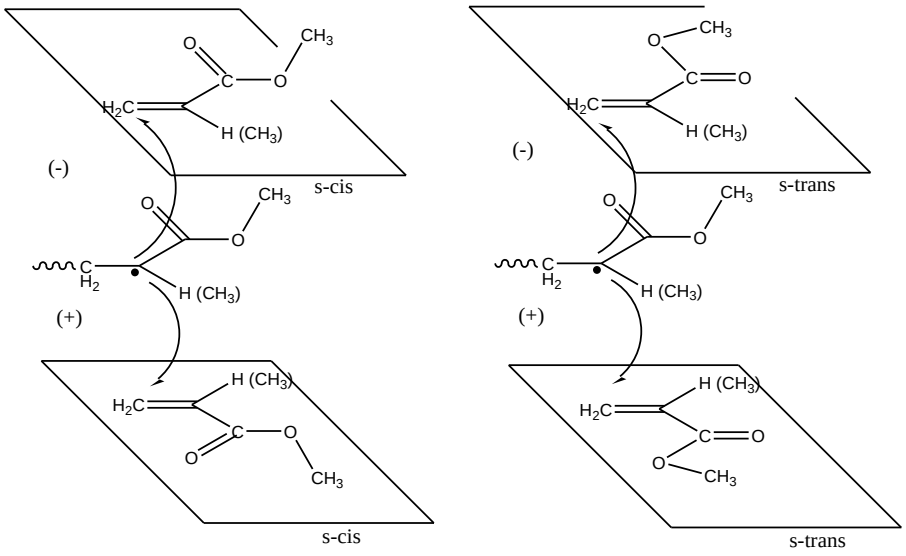

Scheme 5.2. Stereoselective radical (*syn*) addition to MA (MMA) (s-*cis* and s-*trans*).

A rotational potential energy scan is performed for rotation about the forming bond in the search for each transition state. This study reveals that the addition of the *syn*-MA and *syn*-MMA radicals to the s-*cis*-MA and s-*cis*-MMA monomers from the (+) direction yielding a syndiotactic chain is favored over the others (Table 5.3). Nevertheless the attack along the reverse side of the monomer (the (-) direction) leading to an isotactic dimeric chain requires slightly more energy and hence both reactions are competitive with respect to each other. For the syndiotactic polymerization of MA starting from the s-*cis*

stereoconformation two significant minima are found in the rotational potential energy curve : the global minimum is found at torsional angle θ ($C_1C_2C_3C_4$) = 176.83º ; the local minimum corresponding to a gauche addition is barely higher (Figure 5.4). A similar procedure is followed for the isotactic polymerization of MA for which the global minimum along the potential energy surface of the forming bond lies at θ = 49.60º. The local minimum for the transition structure is still the gauche addition (θ = -50.70º) (Figure 5.4).

Table 5.3 also reveals that the reaction barriers of the addition reactions belonging to the other stereoisomers – besides s-*cis*- are somewhat higher, but conclusive remarks should be handled with care since the change of monomer from MA to MMA reduces the reaction barrier differences within a range of 0.9 kcal/mol. In this study, the propagation kinetics for all the monomers of interest will be modeled for the attack of the *syn* radical to the s-*cis* monomer from the (+) direction.

Table 5.3. Relative reaction barriers (B3LYP/6-31+G(d), kcal/mol) for the transition states leading to syndiotactic and isotactic MA(MMA) dimeric chains .

R\M	s-*cis*	s-*trans*
syn (+)	syndiotactic 0.00(0.00)	syndiotactic 1.15(0.69)
syn (-)	isotactic 0.17(0.29)	isotactic 1.04(0.79)
anti (+)	syndiotactic 1.12(0.35)	syndiotactic 2.15(0.87)
anti (-)	isotactic 1.07(0.23)	isotactic 1.91(0.83)

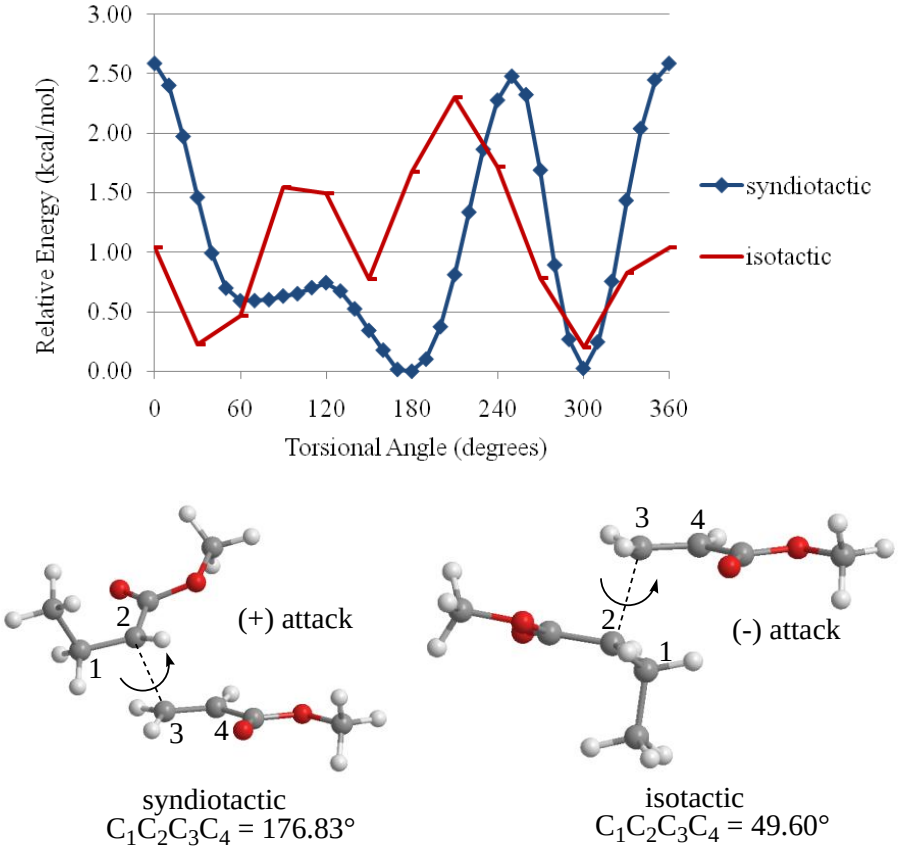

Figure 5.4. Rotational potential energy scan and transition state structures for syndiotactic (syn(+)s-*cis*) and isotactic (syn(-)s-*cis*) propagation of MA (B3LYP/6-31+G(d)).

Similarly, for the syndiotactic polymerization of MMA the global minimum along the potential energy scan around the forming bond lies at torsional angle θ ($C_1C_2C_3C_4$) = 60.13º; The local minimum for the transition structure is the anti addition θ = -170.02º. For the isotactic polymerization of MMA , the global minimum lies at θ = 49.88º. The local minimum for the transition structure is the gauche addition (θ = -71.63º) which corresponds to ~300º (Figure 5.5).

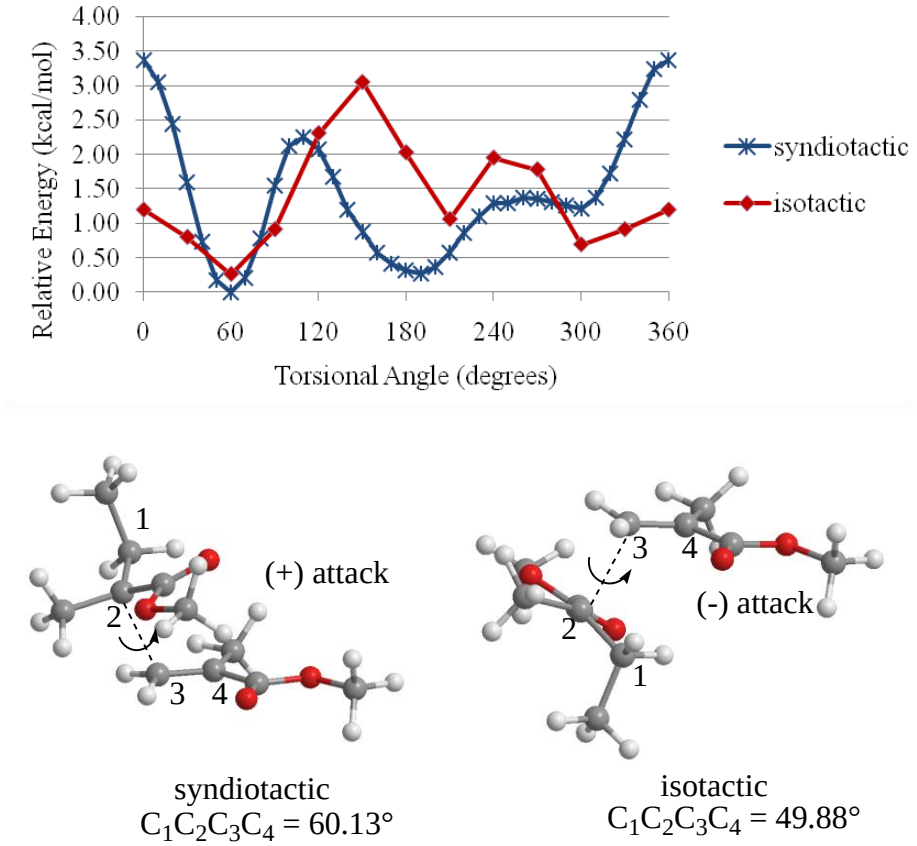

Figure 5.5. Potential energy scan and transition state structures for syndiotactic (syn(+)s-*cis*) and isotactic (syn (-)s-*cis*) propagation of MMA (B3LYP/6-31+G(d)).

A conformer search about the newly formed bond was carried out for the syndiotactic polymers (dimeric chains)- for MMA and MA (Figure 5.6). It is clearly seen that in both cases the growing backbone tends to be in a plane, the carbon atoms of the growing backbone being anti to each other. (Figure 5.7).

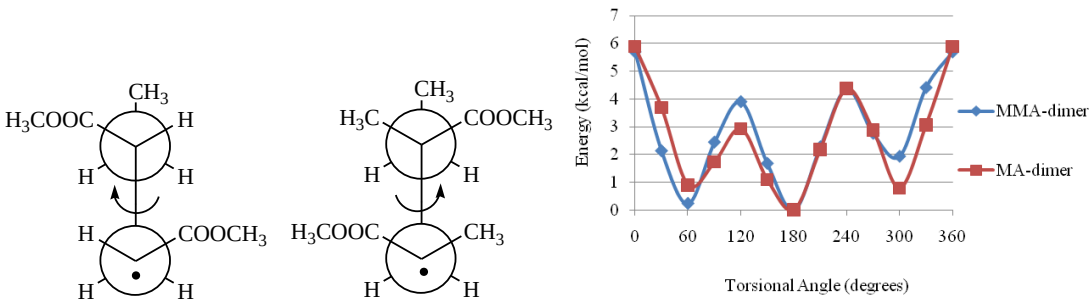

Figure 5.6. Conformational search for the intermediate products (dimeric chains) of MA and MMA and their Newman projections.

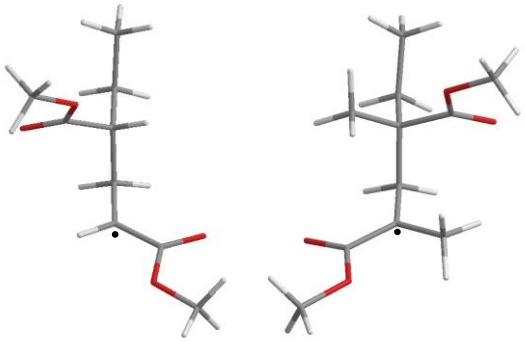

MA-dimer MMA-dimer

Figure 5.7. 3D structures for the intermediate products (dimeric chains) of MA and MMA.

Transition structures for the propagation of the monomers

For all the monomers-except MHMA-, the most favorable transition structures correspond to the attack of the radical in a *syn* conformation to the s-*cis* stereoisomer of the monomer (Figure 5.8). The *s-trans* conformer of MHMA is favored over its *s-cis* conformer, because of the intramolecular hydrogen bonding interactions between the -CH_2OH group and the carbonyl oxygen. The geometries of the transition states are such that the attack of the radical to the monomer is gauche except for MA. The potential energy scans for MMA, ECA, EFA and ECNA have their minima at approximately similar torsional angles of ~ 60º.

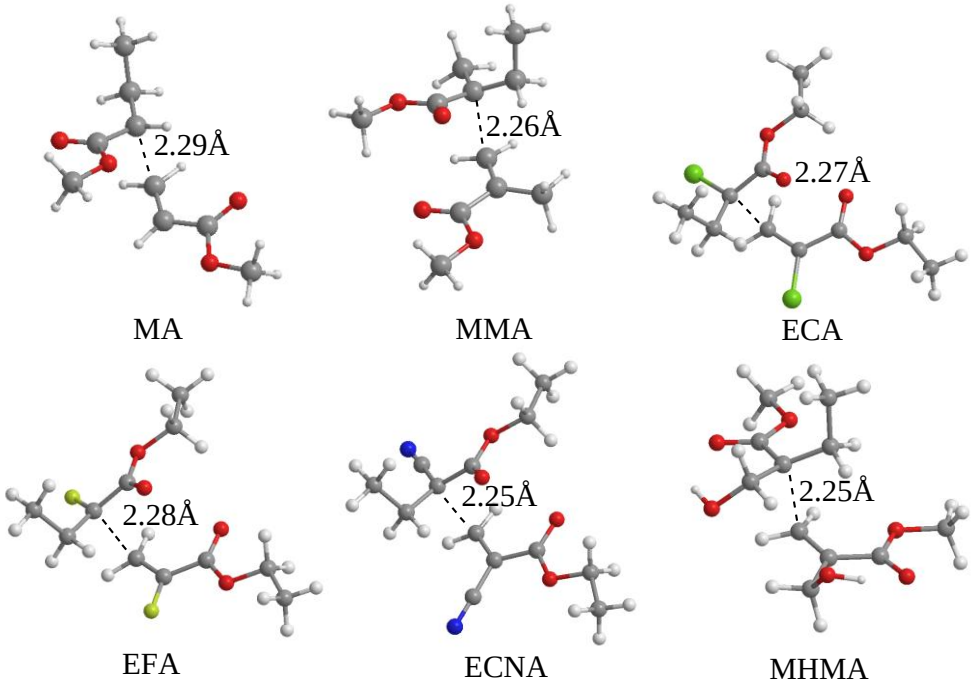

Figure 5.8. Most stable transition structures for the propagation of the monomers (B3LYP/6-31+G(d)).

The C…C bond distance of the forming bond in the transition states shows a relatively good relationship with the heat of the propagation reaction, $-\Delta H_{rxn}$ (Figure 5.9). The longer the C-C distance, the more the structure resembles the separated reactants, the closer is the transition structure to the reactants and finally the more exothermic the reaction is as expected from Hammond's postulate. The addition of a reactive carbon-centered radical to a molecule with a multiple carbon- carbon bond is generally exothermic because a π bond is replaced by a σ bond [30]. Therefore, and according to Hammond's postulate [31], the transition state is early, that is, the cleavage of the π bond and the formation of the σ bond are far from being complete in the transition structure.

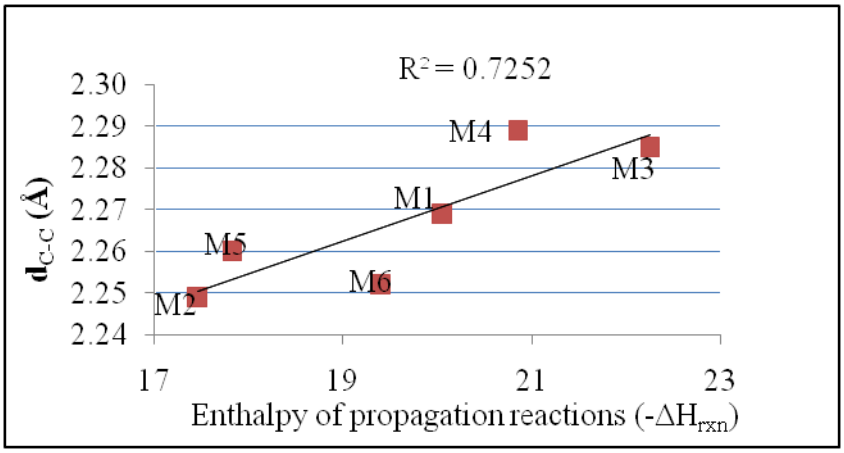

Figure 5.9. Dependence of the C…C bond distance on the heat of reaction ($-\Delta H_{rxn}$) in the transition states of the dimeric radicals (MPWB1K/6-311+G(3df,2p)// B3LYP/6-31+G(d)).

Propagation rate constants of the various monomers at different levels of theory

In the preceding subsections the geometrical features and the tacticity control in the free radical polymerization of MA and MMA have been discussed. It has been demonstrated that syndiospecific and isospecific propagations take place with a slight preference for the formation of syndiotactic MA (MMA) dimeric chains. However, the differences in reaction barriers are very low and are not really conclusive due to the rather low level of theory (B3LYP/6-31+G(d)). Nevertheless, this study gives a qualitative overview of the various stereospecific radical polymerization reactions. In what follows we have attempted to have a deeper understanding of the kinetics of the free radical polymerization of the acrylate derivatives with the aim of testing DFT functionals which would yield propagation rate constants closer to the experimental ones. Table 5.4 gathers the free radical propagation rate constants of the various monomers obtained at different levels of theory together with the experimental results. A reliable methodological approach for studying radical propagation reactions is expected to stem from this study. The transition structures for the dimeric syndiotactic chains (syn(+)s-*cis*) are considered in every case. The level of theory (LOT) study showed that the most reliable results are obtained by using MPWB1K and MPW1B95 methods (Figure 5.10). Nevertheless the experimental trend is best reproduced with MPWB1K and the kinetics in this study are evaluated with this method.

Table 5.4. Propagation rate constants (k_p) of the monomers at different levels of theories in the temperature range 250 < T < 350 K. Geometries are calculated at the B3LYP/6-31+G(d) level, kinetics are determined with different DFT methods at the 6-311+G(3df,2p) level unless otherwise stated.

	B3LYP /6-31+G(d)	B3LYP	BMK	MPW1K	BB1K	MPWB1K	MPW1B95	Exp. k_p (m^3/mol.s)
ECA	2.45E-04	6.08E-05	8.44E-03	2.02E-03	2.77E-03	3.77E-02	6.09E-02	1.66E-00[c]
ECNA	1.10E-04	4.13E-06	3.58E-03	1.38E-03	1.60E-03	2.14E-02	3.81E-02	1.62E-00[c]
EFA	3.46E-03	8.68E-04	8.01E-03	9.13E-03	4.67E-03	5.24E-02	1.01E-01	1.12E-00[c]
MA	1.29E-02	4.24E-03	2.31E-02	4.47E-02	1.75E-02	1.11E-01	2.36E-01	1.48E+01[a,b]
MMA	7.43E-06	1.70E-06	2.84E-04	7.55E-05	1.72E-04	2.63E-03	3.91E-03	3.64E-01[a,b]
MHMA	3.37E-04		1.34E-02	2.56E-03	1.09E-02	1.63E-01	2.62E-01	

References: [a] [16], [b] [17], [c] [18],

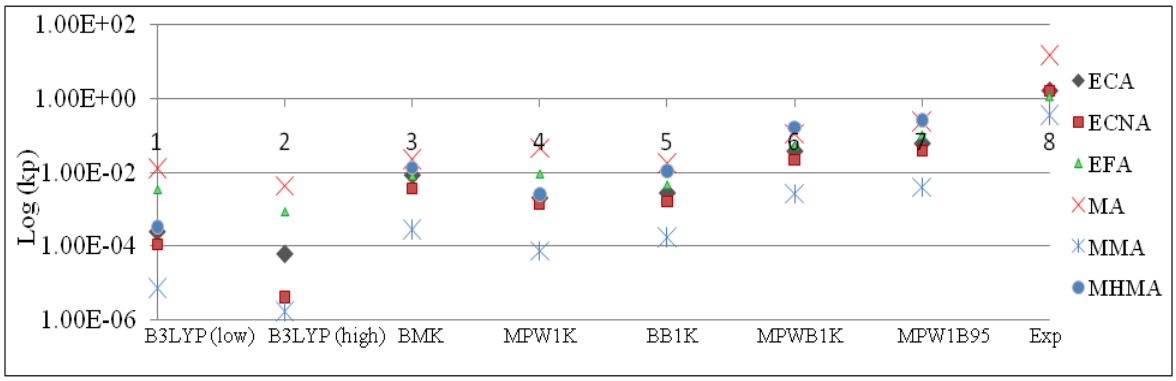

Figure 5.10. Log(k_p) versus different methodologies.

Chain Length Dependency

Earlier studies in the literature have clearly shown that the use of too short chains can incur large errors, and this adds further support to the notion that penultimate unit effects are important in free-radical copolymerization. Coote et al. have shown that for acrylonitrile and vinyl chloride the minimum-sized chemical model that can reliably mimic the polymerization system is the n = 1.5 system (n is an integer that labels the propagation reaction, n = 1 for a unimer, n = 2 for a dimer etc). This model has produced excellent relative values of the barriers and frequency factors, and has produced absolute values of

the rate coefficients that agree to within a factor of 1.6 of their corresponding long chain values. Scheme 5.3 illustrates how the chain length effect on propagation rate constant is modeled. We used the monomeric radical and the monomer itself to calculate k_{P1}. k_{P2} is calculated by the attack of the generated dimeric radical chain to the monomer. The third and fourth steps are also modeled in the same way. The chain length dependency is illustrated by the attack of the radical in a *syn* conformation to the s-*cis* stereoisomer of the monomer while the chain grows.

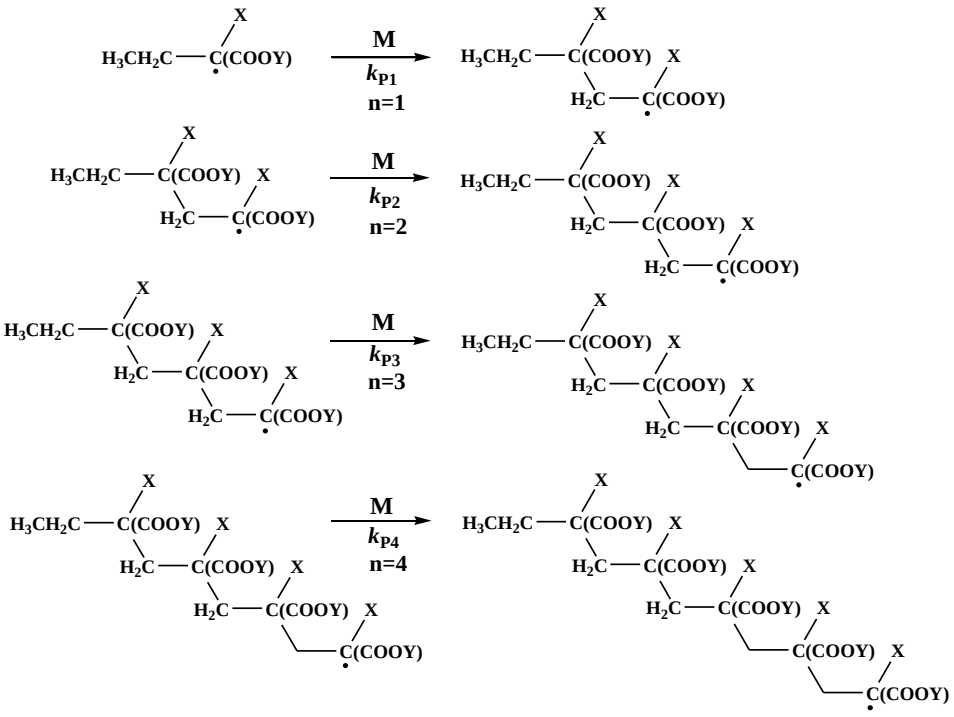

Scheme 5.3. The propagation steps of the growing chain. (X= -H, -CH_3, -F, -Cl, -CN, -CH_2OH; Y= -CH_3 for MA, MMA, MHMA, and Y= -CH_2CH_3 for EFA, ECA, ECNA).

Table 5.5. Chain length dependency of the propagation rate constants k_p (m^3/mol.s) The transition structures for the dimeric syndiotactic chains (syn(+)s-cis) are considered in every case. (MPWB1K/6-311+G(3df,2p)//B3LYP/6-31+G(d) , 250 < T < 350K). Values in parenthesis are rate constants relative to MMA.

	n=1	n=2	n=3	n=4	Exp. k_p
ECA	3.77E-02 (14.34)	4.36E-03 (8.17)	3.49E-03 (2.97)	5.33E-03 (6.11)	1.66E-00 (4.56)
ECNA	2.14E-02 (8.14)	6.85E-03 (12.85)	1.76E-02 (14.98)	5.16E-03 (5.92)	1.62E-00 (4.46)
EFA	5.24E-02 (19.93)	1.82E-02 (34.19)	3.56E-02 (30.24)	2.59E-02 (29.65)	1.12E-00 (3.08)
MA	1.11E-01 (42.16)	1.09E-01 (205.12)	8.72E-02 (74.05)	6.33E-02 (72.64)	1.48E+01 (40.67)
MMA	2.63E-03 (1.00)	5.34E-04 (1.00)	1.18E-03 (1.00)	8.72E-04 (1.00)	3.64E-01 (1.00)
MHMA	1.63E-01 (61.96)	1.53E-01 (287.48)	1.51E-01 (128.65)	1.71E-01 (195.53)	

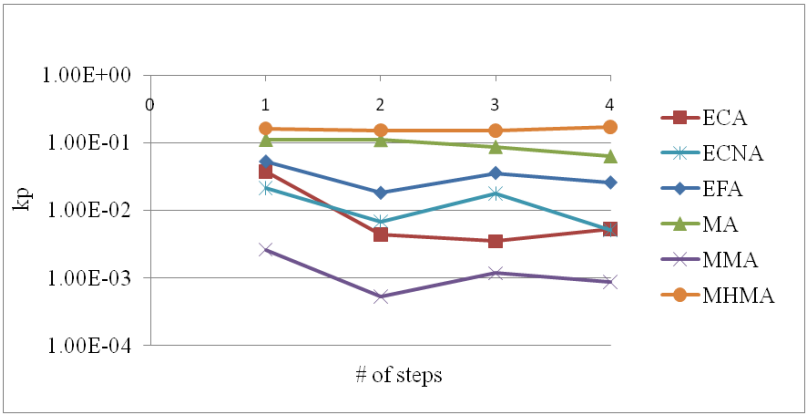

Figure 5.11. Propagation rate constant k_p (m^3/mol.s) as a function of the number of units in growing chain at MPWB1K/6-311+G(3df,2p)//B3LYP/6-31+G(d).

The results in Table 5.5 and Figure 5.11 show that the effect of the chain length on the propagation rate constants can amount to a factor of ten. Some rate constants are oscillating while others exhibit a smooth behavior. A real convergence regime is not yet reached at n=4; in general k_p decreases as the chain gets longer. Among the monomers of interest MMA propagates the slowest experimentally, this finding is reproduced no matter

what the length of the monomer is. In Table 5.5 the relative rate constants, k_p –in parenthesis- show a better agreement with experiment as the chain gets longer. There is one exception - EFA – where the predicted relative trend does not coincide with the experimental findings. The chain length dependence of all the monomers in this study is expected to converge as n increases as in previous studies of Van Cauter et al [11]. and Coote et al [13].

Syndiotactic versus isotactic polymerization of MMA

Isobe et al. have shown that the bulk polymerization of MMA gives an isotactic, atactic and syndiotactic mixture in the ratio of 3/31/66 respectively [2,29]. All the possible transition state structures leading to syndiotactic and isotactic MMA dimeric chains have been located to obtain average rate constants in each case (Figure 5.12). The rate constant for the isotactic transition state is denoted as *ki1* when starting from the s-*cis* monomer, it is denoted as *ki2* when starting from the s-*trans* monomer. Similarly, the rate constants are denoted as *ks1* and *ks2* for the corresponding syndiotactic transition states. The Boltzmann distribution is used to calculate the relative population of the s-*cis* and s-*trans* conformations of the monomer. The overall rate constant is the weight average of the two rate constants. In this way, the average rate constant for the syndiotactic product is $\langle ks \rangle$ = 2.29E-03 (Notice that this value is very close to the rate constant corresponding to the most probable path, 2.63E-03, reported earlier in Table 5.4 and 5.5). The average rate constant $\langle ki \rangle$ for the isotactic product is 1.01E-03. Thus, at the MPWB1K/6-311+G(3df,2p)//B3LYP/6-31+G(d) level the $\langle ks \rangle / \langle ki \rangle$ ratio is 2.28 in qualitative agreement with Isobe's results.[29] Overall, our calculations show the major component of PMMA to be syndiotactic as experimentally observed. The effect of the media on the kinetics and tacticity of the free radical polymerization of MMA has been investigated by Isobe et al., where the syndiotactic specificity of MMA was enhanced by the use of fluoroalcohols, including $(CF_3)_3COH$ as a solvent [29]. Our work in progress includes the free-radical polymerization of MMA in different media in order to assess the origin of the sterocontrol in the free-radical polymerization of MMA and lead experimentalits in their future endeavours.

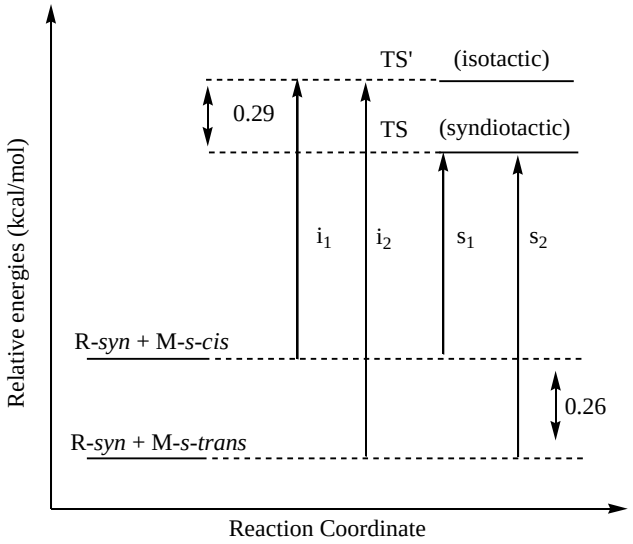

Figure 5.12. Most probable pathways for syndiotactic and isotactic MMA.

Initiation versus propagation reactions of MA and MMA

Even though MA polymerizes 40 times faster than MMA [16,17], the rate coefficients for the initiation of these monomers by the addition of 2-cyano-2-propyl radical generated from the decomposition of the commonly employed initiator 2,2'-azoisobutyronitrile [AIBN]) is 4.30 times faster for MMA [32]. This intriguing behavior of these two commercially widely used monomers has been clarified in what follows.

The MPWB1K/6-311+G(3df,2p)//B3LYP/6-31+G(d) methodology at 315.15K has been used to evaluate the average initiation rate constant $<k_{ini}>$ for MA as 1.95E-04 and the one for MMA as 1.02E-03. Also note that $<k_{ini}>$ in Table 5.6 refers to the average rate constant for the initiation of both MA and MMA relative to both the s-*cis* and s-*trans* conformations of the monomers. Figure 5.13 illustrates the addition of 2-cyano-2-propyl radical (i.e., the radical generated from the decomposition of the commonly employed initiator 2,2'-azoisobutyronitrile [AIBN]) to MA and MMA at 315.15K. Our results indicate the initiation of MMA to be 5.20 times faster than the initiation of MA. This ratio is in good qualitative agreement with the experimental results by Heuts et al. who have determined this ratio to be 4.30 based on the rate coefficients for the addition of 2-cyano-isopropyl radical to MA (0.37 m^3/mol.s) and to MMA (1.59 m^3/mol.s) [32].

Furthermore, Heuts et al. have found the initiation step of MA to have a higher energy barrier (2.7 kcal/mol) than the propagation step. This increase in the activation energy is claimed to be due to the stability of the conjugated cyano radical. Our computational results (Table 5.6) are in agreement with the experimental prediction: in both cases the activation barrier for initiation is higher than the one for propagation by ~2.5 kcal/mol. Experimentally, the accelerated initiation of MMA as compared to MA has been attributed to the magnitude of the preexponential factor, *A* [32]. Our calculations confirm the experimental behavior, the preexpeonential factor *A* is almost 3 times larger for MMA than for MA presumably because tertiary radicals (MMA-R) are expected to be less disordered than secondary radicals (MA-R).

The propagation reaction of MA is faster than the one of MMA because of the higher preexponential entropy factor –the transition state is more disordered- and also because of the lower activation barrier. In the case of MMA steric repulsions between the hydrogen atoms of the methyl groups repel each other (Figure 5.14). Not only steric repulsions but also electronic properties of the transition states have an important effect on the activation barriers (Table 5.6). The dipole moment of the most stable transition state for MMA-anti (μ = 2.036D) is higher than the one for the most stable transition state of MA-gauche (μ = 1.871D).

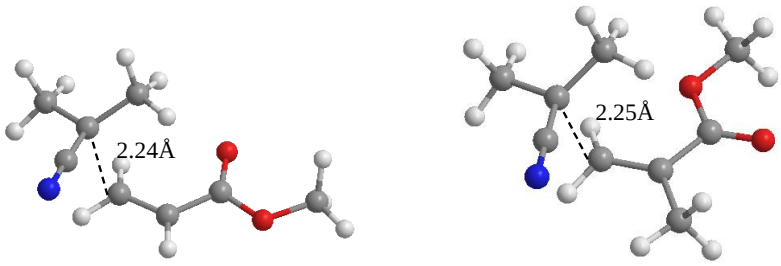

INI-MA-TS INI-MMA-TS

Figure 5.13. Initiation transition state geometries for MA and MMA (B3LYP/6-31+G(d)).

Table 5.6. Kinetic parameters for the initiation and the propagation steps of MA and MMA (MPWB1K/6-311+G(3df,2p)//B3LYP/6-31+G(d), (250 < T < 350K)). A and E_a refer to s-*cis* MA and s-*trans* MMA, $<k_{ini}>$ is the average rate constant for initiation for both conformations in both cases.

	Initiation			Propagation	
Monomer	A *(m^3/mol.s)*	E_a *(kcal/mol)*	Monomer	A *(m^3/mol.s)*	E_a *(kcal/mol)*
MA	2.02E+02	8.42	MA	2.02E+02	8.42
MMA	5.64E+02	8.49	MMA	5.64E+02	8.49

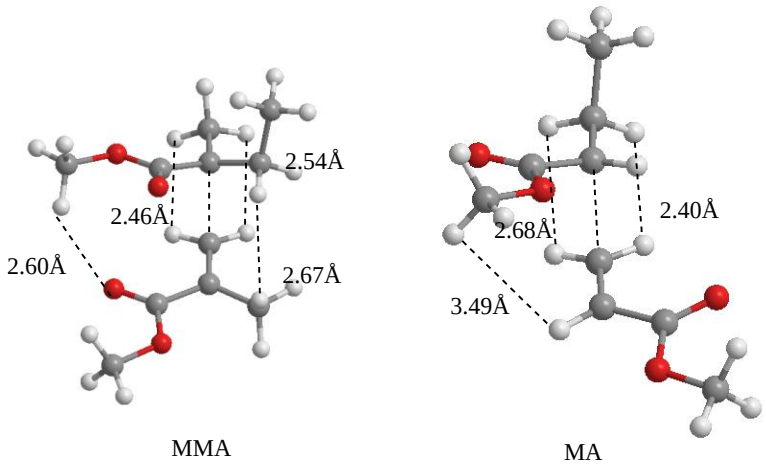

Figure 5.14. Representation of intramolecular interactions in the transition states of MMA and MA.

5.4. Conclusion

In this study, the propagation reaction in the free radical polymerization of methyl acrylate (MA), methyl methacrylate (MMA), ethyl α-fluoroacrylate (EFA), ethyl α-chloroacrylate (ECA), ethyl α-cyanoacrylate (ECNA), methyl α-hydroxymethacrylate (MHMA) has been modeled with DFT. Among the various functionals (BMK, BB1K, MPW1B95, MPW1K, MPWB1K) tested the MPWB1K/6-311+G(3df.2p)//B3LYP/6-31+G(d) methodolgy is found to give best agreement with experiment. The chain length dependency has been examined by the addition of monomeric, dimeric, trimeric and

tetrameric radicals to the monomers. The syndiotactic versus isotactic preference of MMA has been reproduced and finally the initiation versus propagation reactions of MA and MMA has been rationalized. Overall, this study has demonstrated the fact that computational chemistry offers a viable alternative to experiment: relative propagation rate coefficients as well as tacticity can be predicted prior to FRP.

5.5. References

1. (a) Heuts, J. P. A.; Russell, G. T.; Simith, G. B.; Van Herk, A. M. *Macromol. Symp.* **2007**, *248*, 12-22. (b) Buback, M.; Gilbert, R. G.; Hutchinson, R. A.; Klumperman, B.; Kuchta, F. D.; Manders, B. G.; O'Driscoll, K. F.; Russell, G. T.; Schweer, *J. Macromol. Chem. Phys*. **1995**, *196*, 3267. (c) Beuermann, S.; Buback, M.; Davis, T. P.; Gilbert, R. G.; Hutchinson, R. A.; Olaj, O. F.; Russell, G. T.; Schweer, J.; van Herk, A. M. *Macromol. Chem. Phys*. **1997**, *198*, 1545.

2. (a) Isobe, Y.; Yamada, K.; Nakano, T.; Okamoto, Y. *Macromolecules* **1999**, *32*, 5979-5981. (b) Nakano, T.; Okamoto, Y. In Controlled Radical Polymerization Matyjazsewski, K.; Ed.; ACS Symposium Series 685; American Chemical Society: Washington DC. **1998**; pp. 451- 462. (c) Pino, P.; Suter, U. W. *Polymer* **1976**, *17*, 977-995 (d) Hatada, K.; Kitayama, T.; Ute, K. *Prog. Polym. Sci.* **1988**, *13*, 189-276. (e) Yuki, H.; Hatada, K. *Adv. Polym. Sci*. **1979**, *31*, 1-45.

3. Coote, M. *Aust.J.Chem.* **2004**, *57*, 1125-1132.

4. Olaj, O. F.; Vana, P.; Zoder, M.; Kornherr, A.; Zifferer, G. *Macromol. Rapid Commun*. **2000**, *21*, 913-920.

5. Willemse, R. X. E.; Staal, B. B. P.; van Herk, A. M.; Pierik, S. C. J.; Klumperman, B. *Macromolecules* **2003**, *36*, 9797-9803.

6. Olaj, O. F.; Zoder, M.; Vana, P.; Kornherr, A.; Schnöll-Bitai, I.; Zifferer, G. *Macromolecules* **2005**, *38*, 1944-1948.

7. Heuts, J. P. A.; Gilbert, R. G.; Radom, L. *Macromolecules* **1995**, *28*, 8771-8781.

8. Heuts, J. P. A.; Gilbert, R. G.; Radom, L. *J. Phys. Chem*. **1996**, *100*, 18997-19006.

9. (a) Vansteenkiste, P.; Van Neck, D.; Van Speybroeck, V.; Waroquier, M. *J. Chem. Phys.* **2006**, *124* (4). (b) Art. No. 044314. Van Speybroeck, V.; Van Cauter, K.; Coussens, B.; Waroquier, M. *ChemPhysChem*. **2005**, *6* (1), 180-189. (c) Van Speybroeck, V.; Van Neck, D.; Waroquier, M.; Wauters, S.; Saeys, M.; Marin, G. B. *J. Phys. Chem. A*. **2000**, *104*, 10939-10950.

10. Van Speybroeck, V.; Van Neck, D.; Waroquier, M. *J. Phys. Chem. A*. **2002**, *106* (38), 8945-8950.

11. Van Cauter, K.; Van Speybroeck, V.; Vansteenkiste, P.; Reyniers, M. F.; Waroquier, M. *ChemPhysChem* **2006,** *7*, 131 – 140.

12. Huang, D. M.; Monteiro, M. J.; Gilbert, R. G. *Macromolecules* **1998**, *31*, 5175-5187.

13. Izgorodina, E. I.; Coote, M. *Chem. Phys.* **2006**, *324*, 96-110.

14. Yu, X.; Pfaendtner, J.; Broadbelt, L. J. *J. Phys. Chem. A*. **2008**, *112*, 6772-6782.

15. Değirmenci, I.; Avcı, D.; Aviyente, V.; Van Cauter, K.; Van Speybroeck, V.; Waroquier, M. *Macromolecules* **2007**, *40*, 9590-9602.

16. Buback, M.; Kurz, C. H.; Schmaltz, C. J. *Macromol. Chem. Phys*. **1998,** *199*, 1721-1727.

17. (a) Beuermann, S.; Buback, M.; Thomas, P. D.; Gilbert, R. G.; Hutchinson, R. H.; Olaj, O. F.; Russell, G. T.; Schweerh, J.; Van Herk, A. M. *Macromol. Chem. Phys*. **1997**, *198*, 1545-1560. (b) Zammit, M. D.; Coote, M.; Davis, T. P.; Willett, G. *Macromolecules* **1998**, *31*, 955-963. (c) Bauerman, S.; Buback, M. *Prog. Polym. Sci.* **2002**, *27*, 191-254. (d) Van Herk, A. M. *Macromol. Theory Simul*. **2000**, *9*, 433-441.

18. Yamada, B.; Kontani, T.; Yoshioka, M.; Otsu, T. *J. Polym. Sci. Polym. Chem. Ed.* **1984**, *22*, 2381-2393.

19. Avcı, D.; Mathias, L. J.; Thigpen, K. *J. Polym. Sci., Part A: Polym. Chem.* **1996**, *34* (15), 3191-3201.

20. Van Cauter, K.; Van Speybroeck, V.; Waroquier, M. *ChemPhysChem*, **2007**, *8*, 541-552.

21. Gaussian 03, Revision D.01, Frisch, M. J.; Trucks, G. W.; Schlegel, H. B.; Scuseria, G. E.; Robb, M. A.; Cheeseman, J. R.; Montgomery, Jr., J. A.; Vreven, T.; Kudin, K. N.; Burant, J. C.; Millam, J. M.; Iyengar, S. S.; Tomasi, J.; Barone, V.; Mennucci, B.; Cossi, M.; Scalmani, G.; Rega, N.; Petersson, G. A.; Nakatsuji, H.; Hada, M.; Ehara, M.; Toyota, K.; Fukuda, R.; Hasegawa, J.; Ishida, M.; Nakajima, T.; Honda, Y.; Kitao, O.; Nakai, H.; Klene, M.; Li, X.; Knox, J. E.; Hratchian, H. P.; Cross, J. B.; Bakken, V.; Adamo, C.; Jaramillo, J.; Gomperts, R.; Stratmann, R. E.; Yazyev, O.; Austin, A. J.; Cammi, R.; Pomelli, C.; Ochterski, J. W.; Ayala, P. Y.; Morokuma, K.; Voth, G. A.; Salvador, P.; Dannenberg, J. J.; Zakrzewski, V. G.; Dapprich, S.; Daniels, A. D.; Strain, M. C.; Farkas, O.; Malick, D. K.; Rabuck, A. D.; Raghavachari, K.; Foresman, J. B.; Ortiz, J. V.; Cui, Q.; Baboul, A. G.; Clifford, S.; Cioslowski, J.; Stefanov, B. B.; Liu, G.; Liashenko, A.; Piskorz, P.; Komaromi, I.; Martin, R. L.; Fox, D. J.; Keith, T.; Al-Laham, M. A.; Peng, C. Y.; Nanayakkara, A.; Challacombe, M.; Gill, P. M. W.; Johnson, B.; Chen, W.; Wong, M. W.; Gonzalez, C.; and Pople, J. A.; Gaussian. Inc., Wallingford CT, **2004**.

22. Smith, D. M.; Nicolaides, A.; Golding, B. T.; Radom, L. *J. Am. Chem. Soc*. **1998**, *120*. 10223-10233.

23. Boese, A. D.; Martin, J. M. L. *J. Chem. Phys.* **2004**, *121* (8), 3405-3416.

24. (a) Zhao, Y.; Lynch, B. J.; Truhlar, D. G. *J. Phys. Chem. A* **2004**, *108*, 2715-2719. (b) Zhao, Y.; González-García, N.; Truhlar, D. G. *J. Phys. Chem. A* **2005**, *109*, 2012-2018. (c) Sousa, S. S.; Fernandes, A. P.; Ramos, M. J. *J. Phys Chem A.* **2007**, *111*, 10439-10452.

25. Zhao, Y.; Truhlar, D. G. *J. Phys. Chem. A.* **2004**, *108* (33), 6908-6918.

26. Lynch, B. J.; Fast, P. L. Harris, M.; Truhlar, D. G.; *J. Phys. Chem. A* **2000**, *104* (21). 4811-4815.

27. McQuarrie, D. A.; Simon, J. D. *Physical Chemistry-A molecular approach; University Science Books*: Sausalito, CA, 1997.

28. (a) Reed, A. E.; Weinstock, R. B.; Weinhold, F. *J. Chem. Phys*. **1985** , *83* (2), 735-746. (b) Foster, P.; Weinhold, F. *J. Am. Chem. Soc.* **1980**, *102*, 7211-7218. (c) Reed, A.;

Weinhold, E. F. *J. Chem. Phys.* **1983**, *78*, 4066-4073. (d) Reed, A. E.; Weinhold, F. *J. Chem. Phys.* **1985**, *83*, 1736-1740. (e) Reed, A. E.; Curtiss, L. A.; Weinhold, F. *Chem. Rev.* **1988**, *88*, 899-926.

29. Isobe, Y.; Yamada, K.; Nakano, T.; Okamoto, Y. *J. Polym. Sci.. Part A: Polym. Chem.* **2000**, *38*, 4693–4703.

30. Fischer, H.; Radom, L. *Angew. Chem. Int. Ed.* **2001**, *40*, 1340 – 1371.

31. Hammond, G. S. *J. Am. Chem. Soc.* **1955**, *77*, 334-338.

32. Heuts, J. P. A.; Russell, G. T. *Euro. Polym. Jnl.* **2006**, *42*, 3–20.

6. MODELING THE SOLVENT EFFECT ON THE TACTICITY IN THE FREE RADICAL POLYMERIZATION OF METHYL METHACRYLATE

6.1. Introduction

The mechanical, thermal and chemical properties of polymers substantially depend on their primary structures as represented by tacticities, molecular weights, and their distributions [1]. The control of tacticity and molecular weight for synthetic polymers contributes to the development of new materials [2]. The precise control of the molecular weight and/or the chain microstructure during radical polymerization is one of the important issues in the field of polymer synthesis because the polymer properties, such as toughness, solvent resistance, surface properties, and thermal resistance, are significantly influenced by their stereoregularity [3]. The stereoregularity of a polymer main chain is referred to as tacticity. Tacticity deals with the relationship between two adjacent monomer units consisting of meso (*m*) and racemo (*r*) diads. In general, stereocontrol based on radical polymerization is difficult to attain because of the planar characteristics of the propagating radical at the chain-end carbon [4]. Although most of the stereospecific polymerizations were reported for the coordination polymerizations of olefins such as propylene, the stereocontrol during free radical polymerization reactions has recently become possible [5]. Many attempts to produce stereospecific or stereoregular polymers have been made in confined media, such as the solid state, inclusion compounds, porous materials, and templates [6,7]. In solution polymerization, it is more difficult to provide a stereospecific environment around the growing radical center, because the monomer and growing radical species move freely and diffuse in the reaction media. Therefore, vinyl monomers ordinarily produce polymers with an inherent tacticity specific to their chemical structures. From the viewpoint of production cost, solvent or additive-mediated systems might be the most promising solutions to obtain stereospecific polymers.

Okamoto and coworkers have reported the synthesis of highly stereocontrolled polymethacrylates [8], polyacrylamides [9-11], and polymethacrylamides [10-12] through radical polymerization using Lewis acids such as rare earth metal trifluoromethanesulfonates. Furthermore, fluorinated alcohols play an efficient role in controlling the stereospecificity of radical polymerizations of vinyl monomers [13-15]. A relevant study on how tacticity can arise by chain-end control in free radical polymerization of acrylates is given by Tanaka and Niwa [16]. The study suggested that the growing polymer radical end could control the stereochemistry of free radical polymerization depending on the s-*trans* and s-*cis* conformations of the monomer. Many industrially important vinyl polymers including PMMA are produced by free radical polymerization, which is generally poor in stereocontrol. Hence, the development of stereoregulation methods for radical polymerization can contribute to the industrial production of polymers with improved properties [17]. The control of the stereochemistry in MMA polymerization is important because the physical properties of PMMA are often significantly affected by the main-chain tacticity. In the free radical polymerization of MMA three different products are to be expected: syndiotactic (*rr*), isotactic (*mm*) and heterotactic (*mr*). Isobe *et al*. have enhanced the syndiotactic specificity of PMMA by using fluoroalcohols: the polymerization of MMA in perfluoro-*tert*-butyl alcohol (PFTB) $(CF_3)_3COH$ at -98 °C was achieved with the highest syndiotacticity (*rr* = 93 per cent), whereas the syndiotacticity of PMMA is only 85 per cent in methanol at -78 °C. Table 6.1 displays the tacticity ratios in the free radical polymerization of MMA at 20 °C .

Table 6.1. Tacticity in the Free Radical Polymerization of MMA in various solvents at 20 ºC [13c].

	Solvent	Tacticity mm/mr/rr
1	Bulk	3/31/66
2	CH_3OH	3/32/66
3	$(CF_3)_3COH$	1/24/75

Another issue concerns the solvent influence on the propagation kinetics in free radical polymerization. For a long time it was assumed that the solvent effects on the rate coefficients were rather small [18]. Propagation rate coefficients for styrene and methyl methacrylate (MMA) polymerizations in a wide variety of solvents (acetonitrile, dimethyl formamide, anisole, methyl isobutyrate, bromobenzene, benzene and 1,2-dichloroethane) only change mostly by around 10 per cent. (see review of S. Beuermann and references cited therein [18]). On the other hand certain solvents, such as benzyl alcohol [19,20], dimethylsulfoxide [20], N-methylpyrrolidinone [20], 2,6-dithiaheptane [21], and 1,5-dithiacyclooctane [21] turn out to induce a significant increase of k_p. In many cases hydrogen bonding is responsible for this observed increase. Experiments provided by data for acrylamide and N-isopropylacrylamide (NIPAM) suggest a strong increase of k_p upon addition of water to the system [22].

In this study, the role of methanol (CH_3OH) and 1,1,1,3,3,3-hexafluoro-2-(trifluoromethyl)propan-2-ol ($(CF_3)_3COH$) on the tacticity of MMA polymerization will be considered by examining the propagation rate constants for the syndiotactic and isotactic free radical polymerization of MMA.

6.2. Computational procedure

The B3LYP method combined with 6-31+G(d) basis set within the Gaussian 03 program package [23] was chosen as a cost effective and accurate method for geometry optimizations [24]. To verify that the transition states indeed connect the products and pre-reactive complexes, intrinsic reaction coordinate (IRC) [25] calculations were performed. All transition states are characterized by only one imaginary frequency and are true first order saddle points on the potential energy surface.

The energetics and kinetics have been evaluated with the MPWB1K/6-311+G(3df,2p)//B3LYP/6-31+G(d), B3LYP/6-311+G(3df,2p)//B3LYP/6-31+G(d), B3LYP/6-31+G(d)//B3LYP/6-31+G(d) and B2-PLYP/6-31+G(d)//B3LYP/6-31+G(d) methodologies.

The MPWB1K method has proven to be very successful for describing thermochemistry, reaction kinetics, hydrogen bonding, and weak interactions [26-29]. The B2-PLYP method, which combines the BLYP [30] functional with Hartree-Fock exchange and a perturbative second-order correlation part, is also used since it is a promising functional with a high accuracy, taking into account dispersion interactions [31].

To study the solvent effect, we first apply an explicit solvent model. Isobe *et al* have shown experimentally that the concentration of the MMA-$(CF_3)_3COH$ complex was highest when the molar ratio of the two components was approximately 1/1, indicating that the stoichiometry of the reaction was 1/1 [13c]. The interaction of the MMA monomer (M) and the radical ($R^{\cdot}$) with the solvent (S) has been considered as a two-step mechanism that involves a fast preequilibrium between the reactants and the solvent ($M\cdots S$ and $S\cdots R^{\cdot}$) followed by the formation of a pre-reactive complex $(S\text{-}R\text{-}M\text{-}S)^{\cdot}$, this procedure was performed earlier in reference 32.

Step 1:

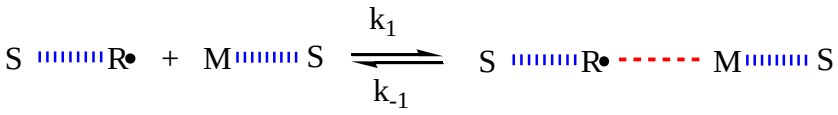

Step 2:

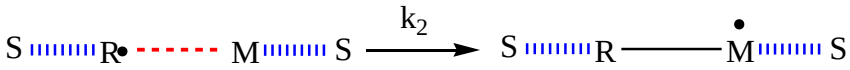

If k_1 and k_{-1} are the rate constants for the forward and reverse reactions in the first step and k_2 corresponds to the second step, the apparent kinetic parameters can be split up in two contributions : the rate coefficient (k_2) and the equilibrium constant K_1 for the formation of the pre-reactive complex (PRC) [33]. A schematic representation of the role of the pre-reactive complex in the apparent reaction rate coefficient is given in Scheme 6.1.

$$k_{app} = K_1 k_2 = \frac{k_1 k_2}{k_{-1}+k_2} \approx \frac{k_1 k_2}{k_{-1}} \qquad (1)$$

with the equilibrium constant of the fast equilibrium between the reactants and the pre-reactive complex obeying the basic statistical thermodynamic principles

$$K_1 = \frac{Q_{PRC}}{Q_R} \exp[\Delta E_0^{PRC}/RT] \quad (2)$$

ΔE_0^{PRC} represents the molar energy difference at 0 Kelvin between the reactants and the PRC including zero-point vibration energies (ZPVE) .

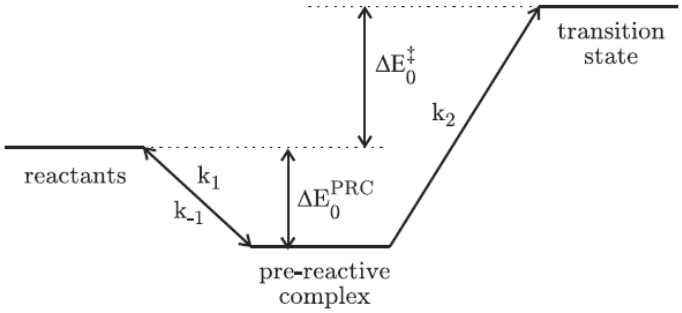

Scheme 6.1. Representation of the role of the pre-reactive complex in the apparent rate coefficient.

Q_{PRC} and Q_R are the pre-reactive complex and the reactants partition functions, respectively.

Similarly, the classical TST formula can be used to calculate k_2 [34]

$$k_2 = \sigma \frac{k_B T}{h} \frac{Q_{TS}}{Q_{PRC}} \exp\left[-(\Delta E_0^{\ddagger} + \Delta E_0^{PRC})/RT\right] \quad (3)$$

with $\Delta E_0^{\ddagger}$ the reaction barrier for the transition state including ZPVE. σ is the reaction path degeneracy that accounts for the number of equivalent reaction paths. k_B represents Boltzmann's constant, T is the temperature, h is Planck's constant. Finally, the apparent reaction rate coefficient k_{app} becomes

$$k_{app} = \sigma \frac{k_B T}{h} \frac{Q_{TS}}{Q_R} \exp[-\Delta E_0^{\ddagger}/RT] \quad (4)$$

This also means that calculating the reaction rate from separated reactants will result in exactly the same rate coefficients as compared to calculating the product of the equilibrium constant K_1 and the unimolecular reaction rate k_2. Although one could start from the separated reactants, the PRC concept is very valuable to get more insight into the role of the solvent molecules and their ability to stabilize the transition state [32].

Equation (4) can be rewritten in terms of the molecular Gibbs free energy difference $\Delta G^{\ddagger}$ between the activated complex and the reactants (with inclusion of zero point vibration energies):

$$k_{app} = \kappa \frac{k_B T}{h} \frac{RT}{p^{\theta}} \exp\left[-\Delta G^{\ddagger}/RT\right] \qquad (5)$$

where R represents the universal gas constant and κ the transmission coefficient which is assumed to be about 1 and p^{θ} is the standard pressure 10^5 Pa (1 bar) [35].

In the case where the solvent effect is considered implicitly as a polarized continuum medium, the effect of the environment was taken into account by use of the self-consistent reaction field (SCRF) theory, utilizing the integral equation formalism-polarizable continum (IEF-PCM) model [36]. In the case where the solvent effect has been modeled explicitly and implicitly the effect of the solvent is modeled as the sum of two contributions : one resulting from the explicit coordination with the individual solvent molecules in the reactants and transition states and one originating from the bulk solvent effect as in earlier publications [37].

6.3. Results

The free radical polymerization of MMA is known to start by the generation of free radicals from the non-radical species (initiator).

$$I \xrightarrow{k_d} R\bullet \qquad \text{(initiation)}$$

The radical $R^{\cdot}$, taken in this study as the methyl ($CH_3^{\cdot}$) radical, adds to the acrylate

monomer and forms a backbone with 3 C atoms. This radical species then adds to the monomer to generate the propagating polymer chain (propagation reaction). $CH_3^{\cdot}$ addition to the carbon-carbon double bond (C=C) was investigated elaborately by Radom et al [38]. Radical addition reaction kinetics of some vinyl monomers was modeled by Coote et al [39-41]. Head to tail propagation was assumed to be the most favorable mode of attack [34,42]. Several groups have modeled the structure-reactivity relationship of various acrylates and methacrylates by using quantum chemical tools [27-29,41,43].

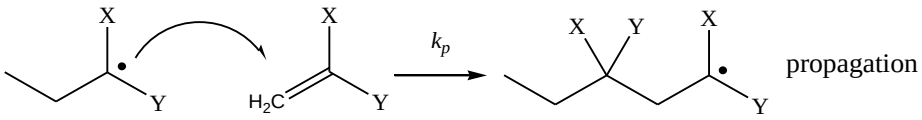

This study aims in elucidating the origins of the syndiotactic/isotactic stereospecificity in the free radical polymerization of MMA as depicted in Scheme 6.2.

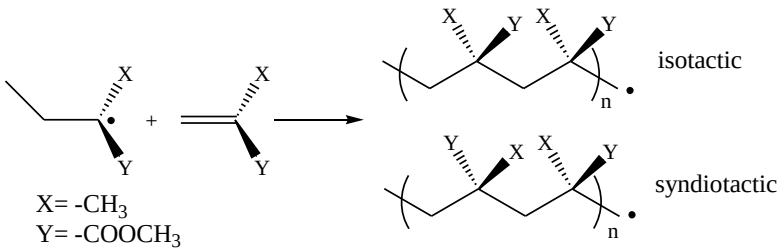

Scheme 6.2. Representation of isotactic and syndiotactic radical polymerization of MMA.

6.2.1. A Free Radical Polymerization of MMA in CH_3OH as solvent

MMA-CH_3OH complex

In vacuum, the most stable conformation of MMA is found to be s-*trans* ($C_1C_2C_4O_7$ = 180º) as shown in Scheme 6.3.

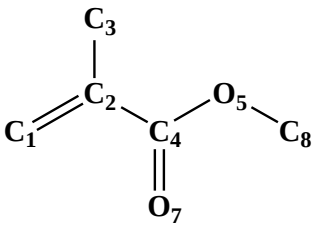

s-*cis* $C_1C_2C_4O_7$ = 0°
(0.39)

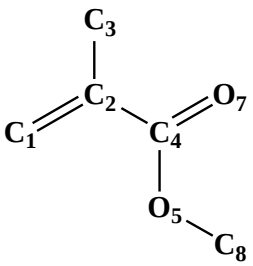

s-*trans* $C_1C_2C_4O_7$ = 180°
(0.00)

Scheme 6.3. Most stable conformations of MMA, relative energies in (kcal/mol) are given in parentheses (MPWB1K/6-311+G(3df,2p)//B3LYP/6-31+G(d)).

A conformational search for the MMA-CH_3OH complex was carried out in order to find out the most stable solvated structures of the monomer-solvent entity. For both s-*cis* and s-*trans* conformations the carbonyl oxygen is the only site to be prone to hydrogen bonding Among the conformations shown in Figure 6.1 complexation to the s-*trans* conformation of MMA from its methoxy side renders this complex (s-*trans*-m2) slightly more stable than the others. The relative energies of the s-*cis*/s-*trans* monomer-CH_3OH complexes range from 0.3 to 0.7 kcal/mol (Figure 6.1).

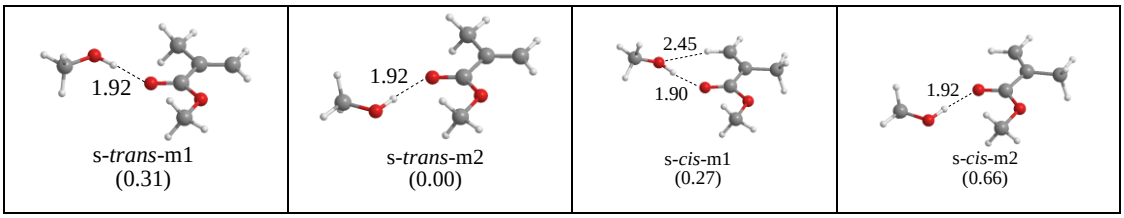

Figure 6.1. Relative energies (kcal/mol) of the s-*cis* and s-*trans* conformers of MMA with CH_3OH (MPWB1K/6-311+G(3df,2p)//B3LYP/6-31+G(d)).

MMAR-CH_3OH complex

In the gas phase the *syn* and *anti* conformation of the radical are almost isoenergetic, and both have been considered for the formation of possible MMAR-CH_3OH complexes (Scheme 6.4).

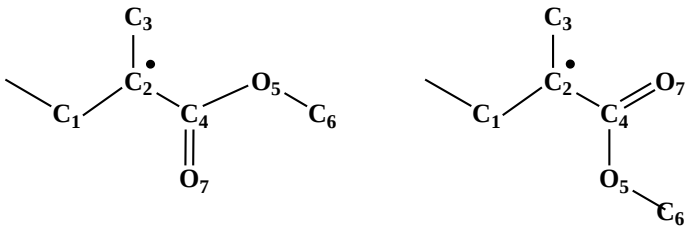

syn-r $C_1C_2C_4O_7$ = 0° (0.00)

anti-r $C_1C_2C_4O_7$ = 180° (0.01)

Scheme 6.4. Most stable conformations of MMAR, relative energies in (kcal/mol) are given in parentheses (MPWB1K/6-311+G(3df,2p)//B3LYP/6-31+G(d)).

Complexation of the radical with the methanol solvent does not alter significantly the energetics : the difference in binding energy between the *syn*-r and *anti*-r remains negligible (Figure 6.2). CH_3OH preferentially binds to the carbonyl oxygen (*syn*-r1 and *syn*-r2) of the radical. The global minimum for the *syn* conformer of the radical is found to be the structure where methanol forms a hydrogen bond with the carbonyl oxygen with the methyl group away from the propagating chain, the *anti* conformation is slightly more stable than *syn* conformation. The relative energies of the radicals range from 0.1 to 0.5 kcal/mol (Figure 6.2).

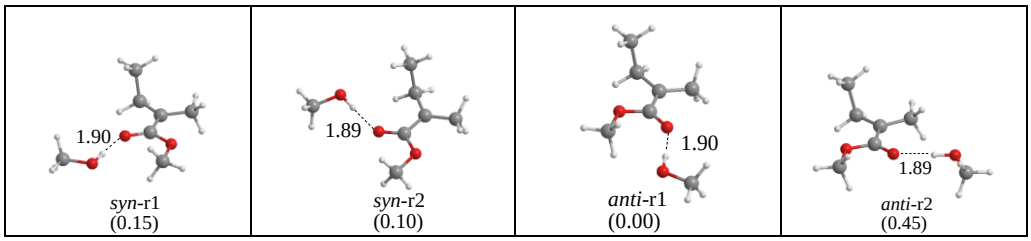

syn-r1 (0.15) | *syn*-r2 (0.10) | *anti*-r1 (0.00) | *anti*-r2 (0.45)

Figure 6.2. Relative energies (kcal/mol) of the various conformations of the MMAR-CH_3OH complexes (MPWB1K/6-311+G(3df,2p)//B3LYP/6-31+G(d).

Transition Structures and Pre-reactive Complexes

The radical can attack the double bond of the monomer to yield either the isotactic or syndiotactic dimer based on the relative orientation of the two species (Scheme 6.5).

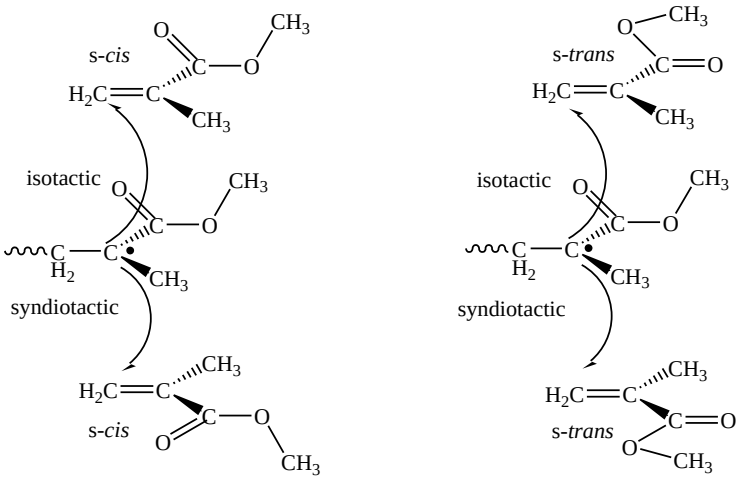

Scheme 6.5. Stereoselective radical (*syn*) addition to MMA (s-*cis* and s-*trans*).

As already discussed in a previous study of the authors, the attack of the radical to the monomer is gauche in the syndiotactic and isotactic polymer chains [43a].

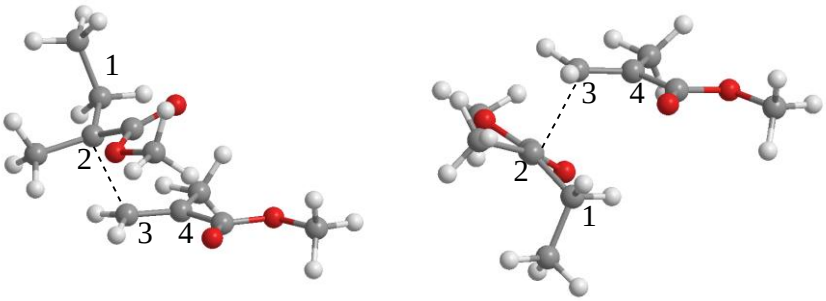

syndiotactic
$C_1C_2C_3C_4$ = 60.13°
(0.00)

isotactic
$C_1C_2C_3C_4$ = 49.88°
(0.79)

Figure 6.3. Dimeric transition structures for the free radical polymerization of MMA in vacuo. (MPWB1K/6-311+G(3df,2p)//B3LYP/6-31+G(d)).

Solvation of the transition state is studied by including only one methanol solvent molecule per monomer. In this picture the propagating radical attacks the monomer while a solvent molecule –CH_3OH- can form a hydrogen bond with the monomer (MMA) and the propagating radical (MMAR) as depicted in Scheme 6.6. Our previous study [43a] has shown that the most stable transition structures correspond to the attack of the monomeric radical of MMA in a *syn* conformation to the s-*cis* isomer of the monomer. The solvent can approach the monomer and the radical either from the direction in between the propagating

species (inner approach –i) or from outside (outer approach -o). As displayed in Scheme 6.6, alternative approaches of the solvent molecule to the propagating syndiotactic and isotactic polymer chains have been modeled, the most stable ones in each case have been reported. The nomenclature *syn*_oo, *syn*_oi, *syn*_io, *syn*_ii has been used to identify the approach of the solvent to the syndiotactic chain, similar notation *iso*_oo, *iso*_oi, *iso*_io, *iso*_ii has been employed for the isotactic chain.

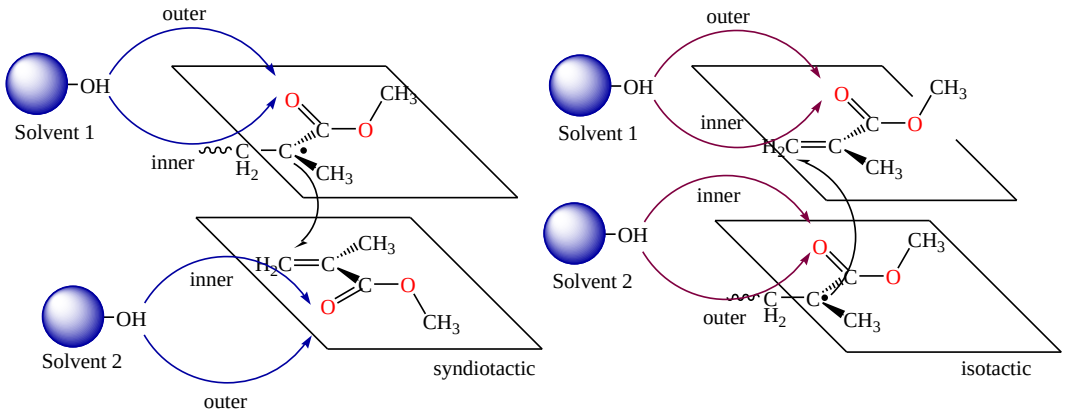

Scheme 6.6. Representation of solvent attack to the syndiotactic and isotactic propagating chains.

In the transition structures for the syndiotactic and isotactic propagating chains the carbonyl oxygen coordinates with methanol with distances varying from 1.86 Å to 1.91 Å, while the oxygen atom of the methanol is also involved in secondary long range stabilizing interactions with the methyl hydrogens in close proximity (2.43 Å to 2.52 Å). The presence of these bridge-type hydrogen bonds are decisive for determining the most stable transition structures. They elucidate mainly why syndiotactic structures are slightly better stabilized by the solvent by 1-3 kcal/mol (MPWB1K/6-311+G(3df,2p)//B3LYP/6-31+G(d), Figure 6.4). In all transition structures the forming C- - - C bond distances between the monomer and the radical vary between 2.24 Å and 2.26 Å. Also note that even though the nomenclature i(inner)/o(outer) is adopted for the approach of methanol to the dimeric chain, optimizations have led to structures where the methanol molecules H-bonded to the carbonyl oxygens lie more or less between the monomer and radical moieties in the dimeric structures.

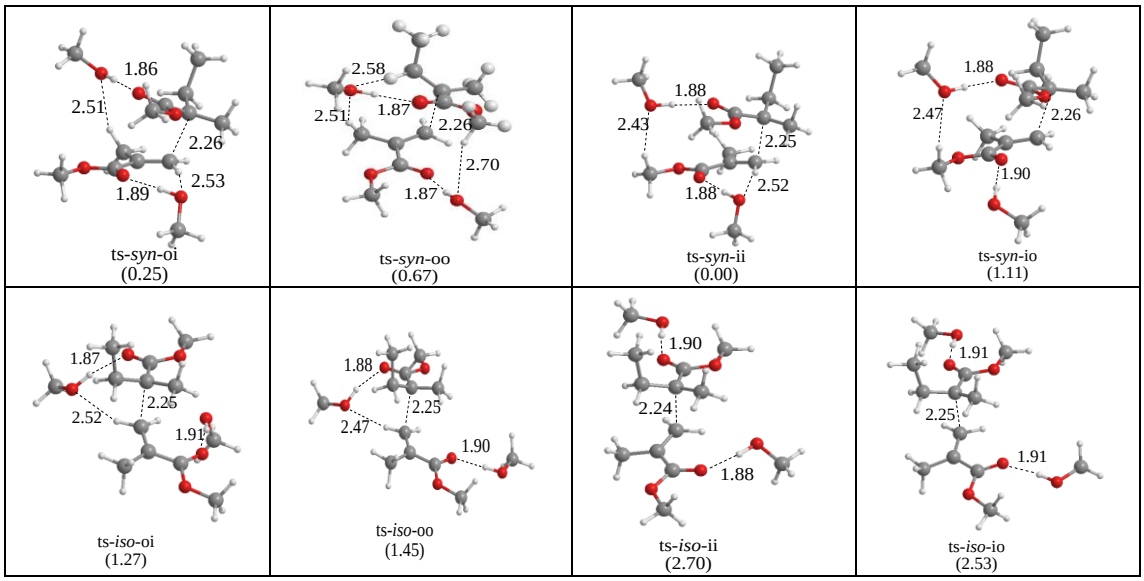

Figure 6.4. Relative energies (kcal/mol) of the most stable transition structures with CH_3OH (MPWB1K/6-311+G(3df,2p)//B3LYP/6-31+G(d)).

IRC calculations have yielded the pre-reactive complexes corresponding to the transition structures. The pre-reactive complexes correspond to stationary points along the potential energy surface of the propagation reaction where the two CH_3OH solvent molecules keep the monomer and the propagating radical in close proximity to each other before these two species have the proper orientation to react. The most favorable reaction paths for both syndiotactic and isotactic dimerizations are shown in Figures 6.5 and 6.6. The syndiotactic polymer chain is better stabilized and reacts faster than the isotactic polymer chain ($\Delta E_0^{\ddagger}$ amounts to 3.95 kcal/mol and 5.40 kcal/mol respectively).

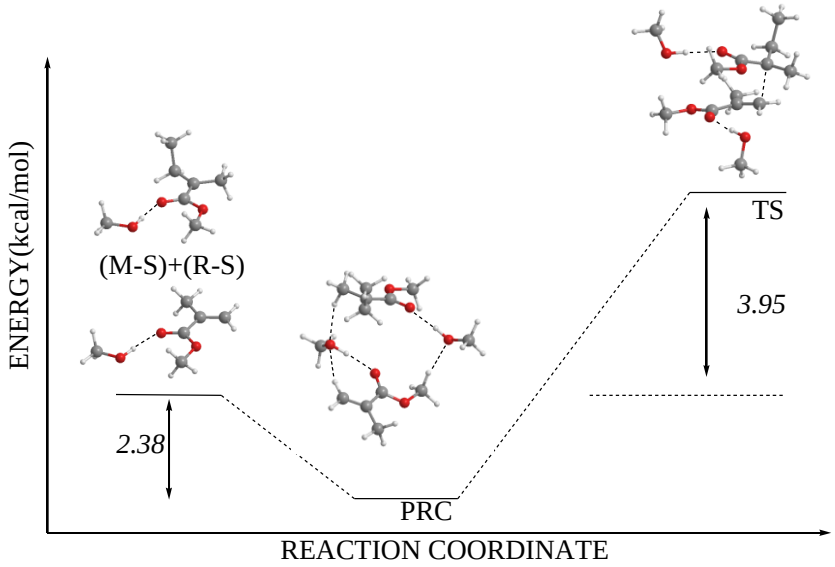

Figure 6.5. Energetics for syndiotactic dimeric-MMA formation (*syn*-ii) with CH_3OH (MPWB1K/6-311+G(3df,2p)//B3LYP/6-31+G(d)).

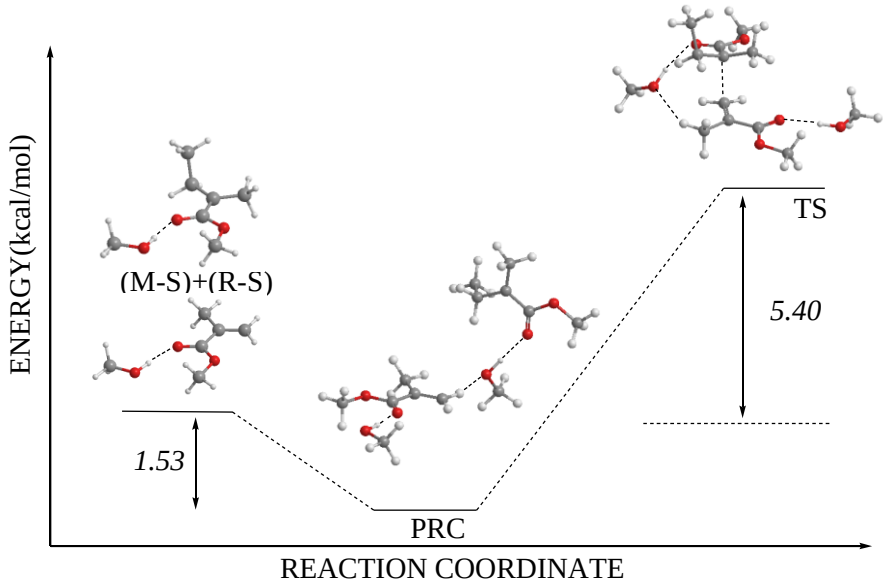

Figure 6.6. Energetics for isotactic dimeric-MMA formation (*iso*-oo) with CH_3OH (MPWB1K/6-311+G(3df,2p)//B3LYP/6-31+G(d)).

The kinetics of all the paths corresponding to the transition structures depicted in Figure 6.4 have been considered, the contribution of the *syn*-ii and *iso*-oo structures is found to be higher than the others. As shown in Figure 6.5, Figure 6.6 and Table 6.2 the energy barrier for the syndiotactic reaction (*syn*-ii) is smaller than the one for the isotactic

reaction (*iso*-oo) about 1.45 kcal/mol by using explicit solvent. This difference is mainly due to the presence of steric effects in the isotactic transition structure. However as displayed in Table 6.3, the ratio k_{syn} / k_{iso} is smaller than the one that would be expected based on energy barriers, this is due to entropic contributions to the rate constants. The vibrational partition function of the isotactic dimeric transition structure ($0.74x10^{31}$) is greater than the one of the syndiotactic structure ($0.17x10^{30}$) as a result of greater disorder in the former. The isotactic structure is more disordered due to the presence of the pendant groups on the same side of the backbone. Overall the isotactic structure is favored entropically ($\Delta G^{\ddagger}$), whereas the syndiotactic structure is favored energetically ($\Delta E_0^{\ddagger}$) as shown in Table 6.2. The reaction is exothermic slightly in favor of the syndiotactic path. In Table 6.3 the reaction channels have been considered as concurrent reactions where the sum of the reaction rate constants for the syndiotactic (k_{syn}) and isotactic (k_{iso}) paths have been evaluated. The k_{syn} / k_{iso} ratio is reproduced qualitatively with all the methodologies with implicit and explicit solvent.

Table 6.2. Energetics (kcal/mol) for syndiotactic and isotactic paths with explicit CH_3OH at 293.15K ((MPWB1K/6-311+G(3df,2p)// B3LYP/6-31+G(d)).

	$\Delta E_0^{\ddagger}$	$\Delta G^{\ddagger}$	ΔH
syn-oi	4.20	19.73	-17.00
syn-oo	4.62	19.57	-16.50
syn-ii	3.95	19.24	-17.07
syn-io	5.06	19.98	-17.29
iso-oi	5.22	19.40	-16.85
iso-oo	5.40	18.73	-16.94
iso-ii	6.66	19.88	-15.14
iso-io	6.48	19.69	-15.35

Table 6.3. Kinetics (k_{app}) for the syndiotactic and isotactic polymerization of MMA in vacuum and CH_3OH at 293.15K (B3LYP/6-31+G(d) geometries have been considered).

	B3LYP /6-31+G(d)	B3LYP /6-311+G(3df,2p)	MPWB1K/ 6-311+G(3df,2p)	B2PLYP/ 6-31+G(d)
Explicit solvent				
$k_{syn\text{-oi}}$	4.82E-07	6.87E-08	2.91E-04	3.71E-03
$k_{syn\text{-oo}}$	1.68E-06	2.36E-07	3.86E-04	5.87E-03
$k_{syn\text{-ii}}$	2.09E-06	2.12E-07	6.76E-04	2.06E-02
$k_{syn\text{-io}}$	1.29E-06	1.56E-07	1.89E-04	4.96E-03
$k_{iso\text{-oi}}$	2.51E-06	3.65E-07	5.12E-04	5.88E-03
$k_{iso\text{-oo}}$	6.71E-06	1.18E-06	1.64E-03	3.97E-03
$k_{iso\text{-ii}}$	1.54E-06	2.89E-07	2.26E-04	7.53E-04
$k_{iso\text{-io}}$	2.08E-06	4.08E-07	3.12E-04	5.11E-04
$k_{syn\ (tot)}$	5.54E-06	6.73E-07	1.54E-03	3.51E-02
$k_{iso\ (tot)}$	1.28E-05	2.24E-06	2.69E-03	1.11E-02
k_{syn} / k_{iso} *	0.43	0.30	0.57	3.16
Implicit + Explicit solvent				
k_{syn} / k_{iso} *a	-	3.85	9.38	40.57
Vacuum				
k_{syn} / k_{iso}	0.74	0.68	1.75	-
Implicit solvent				
k_{syn} / k_{iso} *b	-	1.04	2.90	-

* $[k_{syn} / k_{iso}]_{exp}$ = 22 in methanol ……($[k_{syn} / k_{iso}]_{exp}$ = 22 in bulk) [13c]

[a] Reaction path within a mixed implicit/explicit solvent model (a solvated monomer and solvated radical embedded in a continuum of dielectric constant ε = 32.63

[b] Reaction path within implicit solvent model embedded in a continuum of dielectric constant ε = 32.63

The incorporation of explicit solvent molecules is expected to lead to a decrease in activation energy resulting to an increase of the reaction rate coefficient as found in a recent work of part of the authors on the effect of explicit water molecules on the propagation rate in acrylamide and methacrylamide [32]. Here the major increase in k_p

values results from usage of the explicit/implicit solvation model. As mentioned earlier by Warshell et al. care needs to be taken in absolute evaluation of these values, as this model can also overshoot the solvent effects [44].

In this study, the presence of explicit and implicit solvent has reproduced qualitatively the experimental expectation in favor of the syndiotactic PMMA.

6.2.2. Free Radical Polymerization of MMA in perfluoro-tert-butyl alcohol $(CF_3)_3COH$

We now investigate the influence of the solvent type on the stereochemistry in MMA polymerization. We have chosen $(CF_3)_3COH$ as the *rr*-tacticity is the largest in this solvent. Four solvated complexes for the monomer MMA-$(CF_3)_3COH$ and radical MMAR-$(CF_3)_3COH$ are found and displayed in Figure 6.7. They all show a hydrogen bond between the alcoholic H and the carbonyl oxygen but due to the larger polarizability of $(CF_3)_3COH$ the coordination distance is found slightly smaller (1.75 Å) than the one for methanol (1.90 Å).

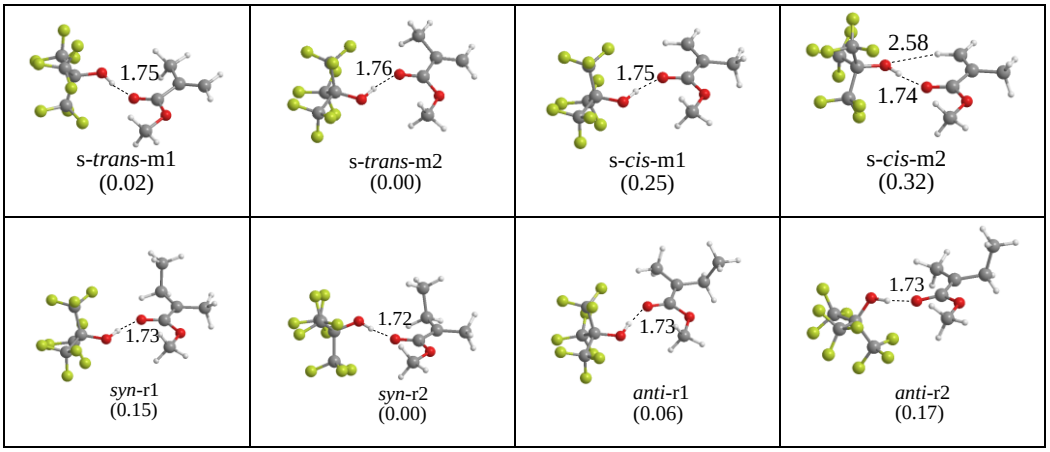

Figure 6.7. Relative energies (kcal/mol) of MMA-$(CF_3)_3COH$ and MMAR-$(CF_3)_3COH$ complexes (MPWB1K/6-311+G(3df,2p)//B3LYP/6-31+G(d)).

In the transition structures along the formation of the syndiotactic and isotactic products notice that the F atoms of the $(CF_3)_3COH$ solvent are in close proximity in the

isotactic chains rather than in the syndiotactic chains. The steric repulsion between the bulky solvent molecules is much more pronounced in $(CF_3)_3COH$ rather than in CH_3OH.

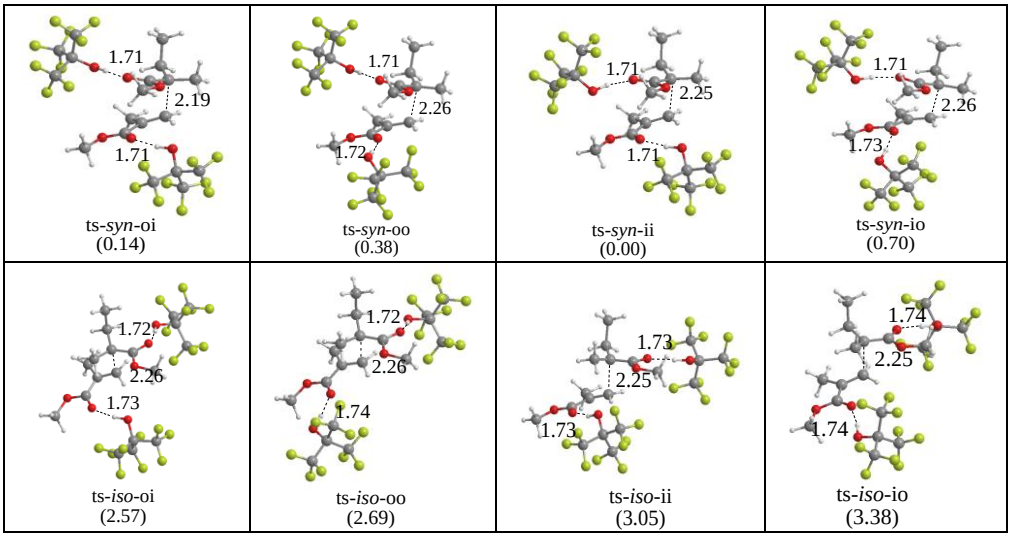

Figure 6.8. Relative energies (kcal/mol) of the most stable transition structures with $(CF_3)_3COH$ (MPWB1K/6-311+G(3df,2p)//B3LYP/6-31+G(d)).

In PFTB the reaction barrier for the syndiotactic path (*syn*-ii) is smaller than the one for the isotactic path (*iso*-oi) by about 2.57 kcal/mol due to the presence of steric effects in the isotactic transition structure (Table 6.4). As displayed in Table 6.5, the k_{syn} / k_{iso} ratio illustrates the same behavior as the activation barriers in contrast to the FRP of MMA in CH_3OH. The FRP of MMA in PFTB favors the syndiotactic path both energetically and entropically; this is probably due to the nature of the H-bonds which are shorter and stronger in PFTB and stabilize better the pendant groups which are more ordered as compared to the ones in CH_3OH. Also note that the free radical polymerization of MMA in PFTB is exothermic ($\Delta H < 0$) in favor of the syndiotactic path.

Table 6.4. Energetics for syndiotactic and isotactic paths with explicit $(CF_3)_3COH$ (MPWB1K/6-311+G(3df,2p)// B3LYP/6-31+G(d)) at 293.15K.

	$\Delta E_0^{\ddagger}$	$\Delta G^{\ddagger}$	ΔH
syn-oi	2.97	17.44	-20.23
syn-oo	3.22	18.31	-20.12
syn-ii	2.84	17.10	-19.58
syn-io	3.54	18.47	-19.77
iso-oi	5.41	20.93	-18.06
iso-oo	5.52	20.51	-17.57
iso-ii	5.89	19.86	-16.94
iso-io	6.21	19.10	-16.52

The dielectric constant of perfluoro-tert-butyl alcohol $(CF_3)_3COH$ has been calculated in order to treat it as a polarizable continuum. The Debye Equation has been used to evaluate the dielectric constant of $(CF_3)_3COH$ as shown in Eq. (6)

$$\frac{\varepsilon_r - 1}{\varepsilon_r + 2} = \frac{\rho P_m}{M} \qquad (6)$$

ρ is the density of $(CF_3)_3COH$, M is its molecular weight, and P_m is the molar polarization. The formalism displayed in Eq. 6 has been used to find ε = 4.49 for $(CF_3)_3COH$ and calculations in a continuum with ε = 4.49 have been carried out (Table 6.5). The experimentally observed enhancement of the stereoselectivity in $(CF_3)_3COH$ is pretty well reproduced qualitatively both with the MPWB1K/6-311+G(3df,2p)//B3LYP/6-31+G(d) and the B2PLYP/6-31+G(d)//B3LYP/6-31+G(d) methodologies.

Table 6.5. Kinetics (k_{app}) for syndiotactic and isotactic polymerization of MMA in vacuum and $(CF_3)_3COH$ at 293.15K (B3LYP/6-31+G(d) geometries have been considered).

	B3LYP/6-31+G(d)	B3LYP/6-311+G(3df,2p)	MPWB1K/6-311+G(3df,2p)	B2PLYP/6-31+G(d)
Explicit solvent				
$k_{syn\text{-oi}}$	7.82E-07	2.13E-06	1.47E-02	1.82E+00
$k_{syn\text{-oo}}$	1.80E-07	4.83E-07	3.29E-03	2.55E-01
$k_{syn\text{-ii}}$	1.38E-06	3.49E-06	2.65E-02	3.25E+00
$k_{syn\text{-io}}$	2.03E-07	5.21E-07	2.53E-03	2.80E-01
$k_{iso\text{-oi}}$	8.74E-09	3.14E-08	3.68E-05	1.08E-03
$k_{iso\text{-oo}}$	2.14E-08	6.38E-08	7.65E-05	8.75E-04
$k_{iso\text{-ii}}$	5.45E-08	1.73E-07	2.31E-04	3.32E-03
$k_{iso\text{-io}}$	3.09E-07	9.38E-07	8.58E-04	6.26E-03
$k_{syn\ (tot)}$	2.55E-06	6.63E-06	4.70E-02	5.61E+00
$k_{iso\ (tot)}$	3.94E-07	1.21E-06	1.20E-03	1.15E-02
k_{syn} / k_{iso}	6.47	5.50	39.07	486.06
Implicit + Explicit solvent				
k_{syn} / k_{iso} [a]		13.19	79.79	477.03
Vacuum				
k_{syn} / k_{iso}	0.74	0.68	1.75	-
Implicit solvent				
k_{syn} / k_{iso} [b]	-	1.06	2.85	-

* $[k_{syn} / k_{iso}]_{exp}$ = 75 in $(CF_3)_3COH$ [13c]

[a] Reaction path within a mixed implicit/explict solvent model (a solvated monomer and solvated radical embedded in a continuum of dielectric constant ε = 4.49 .

[b] Reaction path within implicit solvent model embedded in a continuum of dielectric constant ε = 4.49.

6.2.3. Comparison of the Free Radical Polymerization of MMA in CH_3OH and in $(CF_3)_3COH$

The comparison of activation barriers for the propagation reaction in vacuum, in methanol, and in fluorinated alcohol emphasizes the fact that the solvent stabilizes transition states more than the reactants (Table 6.6). The reaction barriers $\Delta E_0^{\ddagger}$ for the most favorable reaction paths leading to syndiotactic and isotactic dimeric growing polymer chains are in agreement with the experimental findings at 20ºC where PMMA is 66 per cent syndiotactic in methanol and 75.3 per cent in PFTB; whereas it is 1.2 per cent isotactic in PFTB and 2.5 per cent in methanol respectively (Table 6.6) [13b]. On the energetic and kinetic basis the syndiotactic propagation is accelerated as the interaction with the surrounding medium increases. Notice also that the solvent stabilizes less the isotactic transition structures as compared to the syndiotactic ones: for isotactic PMMA even though interactions with the solvent molecules are favorable, their close proximity inhibits this rearrangement. The size of PFTB molecules being larger than the one of CH_3OH molecules there is greater repulsion between PFTB molecules, this behavior is perfectly well reflected in k_{iso} in methanol ($3.03x10^8$) being larger than k_{iso} in PFTB ($2.64x10^8$).

Table 6.6. Reaction barriers $\Delta E_0^{\ddagger}$ (kcal/mol) and rate constants for the most favorable reactions (MPWB1K/6-311+G(3df,2p)//B3LYP/6-31+G(d)).

	vacuum	CH_3OH	$(CF_3)_3COH$
$\Delta E_0^{\ddagger}$ (syn)	5.33	3.95	2.84
$\Delta E_0^{\ddagger}$ (iso)	6.12	5.40	6.21
k_{syn}*		2.17E+09	4.31E+10
k_{iso}*		3.03E+08	2.64E+08

* Rate constants have been calculated with IEF-PCM in a polar environment

The experimentally observed reaction outcomes have also been rationalized by a comparative analysis of the transition state structures via the distortion/interaction model

[45]. The activation strain model of chemical reactivity by Bickelhaupt [45b], was employed.

$$\Delta E_0^{\ddagger} = \Delta E_{int}^{\ddagger} + \Delta E_{dist}^{\ddagger} \quad (7)$$

The distortion/interaction model separates the activation energy ($\Delta E_0^{\ddagger}$) into distortion energy ($\Delta E^{\ddagger}_{dist}$), and interaction energy ($\Delta E^{\ddagger}_{int}$) between distorted fragments, where the former is associated with the strain caused by deforming the individual reactants, and the latter is the favorable interaction between the deformed reactants.

Table 6.7. Gas phase activation barriers ($\Delta E_0^{\ddagger}$), interaction energies ($\Delta E^{\ddagger}_{int}$), and distortion energies ($\Delta E^{\ddagger}_{dist}$) with explicit solvent (MPWB1K/6-311+G(3df,2p)//B3LYP/6-31+G(d), kcal/mol).

	CH_3OH			$(CF_3)_3COH$		
	$\Delta E_0^{\ddagger}$	$\Delta E^{\ddagger}_{int}$	$\Delta E^{\ddagger}_{dist}$	$\Delta E_0^{\ddagger}$	$\Delta E^{\ddagger}_{int}$	$\Delta E^{\ddagger}_{dist}$
syn-oi	4.20	-6.64	10.84	2.97	-6.75	9.72
syn-oo	4.62	-6.33	10.95	5.52	-6.59	9.81
syn-ii	3.95	-7.09	11.04	2.84	-6.84	9.67
syn-io	5.06	-5.74	10.79	3.54	-6.33	9.87
iso-oi	5.22	-6.66	11.88	5.41	-4.83	10.24
iso-oo	5.40	-5.71	11.11	5.52	-4.69	10.21
iso-ii	6.66	-4.40	11.05	5.89	-4.61	10.50
iso-io	6.48	-3.27	9.75	6.21	-3.81	10.02

When CH_3OH is the solvent, the contribution of the distortion energy is more or less similar for both sydiotactic and isotactic channels. On the other hand when $(CF_3)_3COH$ is used the distortion energy is higher in the isotactic channel as expected based on the proximity of the pendant groups. Also in $(CF_3)_3COH$, the interaction energies stabilize the syndiotactic structures more than the isotactic ones, this is confirmed by the stronger H-bonds (1.71 Å) in these structures as compared to the ones in the syndiotactic structures

(1.72-1.74 Å). Overall, the distortion/interaction model explains the experimentally determined syndiotactic preference of the free radical polymerization of MMA in the presence of $(CF_3)_3COH$.

6.4. Conclusion

In this study, the control of the stereochemistry in methylmethacrylate (MMA) has been modeled with the B3LYP/6-31+G(d)//B3LYP/6-31+G(d), B3LYP/6-311+G(3df,2p)//B3LYP/6-31+G(d), MPWB1K/6-311+G(3df,2p)//B3LYP/6-31+G(d), B2PLYP/6-311+G(3df,2p)//B3LYP/6-31+G(d methodologies. The role of the solvent on the tacticity of MMA polymerization has been investigated by considering the propagation rate constants for the syndiotactic and isotactic free radical polymerization of MMA in vacuum, in methanol (CH_3OH) and in 1,1,1,3,3,3-hexafluoro-2-(trifluoromethyl)propan-2-ol ($(CF_3)_3COH$). The role of $(CF_3)_3COH$ in inhibiting the isotacticity of PMMA has been explained by the steric hindrance of the pendant solvent molecules strongly hydrogen bonded to the carbonyl oxygens (~ 1.7 Å) located on the same side of the backbone. CH_3OH is less effective in reducing the isotacticity because of its small size and because of the relatively loose hydrogen bonds (~ 1.9 Å) with the carbonyl oxygen. The methodologies used in this study within the scope of the terminal unit model have effectively reproduced the solvent effect on the FRP kinetics of MMA. The quantitative reproduction of absolute rates of polymerization in solvent remains a challenge for theoretical methods, however this study proves that qualitative trends on effect of solvent on tacticity can be reproduced by the used theoretical models. Overall, this study has demonstrated the fact that computational chemistry offers a viable alternative to experiment: the effect of solvent on tacticity can be predicted prior to the experiment.

6. 5. References

1. Gladysz, J. A. *Chem. Rev*. **2000**, *100*, 1167-1168.
2. Sugiyama, Y.; Satoh, K.; Kamigaito, M.; Okamoto, Y. *J. Polym. Sci., Part A: Polym. Chem*. **2006**, *44*, 2086–2098.
3. (a) Pino, P.; Suter, U. W. *Polymer* **1976**, *17*, 977–995. (b) Hatada, K.; Kitayama, T.; Ute, K. *Prog. Polym. Sci.* **1988**, *13*, 189–276. (c) Yuki, H.; Hatada, K. *Adv. Polym. Sci.* **1979**, *31*, 1–45.
4. Matsumoto, A. In *Handbook of Radical Polymerization*; Matyjaszewski, K.; Davis, T. P., Eds.; Wiley-Interscience: Hoboken, **2002**; pp 691–773.
5. (a) Habaue, S.; Okamoto, Y. *Chem. Rec.* **2001**, *1*, 46-52. (b) Miura, Y.; Shibata, T.; Satoh, K.; Kamigaito, M.; Okamoto, Y. *J. Am. Chem. Soc.* **2006**, *128*, 16026-16027.
6. Tanaka, H., *Prog. Polym. Sci.* **1992**, *17*, 1107-1152.
7. Satoh, K.; Kamigaito, M. *Chem. Rev.* **2009,** *109,* 5120–5156.
8. Isobe, Y.; Nakano, T.; Okamoto, Y. *J. Polym. Sci., Part A: Polym. Chem.* **2001**, *39*, 1463–1471.
9. Isobe, Y.; Fujioka, D.; Habaue, S.; Okamoto, Y. *J. Am. Chem. Soc.* **2001**, *123*, 7180–7181.
10. Habaue, S.; Isobe, Y.; Okamoto, Y. *Tetrahedron* **2002**, *58*, 8205–8209.
11. Okamoto, Y.; Habaue, S.; Isobe, Y.; Suito, Y. *Macromol. Symp.* **2003**, *195*, 75–80.
12. Suito, Y.; Isobe, Y.; Habaue, S.; Okamoto, Y. *J. Polym. Sci., Part A: Polym. Chem.* **2002**, *40*, 2496–2500.
13. (a) Yamada, K.; Nakano, T.; Okamoto, Y. *Macromolecules* **1998**, *31*, 7598–7605. (b) Isobe, Y.; Yamada, K.; Nakano, T.; Okamoto, Y. *Macromolecules* **1999**, *32*, 5979–5981. (c) Isobe, Y.; Yamada, K.; Nakano, T.; Okamoto, Y. *J. Polym. Sci., Part A: Polym. Chem.* **2000**, *38*, 4693–4703.

14. Miura, Y., Satoh, T., Narumi, A., Nishizawa, O., Okamoto, Y., Kakuchi, T. *J. Polym. Sci., Part A: Polym. Chem.* **2006**, *44*, 1436–1446.

15. (a) Miura, Y.; Satoh, T.; Narumi, A.; Nishizawa, O.; Okamoto, Y.; Kakuchi, T., *Macromolecules* **2005**, *38*, 1041-1043; (b) Miura, Y.; Satoh, T.; Narumi, A.; Nishizawa, O.; Okamoto, Y.; Kakuchi, T., *J. Polym. Sci., Part A: Polym. Chem.* **2006**, *44*, 1436-1446.

16. Tanaka, H.; Niwa, M., *Polymer* **2008**, *49*, 3693-3701.

17. Nakano, T.; Okamoto, Y. In *Controlled Radical Polymerization* Matyjazsewski, K., Ed.; ACS Symposium Series 685; American Chemical Society: Washington, DC, **1998**; pp 451- 462.

18. Beuermann S., *Macromol. Rapid Commun.* **2009**, *30*, 1066-1088.

19. O'Driscoli, K. F.; Monteiro, M. J.; Klumperman, B., *J. Polym. Sci., Part A: Poly. Chem.*, **1997**, *35*, 515-520.

20. Zammit, M. D.; Davis, T. P.; Willett, G. D.; O'Driscoli, K. F., *J. Polym. Sci., Part A: Poly. Chem.* **1997**, *35*, 2311-2321.

21. Harrisson, S.; Barner-Kowollik, C.; Davis, T. P.; Evans, K.; Rizzardo, R.; Stenzel, M.; Yin, M. Z., *Phys. Chem.* **2005**, *219*, 267-281.

22. Ganachaud, F.; Balic, R.; Monteiro, M. J.; Gilbert, R. G., *Macromolecules* **2000**, *33*, 8589 -8596; Seabrook, S. A.; Tonge, M. P.; Gilbert, R. G., *J. Polym. Sci., Part A:Poly. Chem.* **2005**, *43*, 1357-1368.

23. Gaussian 03, Revision D.01, Frisch, M. J.; Trucks, G. W.; Schlegel, H. B.; Scuseria, G. E.; Robb, M. A.; Cheeseman, J. R.; Montgomery, Jr., J. A.; Vreven, T.; Kudin, K. N.; Burant, J. C.; Millam, J. M.; Iyengar, S. S.; Tomasi, J.; Barone, V.; Mennucci, B.; Cossi, M.; Scalmani, G.; Rega, N.; Petersson, G. A.; Nakatsuji, H.; Hada, M.; Ehara, M.; Toyota, K.; Fukuda, R.; Hasegawa, J.; Ishida, M.; Nakajima, T.; Honda, Y.; Kitao, O.; Nakai, H.; Klene, M.; Li, X.; Knox, J. E.; Hratchian, H. P.; Cross, J. B.; Bakken, V.; Adamo, C.; Jaramillo, J.; Gomperts, R.; Stratmann, R. E.; Yazyev, O.; Austin, A. J.; Cammi, R.; Pomelli, C.; Ochterski, J. W.; Ayala, P. Y.; Morokuma, K.; Voth, G. A.;

Salvador, P.; Dannenberg, J. J.; Zakrzewski, V. G.; Dapprich, S.; Daniels, A. D.; Strain, M. C.; Farkas, O.; Malick, D. K.; Rabuck, A. D.; Raghavachari, K.; Foresman, J. B.; Ortiz, J. V.; Cui, Q.; Baboul, A. G.; Clifford, S.; Cioslowski, J.; Stefanov, B. B.; Liu, G.; Liashenko, A.; Piskorz, P.; Komaromi, I.; Martin, R. L.; Fox, D. J.; Keith, T.; Al-Laham, M. A.; Peng, C. Y.; Nanayakkara, A.; Challacombe, M.; Gill, P. M. W.; Johnson, B.; Chen, W.; Wong, M. W.; Gonzalez, C.; and Pople, J. A.; Gaussian. Inc., Wallingford CT, **2004**.

24. Smith, D. M.; Nicolaides, A.; Golding, B. T.; Radom, L. *J. Am. Chem. Soc.* **1998**, *120*, 10223-10233.

25. Gonzáles, C.; Schlegel, H. B. *J. Phys. Chem.* **1990**, *94*, 5523-5527.

26. Zhao, Y.; Truhlar, D. G. *J. Phys. Chem. A* **2004**, *108*, 6908–6918.

27. Furuncuoğlu, T.; Uğur, İ.; Değirmenci, İ.; Aviyente, V. *Macromolecules* **2010**, 43, 1823-1835.

28. Liang,K.; Dossi, M.; Moscatelli, D.; Hutchinson, R. A. *Macromolecules* **2009**, *42*, 7736-7744.

29. Yu, X.; Pfaendtner, J.; Broadbelt, L. J. *J. Phys. Chem. A* **2008**, *112*, 6772–6782.

30. Lee, C. T.; Yang, W. T.; Parr, R. G. *Phys. Rev. B* **1988**, *37*, 785–789 ; Becke, A. D. *Phys. Rev. A* **1988**, *38*, 3098–3100.

31. Grimme, S.; Steinmetz, M.; Korth, M., *J. Chem. Theory Comput.* **2007,** *3*, 42-45. Grimme, S., *J. Chem. Phys.* **2006**, *124*, 174301-12.

32.De Sterck, B.; Roel Vaneerdeweg, R.; Du Prez, F.; Waroquier, M, Van Speybroeck, V. *Macromolecules* **2010**, *43*, 827-836.

33. Singleton, D. L.; Cvetanovic, R. J., *J. Am. Chem. Soc*. **1976,** *98*, 6812-6819.

34. Pilling, M. J.; Seakins, P. W. *Reaction Kinetics*; Oxford University Press: New York, **1996**.

35. *Atkins' Physical Chemistry*, 8th ed.; Atkins, P.; De Paula, J. Oxford University Press, New York, **2006**.

36. (a) Tomasi, J.; Mennucci, B.; Cance`s, E. *J. Mol. Struct.: THEOCHEM* **1999**, *464*, 211-226. (b) Cance`s, M. T.; Mennucci, B.; Tomasi, J. *J. Chem. Phys*. **1997**, *107*, 3032-3041. (c) Mennucci, B. Tomasi, J. *J. Chem. Phys.* **1997**, *106*, 5151-5158. (d) Mennucci, B.; Cance`s, E.; Tomasi, J. *J. Phys. Chem. B* **1997**, *101*, 10506-10517.

37. (a) Kelly, C. P.; Cramer, C. J.; Truhlar, D. G. *J. Phys. Chem. A* **2006**, *110*, 2493–2499. (b) Kamerlin, S. C. L.; Haranczyk, M.; Warshel, A. *ChemPhysChem* **2009**, *10*, 1125–1134. (c) De Sterck, B.; Van Speybroeck, V.; Mangelinckx, S.; Verniest, G.; De Kimpe, N.; Waroquier, M. *J. Phys. Chem. A* **2009**, *113*, 6375–6380. (d) Van Speybroeck, V.; Moonen, K.; Hemelsoet, K.; Stevens, C.; Waroquier, M. *J. Am. Chem. Soc.* **2006**, *128*, 8468–8478. (e) Kelly, C. P.; Cramer, C. J.; Truhlar, D. G. *J. Chem. Theory Comput.* **2005**, *1*, 1133–1152.

38. (a) Heuts, J. P. A.; Gilbert, R. G.; Radom, L. *Macromolecules* **1995**, *28*, 8771-8781. (b) Wong, M. W.; Radom, L. *J. Phys. Chem.* **1995**, *99*, 8582-8588. (c) Heuts, J. P. A.; Gilbert, R. G.; Radom, L. *J. Phys. Chem.* **1996,** *100*, 18997-19006. (d) Wong, M. W.; Radom, L. *J. Phys. Chem. A* **1998,** *102*, 2237-2245. (e) Fischer, H.; Radom, L. *Angew. Chem. Int. Ed.* **2001**, *40*, 1340 -1371. (f) Go´mez-Balderas, R.; Coote, M. L.; Henry, D. J.; Fischer, H.; Radom, L. *J. Phys. Chem. A* **2003,** *107*, 6082-6090. (g) Go´mez-Balderas, R.; Coote, M. L.; Henry, D. J.; Radom, L. *J. Phys. Chem. A* **2004,** *108*, 2874-2883. (h) Henry, D. J.; Coote, M. L.; Go´mez-Balderas, R.; Radom, L. *J. Am. Chem. Soc.* **2004**, *126*, 1732-1740.

39. Izgorodina, E. I.; Coote, M. L. *Chem. Phys.* **2006**, 324, 96–110.

40. Coote, M. L. *Macromol. Theory Simul*. **2009**, *18*, 388–400.

41. Lin, C. Y.; Izgorodina, E. I.; Coote, M. L. *Macromolecules* **2010**, *43*, 553–560.

42. Van Cauter, K.; Van Speybroeck, V.; Waroquier, M. *ChemPhysChem*, **2007**, *8*, 541-552.

43. a) Değirmenci, İ.; Aviyente, V.; Van Speybroeck, V.; Waroquier, M. *Macromolecules* **2009**, *42*, 3033-3041. b) Değirmenci, İ.; Avcı, D.; Aviyente, V.; Van Cauter, K.; VanSpeybroeck, V.; Waroquier, M. *Macromolecules* **2007**, *40*, 9590–9602. c) Günaydın, H.; Seyhan, S.; Tüzün, N. Ş.; Avcı,D.; Aviyente, V. *Int. J. Quant. Chem.*, **2005**, *103*, 176- 189. d) Salman, S.; Ziylan Albayrak A.; Avcı, D.; Aviyente, V. *J. Polym. Sci., Part A: Poly. Chem.* **2005**, *43*, 2574–2583.

44. Kamerlin, S. C. L.; Haranczyk, M.; Warshel, A. *ChemPhysChem* **2009**, *10*, 1125–1134.

45. a) Ess, D. H.; Houk, K. N. *J. Am. Chem. Soc.* **2007**, *129*, 10646. b)Bento, A. P.; Bickelhaupt, F. M. *J. Org. Chem.* **2008**, *73*, 7290-7299. c) Catak, S.; Matthias D'hooghe, M.; De Kimpe, N.; Waroquier, M.; Van Speybroeck, V. *J. Org. Chem.* **2010**, *75*, 885–896.

7. ROLE OF SOLVENT ON THE PROPAGATION KINETICS OF ACRYLIC ACID AND METHACRYLIC ACID

7.1 Introduction

Water-soluble polymers are of high technical importance, finding widespread application in hydrogels, flocculants, thickeners, coatings, etc to improve the final product properties, including adhesion characteristics and mechanical properties of paints and paper coatings [1,2]. Pulsed-laser polymerization in conjunction with size-exclusion chromatography (PLP-SEC) has been used to detect experimentally the influence of solvents on the propagation kinetics [3,4]. The free radical polymerization for styrene (in ethanol, methanol, toluene, ethylbenzene), methacrylic acid (in methanol, tetrahydrofuran, 2-propanol, toluene, acetic acid), methyl methacrylate (in methanol, ethyl acetate, ethanol, toluene, 2-butanone), and butyl acrylate (in toluene, tetrahydrofuran) showed, so far, that k_p is invariant with monomer concentration [5-7]. For a long time it was assumed that the solvent effects on the rate coefficients were rather small. The propagation rate coefficients for styrene and methyl methacrylate (MMA) polymerizations in a wide variety of solvents [acetonitrile, dimethyl formamide, anisole, methyl isobutyrate, bromobenzene, benzene and 1,2-dichloroethane] only change mostly around 10 %. [see review of S. Beuermann and references cited therein [8]]. On the other hand certain solvents, such as benzyl alcohol [9], dimethylsulfoxide [9], N-methylpyrrolidinone [9], 2,6-dithiaheptane [10], and 1,5-dithiacyclooctane [10] turn out to induce a significant increase of k_p. In many cases hydrogen bonding is responsible for this observed increase.

Recently, measurements of propagation rate coefficients, k_p, in aqueous solution of methacrylic acid (MAA) [7, 11-14], acrylic acid (AA) [7,15-17], 2–4 *N*-isopropyl acrylamide (NIPAM) [18], and acrylamide [19] have been carried by the PLP-SEC method. These studies revealed that polar monomers which are capable of forming hydrogen bonds are affected substantially by the solvent [20-22]. Passing from the bulk system to a highly dilute system, the propagation rate constant k_p of nonionized MAA increases by more than one order of magnitude. The same trend is true for acrylic acid. The significant increase in k_p upon decreasing the monomer concentration is attributed to an

increase in the Arrhenius pre-exponential factor, $A(k_p)$. It is suggested that the increase in the Arrhenius pre-exponential factor, increase in disorder, is due to the fact that the intermolecular interactions between the transition state structure for propagation and a monomer environment are significantly weaker than the ones between this transition structure and a water environment [23].

Along the polymerizations in aqueous phase strong hydrogen bonds between water molecules and the carbonyl group of the monomers competes with hydrogen bonds between carbonyl groups in the macroradical and in the monomer. The rotational degrees of the transition state structure are strongly affected by the competing interactions: the larger the H_2O content, the lower the steric hindrance and the higher the mobility of the radical chain end. The activation energy is not affected by the presence of H_2O, whereas the pre-exponential factor may be increased by one order of magnitude [8].

Chapiro et al. [22] have explained the effect of solvent on the overall reaction rate in the free radical polymerization of AA and MAA by defining two groups of solvents: (i) The first group of solvents, i.e., water, methanol, and dioxane, are good polar solvents for the polymer. Because of hydrogen bonding between the monomers and the solvent the acid exhibits an associated structure forming oligomeric associates and monomer-solvent association complexes. (ii) The second group, i.e., toluene and hexane, are non-polar solvents for the polymer. In this group of solvents only self association of the monomer (formation of cyclic dimers and linear oligomers) and association with the propagating chain is possible. Dilution of the system shifts the equilibrium from a linear oligomeric form to a cyclic dimer while increasing temperature favors the linear oligomer. The reaction rate turns out to be reduced for the cyclic dimer form.

More systematic experimental studies about the solvent influence on k_p for various monomers were conducted over the last couple of years [7,11-19,24], and they give indication that the solvent induces changes which are much larger than originally thought. Also recent theoretical studies point towards the same conclusion, stressing the importance of taking into account the relevant rotational modes of the transition state structure [25, 43a]. Experiments provided by data for acrylamide and N-isopropylacrylamide (NIPAM) suggest a strong increase of k_p upon addition of water to the system [26]. If intra- and

intermolecular interactions in the system are varied, they are expected to influence the rotational modes of the transition state. In aqueous phase the propagating radical is surrounded by an environment consisting of water and the monomer. The water molecules compete with interactions between monomer molecules and the propagating chain. If interactions with water are occurring the extent of internal friction of the transition state structure will be lower than in case of interactions with monomer due to the much smaller size of the water molecule. As a consequence of the less hindered rotational modes of the transition state the pre-exponential factor is enhanced in the presence of water [27].

In this study, the solvent effect on the propagation rate constant of AA and MAA will be considered. Comparisons of geometrical features of propagating species in bulk and solvent media will elucidate the role of the solvent on the propagation rate constant of these two monomers.

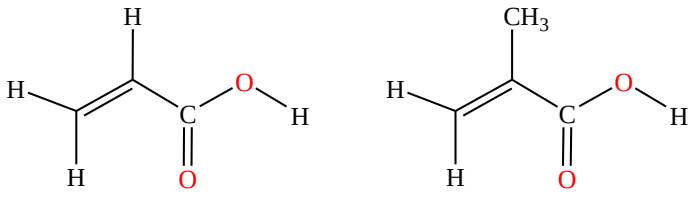

Acrylic Acid (AA) Methacrylic Acid (MAA)

Figure 7.1. Monomers considered in this study.

7.2 Computational Procedure

The B3LYP method combined with 6-31+G(d) basis set within the Gaussian 03 program package [28] was chosen as a cost effective and accurate method for geometry optimizations [29]. The energeties and kinetics have been evaluated with the MPWB1K/6-311+G(3df,2p)//B3LYP/6-31+G(d), B3LYP/6-311+G(3df,2p)//B3LYP/6-31+G(d), and B3LYP/6-31+G(d)//B3LYP/6-31+G(d), methodologies. The MPWB1K method has proven to be very successful for describing thermochemistry, reaction kinetics, hydrogen bonding, and weak interactions [30,31]. Especially polymerization reaction of acrylates the method has proven to be very successful [42,43].

The conventional transition state theory (TST) is used to calculate the rate constants. The rate equation of a bimolecular reaction $A+B\rightarrow C$ is given by [32]

$$k_{app} = \sigma \frac{k_B T}{h} \frac{Q_{TS}}{Q_R} e^{-\Delta E_0^{\ddagger}/RT}$$

$\Delta E_0^{\ddagger}$ is the reaction barrier for the transition state including ZPVE. σ is the reaction path degeneracy that accounts for the number of equivalent reaction paths. k_B represents Boltzmann's constant, T is the temperature, h is Planck's constant.

This equation can be rewritten in terms of the molecular Gibbs free energy difference $\Delta G^{\ddagger}$ between the activated complex and the reactants (with inclusion of zero point vibration energies) :

$$k_{app} = \kappa \frac{k_B T}{h} \frac{RT}{p^{\theta}} e^{-\Delta G^{\ddagger}/RT}$$

where R represents the universal gas constant and κ is the transmission coefficient which is assumed to be about 1 and p^{θ} is the standard pressure 10^5 Pa (1 bar) [33].

In the case where the solvent effect is considered implicitly only, the effect of a polar environment was taken into account by use of the self-consistent reaction field (SCRF) theory, utilizing the integral equation formalism-polarizable continuum (IEF-PCM) model [34]. In the case where the solvent effect has been modeled explicitly and implicitly, the effect of the solvent is modeled as the sum of two contributions: one resulting from the explicit coordination with solvent molecules in the reactants and transition states and one originating from the bulk solvent effect as in earlier publications [35].

7.3 Results

The free radical polymerization of a monomer starts with the generation of free radicals from initiator (the non-radical species).

$$I \xrightarrow{k_d} R\bullet \qquad \text{(initiation)}$$

The methyl ($CH_3^{\cdot}$) radical was taken as the radical $R^{\cdot}$ in this study. Addition to a monomer of this radical produces the monomeric radical which consists of a backbone with three carbon atoms. This monomeric radical then adds to the monomer to generate the propagating polymer chain (propagation reaction). Radom et al. studied previously $CH_3^{\cdot}$ addition to the carbon-carbon double bond (C=C) by the aid of quantum chemical tools [36].

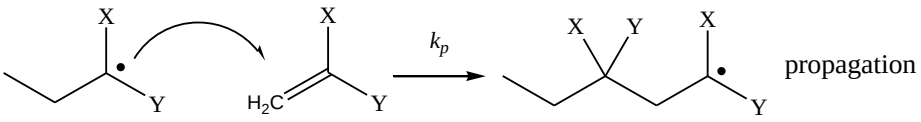

X=-H for AA and -CH_3 for MAA
Y=-COOH

Similar studies were conducted by Coote et al.[37-39] on vinyl monomers. They used high-level composite ab initio molecular orbital theory method (G3(MP2)-RAD [46]) that approximates CCSD(T) calculations with a large triple-ζ basis from calculations with a double-ζ basis set, via basis set corrections carried out at the R(O)MP2 level of theory. They calculated the rate coefficients and Arrhenius parameters with this composite method for dimer models and have corrected their gas phase results by computing solution phase calculations with the COSMO-RS [47] method. Experimentally observed head to tail propagation [40] which is assumed to be the most favorable mode of attack was proven by theoretical methods [41].

Geometrical Features of the monomers and the radicals

A conformational search was carried out for the monomers and the radicals. The s-*cis* geometry has the lowest energy for AA, while on the other hand the s-*trans* conformer of MAA has the lowest energy (Figure 7.2). Although the energy difference between s-cis and s-*trans* conformers is only 0.32 kcal/mol and 0.47 kcal/mol for AA and MAA respectively (Figure 7.3), the rotational barriers between s-cis and s-trans conformers of both monomers are more than 5 kcal/mol at B3LYP/6-31+G(d) level (Figure 7.2). These results are consistent with previous theoretical studies [43]. The general tendency of acrylates is to exist in the s-*cis* conformations whereas methacrylates exist in s-*trans* forms.

Notice that in both cases long range electrostatic interactions between the carbonyl oxygen and hydrogens stabilize these structures. In the case of MAA s-*trans* is preferred because of the bifurcation of the carbonyl oxygen between the hydrogens of the methyl group.

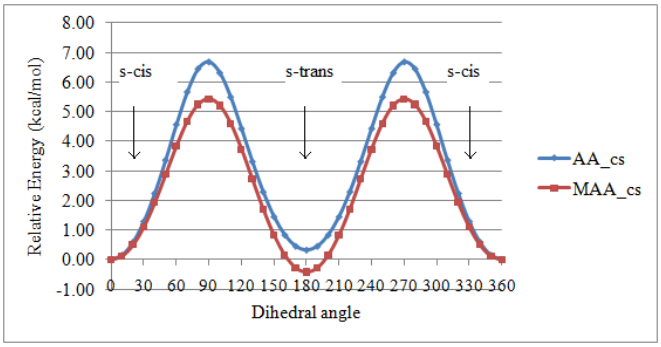

Figure 7.2. Rotational potential (kcal/mol) as a function of the dihedral angle CαCβCO for AA and MAA. (B3LYP/6-31+G(d)).

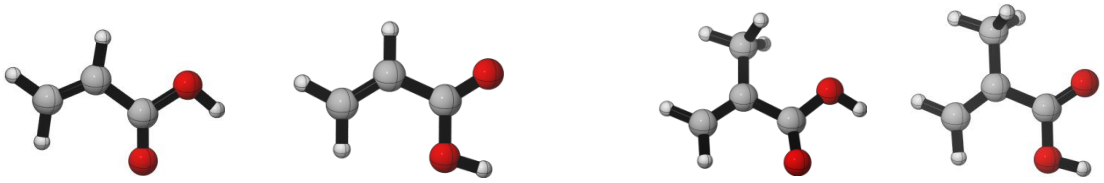

s-cis AA	s-trans AA	s-cis MAA	s-trans MAA
ΔE = 0.00 kcal/mol	0.20 kcal/mol	0.62 kcal/mol	0.00 kcal/mol
ΔG = 0.00 kcal/mol	0.18 kcal/mol	0.66 kcal/mol	0.00 kcal/mol

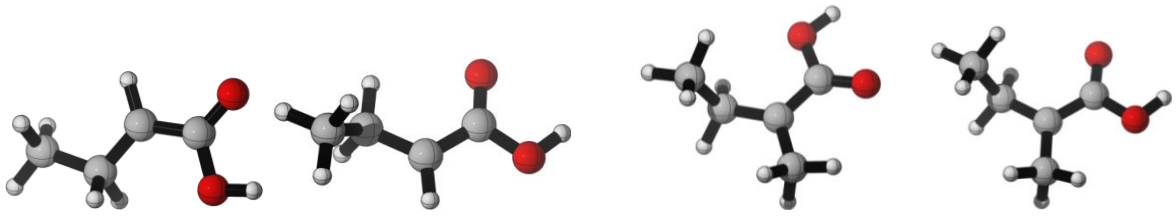

anti-AA-R	syn-AA-R	anti-MAA-R	syn-MAA-R
ΔE = 0.47 kcal/mol	0.00 kcal/mol	0.00 kcal/mol	0.04 kcal/mol
ΔG = 0.00 kcal/mol	0.00 kcal/mol	0.49 kcal/mol	0.00 kcal/mol

Figure 7.3. Relative energies and Gibbs Free Energies for the most stable conformers of the monomers and the radicals of AA and MAA at MPWB1K/6-311+G(3df,2p)//B3LYP/6-31+G(d) (kcal/mol).

Propagation Reaction

The addition of the radical to the monomer yielding syndiotactic and isotactic dimers is depicted in Scheme 7.1. The attack of the most stable radical -syn and anti conformers- to the most stable monomer–*s-cis* and *s-trans* conformers- is summarized Scheme 7.1.

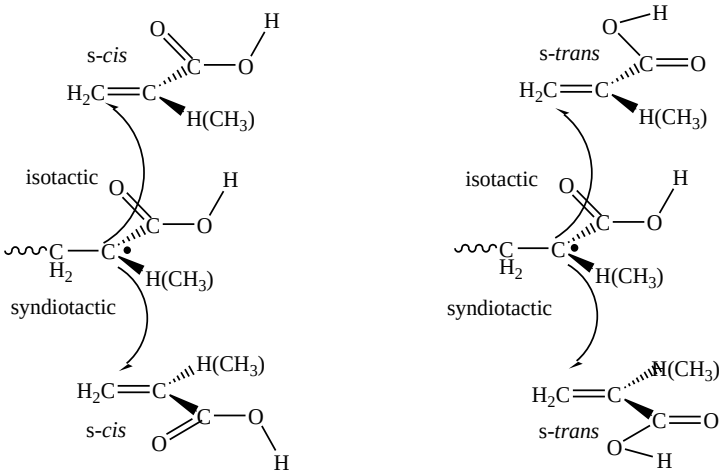

Scheme 7.1. Stereoselective radical (*syn*) addition to **AA** and **MAA** (s-*cis* and s-*trans*).

After generating the transition state geometries for eight plausible combinations of the radical and the monomer,a relaxed potential energy scan was carried out around the forming bond (Figure 7.4. and Figure 7.5.) in order to scan for all possible transition state structures.

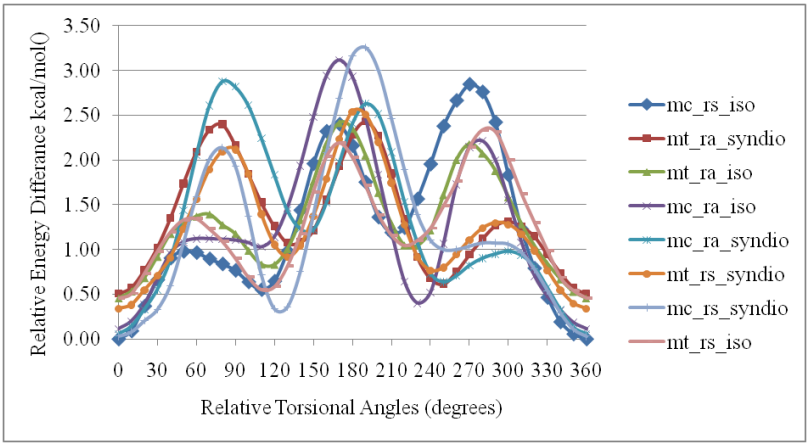

Figure 7.4. Rotational potentials (B3LYP/6-31+G(d)) for the propagation reactions of MAA.

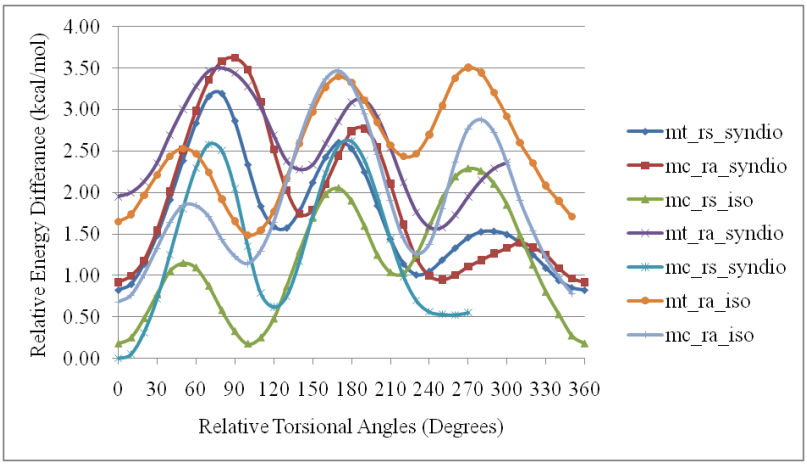

Figure 7.5. Rotational potentials (B3LYP/6-31+G(d)) for the propagation reactions of AA.

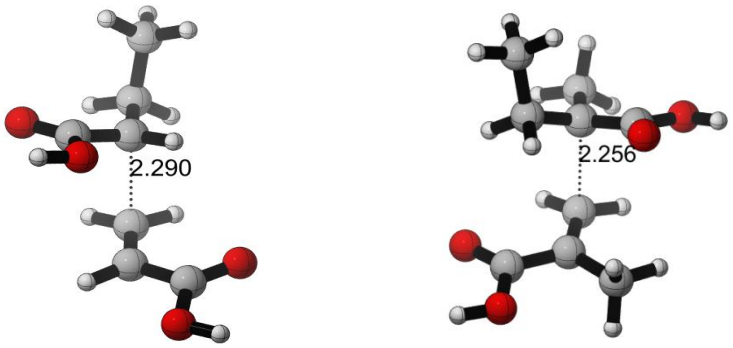

TS-AA TS-MAA

Figure 7.6. Most stable transition state structure of AA and MAA (B3LYP/6-31+G(d)).

According to the relaxed potential energy scan analysis around the forming bond, the most stable transition state structures for AA and MAA are presented in Figure 7.6. The eight plausible transition states of MAA have shown that for syndiotactic formation the addition prefers to be *anti* whereas for the isotactic dimer the *gauche* addition is preferred (Figure 8.6.). These trends are dictated by steric effects as well as by long range interactions between carbonyl oxygen and hydrogens of the methyl group. As in the case of methacrylates, in both cases –syndiotactic and isotactic- the radical is *syn* and the monomer is *s-cis* [42,43b-43d]. On the other hand, the eight possible transition states of

AA have shown that for syndiotactic dimer formation the addition is anti whereas for the isotactic one the gauche addition is preferred.

Table 7.1. Relative reaction barriers (kcal/mol) leading to syndiotactic and isotactic dimers (B3LYP/6-31+G(d)).

		MAA		**AA**	
	R\M	s-*cis*	s-*trans*	s-*cis*	s-*trans*
syndiotactic	*syn*	0.09	0.34	0.00	0.87
isotactic	*syn*	0.00	0.39	0.31	1.38
syndiotactic	*anti*	0.11	0.44	0.98	1.74
isotactic	*anti*	0.23	0.48	0.86	1.62

Explicit Solvent Study

Various complex structures with one water molecule were generated tested to find the most suitable monomer-water interaction geometry (1, 2, 3 in Figure 7.7). Formation of two hydrogen bonds stabilize the complex structure more than the other possibilities (Table 7.2). The complex stabilization energy (CSE) amounts to 8.62 kcal/mol in that case (Figure 7.8). However, the Gibbs free energy change of this geometry is positive, which might possibly ascribed to too much strain in the structure as the water molecule makes contact with the carbonyl and hydroxyl group. Therefore, the number of explicit solvent molecules has been increased to two and new solvated structures have been located (4,5,6,7 in Figure 7.7). The Gibbs free energy change is negative when two water molecules are used and the complex stabilization energy with two water molecules is about 19.05 kcal/mol (Figure 7.8). While water molecules make explicit interaction with methacrylic acid they also form hydrogen bonding with each other. Three water molecules were also used to generate a solvated MAA complex. The complex stabilization energy converges with three water molecules (Table 7.2). The complex stabilization energy difference between a complex with water molecules three water molecules is very small compared to the difference between one –water complex and two-water complex form. Because, the Gibbs free energy becomes positive when the solvent number increases to three, two water molecules can be considered as adequate to solvate MAA.

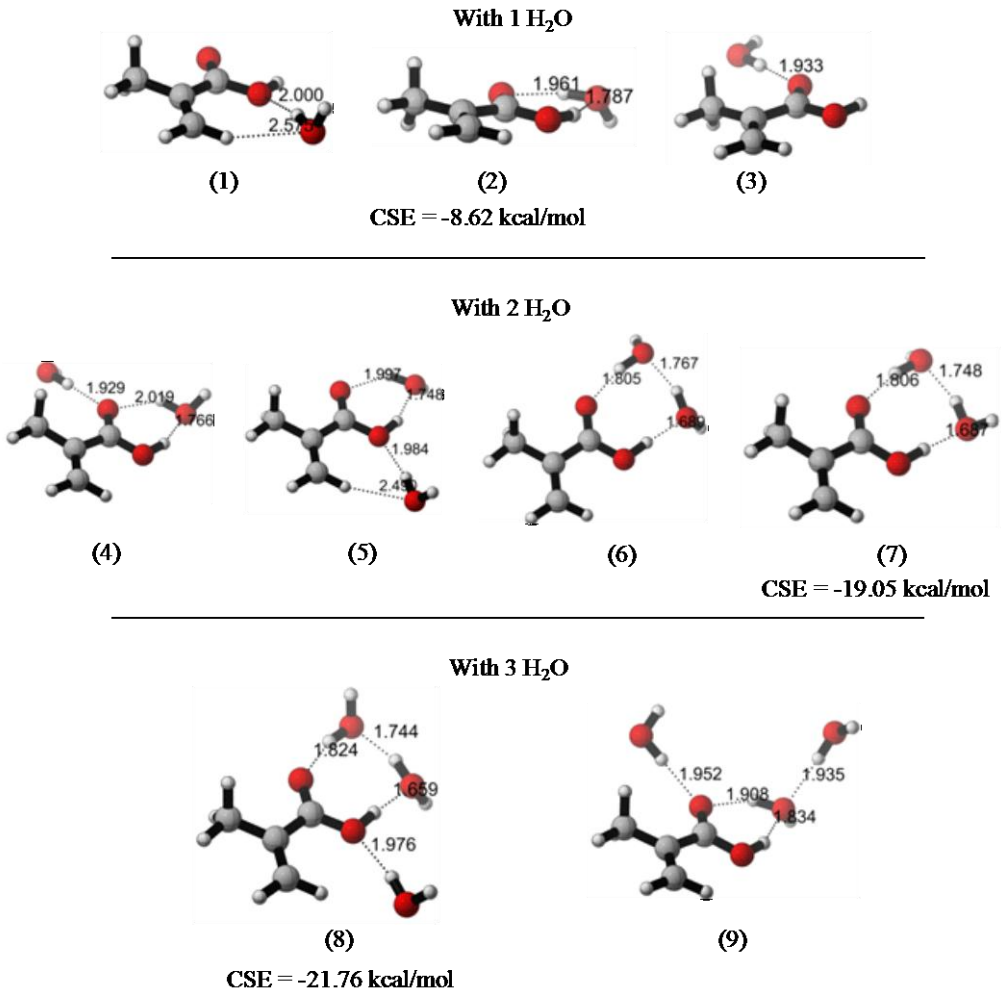

Figure 7.7. Solvation possibilities of MAA with different number of solvent molecules (B3LYP/6-31+G(d)).

Table 7.2. Energetics (kcal/mol) for solvation of MAA (B3LYP/6-31+G(d)).

	with 1 H_2O			with 2 H_2O				with 3 H_2O	
	1	2	3	4	5	6	7	8	9
ΔE^a	*6.74*	**0.00**	*4.69*	*6.75*	*7.97*	*0.55*	**0.00**	**0.00**	*6.23*
ΔG^b	*5.02*	**0.18**	*3.11*	*3.43*	*4.88*	*-1.16*	**-1.55**	**2.89**	*6.94*
CSE^c	*-1.87*	**-8.62**	*-3.93*	*-12.30*	*-11.08*	*-18.49*	**-19.05**	**-21.76**	*-15.53*

[a] relative energy between various solvated structures referred to the most stable one within a fixed number of water molecules,

[b] Gibbs free energy change (solvation energy),

[c] Complex Stabilization Energy.

Energetics about the most stabilized and solvated structures with water molecules which were given as bold data in Table 7.2 were plotted energy change (kcal/mol) versus number of water molecules in Figure 7.8.

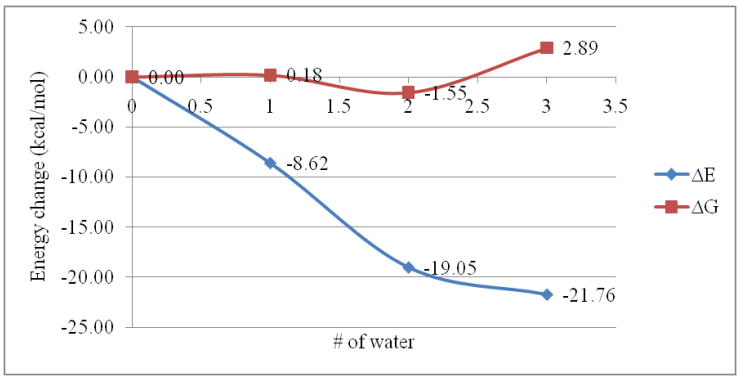

Figure 7.8. Gibbs free energy change and stabilization energies for solvation of MAA with various water molecules (kcal/mol). Only the most stable structures (2, 7, and 8) are taken up shown in Figure 7.7.

Similar to the solvation study of the monomer MAA, AA-water solvated complexes were also generated. In addition the most stable radical structures of both AA and MAA were solvated like the solvated in a similar fashion. In a next step the solvated monomers and radicals are used to locate solvated transition states (Figure 7.9).

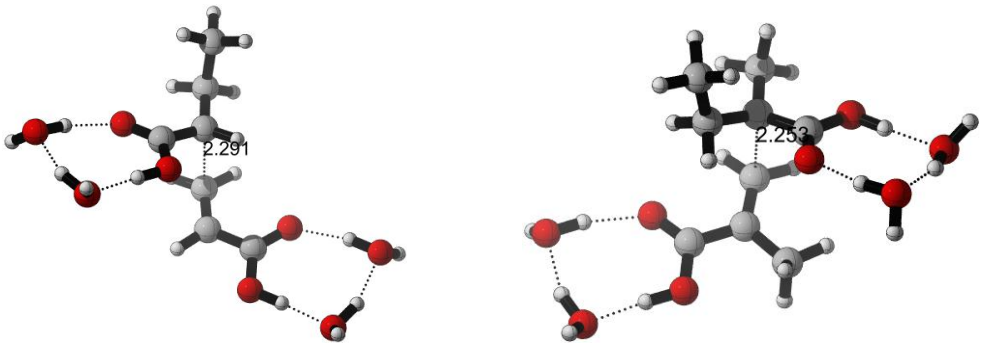

(AA) (MAA)

Figure 7.9. The propagation transition state structures for **AA** and **MAA** with four explicit water molecules.

Table 7.3 summarizes kinetic and energetic results for the propagation reaction of both monomers at room temperature. Results with/without explicit solvent and in polar continuum medium are presented in the Table 7.3. The experimental study has shown that, the propagation rate constant of AA is about 30 times faster than the propagation rate constant of MAA. This behavior was reproduced qualitatively in the gas phase. On the other hand, the propagation rate constant was not reproduced satisfactory with explicit solvent molecules.

Table 7.3. Kinetics (k_p is $l.mol^{-1}s^{-1}$) and energetics (kcal/mol) for AA and MAA at 298.15K. (UAKS cavity was used).

		B3LYP/6-31+G(d)			MPWB1K/6-311+G(3df,2p)			Exp.
		E_a	$\Delta G^{\neq}$	k_p	E_a	$\Delta G^{\neq}$	k_p	k_p
AA	gas	6.43	17.68	1.68E+01	5.09	16.34	1.62E+02	**20.1E+03**[a]
	explicit	6.49	18.04	9.13E+00	5.19	16.74	8.32E+01	
	implicit*	-	17.78	1.43E+01	-	15.85	3.73E+02	**11.9E+04**[b]
	explicit+implicit*	-	17.75	1.50E+01	-	15.81	3.94E+02	
MAA	gas	8.84	21.75	1.77E-02	6.10	19.00	1.83E+00	**5.74E+02**[c]
	explicit	8.71	22.38	6.05E-03	5.80	19.47	8.21E-01	
	implicit*	-	21.75	1.75E-02	-	20.63	1.15E-01	**3.83E+03**[b]
	explicit+implicit*	-	24.96	7.76E-05	-	21.14	4.91E-02	

*****6-311+G(3df,2p)

[a] Ref. [29], [b] Ref. [30], [c] Ref. [31] (15 wt % MAA)

Table 7.4. Relative ratios of kinetic dates about AA and MAA.

	B3LYP/6-31+G(d)			MPWB1K/6-311+G(3df,2p)			Exp.
	A	B	C	A	B	C	A
Gas	949.15	-	-	88.52	-	-	35.02
explicit	1509.09	0.54	0.34	101.34	0.51	0.45	31.07
implicit	817.14	0.85	0.99	3243.48	2.30	0.06	
explicit+implicit	193298.97	0.89	0.00	8024.44	2.43	0.03	

A is kp_{AA}/kp_{MAA}, B is $kp_{AA\ in\ water}/kp_{AA\ in\ gas\ phase}$, C is $kp_{MAA\ in\ water}/kp_{MAA\ in\ gas\ phase}$, kp_{AA}/kp_{MAA} in bulk is 5.92 and it is in water 6.67.

The gas phase study has shown that AA has an earlier transition state than MAA. The forming bond distance at the transition state is 2.29 Å for AA while it is 2.26 Å for MAA (Figure 7.6). These geometrical properties of the transition state can influence the reaction barrier of AA significantly. Most probably these geometrical features can be ascribed to additional steric effects present in MAA due to the the methyl group at α position of the monomer. The early transition state and absence of the steric group close to the reactive center for the addition reaction leads to a higher rate for the propagation reaction in case of AA.

A molecular dynamic study with the CHARMM force field was conducted on the monomers in order to understand the complexation behavior of MAA. Therefore 1000 monomers were placed in a periodic box and a NPT simulation was conducted at T = 298.15K and P = 1atm. This study has shown that the MAA monomer prefers a dimeric complex form in the bulk. Based on MD findings, dimeric complex forms of AA and MAA were generated by the standard static methods (Figure 7.10).

The dimeric complex form of the MAA (monomers CSE is -15.27 kcal/mol) is 3.78 kcal/mol less stabilized than the one with two water molecules (CSE is -19.05 kcal/mol). This behavior points to the fact that MAA prefers to be solvated by water instead than by other monomers present in the reaction medium. The same behavior was found for AA.

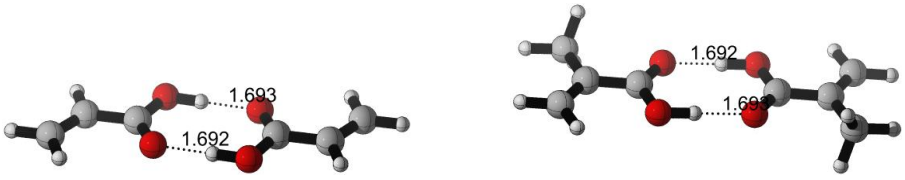

AA-AA-dimer
(CSE = -15.25 kcal/mol)
(ΔG = -3.99 kcal/mol)

MAA-MAA-dimer
(CSE = -15.27 kcal/mol)
(ΔG = -4.03 kcal/mol)

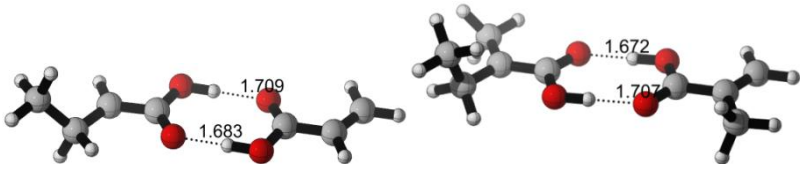

AA-AA-R-dimer MAA-MAA-R-dimer

Figure 7.10. Dimeric complexes of monomers and radicals for AA and MAA.

As seen from the 3D structures, the dimers are held tight together with two H-bonds. The Gibbs free energy change associated with complexation of two monomers both for AA and MAA show that the complexation energy of these two monomers is almost the same at the dimeric complex form (the free energy change of solvation amount to -3.99 kcal/mol for AA and -4.03 kcal/mol for MAA). The trimeric complex forms of MAA have also been modeled, but dimeric complex forms of MAA are found to be more solvated than trimeric complex forms. The Gibss Free energy change difference between dimeric and trimeric form is 4.69 kcal/mol at B3LYP/6-31+G(d) level and 298.15K. This means that the monomer prefers to form a dimeric complex instead of a trimeric complex.

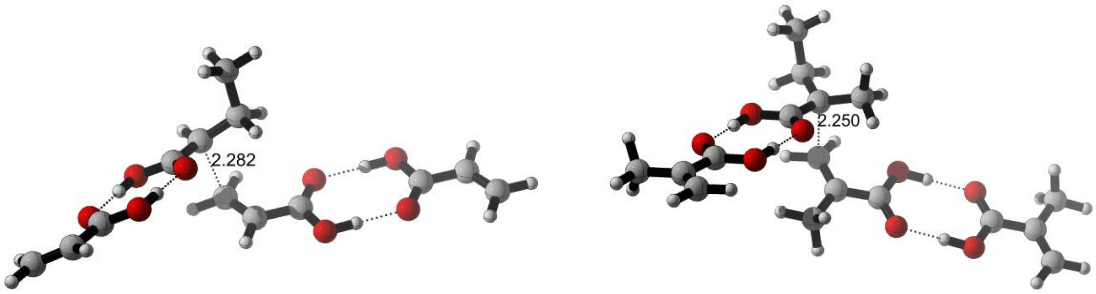

Figure 7.12. The transition states of propagation reaction for AA and MAA with dimeric complex form.

Dimeric complex forms of the transition states for propagation reaction of **AA** and **MAA** have also been located (Figure 7.12). The propagation rate constants of dimeric complex geometry for AA is 1.36E+02 $L.mol^{-1}.s^{-1}$ and for MAA is 5.34E+00 $L.mol^{-1}.s^{-1}$ at MPWB1K/6-311+G(3df,2p)//B3LYP/6-31+G(d) level of theory. Modeling the propagation reaction of the monomers with these dimeric complex structures does not give a reasonable explanation for the difference between polymerization behavior of AA with respect to MAA. Further research is needed at this point to also investigate the possible role of prereactive complexes to fully explain the relative ratios of polymerization between AA and MAA with the solvated structures.

7.4. Conclusions

The relative propagation rate constants for AA and MAA have been reproduced with quantum chemical tools in the gasphase. The faster polymerization of AA can be ascribed to an earlier transition state and less steric hindrance. Furthermore solvated structures were localized for MAA and AA monomers, radicals and transition states. For the monomers it was found that both in case of AA and MAA solvation with two water molecules is preferred. In addition it was tested in how far the monomer has the tendency to be solvated with other monomers in the reaction medium. Therefore preliminary structures were localized with MD simulations which were then further optimized at the B3LYP level of theory. We found that both for AA and MAA the monomers are best solvated with water and not with other monomers present. In addition we tried to reproduce the relative ratios for polymerization between AA en MAA also with solvent molecules. When only explicit solvent molecules are included the relative ratio is slightly too high compared to the experimental data. When a combined explicit/implicit solvent model is used the ratios are not in the right order of magnitude. Therefore further studies will be conducted to elucidate in how far pre-reactive complexes can play an important role in the kinetics of the MAA and AA monomers. This study shows that the proper modeling of solvent effects for free radical polymerization is not straightforward.

7.5. References

1. *Handbook of Polyelectrolytes and their Applications*, Tripathy, S. K., Kumar, J., Nalva, H. S., Eds.; American Scientific Publishers: Stevenson Ranch, CA, 2002.

2. Kirsh, Yu. E. *Water Soluble Poly-N-Vinylamides Synthesis and Physiochemical Properties*; John Wiley & Sons Ltd.: Chichester, U.K., 1998.

3. Beuermann, S.; Buback, M. *Prog. Polym. Sci.* **2002**, *27*, 191–254.

4. Olaj, O. F.; Schnöll-Bitai, I.; Hinkelmann, F. *Makromol. Chem.* **1987**, *188*, 1689–1702.

5. Methacrylic acid: Beuermann, S.; Paquet, D. A.; McMinn, J. H.; Hutchinson, R. A. *Macromolecules* **1997**, *30*, 194. Acrylic acid: Santos, A. M. *Entropie* **1998**, *212/213*, 31.

6. Davis, T. P.; O'Driscoll, K. F.; Piton, M. C.; Winnik, M. A. *Macromolecules* **1989**, *22*, 2785. Morrison, B. R.; Piton, M. C.; Winnik, M. A.; Gilbert, R. G. *Macromolecules* **1993**, *26*, 4368. Beuermann, S.; Buback, M.; Russell, G. T. *Macromol. Rapid Commun.* **1994**, *15*, 647. Hutchinson, R. A.; Richards, J. R.; Aronson, M. T. *Macromolecules* **1994**, *27*, 4530. Lyons, R. A.; Hutovic, J.; Pinton, M. C.; Christie, D. I.; Clay, P. A.; Manders, B. G.; Kable, S. H.; Gilbert, R. G. *Macromolecules* **1996**, *29*, 1918.

7. Kuchta, F. D.; Van Herk, A. M.; German, A. L. *Macromolecules*, **2000**, *33*, 3641-3649.

8. Beuermann, S., *Macromolecular Rapid Comminications*, **2009**, *30*, 1066-1088.

9. O'Driscoli, K. F.; Monteiro, M. J.; Klumperman, B., *J. Polym. Sci., Part A: Poly. Chem.*, **1997**, *35*, 515 ; Zammit, M. D.; Davis, T. F.; Willett, G. D.; O'Driscoli, K. F., *J. Polym. Sci., Part A: Poly. Chem.*, **1997**, *35*, 2311.

10. Harrisson, S.; Barner-Kowollik, C.; Davis, T. P.; Evans, K.; Rizzardo, R.; Stenzel, M.; Yin, M.; Z. *Phys. Chem.*, **2005**, *219*, 267.

11. Beuermann, S.; Buback, M.; Hesse, P.; Lacı´k, I. *Macromolecules* **2006**, *39*, 184–193.

12. Beuermann, S.; Buback, M.; Hesse, P.; Kukuckova, S.; Lacík, I. *Macromol. Symp.* **2007**, *248*, 23–32.

13. Beuermann, S.; Buback, M.; Hesse, P.; Kukuckova, S.; Lacík, I. *Macromol. Symp.* **2007**, *248*, 41–49.

14. Beuermann, S.; Buback, M.; Hesse, P.; Kuchta, F.-D.; Lacík, I.; van Herk, A. M. *Pure Appl. Chem.* **2007**, *79*, 1463–1469.

15. Lacík, I.; Beuermann, S.; Buback, M. *Macromolecules* **2001**, *34*, 6224– 6228.

16. Lacík, I.; Beuermann, S.; Buback, M. *Macromolecules* **2003**, *36*, 9355– 9363.

17. Lacík, I.; Beuermann, S.; Buback, M. *Macromol. Chem. Phys.* **2004**, *205*, 1080–1087

18. Ganachaud, F.; Balic, R.; Monteiro, M. J.; Gilbert, R. G. *Macromolecules* **2000**, *33*, 8589–8596.

19. Seabrook, S. A.; Tonge, M. P.; Gilbert, R. G. *J. Polym. Sci., Part A: Polym. Chem.* **2005**, *43*, 1357–1368.

20. Plochocka, K. *J. Macromol. Sci., Rev. Macromol. Chem.* **1981**, *20*, 67.

21. Chapiro, A.; Dulieu, J. *Eur. Polym. J.* **1977**, *13*, 563. Chapiro, A. *Pure Appl. Chem.* **1981**, *53*, 643.

22. Gromov, V. F.; Galperina, N. I.; Osmanov, T. O.; Khomikovskii, P. M.; Abkin, A. D. *Eur. Polym. J.* **1980**, *16*, 529.

23. Buback, M.; Pascal Hesse, P.; Hutchinson, R. A.; Kasák, P.; Lacík, I.; Stach, M.; Utz, I. *Ind. Eng. Chem. Res.* **2008,** *47*, 8197–8204.

24. S. A. Seabrook, M. P. Tonge, R. G. Gilbert, *J. Polym. Sci., Part A: Polym. Chem.* **2005**, 43, 1357.

25. Heuts, J. P. A.; Gilbert, K. G.; Radom, L. *Macromolecules*, **1995**, *28*, 8771. Heuts, J. P. A.; Gilbert, K. G.; Mazwell, I. A. *Macromolecules*, **1997**, *30*, 726. Thicket, S. C.; Gilbert, K. G.; *Polymer*, **2004**, *45*, 6993. Igorodina, E. I.; Coote, M. L.; *Chem. Phys.*, **2006**, *324*, 96, Van Speybroeck, V.; Van Neck, D.; Waroquier, M.; Wauters, S.; Saeys, M.; Marin, G. B. *J. Phys. Chem. A* **2000**, *104* (46), 10939- 10950, Vansteenkiste, P.; Van Speybroeck, V.; Marin, G. B.; Waroquier, M. *J. Phys. Chem. A* **2003**, *107* (17), 3139-3145, Van Speybroeck, V.; Vansteenkiste, P.; Van Neck, D.; Waroquier, M. *Chem. Phys. Lett.* **2005**, *402*, 479-484.

26. Ganachaud, F.; Balic, R.; Monteiro, M. J.; Gilbert, K. G. *Macromolecules*, **2000**, *33*, 8589. Seabrook, S. A.; Tonge, M. P.; Gilbert, K. G. *J. Polym. Sci., Part A: Poly. Chem.*, **2005**, *43*, 1357.

27. Beuermann, S. *Macromol. Rapid Commun.* **2009**, 30, 1066–1088.

28. Gaussian 03, Revision D.01, Frisch, M. J.; Trucks, G. W.; Schlegel, H. B.; Scuseria, G. E.; Robb, M. A.; Cheeseman, J. R.; Montgomery, Jr., J. A.; Vreven, T.; Kudin, K. N.; Burant, J. C.; Millam, J. M.; Iyengar, S. S.; Tomasi, J.; Barone, V.; Mennucci, B.; Cossi, M.; Scalmani, G.; Rega, N.; Petersson, G. A.; Nakatsuji, H.; Hada, M.; Ehara, M.; Toyota, K.; Fukuda, R.; Hasegawa, J.; Ishida, M.; Nakajima, T.; Honda, Y.; Kitao, O.; Nakai, H.; Klene, M.; Li, X.; Knox, J. E.; Hratchian, H. P.; Cross, J. B.; Bakken, V.; Adamo, C.; Jaramillo, J.; Gomperts, R.; Stratmann, R. E.; Yazyev, O.; Austin, A. J.; Cammi, R.; Pomelli, C.; Ochterski, J. W.; Ayala, P. Y.; Morokuma, K.; Voth, G. A.; Salvador, P.; Dannenberg, J. J.; Zakrzewski, V. G.; Dapprich, S.; Daniels, A. D.; Strain, M. C.; Farkas, O.; Malick, D. K.; Rabuck, A. D.; Raghavachari, K.; Foresman, J. B.; Ortiz, J. V.; Cui, Q.; Baboul, A. G.; Clifford, S.; Cioslowski, J.; Stefanov, B. B.; Liu, G.; Liashenko, A.; Piskorz, P.; Komaromi, I.; Martin, R. L.; Fox, D. J.; Keith, T.; Al-Laham, M. A.; Peng, C. Y.; Nanayakkara, A.; Challacombe, M.; Gill, P. M. W.; Johnson, B.; Chen, W.; Wong, M. W.; Gonzalez, C.; and Pople, J. A.; Gaussian. Inc., Wallingford CT, **2004**.

29. Smith, D. M.; Nicolaides, A.; Golding, B. T.; Radom, L. *J. Am. Chem. Soc.* **1998**, *120*, 10223-10233.

30. Zhao, Y.; Truhlar, D. G. *J. Phys. Chem. A* **2004**, *108*, 6908–6918.

31. Liang,K.; Dossi, M.; Moscatelli, D.; Hutchinson, R. A. *Macromolecules*, **2009**, *42*, 7736-7744.

32. McQuarrie, D. A.; Simon, J. D. *Physical Chemistry-A molecular approach; University Science Books*: Sausalito, CA, 1997.

33. *Atkins' Physical Chemistry*, 8th ed.; Atkins, P.; De Paula, J.; Oxford University Press, New York, **2006**.

34. (a) Tomasi, J.; Mennucci, B.; Cance`s, E. *J. Mol. Struct.: THEOCHEM* **1999**, *464*, 211-226. (b) Cance`s, M. T.; Mennucci, B.; Tomasi, J. *J. Chem. Phys.* **1997**, *107*, 3032-3041. (c) Mennucci, B. Tomasi, J. *J. Chem. Phys.***1997**, *106*, 5151-5158. (d) Mennucci, B.; Cance`s, E.; Tomasi, J. *J. Phys.Chem. B* **1997**, *101*, 10506-10517.

35. Kelly, C. P.; Cramer, C. J.; Truhlar, D. G. *J. Phys. Chem. A* **2006**, *110*, 2493–2499. Kamerlin, S. C. L.; Haranczyk, M.; Warshel, A. *ChemPhysChem* **2009**, *10*, 1125–1134. De Sterck, B.; Van Speybroeck, V.; Mangelinckx, S.; Verniest, G.; De Kimpe, N.; Waroquier, M. *J. Phys. Chem. A* **2009**, *113*, 6375–6380. Van Speybroeck, V.; Moonen, K.; Hemelsoet, K.; Stevens, C.; Waroquier, M. *J. Am. Chem. Soc.* **2006**, *128*, 8468–8478. Kelly, C. P.; Cramer, C. J.; Truhlar, D. G. *J. Chem. Theory Comput.* **2005**, *1*, 1133–1152.

36. (a) Heuts, J. P. A.; Gilbert, R. G.; Radom, L. *Macromolecules* **1995**, *28*, 8771-8781. (b) Wong, M. W.; Radom, L. *J. Phys. Chem.* **1995**, *99*, 8582-8588. (c) Heuts, J. P. A.; Gilbert, R. G.; Radom, L. *J. Phys. Chem.* **1996,** *100*, 18997-19006. (d) Wong, M. W.; Radom, L. *J. Phys. Chem. A* **1998,** *102*, 2237-2245. (e) Fischer, H.; Radom, L. *Angew. Chem. Int. Ed.* **2001**, *40*, 1340 -1371. (f) Go´mez-Balderas, R.; Coote, M. L.; Henry, D. J.; Fischer, H.; Radom, L. *J. Phys. Chem. A* **2003,** *107*, 6082-6090. (g) Go´mez-Balderas, R.; Coote, M. L.; Henry, D. J.; Radom, L. *J. Phys. Chem. A* **2004,** *108*, 2874-2883. (h) Henry, D. J.; Coote, M. L.; Go´mez-Balderas, R.; Radom, L. *J. Am. Chem. Soc.* **2004**, *126*, 1732-1740.

37. Izgorodina, E. I.; Coote, M. L. *Chem. Phys.* **2006**, 324, 96–110.

38. Coote, M. L. *Macromol. Theory Simul*. **2009**, *18*, 388–400.

39. Lin, C. Y.; Izgorodina, E. I.; Coote, M. L. *Macromolecules* **2010**, *43*, 553–560.

40. Pilling, M. J.; Seakins, P. W. *Reaction Kinetics*; Oxford University Press: New York, **1996**.

41. Van Cauter, K.; Van Speybroeck, V.; Waroquier, M. *ChemPhysChem*, **2007**, *8*, 541-552.

42. Yu, X.; Pfaendtner, J.; Broadbelt, L. J. *J. Phys. Chem. A* **2008**, *112*, 6772–6782.

43. a) Değirmenci, İ.; Avcı, D.; Aviyente, V.; Van Cauter, K.; VanSpeybroeck, V.; Waroquier, M. *Macromolecules* **2007**, *40*, 9590–9602. b) Değirmenci, İ.; Aviyente, V.; Van Speybroeck, V.; Waroquier, M. *Macromolecules* **2009**, *42*, 3033-3041. c) Furuncuoğlu, T.; Uğur, İ.; Değirmenci, İ.; Aviyente, V. *Macromolecules* **2010**, 43, 1823-1835. d)Değirmenci, İ.; Eren, Ş.; Aviyente, V.; De Sterck, B.; Hemelsoet, K.; Van Speybroeck, V.; Waroquier, M.; *Macromolecules*, **2010**, *43*, 5602–5610.

44. Günaydın, H.; Seyhan, S.; Tüzün, N. Ş.; Avcı,D.; Aviyente, V. *Int. J. Quant. Chem.*, **2005**, *103*, 176- 189. d) Salman, S.; Ziylan Albayrak A.; Avcı, D.; Aviyente, V. *J. Polym. Sci., Part A: Poly. Chem.* **2005**, *43*, 2574–2583.

45. Liang,K.; Dossi, M.; Moscatelli, D.; Hutchinson, R. A. *Macromolecules* **2009**, *42*, 7736-7744.

46. Henry, D. J.; Sullivan, M. B.; Radom, L. *J. Chem. Phys*. **2003**, 118, 4849–4860.

47. (a) Klamt, A. *J. Phys. Chem*. **1995**, 99, 2224–2235.(b) Klamt, A. COSMO-RS: From Quantum Chemistry to Fluid Phase Thermodynamics and Drug Design; Elsevier Science Ltd.: Amsterdam, The Netherlands, 2005. (c) Klamt, A.; Jonas, V.; Burger, T.; Lohrenz, J. C. W. *J. Phys. Chem. A* **1998**, 102, 5074–5085.

8. ROLE OF CHAIN TRANSFER AGENTS IN FREE RADICAL POLYMERIZATION KINETICS

8.1. Introduction

The molecular weight control of polymers is a subject of increasing interest since many of their properties such as physical and mechanical properties depend on the chain length [1]. In the conventional free radical polymerization the control of the polymer chain length is difficult to attain. The classical method of controlling molecular weights is the addition of chain transfer agents to the polymerization medium. For many industrially important systems, a chain transfer agent is added to the polymerization composition in order to lower the polymer molecular weight [2]. A growing macro radical abstracts a hydrogen atom from the chain transfer agent giving a terminated polymer chain and a new initiating radical, which adds to the monomer giving a new propagating species. The general chain transfer constant, C_s, defined as the ratio of the chain transfer and propagation rate coefficients, k_{ct}/k_p is a measure of the reactivity of a chain transfer agent. The higher is C_s, the lower the concentration of the chain transfer agent required for a particular molecular weight reduction [3].

$$C_s = \frac{k_{ct}}{k_p}$$

The decrease of the molecular weight by the addition of a chain transfer agent is quantitatively given by the Mayo equation [4], which expresses the reciprocal of the polymerization degree (D_{Pn}) as a function of the rate of the chain growth and the chain stopping,

$$\frac{1}{D_{Pn}} = \frac{1+\alpha}{(D_{Pn})_0} + C_s \frac{[CTA]}{[M]}$$

In this equation, $(D_{Pn})_0$ is the polymerization degree in the absence of chain transfer agent, [CTA] is the concentration of the chain transfer agent, [M] is the monomer concentration, and α is the fraction of termination by disproportionation [5].

In the last decade the control of molecular weight has also been achieved by a living radical polymerization such as atom transfer radical polymerization (ATRP) [6-9], nitroxide-mediated polymerization (NMP) [10-11], and reversible addition-fragmentation chain transfer (RAFT) polymerization [12-13]. Catalytic chain-transfer (CCT) agents have also a control on the molecular weight: substituted cobalt porphyrins, or benzoporphyrins have been shown to provide dramatic reductions in the molecular weight of the methacrylate polymers during radical polymerization with little to no reduction in overall yield of polymer [14].

In parallel with experimental developments, quantum mechanical tools have been used to model the chain transfer reactions in free radical polymerization processes. Radom et al. have used the B3LYP/6-31G(d) methodology and the curve-crossing model to study the hydrogen transfer between ethyl radical and ethylene: an example where kinetics does not follow thermodynamics [15]. Gilbert et al. have modeled the short-chain branching in polyethylene with ab initio quantum mechanics up to the QCISD(T) level [16]. Density functional calculations are reported for the bond dissociation energy of a number of dithioacetates, $CH_3C(S)S$-R and selected dithiobenzoates, PhC(S)S-R, used mainly in addition-fragmentation transfer (RAFT) controlled radical polymerization [17]. The usage of quantum chemical tools in elucidating the chain transfer process via the reversible addition fragmentation chain transfer (RAFT) polymerization has been thoroughly investigated by Coote et al [18]. The latter have identified significant penultimate effects in the equilibrium constants between active and dormant species of atom transfer radical systems (ATRP) [19]. The same group has determined the equilibrium constants for the Cu-based atom transfer radical polymerization (ATRP) for a wide range of ligands and initiators in acetonitrile [20] and have reported the thermodynamic and electrochemical properties of alkyl halides used as ATRP initiators [21]. Among others a high-level ab initio study by the group of Coote et al. is on the evaluation of rate coefficients for the intra- and intermolecular hydrogen abstraction reactions in the formation of the various types of defect structures in radical suspension polymerization of vinyl chloride [22]

followed by a study on PVC where hydrogen abstraction reactions, especially backbiting and abstraction from chloroallylic end groups are emphasized [23]. The main reaction routes that lead to the formation of structural defects in PVC have also been studied by Van Speybroeck et al. with the BMK/6-311+G(3df,2p)//B3LYP/6-31+G(d) methodology [24]. A DFT modeling study in our group has shown the chain transfer to play a major role in inhibiting the polymerization of dimethylaminoethyl acrylate [25].

Experimental and theoretical studies on hydrogen and halogen atom transfer reactions have illustrated the structure-reactivity relationship in these reactions as well as the importance of polar effects in the transition states; several theoretical frameworks such as the curve-crossing model of Shaik and Pross have been developed to explain these results [26]. A study on alkyl halides, RX, reports their reduction to the corresponding alkanes, RH, by triethylsilane in the presence of a suitable initiator and an alkanethiol catalyst [27]. The reactions of methanethiyl radicals ($CH_3S\cdot$) with the cyclic anhydrides of glycine, alanine, sarcosine and the acyclic peptides were studied by means of B3LYP/6-311+G(d,p) calculations and it has been concluded that the ultimate site of free-radical damage in proteins will rest at the backbone α C-site, rather than at a thiol [28]. Recently, high level ab initio calculations have been used to understand the hydrogen abstraction by carbon-centered radicals from thiols where a reasonable correlation between the barrier height and the polar effects has been found [29]. Dolbier et al. have highlighted the importance of transition-state polar effects in hydrogen atom transfer reactions: the rate of reduction of fluoroalkyl radicals by PhSH has shown that PhS-H, a very efficient H atom donor to hydrocarbon radicals, reduced perfluoro-n-alkyl radicals - 500 times slower. This result indicates that transition-state polar effects must also play a significant role in such hydrogen atom transfer reactions [30].

In this study, quantum mechanical calculations have been used to model and understand the role of chain transfer agents in the free radical polymerization of ethylene.

8.2. Methodology and Computational Procedure

The free-radical polymerization proceeds via a chain mechanism and consists of four elementary reactions, i.e., initiation, propagation, chain transfer, and termination [31]. The

first step is the production of free radicals from the initiator molecule by light and heat. The initiator radical attacks the monomer to create a new radical. Successive additions of newly formed radicals and monomers is called propagation which is the main reaction of polymerization.

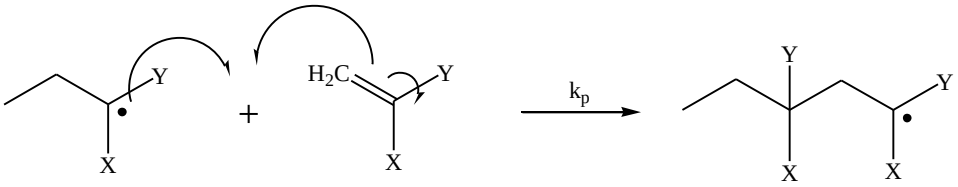

The propagating radical may attack to another monomer by chain transfer and the radical center may be transferred to another chain, so that the molecular weight of the propagating polymer can be controlled.

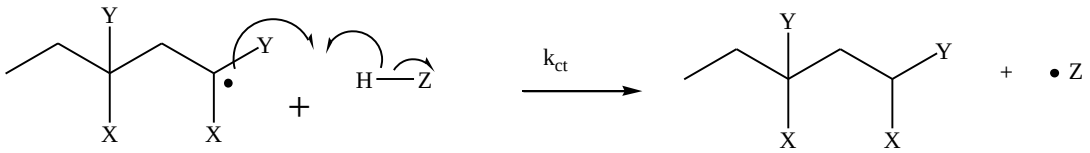

The polymerization reaction ends up by the combination of two radicals.

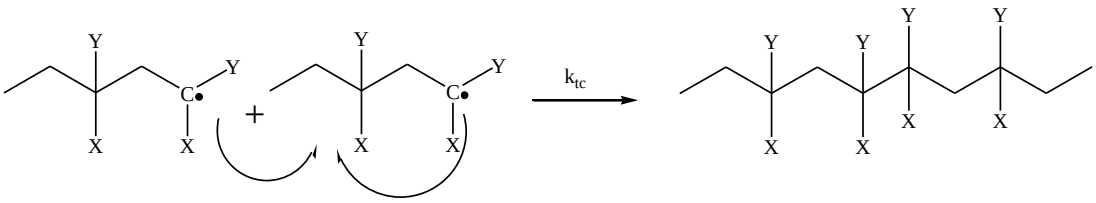

The activated complex theory pictures a reaction between A and B as proceeding through the formation of an activated complex, $C^{\ddagger}$, in a rapid pre-equilibrium:

$$A + B \rightleftharpoons C^{\ddagger} \rightarrow P$$

The activated complex falls apart by a unimolecular decay into the products, P.

Provided that $\overline{K}^{\ddagger}$ is the equilibrium constant (despite one mode of $C^{\ddagger}$ having been discarded), $\Delta G^{\ddagger}$ can be expressed through the definition

$$\Delta G^{\ddagger} = -RTln\overline{K}^{\ddagger}$$

Then the rate constant becomes

$$k_2 = \kappa \frac{kT}{h} \frac{RT}{p^\theta} e^{-\Delta G^\ddagger / RT}$$

where k represents Boltzmann's constant, T is the temperature, h is Planck's constant, $\Delta G^\ddagger$ represents the molecular Gibbs free energy difference between the activated complex and the reactants (with inclusion of zero point vibrational energies), R is the universal gas constant, κ is the transmission coefficient which is assumed to be about 1 and p^θ is the standard pressure 10^5 Pa (1 bar) [32].

Density functional theory was used for all geometry optimizations by using the Gaussian 03 program package [33]. We selected the B3LYP/6-31+G(d) methodology as a cost effective method as it was also used in previous reports to model the free radical propagation reactions [25,34-36]. Although B3LYP is accurate for geometry optimizations, it is not suitable for obtaining kinetic results [37]. Different hybrid meta GGA functionals - MPWB1K [38] and M05-2X [39] - have been used to obtain more realistic kinetic results. A recent study on hybrid meta DFT methods has shown that MPWB1K can be used with confidence for a combination of thermochemistry, thermochemical kinetics, hydrogen bonding, and weak interactions, especially for thermochemical kinetics and noncovalent interactions [38]. M05-2X is a hybrid meta exchange-correlation functional which was designed for very general purposes such as kinetics, thermochemistry of main group elements, noncovalent interactions, ionization potentials and activation energies [39]. For the activation energy barriers, it was found that this method is less accurate than BB1K, PWB6K, MPWB1K, MPW1K, BMK, for H-abstraction reactions, but more accurate than B3LYP and other functional [39].

The transition structures for the addition, hydrogen abstraction and chlorine abstraction reactions have a very low vibrational frequency, corresponding to the internal rotation of the incoming radical about the forming bond. Recent studies of radical addition [25,35,40] and hydrogen abstraction reactions [41] have been modeled by using the 1D-HR approach. In this study we used a mixed harmonic oscillator/hindered rotor (HO/HR) model, in which all the internal motions except the internal rotations corresponding to bond formation are approximated as independent harmonic oscillators. Tunneling corrections for the abstraction of hydrogen have been used in modeling since the abstracted hydrogen atom is light and its wavelength is large compared with the barrier width, thereby enabling

it to ‘tunnel’ through the barrier. Hybrid DFT methods such as MPW1K and B3LYP have been used to obtain reasonable estimates of the tunneling coefficients -to within a factor of 2–3 [42]. In recent studies both Wigner [43] and Eckart [44] methodologies have been used successfully for hydrogen abstraction reactions [25, 45].

To calculate the bond dissociation energies of the chain transfer agents we have made use of isodesmic reactions which conserve the number of each bond type on either side of the reaction resulting in significant improvements in calculated reaction enthalpies due to the cancellation of systematic calculation errors [46].

The bond dissociation energy for R-X (X=H or Cl) can be calculated by using equation (2)

$$R\text{-}X \rightarrow R\cdot + X\cdot \quad (1)$$

$$BDE\ (R\text{-}X) = \Delta_f H^0_{298}(R\cdot) + \Delta_f H^0_{298}(X\cdot) - \Delta_f H^0_{298}(R\text{-}X) \quad (2)$$

The energy of the isodesmic reaction 3 has been expressed in equation 4

$$R\text{-}X + CH_3\cdot \rightarrow R\cdot + CH_3X \quad (3)$$

$$\Delta_{rxn} H^0_{298}\ (3) = \Delta_f H^0_{298}(CH_3X) + \Delta_f H^0_{298}(R\cdot) - \Delta_f H^0_{298}(CH_3\cdot) - \Delta_f H^0_{298}(R\text{-}X) \quad (4)$$

Equation (4) is substituted in equation (2) to evaluate the bond dissociation energy of R-X as displayed in equation (5)

$$BDE\ (R\text{-}X) = \Delta H_{rxn}(3) - \Delta_f H^0_{298}(CH_3X) + \Delta_f H^0_{298}(CH_3\cdot) + \Delta_f H^0_{298}(X) \quad (5)$$

where $\Delta_f H^0_{298}(CH_3Cl)$ = -19.57 kcal mol^{-1} [47], $\Delta_f H^0_{298}(CH_4)$ = -17.78 kcal mol^{-1} [47], $\Delta_f H^0_{298}(CH_3\cdot)$ = 35.05 kcal mol^{-1} [48], $\Delta_f H^0_{298}(Cl)$ = 29.03 kcal mol^{-1} [48], $\Delta_f H^0_{298}(H)$ = 52.10 kcal.mol^{-1} have been used [48].

Similarly for the reaction

$$\text{4-X-PhS-H} \rightarrow \text{4-X-PhS}\cdot + \text{H}\cdot \quad (6)$$

the isodesmic reaction

$$\text{4-X-PhS-H} + \text{HS}\cdot \rightarrow \text{4-X-PhS}\cdot + \text{H}_2\text{S} \quad (7)$$

has been utilized to determine the bond dissociation energy of 4-X-PhS-H as

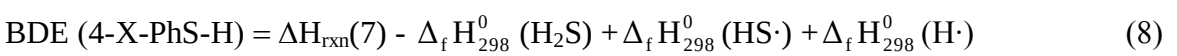

$$\text{BDE (4-X-PhS-H)} = \Delta H_{rxn}(7) - \Delta_f H^0_{298}(\text{H}_2\text{S}) + \Delta_f H^0_{298}(\text{HS}\cdot) + \Delta_f H^0_{298}(\text{H}\cdot) \quad (8)$$

where $\Delta_f H^0_{298}(\text{H}_2\text{S}) = -4.94$ kcal mol^{-1}, $\Delta_f H^0_{298}(\text{HS}\cdot) = 34.20$ kcal mol^{-1}, $\Delta_f H^0_{298}(\text{H}) = 52.10$ kcal mol^{-1} have been used [48].

In this study, the propagation of ethylene, the chain transfer reactions of ethylene with various chain transfer agents, the propagation of methyl methacrylate and acrylamide and their chain transfer reactions have been modeled with the B3LYP/6-311+G(3df,2p)//B3LYP/6-31+G(d), MPWB1K/6-311+G(3df,2p)//B3LYP/6-31+G(d) and M05-2X/6-311+G(3df,2p)//B3LYP/6-31+G(d) methodologies. Calculations are carried out at 403.15 K for the free radical polymerization of ethylene, whereas those of methyl methacrylate and acrylamide are carried out at 298.15 K.

8. 3. Results

8.3.1. Propagation of ethylene

Experimental and quantum chemical studies on the chain length dependency of the propagation rate constant of ethylene have been widely carried out [35]. Olaj et al. observed a slight decrease of k_p in terms of chain length [49]. Willemse showed that k_p is only dependent on the chain length in the oligomeric range [50], but this point of view has been later rejected by Olaj et al [51]. The latter claim that a long-range chain length dependence of k_p extends over several hundreds of propagation steps. The effect of extending the chain length of the radical on the calculated frequencies of the transitional modes in the addition of *n*-alkyl radicals to ethylene was investigated by Radom et al [52]. Another computational study about the free radical polymerization of ethylene indicated that the propagation rate coefficient has largely converged to within a factor of 1.3 by the hexyl radical stage, though a weaker chain-length dependence is detected that extends far beyond the oligomeric range [35]. A study of chain length effects in the free-radical polymerization of vinyl chloride and acrylonitrile indicated that rate coefficients had largely converged to their long chain limit at the dimer radical stage [53]. The results from applying the pulsed laser photolysis method to styrene polymerization are consistent with other recent work indicating that the value of k_p, for styrene is chain length dependent at least for chain lengths 3 units [54].

The propagation of ethylene considered in this study is displayed in Scheme 8.1. The hexyl radical is used as the growing chain to model the propagation and the chain transfer reactions. A relaxed potential energy scan study has shown that along the propagation reaction the hexyl radical approaches the ethylene molecule in the gauche geometry (τ = 57.38˚). The reaction barriers for the addition of various gamma-substituted propyl radicals to alkenes were obtained via ab initio molecular orbital calculations [55]: in each case the lowest energy transition structure conformations were those for gauche-addition transition structures in which the monomer substituent was close to both the gamma substituent of the propyl radical and the unpaired electron. As can be seen from the potential surface

energy scan, the eclipsed conformations in the polymer chain are about 0.70 kcal mol^{-1} less stable than the gauche conformations (Figure 8.1). This type of conformation has already been observed in the free radical propagation reaction of acrylates and methacrylates [25, 34, 37].

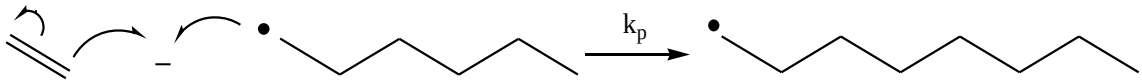

Scheme 8.1. Mechanism for the propagation reaction of ethylene.

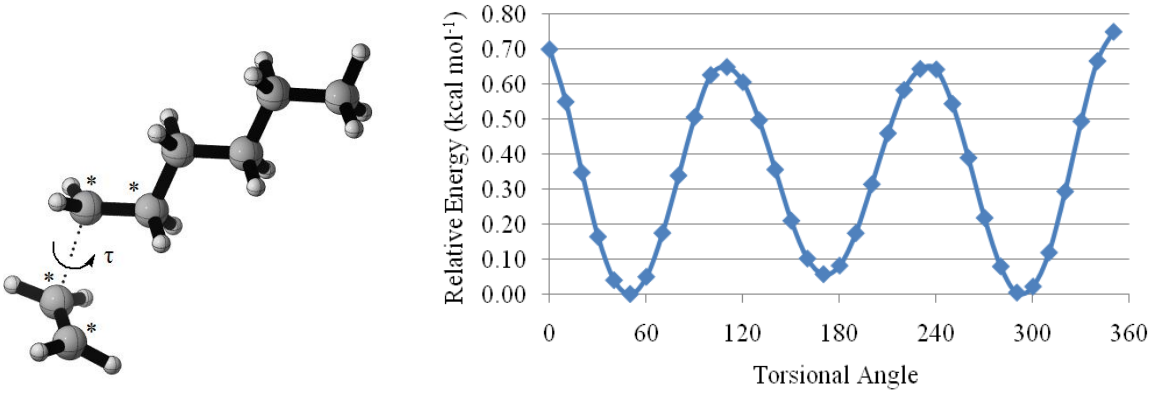

Figure 8.1. Transition state and potential energy scan along τ for the propagation reaction of ethylene (B3LYP/6-31+G(d)).

8.2.2. Chain transfer in the propagation of ethylene

In this study, the substituent effect, the steric effect, the unsaturation, the presence of hetero atoms on the transfer process of H(X) with a polyethylene growing chain are analyzed. This approach will elucidate how different chain transfer agents control the growing chain in the free radical polymerization of ethylene. It is known that halomethanes, which include chloroform, carbon tetrachloride, carbon tetrabromide, and bromotrichloromethane, have been widely used as CTA (telogens) for the preparation of telomers [56]. The perhalomethanes (e.g., carbon tetrachloride, carbon tetrabromide, and bromotrichloromethane) react in the chain transfer process to exchange a halogen atom and form a perhaloalkyl radical that initiates a new propagating chain. The low C_s value for chloroform as compared to the one of carbon tetrachloride is explained by the strength of

the C-H bond in the former. The enhancement of chain transfer reactivity has been postulated to occur by stabilization of the respective transition states for the transfer reactions by contributions from polar effects [57]. The experimental results displayed in Table 8.1 reveal the fact that the electron rich amine derivatives as well as chloromethanes increase the chain transfer constant along the polymerization of polyethylene.

Table 8.1. Chain transfer agents used in the polymerization of ethylene (C_s is the experimental chain transfer constant)

Chain transfer agent			**C_s [58]**
1	Ethene	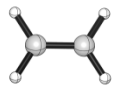	1.00E-05
2	Methane	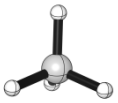	1.00E-04
3	Ethane	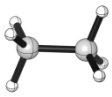	6.00E-04
4	Propane	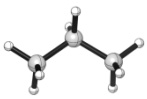	2.70E-03
5	Trimethylamine	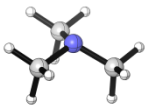	1.80E-02
6	Dimethylamine	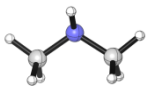	1.90E-01
7	Chloroform	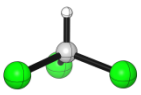	2.90E-01
8	Carbon tetrachloride	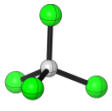	9.80E-01

The chain transfer reactions along the polymerization of ethylene have been modeled by taking into account all the possible reaction mechanisms during the abstraction of the labile atom of the chain transfer agents by the hexyl radical (Scheme 8.2). There is one

possible chain transfer mechanism for ethylene, methane, ethane and tri-methylamine because the hydrogen atoms are equivalent. On the other hand, propane and dimethylamine possess 2 different types of H atoms. In the case of chloroform, there is one labile hydrogen atom and 3 environmentally similar chlorine atoms, in the case of carbon tetrachloride as a chain transfer agent a chlorine atom is transferred to the hexyl radical. Note that the overall rate constant has been taken calculated in all cases, symmetry has not been taken into account by symmetry numbers in the partition functions, instead in the case of C_2H_6 the rate constant for the abstraction of a H atom is multiplied by 6; for $CHCl_3$ the overall rate constant includes the rate constant for H-atom abstraction and 3 times the rate constant for Cl abstraction etc. A similar procedure was followed in a study of H-abstraction by OH radicals where the total rate constant was considered as the sum of the individual rate constants [59].

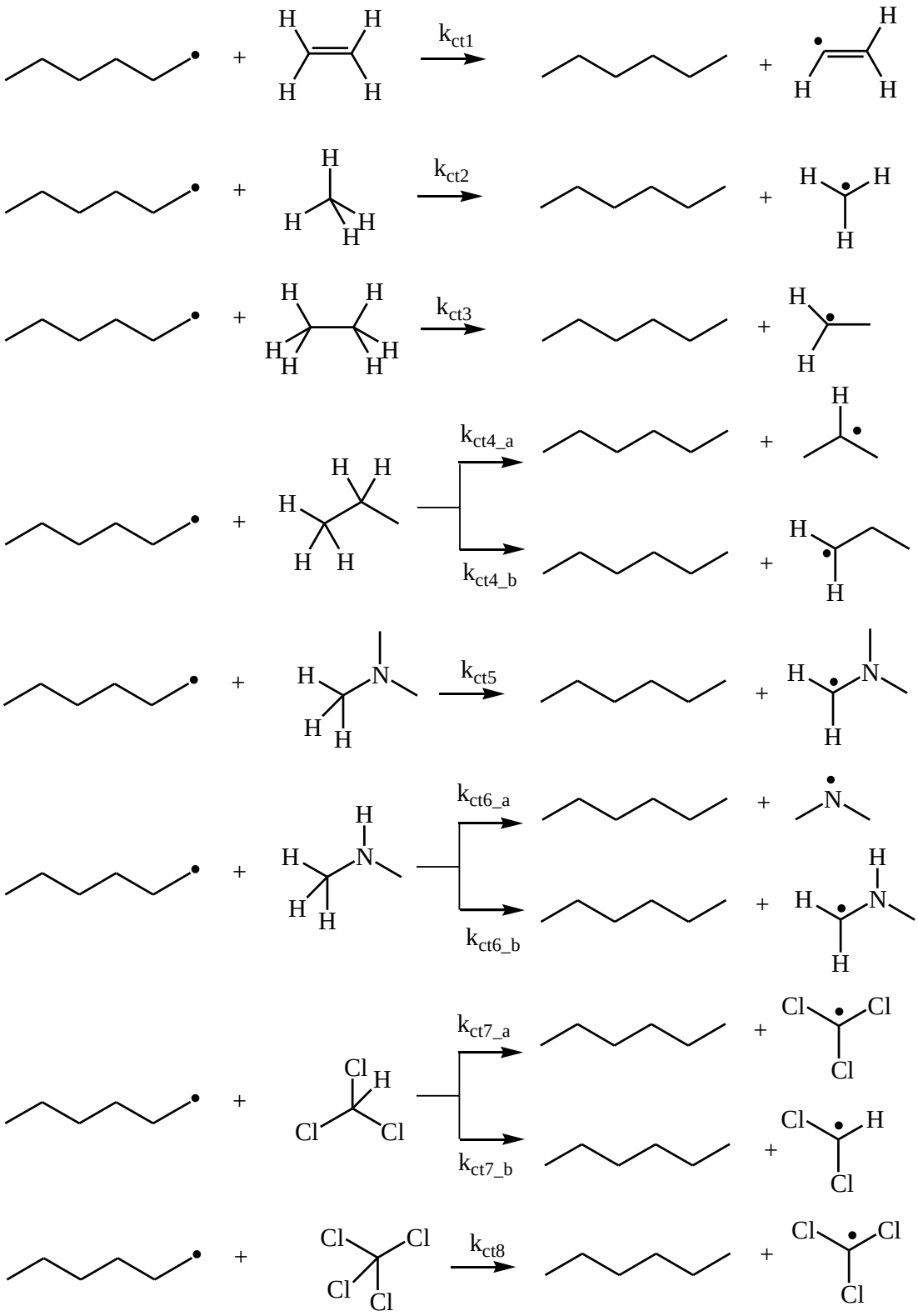

Scheme 8.2. Chain transfer reactions along the polymerization of ethylene.

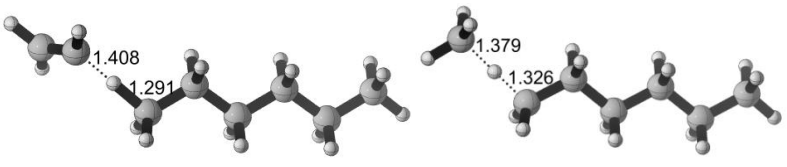

TS-PE-1

TS-PE-2

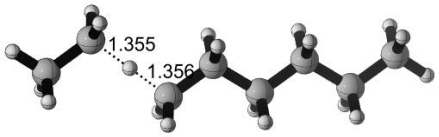

TS-PE-3

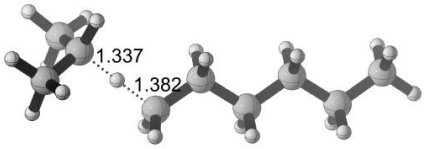

TS-PE-4a

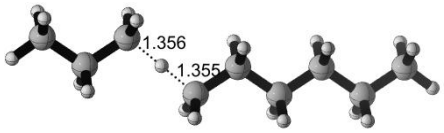

TS-PE-4b

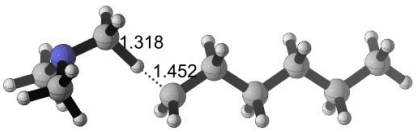

TS-PE-5

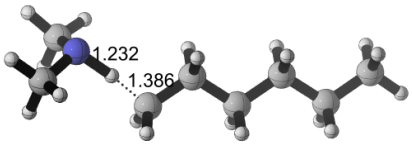

TS-PE-6a

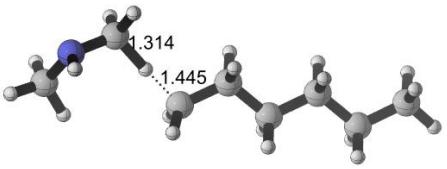

TS-PE-6b

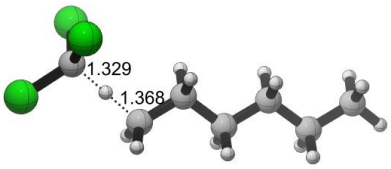

TS-PE-7a

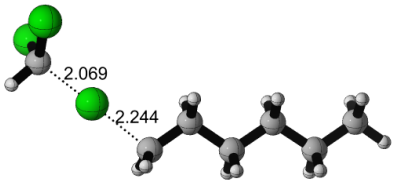

TS-PE-7b

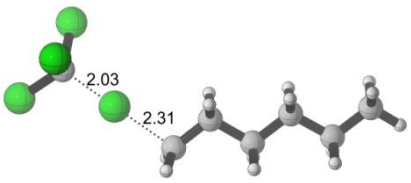

TS-PE-8

Figure 8.2. Transition states of the chain transfer reactions in the propagation of ethylene (B3LYP/6-31+G(d)).

The 3D structures for the transition states of the chain transfer reactions are gathered in Figure 8.2. TS-PE-1 is a late transition state in which a hydrogen atom of ethylene is abstracted by a hexyl radical, in this structure the breaking carbon-hydrogen bond is longer than the forming carbon-hydrogen bond. The hydrogen atom transfer reaction of methane (TS-PE-2), ethane (TS-PE-3) and propane (TS-PE-4b) show similar transition state structures with linear C—X—C features. TS-PE-3 and TS-PE-4b have equal breaking and forming bond distances, due to the similarity of the electronic environment on both sides. On the other hand the electron donor substituents facilitate the H-abstraction and their transition states (TS-PE-5, TS-PE-6a and TS-PE-6b) are early. In the case of chloroform, the hydrogen atom (TS-PE-7a) migrates faster than Cl (TS-PE-7b). The favorable long-range Cl….H interactions in $CHCl_3$ probably inhibits the rupture of the C-Cl bond as compared to the one in CCl_4 where all the four bonds are equivalent (Table 8.2).

Table 8.2. Activation barriers, E_a, (kcal mol^{-1}) for the chain transfer reactions in the FRP of ethylene (MPWB1K/6-311+G(3df,2p)//B3LYP/6-31+G(d)).

Chain transfer agent		**TS**	**E_a**
1	Ethene	TS-PE-1	18.44
2	Methane	TS-PE-2	18.16
3	Ethane	TS-PE-3	15.79
4	Propane	TS-PE-4a	13.80
		TS-PE-4b	16.00
5	Trimethylamine	TS-PE-5	12.22
6	Dimethylamine	TS-PE-6a	10.77
		TS-PE-6b	11.88
7	Chloroform	TS-PE-7a	7.34
		TS-PE-7b	12.95
8	Carbon tetrachloride	TS-PE-8	9.35

The mechanistic details of the chain transfer process in the free radical polymerization of ethylene have been analyzed in details (Table 8.3). Ethylene being a very stable molecule is not a good chain transfer agent, the chain transfer reaction is

endothermic and this is justified by the value of its BDE. Consideration of methane and ethane as chain transfer agents reveals the fact that the addition of a methyl group in ethane decreases the barrier by about 2 kcal mol^{-1} while the heat of the reaction alters by almost 4.5 kcal mol^{-1} due to the electron donor methyl group. The additional methyl group in iso-propane facilitates the H-abstraction similarly, however in n-propane the end methyl group does not assist the H-abstraction reaction and n-propane behaves like ethane. The enthalpies of activation of the amine derivatives are lower as compared to the ones of the hydrocarbons due to the presence of the electron donor group; Hammond's postulate is obeyed as reflected in the exothermicity of these chain transfer reactions. Among the chloromethanes chlorine abstraction from CCl_4 is easier than the others; CCl_3-Cl has the lowest BDE as determined experimentally [21,60]. Nevertheless as seen from the barrier heights, H abstraction is easier than chlorine abstraction due probably its smaller size and $CHCl_3$ acts as a chain transfer agent preferentially via its H. The hydrogen abstraction by carbon-centered radicals from chloroalkanes and amines is generally an exothermic process, in which a strong C-H bond is formed at the expense of weaker bonds broken. There is a correlation between the barrier height and the reaction enthalpy and the Evans-Polanyi rule somewhat rule holds for these reactions (Figure 8.3a).

The relative energies of the charge-transfer configurations at the transition structure have been modeled by considering the relative energies of the $C_6H_{13}^{+}AR^{-}$ and $C_6H_{13}^{-}AR^{+}$ using the charge transfer energies between the isolated $C_6H_{13}^{\cdot}$ and the chain transfer agents. "A" is H for the first 9 species and Cl for the last 2 species in Table 8.3. The hexyl radical (C_6H_{13}) is the propagating radical; the $C_6H_{13}^{+}AR^{-}$ configuration is modeled as the difference of the (vertical) ionization energy of the C_6H_{13} radical and (vertical) electron affinity of the AR fragment; whereas the $C_6H_{13}^{-}AR^{+}$ configuration is modeled as the difference of the (vertical) ionization energy of AR and (vertical) electron affinity of the C_6H_{13} fragment. The $C_6H_{13}^{+}AR^{-}$ species are lower in energy than the $C_6H_{13}^{-}AR^{+}$ species confirming the charge transfer to the chain transfer agent. The amount of charge transferred to the agent exceeds the one on the alkyl fragment in most cases as expected. There is a reasonable correlation between the activation energy and the charge separation in the transition structures reflecting the increasing ability of charge-transfer stabilization in the transition state: CCl_4 with the lowest barrier has the highest charge difference, ΔQ (Figure 8.3b).

Table 8.3. Forward Barrier[a] ($\Delta H^{\neq}_{fwd}$), Reverse Barrier[a] ($\Delta H^{\neq}_{rev}$), Enthalpy[a] (ΔH), Charge – Transfer Energies ($C_6H_{13}^{+}AR^{-}$ and $C_6H_{13}^{-}AR^{+}$), NBO Charges[a] (Q) on the Hexyl Group the Chain Transfer Agents in the Transition Structures (A=H or Cl). The last column displays the Bond Dissociation Energies (kcal mol^{-1}) (MPWB1K/6-311+G(3df,2p)//B3LYP/6-31+G(d)).

R-H	$\Delta H^{\neq}_{fwd}$	$\Delta H^{\neq}_{rev}$	ΔH	$C_6H_{13}^{+}AR^{-}$	$C_6H_{13}^{-}AR^{+}$	$Q(C_6H_{13})$	Q(R)	BDE
CH_2CH-H	18.06	8.92	9.14	6.22	9.90	-0.092	-0.096	109.84 (110.7)[b]
CH_3-H	17.40	13.09	4.32	6.58	13.61	-0.097	-0.104	104.94 (104.99)[b]
CH_3CH_2-H	15.40	15.65	-0.25	6.64	11.84	-0.105	-0.101	100.38 (101.1)[b]
$(CH_3)_2CH$-H	13.64	17.42	-3.78	6.72	11.18	-0.109	-0.105	96.86 (98.6)[b]
$CH_3CH_2CH_2$-H	15.74	15.10	0.64			-0.104	-0.105	101.27
$(CH_3)_2NCH_2$-H	12.08	21.89	-9.81	6.81	7.77	-0.146	-0.046	90.86
$(CH_3)_2N$-H	10.49	19.50	-9.01	6.79	8.27	-0.09	-0.211	91.72
CH_3NHCH_2-H	11.67	21.52	-9.85			-0.142	-0.048	90.80
CCl_3-H	7.43	17.43	-10.00	7.53	10.91	0.145	-0.079	90.78 (95.8)[d]
$CHCl_2$-Cl	13.01	36.32	-23.31			0.136	-0.021	93.99 (77.8)[d]
CCl_3-Cl	9.45	39.82	-30.37	8.23	11.02	-0.011	-0.213	87.07(84.27)[c]

C_6H_{13} (Radical) IE = 8.17 eV, EA = 0.52 eV

[a]Barriers and enthalpies are calculated at 403.15 K (kcal mol^{-1}); bond dissociation energies are calculated at 298.15 K; NBO charges are obtained from the MPWB1K/6-311+G(3df,2p) wave function calculated on the B3LYP/6-31+G(d) geometry.

[b]Ref [46, 48]

[c]The BDE of $CH_3COOC(H)(CH_3)$-Cl has been calculated as 84.23 kcal mol^{-1} in reference [21].

[d]Ref [60]

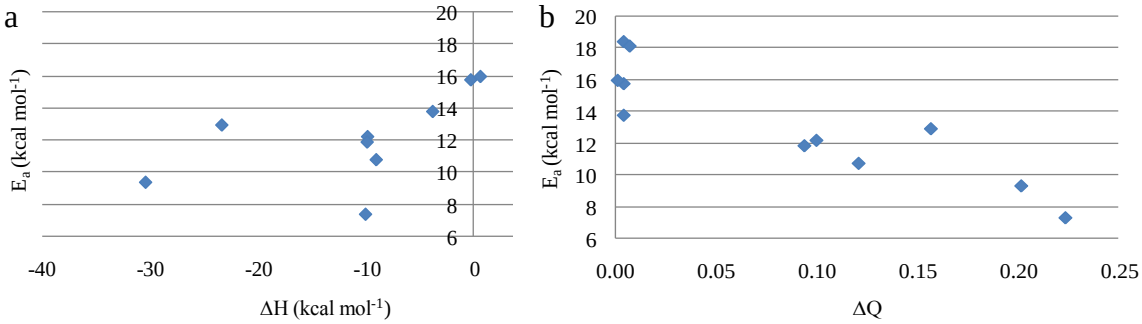

Figure 8.3. (a) Reaction barrier versus reaction enthalpy (MPWB1K/6-311+G(3df,2p) //B3LYP/6-31+G(d)), (b) Reaction barrier versus charge separation between the hexyl radical and the chain transfer agent (MPWB1K/6-311+G(3df,2p)//B3LYP/6-31+G(d)).

8.2.3. Level of Theory Study

The methodology used has been tested and a level of theory (LOT) study has been performed on the chain transfer constant, C_s for the free radical polymerization of ethylene with the MPWB1K, B3LYP and M05-2X methodologies. All the functionals used reproduce qualitatively quite well the experimental trend, the results with the MPWB1K functional have the smallest mean unsigned error (MUE) for the chain transfer constants C_s as depicted in Figure 8.4 (Table 8.4).

Table 8.4. LOT study on the chain transfer constants (C_s) for the various chain transfer agents in the FRP of ethylene (403.15K).

Chain transfer agent		C_s (exp)[a]	C_s (calculated)			
			B3LYP	MPWB1K	M05-2X	MPWB1K[b]
1	Ethene	1.00E-05	1.98E-04	1.53E-05	1.83E-06	1.39E-05
2	Methane	1.00E-04	2.27E-04	3.90E-05	3.59E-06	1.96E-05
3	Ethane	6.00E-04	2.32E-03	4.30E-04	4.83E-05	1.89E-04
4	Propane	2.70E-03	6.90E-03	1.14E-03	2.25E-04	1.29E-03
5	Trimethylamine	1.80E-02	2.69E-01	4.14E-02	2.58E-03	2.25E-03
6	Dimethylamine	1.90E-01	3.14E-01	2.09E-02	2.50E-03	4.08E-02
7	Chloroform	2.90E-01	6.09E-01	1.48E-01	1.34E-02	2.34E+00
8	Carbon tetrachloride	9.80E-01	2.80E+01	4.90E-01	1.76E+00	1.15E-02
MUE*			3.47	0.10	0.16	0.03
R^2			0.91	0.97	0.90	1.00
STDEV			3.24	0.03	0.21	0.00087

[a] Ref [58].

[b] Corrected with HIR and Eckart tunneling corrections.

k_p ($C_6H_{13}\cdot$)(B3LYP/6-311+G(3df,2p)//B3LYP/6-31+G(d)) = 4.74E+00 $Lmol^{-1}s^{-1}$; (MPWB1K/6-311+G(3df,2p)//B3LYP/ 6-31+G(d)) = 4.09E+02 $Lmol^{-1}s^{-1}$; (M05-2X/6-311+G(3df,2p)//B3LYP/ 6-31+G(d)) = 1.03E+05 $Lmol^{-1}s^{-1}$).

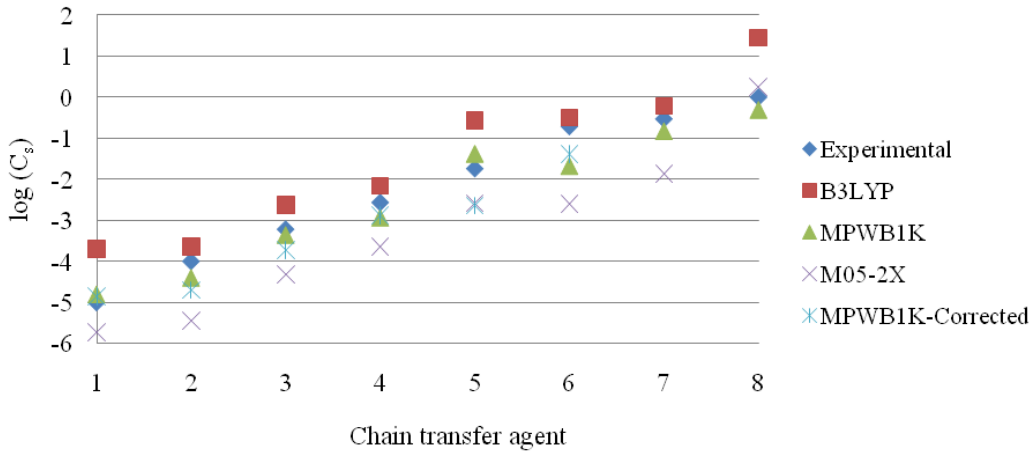

Figure 8.4. log (C_s) against chain transfer agent in the FRP of ethylene (Table 8.4)

8.4. Conclusion

In this study, the reactivity of chain transfer agents in the free radical polymerization of ethylene, methylmethacrylate and acrylamide has been modeled with quantum chemical tools. The B3LYP/6-311+G(3df,2p)//B3LYP/6-31+G(d), MPWB1K/6-311+G(3df,2p)//B3LYP/6-31+G(d) and M05-2X/6-311+G(3df,2p)//B3LYP/6-31+G(d) methodologies have been tested against the experimental results in order to assess the level of theory. In all cases, the MPWB1K/6-311+G(3df,2p)//B3LYP/6-31+G(d) methodology is found to reproduce the experimental trend the best. In the case of polyethylene chloromethanes and amines are found to control the polymerization better than alkanes and alkenes. Overall, the models used in this study have proved to be adequate in the rationalization of the FRP kinetics. Similar calculations can be carried out with confidence to predict the characteristics of the chain transfer agent prior to experimental results.

8. 5. References

1. Valdebenito, A.; Encinas, M. V. *Polymer* **2005**, *46*, 10658–10662.

2. Valdebenito, A.; Encinas, M. V. *Journal of Photochemistry and Photobiology A: Chemistry* **2008**, *194*, 206–211.

3. Heuts, J. P. A.; Davis, T. P.; Russell, G.T. *Macromolecules* **1999**, *32*, 6019-6030.

4. Mayo, F. R. *J. Am. Chem. Soc.* **1943**, *65*, 2324–2329.

5. *Polymer Handbook*, 4th ed.; Brandrup, J.; Immergut, E. H.; Grulke, E. A., Eds.; Wiley-Interscience: Hoboken, NJ, **1999**.

6. Wang, J. S.; Matyjaszewski, K. *J. Am. Chem. Soc.* **1995**, *117*, 5614- 5615.

7. Patten, T. E.; Xia, J.; Abernathy, T.; Matyjaszewski, K. *Science* **1996**, *272*, 866-868.

8. Matyjaszewski, K.; Xia, J. *Chem. Rev.* **2001**, *101*, 2921-2990.

9. Kamigaito, M.; Ando, T.; Sawamoto, M. *Chem. Rev.* **2001**, *101*, 3689-3745.

10. Georges, M. K.; Veregin, R. P. N.; Kazmaier, K. M.; Hamer, G. K. *Macromolecules* **1993**, *26*, 2987-2988.

11. Hawker, C. J.; Bosman, A. W.; Harth, E. *Chem. Rev.* **2001**, *101*, 3661-3688.

12. Chiefari, J.; Chong, Y. K.; Ercole, F.; Krstina, J.; Jeffery, J.; Le, T. P. T.; Mayadunne, R. T. A.; Meijs, G. F.; Moad, C. L.; Moad, G.; Rizzardo, E.; Thang, S. H. *Macromolecules* **1998**, *31*, 5559-5562.

13. Goto, A.; Sato, K.; Tsujii, Y.; Fukuda, T.; Moad, G.; Rizzardo, E.; Thang, S. H. *Macromolecules* **2001**, *34*, 402-408.

14. Gridnev, A. A.; Ittel, S. D. *Chem. Rev.* **2001,** *101*, 3611-3659.

15. Heuts, J. P. A.; Pross, A.; Radom, L. *J. Phys. Chem.* **1996,** *100*, 17087-17089.

16. Toh, J. S. S.; Huang, D. M.; Lovell, P. A.; Gilbert, R.G. *Polymer* **2001**, *42*, 1915–1920.

17. Matyjaszewski, K.; Poli, R. *Macromolecules* **2005,** *38,* 8093-8100.

18. (a) Izgorodina, E. I.; Coote, M. L. *Macromol. Theory Simul*. **2006**, *15*, 394–403. (b) Coote, M. L.; Krenske, E. H.; Izgorodina, E. I. *Macromol. Rapid Commun*. **2006**, *27*, 473–497.

19. Lin, C. Y.; Coote, M. L.; Petit, A.; Richard, P.; Poli, R.; Matyjaszewski, K. *Macromolecules* **2007,** 40, 5985-5994.

20. Tang, W.; Kwak, Y.; Braunecker, W.; Tsarevsky, N. V.; Coote, M. L.; Matyjaszewski, K. *J. Am. Chem. Soc*. **2008**, *130*, 10702–10713.

21. Lin, C.Y.; Coote, M. L.; Gennaro, A.; Matyjaszewski, K. *J. Am. Chem. Soc*. **2008**, *130*, 12762–12774.

22. Purmova, J.; Pauwels, K. F. D.; Van Zoelen, W.; Vorenkamp, E. J.; Schouten, A. J.; *Macromolecules* **2005**, *38*, 6352-6366.

23. Purmova, J.; Pauwels, K. F. D.; Agostini, M.; Bruinsma, M.; Vorenkamp, E. J.; Schouten, A. J.; Coote, M. L. *Macromolecules* **2008**, *41*, 5527-5539.

24. Van Cauter, K.; Van Den Bossche, B. J.; Van Speybroeck, V.; Waroquier, M. *Macromolecules* **2007**, *40*, 1321-1331.

25. Değirmenci, I.; Avcı, D.; Aviyente, V.; Van Cauter, K.; Van Speybroeck, V.; Waroquier, M. *Macromolecules* **2007**, *40*, 9590-9602.

26. Pross, A.; Shaik, S. *Acc. Chem. Res.* **1983**, *16,* 363-370.

27. Cole, S. J.; Kirwan, J. N.; Roberts, B. P.; Willis, C. R. *J. Chem. Soc., Perkin Trans*. 1 **1991**, 103-112.

28. Reid, D. L.; Armstrong, D. A.; Rauk, A.; Von Sonntag, K. *Phys. Chem. Chem. Phys.* **2003**, *5*, 3994–3999.

29. Beare, K. D.; Coote, M. L. *J. Phys. Chem. A.* **2004**, *108,* 7211-7221.

30. Rong, X. X.; Pan, H.; Dolbier, Jr., W. R. *J. Am. Chem. Soc.* **1994**, *116,* 4521-4522.

31. *Handbook of Radical Polymerization*; Matyjaszewski, K.; Davis, T. P.; Wiley-Interscience: Hoboken, NJ, **2002**.

32. *Atkins' Physical Chemistry*, 8th ed.; Atkins, P.; De Paula, J.; Oxford University Press. New York. **2006**.

33. Gaussian 03. Revision D.01; Frisch, M. J.; Trucks, G. W.; Schlegel, H. B.; Scuseria, G. E.; Robb, M. A.; Cheeseman, J. R.; Montgomery Jr., J. A.; Vreven, T.; Kudin, K. N.; Burant, J. C.; Millam, J. M.; Iyengar, S. S.; Tomasi, J.; Barone, V.; Mennucci, B.; Cossi, M.; Scalmani, G.; Rega, N.; Petersson, G. A.; Nakatsuji, H.; Hada, M.; Ehara, M.; Toyota, K.; Fukuda, R.; Hasegawa, J.; Ishida, M.; Nakajima, T.; Honda, Y.; Kitao, O.; Nakai, H.; Klene, M.; Li, X.; Knox, J. E.; Hratchian, H. P.; Cross, J. B.; Bakken, V.; Adamo, C.; Jaramillo, J.; Gomperts, R.; Stratmann, R. E.; Yazyev, O.; Austin, A. J.; Cammi, R.; Pomelli, C.; Ochterski, J. W.; Ayala, P. Y.; Morokuma, K.; Voth, G. A.; Salvador, P.; Dannenberg, J. J.; Zakrzewski, V. G.; Dapprich, S.; Daniels, A. D.; Strain, M. C.; Farkas, O.; Malick, D. K.; Rabuck, A. D.; Raghavachari, K.; Foresman, J. B.; Ortiz, J. V.; Cui, Q.; Baboul, A. G.; Clifford, S.; Cioslowski, J.; Stefanov, B. B.; Liu, G.; Liashenko, A.; Piskorz, P.; Komaromi, I.; Martin, R. L.; Fox, D. J.; Keith, T.; Al-Laham, M. A.; Peng, C. Y.; Nanayakkara, A.; Challacombe, M.; Gill, P. M. W.; Johnson, B.; Chen, W.; Wong, M. W.; Gonzalez, C.; and Pople, J. A.; Gaussian. Inc.. Wallingford CT, **2004**.

34. Değirmenci, İ.; Aviyente, V.; Van Speybroeck, V.; Waroquier, M. *Macromolecules* **2009**, *42*, 3033-3041.

35. Van Cauter, K.; Van Speybroeck, V.; Vansteenkiste, P.; Reyniers, M. F.; Waroquier, M. *ChemPhysChem* **2006,** *7*, 131-140. Speybroeck, V.; Van Cauter, K.; Coussens, B.; Waroquier, M. *ChemPhysChem* **2005**, *6*, 180-189.

36. (a) Gomez-Balderas, R.; Coote, M. L.; Henry, D. J.; Radom, L. *J. Phys. Chem. A* **2004**, *108*, 2874-2883; (b)Coote, M. L. *J. Phys. Chem. A* **2004**, *108*, 3865-3872.

37. Smith, D. M.; Nicolaides, A.; Golding, B. T.; Radom, L. *J. Am. Chem. Soc*. **1998**, *120*, 10223–10233.

38. Zhao, Y.; Truhlar, D. G. *J. Phys. Chem. A* **2004**, *108*, 6908–6918.

39. Zhao, Y.; Schultz, N. E.; Truhlar, D. G. *J. Chem. Theory Comput* **2006,** *2*, 364-382.

40. (a) Van Speybroeck, V.; Van Neck, D.; Waroquier, M.; Wauters, S.; Saeys, M.; Marin, G. B. *J. Phys. Chem. A* **2000**, *104*, 10939-10950. (b) Sabbe, M. K.; Vandeputte, A. G; Reyniers, M. F.; Van Speybroeck, V.; Waroquier, M.; Marin, G. B. *J. Phys. Chem. A* **2007,** *111*, 8416-8428. (c) Van Cauter, K.; Hemelsoet, K.; Van Speybroeck, V.; Reyniers, M. F.; Waroquier, M. *International Journal of Quantum Chemistry* **2005**, *102*, 454–460.

41. (a) Hemelsoet, K.; Van Speybroeck, V.; Moran, D.; Marin, G. B.; Radom, L.; Waroquier, M. *J. Phys. Chem. A* **2006,** *110,* 13624-13631. (b) Van Speybroeck, V.; Hemelsoet, K.; Minner, B.; Marin, G. B.; Waroquier, M. *Molecular Simulation* **2007**, *33*, 879–887. (c) Vandeputte, A. G.; Sabbe, M. K.; Reyniers, M. F.; Van Speybroeck, V.; Waroquier, M.; Marin, G. B. *J. Phys. Chem. A* **2007,** *111*, 11771-11786.

42. Coote, M. L. ; Collins, M. A.; Radom, L. *Mol. Phys.* **2003**, *101*, 1329-1338.

43. Wigner, E. Z. *Phys. Chem. B.* **1932**, *19*, 203.

44. Eckart, C. *Phys. Rev.* **1930**, *35*, 1303-1309.

45. Hemelsoet, K.; Van Speybroeck, V.; Waroquier, M. *ChemPhysChem*. **2008**, *9*, 2349–2358.

46. Da Silva, G.; Chen, C.; Bozzelli, J. W. *Chem. Phys. Lett.* **2006,** *424*, 42–45.

47.*CRC Handbook of Chemistry and Physics*, Lide, D. R., **1990-91**.

48. Blanksby, S. J.; Ellison, G. B. *Acc. Chem. Res.* **2003,** 36, 255-263.

49. Olaj, O. F.; Vana, P.; Zoder, M.; Kornherr, A.; Zifferer, G. *Macromol. Rapid Commun*. **2000**, *21*, 913-920.

50. Willemse, R. X. E.; StAMl. B. B. P.; Van Herk, A. M.; Pierik, S. C. J.; Klumperman, B. *Macromolecules* **2003**, *36*, 9797-9803.

51. Olaj, O. F.; Zoder, M.; Vana, P.; Kornherr, A.; Schnöll-Bitai, I.; Zifferer, G. *Macromolecules* **2005**, *38*, 1944-1948.

52. Heuts, J. P. A.; Gilbert, R. G.; Radom, L. *J. Phys. Chem.* **1996**, *100*, 18997-19006.

53. Izgorodina, E. I.; Coote, M. L. *Chem. Phys*. **2006**, *324*, 96–110.

54. Deady, M.; Mau, A. W. H.; Moad, G.; Spurling, T. H. *Makromol. Chem*. **1993**, *194*, 1691-1705.

55. Coote, M. L.; Davis, T. P. *Macromolecules* **1999**, *32*, 5270-5276.

56. Boutevin. B. *J. Polym. Sci.; Part A: Polym. Chem.* **2000**, *38*, 3235-3243.

57. *Principles of Polymerization*; Odian, G. Wiley-Interscience, New York, **1991**.

58. Mortimer, G. A.. *J. Polym. Sci. : Part A-1* **1966**, *4*, 881-900.

59. Atadinc, F.; Selcuki, C.; Sarı, L.; Aviyente, V. *Phys. Chem. Chem. Phys.* **2002**, *4*, 1797-1806.

60. McGivern, S. W.; Derecskei-Kovacs, A.; North, S. W.; Francisco, J. S. *J. Phys Chem. A* **2000**, *104* , 436-442.

9. GENERAL CONCLUSIONS

In this study, polymerization trends of acrylates and methacrylates were modeled by density functional based methods in order to understand structure-reactivity relations between the monomer and overall rate of polymerization. The kinetics of the various reactions was modeled by means of Transition State Theory, in which uses the properties of reactants, transition state and products along the reaction path to calculate the reaction rate constant. These properties obtained from the first principles calculations are the energies and molecular partition functions. As observed earlier in literature, the obtained results might be influenced a lot by the electronic level of theory used during the calculations. To this end various levels of theory were tested to investigate the influence of the obtained results with respect to the electronic structure method. All geometries were generated by the B3LYP/6-31+G(d) level of theory which is known to be reliable for these purposes. Of all tested levels of theory the MPWB1K functional in combination with the 6-311+G(3df,2p) basis set is found to give the most reliable results, compared to the experimental data. The proposed method gives a good compromise between accuracy and computational efficiency. Our findings are in agreement with other literature data in this field. However some more groups have also proposed the usage of computationally more expensive methods such as the CCSD(T) calculations, but in view of the size of the systems under study here these methods were not feasible.

Another point of interest concerns the appriopriate treatment of the low vibrational frequencies. In standard ab initio packages, all vibrational modes are treated within the Harmonic Oscillator approximation (HO). Most of the reactions modeled in this thesis are radical addition reactions for which the transition state is characterized by a low vibrational mode that corresponds to rotation about the forming bond. A correct description of all possible transition states. i.e. trans and gauche additions, requires the treatment of these modes in the hindered rotor approach. For all addition reactions studied in this thesis, rotational potentials for this particular mode were generated and all possible transition states were taken into account. The hindered rotor approach made substantial

corrections to the propagation rate constant of acrylates while it is negligible for alkyl α-hydroxymethacrylates. The rotational barrier is relatively small for acrylates in comparison with alkyl α-hydroxymethacrylates. Therefore, the hindered rotor correction gains importance for calculating the rate constant of the propagation reaction of acrylates.

This procedure was first applied to study the polymerization behavior of a series of acrylates and methacrylates for which experimental rates of polymerization were available. We could indeed reproduce the experimentally observed trends.

In a next step this study was further extended to a series of alpha substituted acrylates and methacrylates. Following monomers were taken into account : methyl acrylate (MA), methyl methacrylate (MMA), ethyl α-fluoroacrylate (EFA), ethyl α-chloroacrylate (ECA), ethyl α-cyanoacrylate (ECNA), methyl α-hydroxymethacrylate (MHMA). In addition also the chain length dependence has been examined by the addition of monomeric, dimeric, trimeric and tetrameric radicals to the monomers. has been modeled with DFT. The proposed methodology succeeds in predicting the experimentally observed trends for the propagation kinetics.

Another highly relevant but difficult issue concerns the influence of solvent on the free radical polymerization behavior. When starting this thesis most studies available in literature used continuum models to study these effects. However when particular interactions between solvent molecules and reacting monomers or radical play a role such approach is not sufficient anymore. Therefore we used a combination of an explicit and implicit solvation model. In such approach some discrete molecules are added to the modeled cluster which is then further embedded in a continuum with constant dielectricum constant.

The solvent effect on the tacticity control of MMA polymerization has been investigated by using MPWB1K/6-311+G(3df,2p)//B3LYP/6-31+G(d) level of theory. The propagation reaction of MMA in vacuum, in methanol (CH_3OH) and perfluoro-tert-butyl alcohol ($(CF_3)_3COH$) was modeled by considering syndiotactic and isotactic addition geometries of the monomer. The special effect of $(CF_3)_3COH$ on the stereoregularity of PMMA has been explained by both the steric hindrance and hydrogen bonding of solvent

molecule. While it makes strongly hydrogen bonds to the carbonyl oxygens (~ 1.7 Å) located on the same side of the backbone it also leads to steric hindrance. CH_3OH has relatively small size and it makes relatively weak hydrogen bonds (~ 1.9 Å) with the carbonyl oxygen. Therefore it has less effectiveness to reduce the istacticty of PMMA.

This study has been extended to acrylic acids and methacrylic acids for which available literature date indicates that the polymerization rate varies strongly with pH and degree of ionization. In addition to solvating the monomers and radicals with water molecules, we also explored the possiblility of solvation by other monomers present in the reaction medium.

Overall within the present approach the polymerization trends are qualitatively well reproduced with k_p. The quantitative reproduction of absolute rates of polymerization in bulk and solvent remains a challenge for theoretical methods. A particular problem occurs for longer radicals for which a myriad of conformations are possible. In that case simple selection of one reactant complex or transition state is not possible. Another challenge remains the treatment of solvation effects. Although we were able to model in most case the experimentally observed trends with static methods, the proper account of all possible minima on the potential energy surface is not straightforward. Moreover various prereactive complexes can play an important role which complicates the calculation of the reaction rates. Nowadays molecular dynamics methods are fully developed to study reactions in which all reaction partners are properly embedded in a full solvated box. Up to this point these methods are still computationally very expensive and cannot be used straightforward for a large number of monomers.

Within the current limits of computational power and numerical methods, this study has demonstrated the fact that computational chemistry offers a viable alternative and complement to experiment: relative propagation rate coefficients as well as tacticity and solvent effect on tacticity can be predicted prior to FRP.